The Electrophysiology of Neonatal Abstinence Syndrome

By

Richard George Boulton

B.Sc. (Hons), Pg.Dip.

Submitted in fulfilment of the requirements for the degree of Doctor of Philosophy

Department of Clinical Physics and Bioengineering,

College of Medical, Veterinary & Life Sciences

University of Glasgow

December 2014

No part of this thesis has been submitted in support of an application for another degree or qualification of this or any other university.

Abstract

Background

The recommended treatment for pregnant drug misusing women is maintenance methadone. This is of proven benefit in terms of improving maternal well-being, but is commonly associated with neonatal abstinence syndrome (NAS). NAS reflects withdrawal at birth from *in utero* exposure to licit (including maintenance methadone prescribed to reduce illicit drug use) or illicit opioids (heroin). Symptoms include diarrhoea, extreme irritability, feeding problems, jitteriness and sleep disturbance and in some cases seizures. These signs suggest impaired regulation of homoeostatic processes, postulated to be due to dysfunctional vagal regulation. At present NAS cannot be predicted in individual cases, therefore management must include prolonged hospital stay to monitor for symptoms, and pre-emptive treatment is not feasible. Resting heart rate variability (HRV) is a well-established measure of the parasympathetic autonomic nervous system, reflective of cardiac vagal tone (CVT). The purpose of this study was to develop a better understanding of the electrophysiology of methadone-exposed neonates using EEG, ECG and CVT, with the aim of improving short and longer term management of the *in utero* drug exposed infant.

Materials and Methods

Twenty six methadone-exposed infants and thirty controls matched for gestation, birth weight, and postcode of residence underwent a one hour sleep polysomnogram (PSG) incorporating an electroencephalogram (EEG) and electrocardiogram (ECG), recorded within the first 48 hours of life (preceding onset of any NAS). *In utero* drug exposure was described by a combination of maternal drug and alcohol history and urinalysis, and infant meconium and urine toxicology. PSGs were scored for sleep state (quiet; intermediate; active), and artefact-free epochs extracted by an experienced paediatric neurologist. EEG spectral analysis was performed and HRV used to estimate CVT.

Results

PSGs from 45 infants (80% of those tested), including 20 methadone-exposed infants, were deemed suitable for a sleep study analysis. For the 20 methadone-exposed infants, additional drug exposure was as follows: opioids 12/20 (60%): benzodiazepines 11/20 (55%): amphetamines 7/20 (35%): cocaine 4/20 (20%) and cannabis 13/20 (65%). Three of these 20 infants developed significant NAS requiring treatment. The EEG analysis showed cases tended to have increased EEG power and lower spectral edge frequencies but no group differences reached significance. The ECG analysis showed higher power amongst cases for many of the HRV parameters, but none reached significance between groups. However, control infants had lower CVT for all sleep states than methadone-exposed infants: active sleep CVT 1.9 vs 3.5 ($p=0.002$), indeterminate sleep CVT 2.4 vs 3.7 ($p=0.033$) and quiet sleep CVT 3.2 vs 4.6 ($p=0.362$).

Conclusion

Newly born infants of opioid-dependent mothers prescribed maintenance methadone have increased CVT consistent with impaired homeostatic regulation of the autonomic nervous system. Although CVT did not predict NAS for the small number of infants who required treatment, CVT may have potential as a predictor of NAS in conjunction with other neonatal and maternal parameters.

List of Contents

List of tables

List of Figures

Preface

During the early 2000s an increase in the number of children referred to Opthalmology at the Royal Hospital for Sick Children in Glasgow with nystagmus and possible delayed visual maturation was observed. Dr Ruth Hamilton and Prof. Gordon Dutton of the departments of Clinical Physics and Ophthalmology recognised that many of these children had a history of *in utero* exposure to methadone and/or illicit drugs (Hamilton et al., 2010). It was also noted that there had been a contemporaneous increase in the number of drug-misusing mothers prescribed methadone within Greater Glasgow and Clyde.

The author of this thesis contributed to a subsequent pilot study undertaken at the Princess Royal Maternity (McGlone et al., 2008). Visual evoked potentials (VEPs) were recorded within three days of birth from 21 term infants of opioid-dependent woman prescribed methadone in pregnancy and from 20 controls. VEPs from drug-exposed infants were less likely to be of typical waveform and more likely to be immature or non-detectable ($p<0.01$) than those of control infants. VEPs were also smaller in amplitude (median 11 vs 24 µV, $p<0.001$). VEPs of drug-exposed infants had matured after 1 week but remained of lower amplitude than VEPs of newborn controls ($p<0.01$) and continued to be non-detectable in 15%. This pilot study indicated that further study was required to address the specific effects of maternal methadone and/or other illicit drug misuse upon infant VEPs, as well as possible associations between *in utero* drug exposure and subsequent visual and general neurological development.

This led to the ‘Vision in Drug-Exposed Infants’ (VIDI) study (McGlone et al., 2014, 2013), funded by Yorkhill Children’s Charity and TENOVUS Scotland. The VIDI study obtained uniquely comprehensive toxicology information, identifying the extent of *in utero* drug exposure for a cohort of 100 infants and related this to newborn VEPs as well as visual and general neurological development at six months of age. Dr Laura McGlone, a paediatric trainee, recruited all the infants for the VIDI study and undertook the assessments. In a nested study, the author investigated the effects of *in utero* exposure to methadone and other illicit drugs on neonatal sleep states and cardiac vagal tone (CVT), by means of polysomnography and calculation of heart rate variability (HRV). The nested study is described in this thesis.

Author's Declaration

The material presented in this thesis is the author's own work with the following exceptions:

Dr Laura McGlone recruited the mothers and infants to the study as part of the wider VIDI study, and was in attendance during the recording sessions.

Dr Mary O'Regan scored the polysomnograms for each sleep state.

Dr Stig Hansen made the Neuroscope™ proprietary software available for measuring CVT. He also provided the software routine which translated my data in EDF format to the data input format required by the Neuroscope™ software. Dr Hansen modified this software when my test data highlighted a fault.

Dr William Borland was responsible for the toxological analysis of the maternal urine samples for the VIDI study.

Dr Gail Cooper and Mrs Huda Hassan undertook the toxicological analysis of the meconium samples for the VIDI study.

Presentations and Awards

Material contained in this thesis has been disseminated at local and national meetings:

Boulton R. Predicting neonatal abstinence syndrome with ECG. Department of Clinical Physics and Bioengineering 60th anniversary symposium, Glasgow Science Centre, Glasgow, November 7th 2013. *Awarded best presentation.*

Boulton R. Predicting neonatal abstinence syndrome with ECG. Scottish Paediatric Society St. Andrew's Day Symposium, Edinburgh, November 22nd 2013. *Awarded the Oman Craig Trophy for the best scientific presentation.*

Publications

The pilot data which were a precursor to the VIDI study has been published in the following paper:

McGlone L, Mactier H, Hamilton R, Bradnam MS, **Boulton R,** Borland W, Hepburn M, McCulloch DL. Visual evoked potentials (VEPs) in infants exposed to methadone *in utero*. Arch Dis Child 2008; 93: 784-6

Published Abstracts

Material obtained as part of the VIDI study has resulted in the following published abstracts:

Mactier H, McGlone, Hamilton R, **Boulton R,** McDulloch DL, Bradnam MS, Borland W, Cooper G, Hassan H, Weaver LT. Abnormal visual evoked potentials in newborn infants of drug-misusing mothers: is prescription of substitute methadone to blame? Arch Dis Child Fetal Neonatal Ed 2011;96: Fa45-46

McCulloch DL, McGlone L, **Boulton RG,** Doherty E, Hamilton R, Bradnam MS, Mactier H. Neonatal VEPs to transient and steady-state luminance stimuli: normative data. Doc Opthalmol 2010;121(suppl):4.

McCulloch DL, McGlone L, Bradnam MS, Hepburn M, Hamilton R, Borland W, **Boulton R**, Pieh C, Bach M, Mactier H. Flash and flicker VEPs in newborn term infants of drug-misusing mothers. Doc Opthalmol 2007; 115:30.

In utero methadone exposure adversely affects the neonatal flash VEP. Hamilton R, McGlone L, McCulloch DL, **Boulton R**, Bradnam M, Weaver LT, Mactier H. 49th ISCEV International Symposium, Quebec City 2011.

Acknowledgement

The author gratefully acknowledges the financial assistance of the Yorkhill Children's Charity (formerly the Yorkhill Children’s Foundation), Tenovus Scotland and the Princess Royal Maternity Special Care Baby Unit Fund.

I would like to thank my supervisors, Dr Michael Bradnam, Dr Ruth Hamilton and Dr Helen Mactier for their continued support and patience throughout the project. Dr Bradnam provided weekly tutorials, insightful suggestions and help with understanding the fundamentals of digital signal processing. To Dr Hamilton my particular thanks for ongoing electrophysiological support and much constructive criticism during the thesis writing. Finally thanks go to Dr Mactier for her encouragement, and help in understanding the importance of drug-misuse in pregnancy and how medical physics can play an important role in a neonatal unit.

To Dr Laura McGlone, I extend my gratitude for her hard work and cooperation during the VIDI study, showing that collaboration between clinicians and scientists can be highly productive.

Thanks also to Dr Stig Hansen for introducing me to cardiac vagal tone and allowing access to the software necessary to undertake analysis of the study data.

A special thank you to Dr Mary O'Regan for tirelessly reporting on the polysomnograms and helping me to understand the mysteries of the newborn EEG.

To Hillary Reidpath I extend my thanks for her practical training in the recording of polysomnography.

To Dr David Young, my gratitude for insightful explanation of statistical techniques, and highlighting where statistics were most useful.

In relation to the toxicology analysis, I would like to thank Dr William Borland, Dr Gail Cooper and Mrs Huda Hassan for their respective roles in helping to clarify drug exposure.

From the Department of Clinical Physics and Bioengineering I would like to thank Professors Alex Elliott and David Keating for giving me the opportunity to undertake this research.

I am also grateful to Dr Ajaz Mohammed who helped develop my interest and enthusiasm for coding and the open-source movement in general.

Michelle McIntosh, whose patience, support and enthusiasm were unwavering, I dedicate this thesis to you.

Definitions/Abbreviations

Abbreviation	Description
ANS	Autonomic nervous system
AS	Active sleep
BPM	Beats per minute
CFM	Cerebral function monitor
CIPA	Cardiac parasympathetic activity
CVT	Cardiac vagal tone
DFT	Discrete Fourier Transform
ECG	Electrocardiogram
EEG	Electroencephalogram
EMG	Electromyogram
FFT	Fast Fourier transformation
FIR	Finite impulse response
GA	Gestational age
HF	High frequency
HRV	Heart rate variability
IUGR	Intrauterine growth restriction
IIR	Infinite impulse response
IS	Indeterminate sleep
LF	Low frequency (HRV)
MF	Mid frequency (HRV)
NAS	Neonatal abstinence syndrome
NICU	Neonatal intensive care unit
NREM	Non-rapid eye movement
PSD	Power spectral density
PSG	Polysomnogram
QS	Quiet sleep
REM	Rapid eye movement
RMSSD	Root mean square of successive differences
RR	RR interval
SDNN	Standard deviation of the RR intervals
SUDI	Sudden Unexpected Death in Infancy
STFT	Short time Fourier transform
VLF	Very low frequency (HRV)

1 Clinical Background

1.1 Treatment for Opioid Dependency

Standard treatment for the pregnant opioid-dependent woman in the UK involves prescription of methadone, a synthetic opioid (Ajayi, 2008; Mattick et al., 2003). Methadone is used as an analgesic as well as for maintenance treatment of patients using illicit opioids. Methadone acts on the opioid receptors, producing many of the same effects as illicit opioids. It is useful in treatment of opioid dependence because it can be given orally and its long duration of effect helps to stop cravings associated with opioid withdrawal.

Higher doses of methadone can block the euphoric effects of heroin, morphine, and similar drugs. The hope is that with properly prescribed methadone patients can reduce or stop altogether their use of illicit opioids.

Methadone maintenance was first used in the US in the 1950's and a large evidence base now exists. In pregnant opioid-dependent women, methadone reduces the likelihood of preterm birth and intrauterine growth restriction (IUGR) as well as risk taking behaviours (Burns et al., 2007; Mattick et al., 2003).

The main problem with methadone maintenance treatment during pregnancy is the high incidence of neonatal abstinence syndrome (NAS) relating to infant opioid withdrawal, variably reported between 19% and 80% (Baar et al., 1989; Dashe, 2002; Dryden et al., 2009; Fajemirokun-Odudeyi et al., 2006; McCarthy et al., 2005). The variability in incidence is due at least in part to different methods of assessing the severity of NAS. Although higher prescribed maternal methadone doses increase the likelihood of the infant requiring treatment for NAS (Dryden et al., 2009), the relationship between maternal drug use and NAS is complex and NAS cannot be predicted in individual cases (Mactier, 2011).

Buprenorphine is a synthetic opioid, and like methadone can help stabilise lifestyle and reduce illicit drug use. Studies by Fischer et al., (2006) and Jones et al., (2005) suggest that when compared with methadone, *in utero* buprenorphine exposed infants have reduced length of hospital stay and reduced severity of symptoms. Retention to treatment was however poorer with the buprenorphine group. Currently both drugs are used in clinical practice in the UK, but methadone is still the predominant treatment in Scotland.

1.2 Neonatal Abstinence Syndrome

NAS is a group of signs and symptoms occurring in a newborn infant as a result of withdrawal from physically addictive substances taken by the mother during pregnancy.

These substances can include opiates (derivatives of the opium poppy), or synthetic opioid substances including methadone or buprenorphine used to treat opioid addiction. Other substances causing NAS include benzodiazepines, cocaine and amphetamines as well as caffeine, nicotine and some antidepressant agents such as selective serotonin re-uptake inhibitors (Castellanos and Rapoport, 2002). This thesis will consider primarily the effects of opioid use in pregnancy. For clarity the term opioid will be used to include both synthetic and natural substances with opioid activity.

1.2.1 Pathophysiology

All opioid substances are physically addictive, meaning that the individual patient develops tolerance, requiring increasingly larger doses to achieve the same effect. Drug addiction is a complex interaction of physical and psychological dependence, and does not occur in every subject who takes opioids. During pregnancy, opioids and other drugs of misuse cross the placental barrier; this occurs in varying degrees, depending on the pharmaco-kinetic properties of the individual drugs. Once drugs cross the placenta, they tend to accumulate in the foetus because of the immaturity of the foetal renal system and enzymes used to metabolise opioids. Abrupt disruption of the passage of drugs

when the umbilical cord is clamped at birth results in the infant going “cold turkey” and (depending upon how much drug is in the foetal system, and how quickly this residual drug is metabolised) sometimes also results in NAS.

Aside from withdrawal symptoms in the first week or two of life, common findings in infants exposed to opioids include low birth weight, prematurity and IUGR.

1.2.2 Diagnosis

Signs of NAS fall under three main categories; neurological, cardiorespiratory and gastrointestinal. These signs can include trembling, irritability and excessive crying, disordered sleep, increased muscle tone, rapid breathing (tachypnoea), sweating, fever and unstable temperature, poor feeding and incoordinate sucking, vomiting, diarrhoea and dehydration. Seizures may also occur in infants suffering from NAS but are rare.

The pattern and timing of neonatal abstinence reflect the pharmacology of the substance(s) from which the infant is withdrawing, including drug half-life and its distribution in bodily fat or fluids. The half-life of a particular drug is dependent upon its metabolism, which in turn may be influenced by genetic variation between subjects (Eap et al., 2002). For example, withdrawal from heroin, which has a very short half-life of 3 minutes (Inturrisi et al., 1984), occurs within the first 24 - 48 hours, whereas the onset of withdrawal from methadone, which has a very variable half-life of between 12 and 60 hours (Eap et al., 2002), is typically delayed until day 3 to 5 . Withdrawal from benzodiazepines may be delayed for up to two weeks.

The severity of NAS is commonly assessed using either the Lipsitz or Finnegan scoring tools (Finnegan et al., 1974; Lipsitz, 1975) which each produce a cumulative score of the various signs of NAS. The scoring system currently used in the Glasgow neonatal units is a modification of the Lipsitz scoring system. NAS is the likely diagnosis if an infant presents with the signs described above, when its mother is known to have used addictive substances during pregnancy, but caution must be exercised in the diagnosis as other conditions (such as intracerebral bleeds, hypocalcaemia and thyrotoxicosis) may mimic NAS.

1.2.3 Management

Standard management for an infant at risk of developing NAS generally involves a prolonged postnatal stay in hospital where the infant can be closely supervised. In Glasgow, the median postnatal stay for healthy maternal drug-exposed infants who do not require pharmacological treatment for NAS is three times longer than the median stay for healthy non-maternal drug exposed infants (Dryden et al., 2009). Although NAS is more common in infants born to women prescribed higher doses of methadone, NAS cannot be predicted in individual cases, hence the prolonged hospital stay is applied to all infants of drug-misusing women. Being able to predict which infants will develop NAS would allow for early discharge of unaffected infants, which is likely to not only cause less distress to both mother and infant (and almost certainly less adverse effects on parenting), but also produce significant cost savings to the NHS. The ability to predict NAS would also allow trials of pre-emptive medication (shown to be useful in adults).

The majority of infants with NAS in Glasgow are withdrawing from opioids (Dryden et al., 2009; Jackson et al., 2004), with or without additional benzodiazepines. Almost all pregnant opioid-dependent women smoke in pregnancy; it is not known how much nicotine withdrawal contributes to NAS. Simple measures including nursing, swaddling, pacifiers and demand feeding are used to control mild NAS, and the infant is kept with mother whenever possible. NHS Greater Glasgow and Clyde neonatal network guidelines indicate that pharmacological treatment should be started if the Lipsitz score is ≥ 5 on two occasions 12 hours apart, despite efforts to console the infant by nursing/carrying. Pharmaceutical treatment is based on the mother's drug use during pregnancy; if, as is usually the case, the newborn has been exposed to opioids *in utero*, oral morphine solution is prescribed to the infant at a starting dose of 60 micrograms/kg four hourly, otherwise oral phenobarbital is used (Jackson et al., 2004; Osborn et al., 2010). For infants with the most severe NAS whose signs and symptoms are not controlled by oral morphine replacement, phenobarbital is added as second line therapy.

1.2.4 Extent

In Scotland, the estimated number of illicit drug users in 2009/10 was 59,600 (CI 58,300 – 61,000) of which 17,300 (30%) were female (Team, 2013). In England approximately 46,500 female addicted to heroin are receiving treatment, the vast majority of whom are of child bearing age (Health and Social Care Information Centre, 2012). The true extent of drug misuse in pregnancy has not been properly described, although accurate records of women prescribed methadone do exist.

1.3 Effects of Maternal Opioid Dependence on the Foetus and Child

1.3.1 Growth

Intrauterine growth restriction (IUGR) refers to the poor growth of an unborn infant during pregnancy. Specifically, it means that the developing infant has not achieved its genetic growth potential and is commonly defined as weighing <10th centile for gestational age. IUGR is due to dysfunction of the placenta and is a risk factor for an impaired neuro-developmental outcome (Allen, 1984; Teberg et al., 1988).

The growth of infants born to opioid dependent mothers is poor in the neonatal period and longitudinal growth is compromised for at least the first 3 years of life. Head growth and weight do however tend to catch up over the first 18 months (Hunt et al., 2008; Lifschitz et al., 1985; Ornoy et al., 2001, 1996). One author has reported continued poor head growth in children exposed to heroin *in utero* (Wilson et al., 1979).

In humans, reduced *in utero* head growth in infants of drug exposed mothers and is relatively greater than reduction in birth weight (Dryden et al., 2009; Hunt et al., 2008; Jones et al., 2005; McGlone et al., 2014; Rosen and Johnson, 1982; Whitham et al., 2007). Head growth is a proxy for brain growth and may be more impaired in infants exposed to methadone compared with buprenorphine (Fajemirokun-Odudeyi et al.,

2006).

1.3.2 Development of the Brain

In animal studies, mice exposed to heroin *in utero* showed behavioural deficits (Vatury et al., 2004) and in rats, opioid exposure reduced mu-opioid receptor binding affinity and concentration of neurotransmitters (Darmani et al., 1992; Robinson and Smotherman, 1997). Further animal evidence indicates that *in utero* exposure to buprenorphine adversely affects brain myelination (Sanchez et al., 2008).

Foetal neurobehaviour serves as a window to the developing nervous system (Nijhuis, 2003) and it is likely that disruption to foetal neurobehaviour reflects adverse effects upon the neuro-development of the foetus.

As in animal studies preliminary MRI findings in methadone-exposed infants and children suggest possible alterations in mylinations. Walhovd et al., (2012) used diffusion tensor imaging to compare the early cerebral connective tract development of infants born to methadone with comparison infants. They showed that methadone-exposed infants exhibited higher mean diffusivity, suggesting altered maturation of connective tracts.

Hunt et al., (2008) reviewed fourteen studies examining the neuro-developmental outcomes of infants exposed to opioids *in utero*. A variety of psychological tests were employed for the assessment of outcomes. He concluded that “opioid-exposed infants had significantly lower scores with all assessment tools used except for the psycho-motor development index of the Bayley Scales of Infant Development.” These data were shown to be most significant at the 18 month stage. Differences in neuro-developmental outcome remained at the three year assessment. A weakness of the studies was that male infants were over-represented in the opioid exposed group. Further studies examining the role of social deprivation at three years (Ornoy et al., 1996) and at eight years of age (Ornoy et al., 2001) showed that children of heroin-addicted mothers who had been adopted performed better at psychometric testing than the children who remained with their natural parents. There is a likely interplay between

genetic potential, *in utero* environment and upbringing which makes interpretation of follow up studies very difficult.

1.3.3 Visual Development

The first reports of abnormal visual findings in children of methadone-maintained mothers were published over 30 years ago (Rosen and Johnson, 1982). Abnormalities include strabismus (misaligned eyes), nystagmus (involuntary eye movements), refractive errors and delayed visual maturation. Visual evoked potentials (VEPs) can be used as an objective measure of the maturity and integrity of the visual pathway. VEPs in prenatally exposed rats at birth and at six months (Pinto et al., 1986) and in adult humans (Bauer, 1998) with a history of chronic methadone exposure show a tendency to be smaller and delayed in onset. In the early newborn period, McGlone et al., (2013, 2014) demonstrated immature VEPs and subsequently impaired vision at 6 month in infants of opioid-dependent women prescribed maintenance methadone in pregnancy. A non-randomised study by Whitham et al., (2010) showed that, at 4 months of age, infants exposed to methadone *in utero* had relatively delayed VEPs when compared to controls and to infants exposed to buprenorphine.

1.4 Electrophysiology of Opioid Exposure

1.4.1 Electroencephalography (EEG) and Polysomnography (PSG)

EEG is a non-invasive tool that can be used to measure cortical activity both in adults and infants. PSG is a technique including EEG and other physiological measurements such as ECG and respiratory rate used for monitoring sleep activity.

In adults, differences based on EEG spectral analysis (a lower frequency alpha peak) were present in the EEG of chronic methadone subjects compared with abstinent

controls. Such differences appeared to be dose related (Gritz et al., 1975), consistent with methadone dose related changes in EEG found in the rat model (Mitra et al., 1981).

Much of the research that has been undertaken in adults focuses on understanding the long term effects of these drugs on the adult brain. The subject often has a long term history of drug exposure and may or may not be undergoing a period of abstinence.

By contrast, EEG work carried out on the neonate is directed by a clinical need to understand the effects of *in utero* drug exposure, and the effects of NAS. The agitated nature of infants diagnosed with NAS suggests abnormal cortical function which must be important as the neonatal period is a time of crucial neurological development. As a neonate spends much of its time asleep, it is important to study EEG patterns in the various sleep states.

One of the earliest studies was performed by Schulman, (1969), who compared sleep states of three groups using PSG. The control group was healthy neonates, whilst the other groups were either infants at risk of central nervous system (CNS) impairment or infants born to opioid addicted mothers. The study found that the infants born to opioid addicted mothers contained no identifiable quiet sleep (Non REM) components, and an excess of motor activity during REM sleep.

Sisson et al., (1974) examined sleep patterns of ten fullterm newonates whose mothers had been exposed to either heroin or a combination of heroin and methadone. They found that such *in utero* drug exposure dramatically altered the sleep patterns, with both heroin and methadone suppressing REM (rapid eye movement) sleep and reducing the amount of quiet sleep. A later study by Dinges et al., (1980) of 58 fullterm neonates (28 exposed to methadone and/or heroin, and 30 unexposed) showed the opposite effect, with an *increase* in REM sleep in drug-exposed infants. The authors did however note a similar reduction in quiet sleep in drug-exposed infants. Manfredi et al., (1983) compared PSG, at 10, 20 and 30 days after birth, from 31 fullterm neonates of “drug addict mothers" (predominately opioid exposure) with these of 10 control neonates. They showed that although the signs of NAS had diminished within the first ten days of life, sleep patterns at both 10 and 20 days still showed significant differences from the control group. Specifically, the drug-exposed infants went into REM sleep more quickly that the controls, but showed a decreased duration of REM periods. By 30 days of life,

there were no significant differences between the exposed and unexposed groups, suggesting that the effects of *in utero* drug exposure on sleep patterns may have passed after the first month of life.

Pinto et al., (1988) monitored PSG activity at 2 and at 4-5 weeks of life in a group of 13 infants whose mothers were chronically addicted to heroin with at least a one year history of drug abuse. Of these 13, only one showed no signs of NAS, and did not require any treatment. The authors found that amounts of quiet and active sleep were reduced, and sleep pattern changes increased, with a general lack of sleep wave cycling between sleep states.

A PSG study by O'Brien and Jeffery, (2002), compared 21 neonates aged between two and 10 days and exposed to opioids during pregnancy with a group of 15 healthy controls. Both treated and non-treated opioid-exposed groups had reduced levels of quiet sleep, and the treated group also showed higher levels of intermediate sleep and arousals.

Sarfi et al., (2009) measured the patterns of sleep-wakefulness in three month old infants exposed to either methadone or buprenorphine. Parents were instructed to complete a 24 hour chart indicating their infant's state of awareness i.e. awake, agitated, asleep and crying. The study population was 71 infants, of whom 36 were born to mothers in a high-dose maintenance treatment (either methadone or buprenorphine). They concluded that the *in utero* drug-exposed group did not differ in terms of sleep-wakefulness from an unexposed control group at three months of age. These findings are consistent with the conclusions of Manfredi et al., (1983), that the effects of *in utero* drug exposure on sleep decline by three months of age.

A normal phenomenon called benign neonatal sleep myoclonus (BNSM) can be observed in neonates during all stages of sleep. BNSM presents clinically as myoclonic jerks, which are more frequent and prominent during phases of quiet sleep. Held-Egli et al., (2009) investigated the incidence, duration and risk factors of BNSM for infants treated for NAS. By performing PSG investigations on 78 term and nearly term *in utero* drug-exposed neonates, they diagnosed BNSM in 68% of the infants with NAS. In all of these infants, both cranial ultrasound, and neurological investigations were normal. By comparison, only 2.6% of the control infants demonstrated BNSM.

Seizures are a further cause for concern in NAS. A study involving 302 neonates exposed *in utero* to narcotics was published by Herzlinger et al., (1977). They found that 18 neonates (6%) had seizures attributable to NAS, of whom 10 (56%) had been exposed to methadone. Only one of 83 (1.2%) neonates exposed exclusively to heroin went on to develop seizures.

Published studies of *in utero* opioid exposure and sleep studies have been summarised in Table 1.

We are aware that:

- Sleep patterns are dramatically altered in infants exposed to opioids *in utero* during the first days of life (Dinges et al., 1980; Manfredi et al., 1983; Sisson et al., 1974).
- Methadone exposure may be related to a greater level of seizure activity compared to “passively addicted to narcotics” neonates not exposed to methadone (Herzlinger et al., 1977).
- *In utero* drug-exposed infants demonstrate lower levels of quiet sleep, but this is not improved by treatment for NAS (O’Brien and Jeffery, 2002).
- Effects of *in utero* drug exposure on infant sleep are no longer apparent three months after birth (Held-Egli et al., 2009; Manfredi et al., 1983).
- Both methadone and buprenorphine used as treatment for opioid dependence in pregnancy may lead to NAS (Sarfi et al., 2009).
- Benign neonatal sleep myoclonus is more prevalent in neonates who show signs of NAS (Held-Egli et al., 2009).

Year	Author	Age-group and (age at test)	Test	Exposure	Conclusions
1969	Schulman	Neonates	PSG	Heroin	QS did not develop in these neonates, although there were cyclic changes in activity level as a function of changing EEG activity
1974	Sisson *et al.*,	Neonates	PSG	Heroin	Minimal REM (AS)
1977	Herzlinger *et al.*,	Neonates	EEG for seizures	Mixed including methadone	Methadone only group, highest level of seizures.
1980	Dinges *et al.*,	Neonates (2 to 7 days of age)	PSG	Heroin including methadone	Increased REM (AS), less QS and disorganised sleep states.
1983	Manfredi *et al.*,	Neonates – Infants at 10, 20 and 30 days of life	PSG	Mixed opioids	Significant sleep pattern differences at 10 & 20 days. Exposed group entered REM quicker but had less episodes of REM.
1988	Pinto *et al.*,	Neonates and Infants (2^{nd} and 4^{th} or 5^{th} week of life)	PSG	Heroin	QS reduced. AS – decrease in LVI, while mixed frequencies (continuous irregular, low voltage) increased in exposed group. High frequency of sleep pattern changes in addicted infants, little tendency to normal sleep cycling.
2002	O'Brien and Jeffrey.	Neonates (2-10 days of life)	PSG	Opioids	In the treated group, increased wakefulness. Treated and non-treated exposed groups had less QS. Treated showed more IS.
2009	Safri *et al.*,	Neonates	Sleep / awake, no PSG.	Methadone or buprenorphine	No significant difference between the two groups.
2009	Held-Egli *et al.*,	Infants at 3 months	PSG	Opioids	High incidence of jerky movements

Table 1: A summary of the studies involving neonates and infants who have been exposed *in utero* to opioids and investigated using either EEG or PSG. QS: quiet sleep. AS: active sleep. LVI: low voltage irregular.

1.4.2 Electrocardiography (ECG), Respiratory Physiology and Vagal Tone

ECG is a non-invasive technique for measuring the electrical activity of the heart. The mass cellular depolarization and repolarization of cardiac muscle tissue which causes muscle contraction and relaxation creates an electrical signal that is recorded at the skin surface as an ECG. Each heart contraction corresponds to a change in the ECG signal, whose major component is the QRS complex. The dominant peak is the R wave. The time between consecutive R waves is called the RR interval. Pulses that occur before and after the QRS complex are called the P and T waves and are created by atrial depolarization and ventricular repolarization respectively. The QT interval is therefore a measure of the time for the ventricles to depolarize and repolarize.

In adults, methadone exposure affects the ECG by increasing the QT interval (Stringer et al., 2009).

Similar effects have been described in neonates. Parikh et al. (2011) examined the effect of *in utero* methadone exposure on the neonate ECG at days 1, 2, 4 and 7 of life. In the methadone-exposed group of 26 term infants, the QT interval was prolonged on day 1: methadone group 435ms vs control 401ms, $p<0.001$, day 2: 433ms vs 390ms, $p<0.001$), although this effect was gone by day 7. Jansson et al. (2005) and Parikh et al. (2011) investigated the effects of maternal methadone use on foetal and maternal RR interval, heart rate variability (HRV), respiration rate, and respiratory sinus arrhythmia (RSA); heart rate variability during breathing is also an indicator of parasympathetic activity. At peak methadone dosage, foetal heart rate was slower, less variable, and displayed fewer accelerations. Foetuses were less active, and the normal integration between heart rate and motor activity (whereby heart rate increases with increased foetal movement) was attenuated. Maternal heart rate was unchanged, but methadone administration was associated with lower maternal respiratory rate and RSA. Thus maternal methadone administration had significant effects on foetal physiology.

These findings may be of relevance to the relationship between maternal substance misuse and sudden unexplained death in infancy (SUDI), as documented by Kandall et

al., (1993). Infants exposed to methadone, heroin, or a combination of methadone and heroin, had a higher risk (odds ratios of 3.6, 2.3 and 3.2 respectively) than unexposed infants of developing SUDI.

Vagal tone (an indicator of the parasympathetic activity of the 10th cranial nerve) can be inferred from the ECG (this is discussed in greater detail in section 3.6). Jansson et al., (2007) examined vagal tone in 50 methadone-maintained pregnant women at 36 weeks' gestation using HRV from the ECG. After birth, infants showing signs of NAS were more likely to have mothers with changes in vagal tone in response to methadone. The authors concluded that infant vagal tone might be a useful marker for predisposition to NAS because NAS is "essentially attributable to disruption or dysregulation of the autonomic nervous system".

A summary of findings from studies of foetal and neonatal ECG in infants exposed *in utero* to opioids is presented below:

- Measurement of maternal ECG late in pregnancy is partially predictive of the severity of NAS in the infant (Jansson et al., 2007).
- Neonates exposed to methadone *in utero* show prolonged QT intervals in days 1 and 2 of life, but by day 4 this effect has gone (Parikh et al., 2011).

1.4.3 Visual Electrophysiology (VEP)

Pinto et al. (1988) investigated the effect of methadone on the developing foetal visual system by giving methadone to female rats throughout the duration of pregnancy, then performing visual evoked potentials (VEPs), on the neonatal rats. The neonatal rats had delayed flash VEPs, and smaller flicker VEPs compared to a non-exposed control group, although no long term effect (up to 90 days) was shown.

A more recent study performed by Whitham et al. (2010) examined the effects of prenatal exposure to buprenorphine or methadone on 4 month old infant VEPs. Infants prenatally exposed to methadone had prolonged VEP latencies compared with either the control group or the buprenorphine group.

In a prospective cohort study by McGlone et al. (2013), flash VEPs were recorded within 72 hours of birth for 100 healthy infants and 50 matched comparison infants that been exposed to methadone *in utero*. The drug exposed group was more likely to have smaller amplitude (VEPs median 27 μV vs 39 μV $p<0.001$) and more immature waveforms ($p<0.001$). Following up the same cohort of infants after 6 months, McGlone et al. (2014) showed that 40% of the drug-exposed cohort failed clinical visual assessment: the relative risk of abnormal assessment was 5.1 (95% CI 1.3 to 20; $p=0.02$). Additionally, drug-exposed infants' pattern onset VEPs when present - demonstrated smaller (C2 15' check size 10 μV vs 17 μV $p=0.003$) and slower (C2 15' check size 128ms vs 108 ms $p<0.001$) peaks than those of the comparison infants. It was a subset of this study population that was investigated in this thesis.

1.5 Conclusion

The use of methadone to treat opioid dependency is standard practice around the world with recognised benefits for the mother. Few studies have fully considered outcomes for the infant. There is good evidence of reduced foetal brain growth and increasing evidence of adverse effects on developing visual function in childhood of opioid dependency in pregnancy although whether this is due to illicit drug use or prescribed methadone (or indeed other factors) remains unclear.

This chapter has also covered adverse effects on neonatal sleep and measurable consequences on the infants autonomic nervous system patterns resulting from opioid dependency in pregnancy.

1.6 Hypothesis and Aims

The purpose of this study was to develop a better understanding of the electrophysiology of methadone-exposed neonates, with the ultimate aim of improving short and longer term management of the *in utero* drug exposed infant. I sought to accomplish this by recording PSG in infants born to methadone maintained opioid dependent women and compare the results with data obtained from healthy, term controls. This was a nested study within a larger study of drug-exposed infants called the 'Vision in Drug-Exposed Infants study (Mactier et al., 2012; McGlone et al., 2014, 2013) which afforded a unique opportunity for comprehensive toxicology to identify the extent of *in utero* drug exposure.

Overall Aim:

- To investigate the effects of *in utero* methadone exposure on sleep states and vagal tone using polysomnography and heart rate variability in the neonatal period.
- To develop software to undertake customised analysis of electrophysiological data.

Hypothesis 1: That opioid exposed infants differ from controls with regards to EEG parameters recorded during PSG.

Hypothesis 2: That exposed infants differ from controls in ECG parameters measured during PSG and analysed using time domain, frequency domain and/or non-linear methods.

Hypothesis 3: That exposed infants differ from controls in autonomic nervous system function, as represented by CVT derived from ECG recorded during PSG.

Hypothesis 4: That at least one of these electrophysiological measures is predictive of NAS.

2 Electroencephalography

This chapter describes electroencephalography (EEG) and its role in monitoring sleep patterns in the neonate. EEG is the recording of electrical activity resulting from ionic current flow within the brain cells (neurones); in the clinical setting this is generally achieved by measuring electrical activity over a period of time from multiple electrodes placed on the scalp.

The chapter is divided into three sections, including an overview of relevant neuroanatomy and neurophysiology: techniques of EEG - international standards and clinical interpretation: and sleep, its importance to the neonate, and the use of polysomnography to study activity during sleep. The first section, an overview of the anatomy and physiology of the brain, has been drawn from the following references: (Kandel et al., 2000; Marieb and Hoehn, 2007; Nokes et al., 1995; Novák et al., 2004; Nunez and Srinivasan, 2005; Sanei and Chambers, 2007; Teplan, 2002).

2.1 Anatomy and Physiology

2.1.1 The Nervous System

The nervous system is the network of specialised nerve cells that relays messages between the brain and different parts of the body, ultimately controlling almost all of the body functions.

The central nervous system (CNS) consists of the brain and the spinal cord, which are protected by bony structures including the skull and spinal column, by membrane tissues known as the meninges, and by cerebrospinal fluid.

The peripheral nervous system (PNS) consists of nerves that extend beyond the CNS; its main role is to connect the CNS to the limbs and organs of the body. The PNS is not

protected by bone as the CNS is, leaving it at greater risk of damage. The PNS is subdivided into two further systems, the somatic and autonomic nervous systems. The somatic nervous system (SNS) is responsible for voluntary control of movement via skeletal muscles and includes both sensory (afferent) neurons which carry information to the brain and spinal cord and motor (efferent) neurons which transmit information from the CNS to the muscle fibres. The autonomic nervous system (ANS) controls involuntary functions including heart-rate, respiration and blood pressure and has a role in emotional responses such as sweating and crying. The ANS is controlled from the lower brain stem and has both sensory and motor functions. The ANS has two subsystems:

- the sympathetic nervous system controls the body's response to “fight-or-flight” situations by increasing respiratory rate, slowing or stopping digestion and releasing sweat to lower the body’s temperature
- the parasympathetic nervous system which restores equilibrium after a fight-or-flight scenario has passed by governing the reduction of heart-rate and sweat production. The parasympathetic nervous system also increases gut motility and invokes pupillary constriction.

The brain may be considered as having three main sections: the cerebrum, the cerebellum and the brain stem.

The cerebrum is the largest part of the brain and consists of the cerebral cortex and subcortical structures including the hippocampus, the basal ganglia and the olfactory bulbs. It has two hemispheres divided by the central sulcus and is concerned with many functions including movement, sensory processing, olfaction, communication and memory.

The cerebral cortex is the outermost layered structure of neural tissue consisting of neuronal cell bodies and their supporting sections. The major part of the cortex is highly organised with six layers numbered 1- 6 from the surface inwards; more primitive parts of the brain such as the hippocampus have fewer layers.

The cerebral cortex comprises four lobes:

- The frontal lobe deals with cognitive function including reasoning and short term memory. It contains most of the dopamine-sensitive neurons found in the cerebral cortex. At the rear of the frontal lobe, close to the central sulcus, the motor cortex processes information required for movement.
- The parietal lobe integrates sensory information including pain, touch and spatial awareness.
- The temporal lobe is responsible for interpreting sound. The temporal lobe contains the hippocampus and also plays an important role in the formation of long term memories and spatial awareness.
- The occipital lobe includes the primary visual cortex which integrates visual information received via the retina, the photosensitive membrane at the back of the eye.

The cerebellum is located underneath and behind the cerebrum, and is responsible for coordinating movement, balance and posture.

The brain stem consists of the midbrain, the medulla oblongata and the pons. The cranial nerves whose nuclei lie within the brainstem provide the main motor and sensory innervation to the face and neck. The brain stem also contains all the nerve fibres passing to the spinal cord from the cerebellum and the cerebrum. Most importantly, the brain stem regulates breathing and cardiac function and is essential in maintaining consciousness and regulating the sleep cycle.

2.1.2 Neurons

The fundamental building block of the nervous system is the neuron (or nerve cell), of which there are approximately $1x10^{11}$ in the brain of a newly born fullterm human infant. The neuron is a highly specialised electrically excitable cell capable of processing and transmitting information via electrical and chemical signals. Neurons can transmit signals to other neurons via neural networks, or convey signals to or from other tissues, including muscles or receptor cells such as photoreceptors in the retina or

auditory receptors in the cochlea.

Figure 1 shows the basic structure of a neuron. In common with all other cells, neurons contain a nucleus and a cell body, but neurons are distinguished by two types of processes, axons and dendrites. The axon is the neuron's longest process and its main role is to carry outgoing signals from the cell body. Axons extend to the extremities via the PNS. Dendrites deal with incoming signals, facilitated by the enormous surface area created by their many processes.

Axons are coated with a segmented myelin sheath (a white, fatty protein-lipoid) which acts as an insulator of the electrical impulse passing through the axon and helps to conduct the electrical impulses more quickly. Non-myelinated fibres, including the dendrites, conduct electrical impulses more slowly. The myelin sheath is produced by Schwann cells that surround the axon main body; gaps between these cells occur at points known as the nodes of Ranvier. These uninsulated nodes represent points on the axon capable of generating electrical activity.

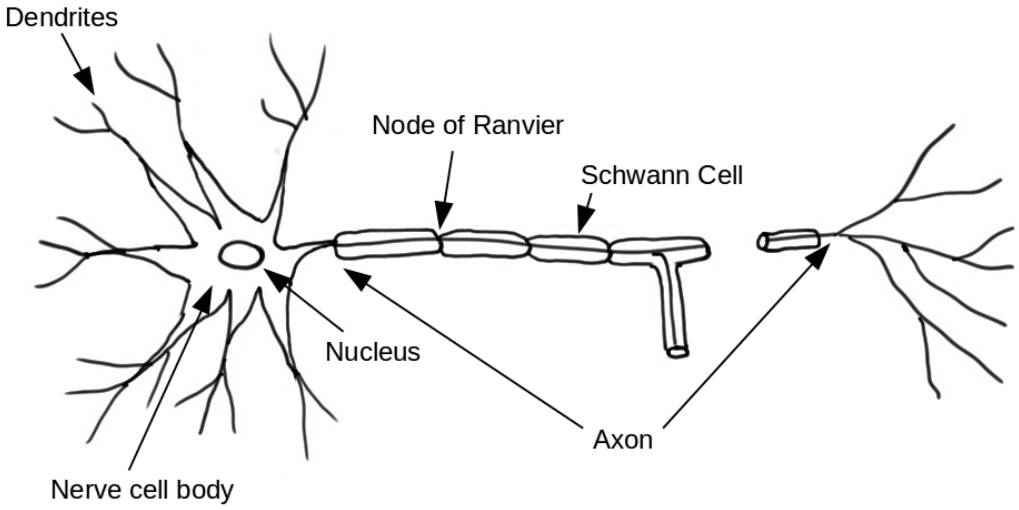

Figure 1: A neuron and its processes showing dendrites. The left shows the main cell body with dendrites extending out. The centre shows an axon which is coated by Schwann cells, with gaps called Nodes of Ranvier.

When a neuron is stimulated, an electrical impulse or action potential is generated along the length of the axon, transmitting information throughout the central and peripheral

nervous systems.

2.1.3 Resting Membrane Potentials and Action Potentials

Communication between neurons is facilitated by both chemical and electrical processes. The key ions in the CNS are sodium (Na^+), potassium (K^+), calcium (Ca^{2+}) and chloride (Cl^-), and there are also negatively charged protein molecules.

A neuron that is not transmitting an impulse is said to be at rest, and has a negative internal charge relative to its exterior (Figure 2). This creates a potential difference of approximately -70 mV, known as the resting membrane potential, maintained by resistance to passage of ions and negatively charged protein molecules across the cell membrane.

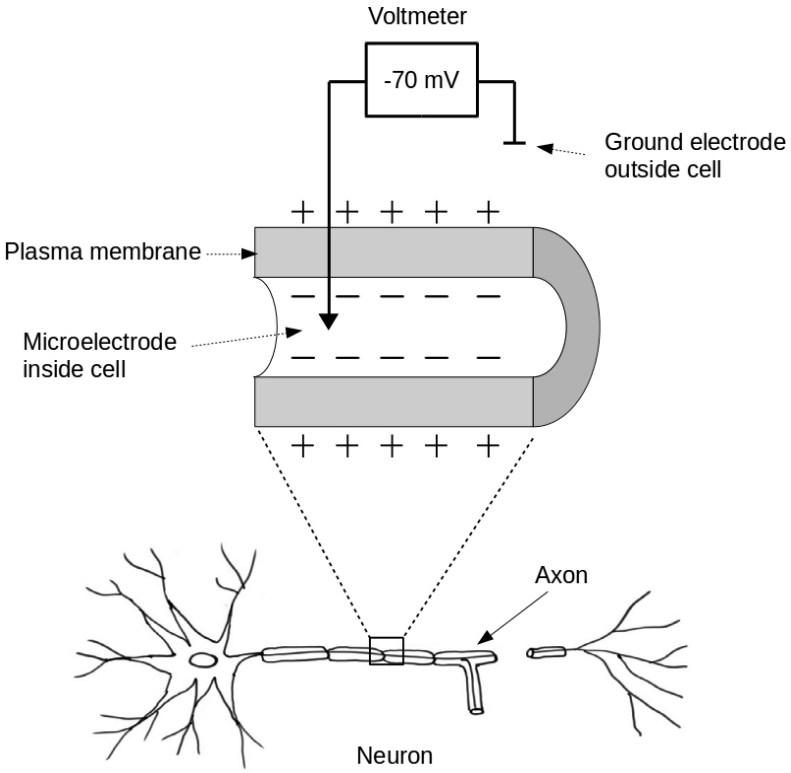

Figure 2: Measurement of resting membrane potential in nerve cells. By attaching a voltmeter across the membrane, a potential difference of -70 mV can be measured.

An action potential is triggered when the resting potential of the cell changes from -70 mV to -55 mV. Once triggered, the action potiential always has the same magnitude, as defined by the 'all or none' principle . The process lasts up to 2 ms and is illustrated in Figure 3.

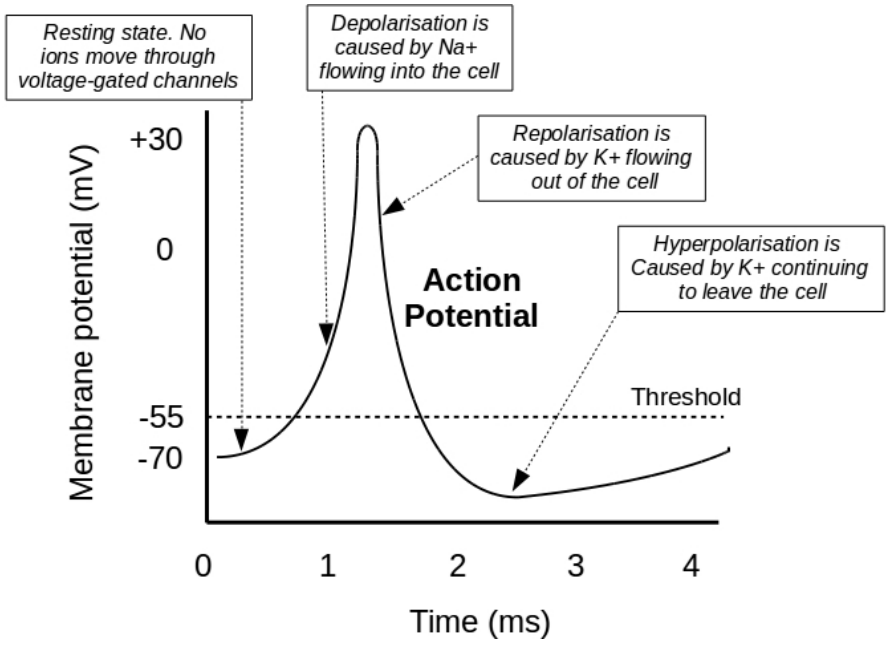

Figure 3: The action potential process showing the change in membrane potential from the resting state, depolarization, repolarisation and finally hyperpolarisation as the potential returns to -70 mV and the resting state.

The action potential occurs because of the exchange of ions across the neuronal membrane. A stimulus triggers opening of the Na^+ channels and due to the transmembrane concentration gradient, Na^+ ions enter the neuron. The neuron then become more positively charged, causing depolarisation and triggering of the action potential. Repolarisation occurs after approximately 1 ms, when the K^+ channels open allowing K^+ ions to leave the cell, and the Na^+ channels start to close. Ion concentration then returns to a state of equilibrium, restoring an internal potential of -70 mV.

2.1.4 Synapses

A synapse is a junction between two neurons. The neuron conducting impulses toward

the synapse is called the pre-synaptic neuron, and that conducting impulses away from the neuron, the post-synaptic neuron. Synapses may be electrical or chemical:

An electrical synapse or gap junction allows positively charged ions to cross a gap of approximately 3.5-4 nm, depolarising the post-synaptic cell. Electrical synapses are very fast (approximately 0.2 ms), and are important for reflex actions. Electrical synapses also allow for synchronised action, and have the capacity to transmit in both directions, although the signal strength is dissipated as it travels. In embryonic nervous tissue, electrical synapses permit guiding cues between neurons, and are important in neuronal development. Over time, many of these early stage electrical neurons are replaced by chemical neurons.

The chemical synapse is more complex and slower by approximately 2 ms than its electrical equivalent, although it can transmit a signal with a constant strength that does not dissipate over distance. The gap in a chemical synapse is larger at approximately 20-40 nm (Hormuzdi et al., 2004). Release of neurotransmitter is triggerered by the arrival of a nerve impulse. Chemical synapses are much more common than electrical synapses.

2.1.5 Neurotransmitters

As noted above, neurotransmitters are chemical compounds which mediate transmission of information across chemical junctions between neurons. Neurotransmitters are released from the axon terminal after an action potential has reached the end of the axon: the neurotransmitter then crosses the synapse to the next neuron where it is taken up in a process termed reuptake (Figure 4).

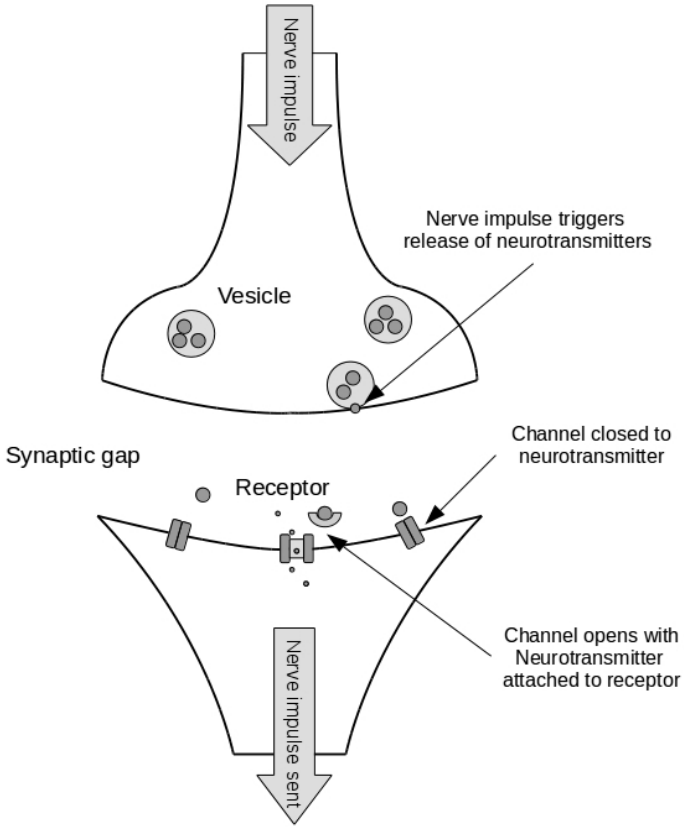

Figure 4: Neurotransmitters crossing the gap junction.

As yet, over 100 chemical neurotransmitters have been discovered; these chemical compounds can be classified by their function:

- Excitatory neurotransmitters increase the likelihood that the receiving neuron will fire an action potential and include epinephrine and norepinephrine. Both of these “stress hormones” are involved in the regulation of heart rate, blood vessel diameter and metabolism.

- Inhibitory neurotransmitters decrease the likelihood that an action potential will be fired by the receiving neuron and include serotonin, which produces feelings of well-being and helps to regulate the sleep cycle, and γ-aminobutyric acid which regulates muscle tone.

- Both excitatory and inhibitory – Some neurotransmitters can both stimulate and inhibit action potentials, the most common being dopamine. Dopamine release is associated with motivation and pleasure as well as movement.

Body functions including heart rate and respiratory rate are regulated by neurotransmitters, depletion of which may result in suboptimal physiological function. Pharmaceutical substances commonly exert their effects via neurotransmitter release and/or reuptake. Illicit drugs including cocaine and amphetamines temporarily block reuptake of dopamine, resulting in euphoria whereas cannabinoids and opioids bind to neuron receptors and block the reuptake of dopamine.

2.1.6 Development of the Human Nervous System

Electrical activity in the human brain starts to occur around the 17th to 23rd week of gestation. By term age (40 weeks' gestation) the brain contains approximately $1x10^{11}$ neurons and the average neuronal density is around 104 neurons per mm^3 (Nunez and Srinivasan, 2005). The number of synaptic connections increases until adulthood when there is a complement of approximately $5x10^{14}$ synapses (Teplan, 2002). About 80% of dendrites form after birth, a large number of them during the first three years of life. Throughout the early years of life, synaptic pruning and synapses that are rarely used are removed, thus reinforcing the role of more important synapses.

As levels of stimuli increase after birth, more myelin is produced, which speeds up signal transmission within the central and peripheral nervous system.

2.2 The Electroencephalogram (EEG)

The electrical potentials generated by single neurons cannot be detected using surface scalp electrodes, and so a standard EEG as measured in clinical practice is the summation of the synchronous activity of millions of neurons with a similar spatial orientation.

The EEG waveform generated depends on the orientation and distance of the firing neurons in relation to the placement of the recording electrode. In accordance with the inverse square law, the generated electric field drops over distance, thus electrical

activity from deep sources is more difficult to detect than activity generated near the scalp. Although neurons in deeper brain structures do not contribute directly to the surface EEG recording, their signals still have a significant effect on the overall EEG. For example, the thalamo-cortical connections are involved in synchronisation of synaptic activity, especially in the generation of sleep spindles.

The technical aspects of recording the EEG will be covered in the following sections, with particular emphasis on recording the EEG in the neonatal period.

2.2.1 International Standards

Guidelines for recording EEG in the neonate have been established by the American Clinical Neurophysiology Society (ACNS) and the International Federation of Clinical Neurophysiology (IFCN).

Key American guidelines are as follows:

- ACNS Guideline One: Minimum technical requirements for Performing Clinical Electroencephalography (Epstein and others, 2006).
- IFCN – Chapter 1-1: The ten-twenty electrode system of the IFCN (Klem et al., 1999).
- IFCN – Chapter 1-2: Instrumentation (Ebner et al., 1999).
- IFCN – Chapter 1-3: IFCN standards for digital recording of clinical EEG (Nuwer et al., 1998).
- IFCN – Chapter 3-3: Neonatal EEG (De Weerd et al., 1999).
- ACNS Guideline on Continuous EEG monitoring in Neonates (Shellhaas et al., 2011).

Following these best practice guidelines is important in order to ensure consistency in EEG recordings. In the neonate this is of particular importance as the EEG varies with increasing maturity, and so the age and maturity of the infant must be taken into account

in interpretation of the final trace.

2.2.2 Electrode Placement

Ag-AgCl scalp electrodes are most commonly used for EEG recording, and are attached to the head with reference to the International 10/20 positioning system (Jasper, 1958), devised to standardise the positions of electrodes (Figure 5). Measurements from key bony landmarks on the scalp determine the correct placement of electrodes. These landmarks are the nasion, the inion, and the left and right preauricular points above the ear (A1 and A2 on Figure 5). The 10-20 system is based on the percentage of distance between these landmarks e.g. 10% posteriorly of the total distance between nasion and inion. Even numbered electrodes are placed on the right hand side of the head, and odd numbered electrodes on the left. Midline electrodes are labelled ‘z' (Rennie et al., 2008).

The standard placements for a neonatal recording are Fp1, Fp2, T3, T4, C3, C4, O1, O2, Oz, Cz, as well as the reference at the vertex, or Cz. The ground electrode is often placed on the forehead or on a bony mass near the ear (Shellhaas et al., 2011).

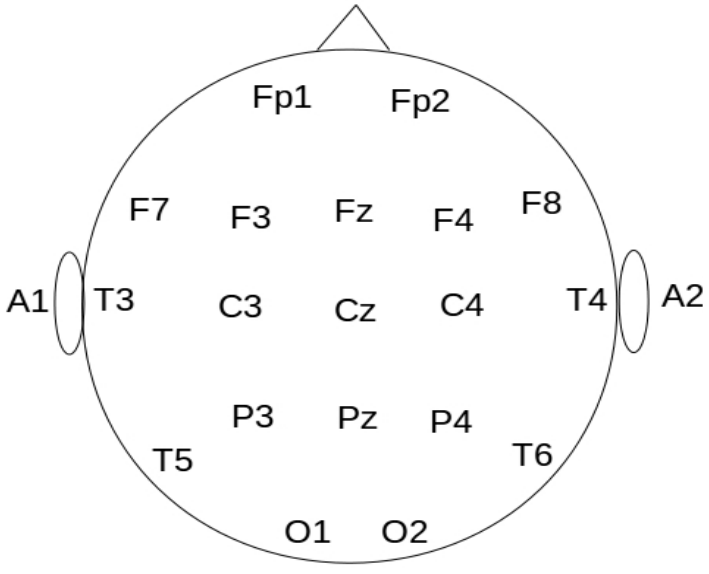

Figure 5: The 10-20 electrode placement system.

2.2.3 Amplification

The EEG signal requires to be amplified from the small signals (10-100 μV) recorded on the scalp. This is done using a differential amplifier.

A differential amplifier has two inputs; one from the active electrode and one from the reference electrode. The amplifier subtracts the reference from the active input, so that identical signals occurring on both input electrodes are cancelled out and artefacts common to both inputs are removed. Only the difference between input signals is amplified, i.e. if the two inputs change by the same amount with respect to ground, then this change does not appear at the amplifiers output. Thus only the difference between the two inputs is amplified (Figure 6).

The ability of a differential amplifier to reject signals common to both inputs is governed by its common mode rejection ratio (CMRR), which under ideal situations is at least 120dB. A typical common mode signal which requires to be rejected is 50Hz mains interference, as this is likely to present approximately equally on both active and reference electrodes (Rowan and Tolunsky, 2003).

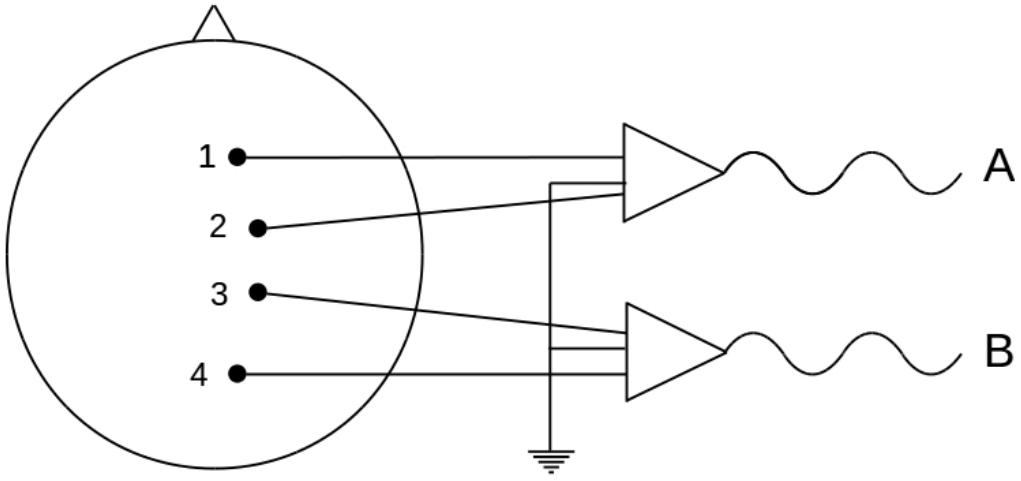

Figure 6: Illustration of a two channel recording system. The output signals (A and B) are the amplified difference between the two inputs, 1 and 2 for output A, and 3 and 4 for output B.

2.2.4 Montages

A montage describes the combination of electrodes used for each EEG channel. It is

usual for montages to use equidistant pairs of electrodes running from the front to the rear of the head with the same reference electrode used for all channels (Rennie et al., 2008). The data may be viewed post-acquisition using different montages. For example, if channel 1 montage is Oz-Fz, and channel 2 montage is Pz-Fz, then a new montage can be created by subtracting channel 2 from channel 1: (Oz-Fz)–(Pz-Fz) = Oz-Fz-Pz+Fz = Oz-Pz.

Montages can be referential or bipolar. Referential montages (left hand illustration, Figure 7) use a common electrode as reference input for all channels. This common reference point is usually placed along the midline of the head, such as at location Cz, to avoid hemispheric bias (Rennie et al., 2008). The bipolar montage (right hand illustration in Figure 7) uses two electrodes per channel, as well as a ground. The two electrodes are called electrode pairs.

Mizrahi et al., (2003) advise that a bipolar montage should be used for infant recordings to give broad coverage of the entire scalp. This same recommendation is made in the ACNS standards (Shellhaas et al., 2011). Rennie et al., (2008) recommend that the following regions should be covered: right and left frontal, temporal, occipital, central (or parietal) and the mid central region.

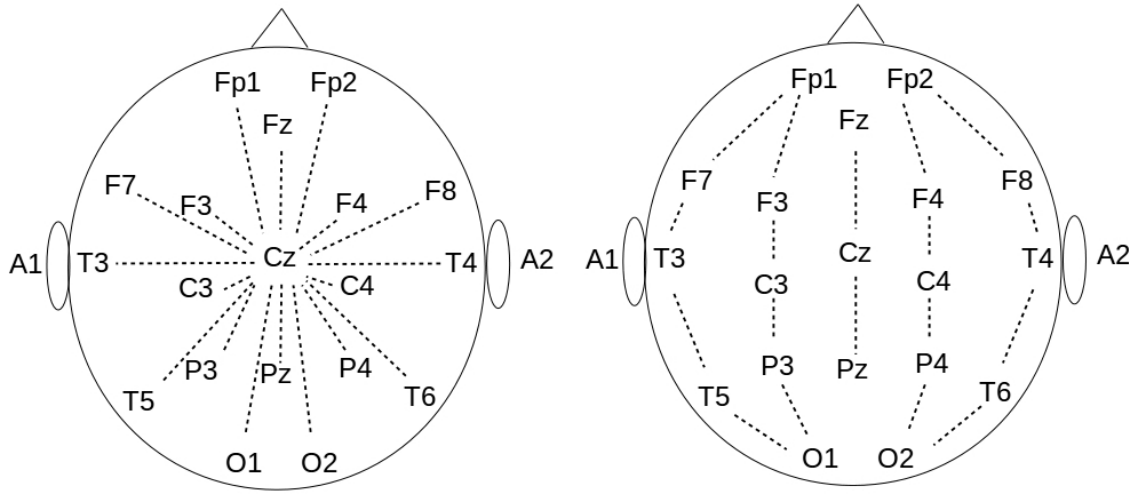

Figure 7: Montage types : Referential on the left and bipolar on the right. A line joining two electrodes indicates the pairing for the twin inputs to the amplifiers.

2.2.5 Practical Considerations for Infant EEG

The EEG is often performed whilst the infant is asleep to ensure adequate artefact-free data, although twitches or jolts may still occur. Care is required to place electrodes without waking the infant. Electrodes should avoid the fontanelles (fibrous areas between the bony plates of the skull) or any haematoma (Rennie et al., 2008). An awake infant can pull at electrode leads which are easily dislodged.

An environment conducive to sleep (dim lighting, warm and quiet) is helpful, as is recording after a feed when the infant is more likely to be settled. It is normal practice to video the recording session and to make contemporary annotations to aid in later interpretation of artefacts (Rennie et al., 2008).

2.2.6 EEG Trace Characteristics

In order to interpret and describe an EEG recording the following nomenclature is used.

Frequency: The number of occurrences of an event within a certain length of time. The frequency can be described in three ways:

1. Rhythmic - Events having a constant and regular frequency.
2. Arrhythmic - Events having no stable rhythm within the signal.
3. Dysrhythmic - An abnormality or event in an otherwise normal rhythm.

Voltage (Amplitude): Either the average or peak voltage of the signal over a given period of time.

- Attenuation - Also known as suppression or depression, the result of a gradual reduction in the amplitude of the signal.
- Hypersynchrony - Increase in voltage and regularity of rhythmic activity. This implies that there is an increase in the amount of neural activity contributing to the EEG rhythm.
- Paroxysmal - Sudden and abrupt increase in activity above the background level that can often involve much higher voltages, before the level returns to the lower levels. This is typical of seizure activity.

Morphology: The morphology of an EEG trace refers to its wave shape. This is defined by the frequencies that make up the waveform and their phase and voltage relationships. Such patterns can be defined as follows:

- Monomorphic - EEG activity that appears to have one dominant factor or source.
- Polymorphic - A complex EEG waveform that is composed of a number of frequency components.
- Sinusoidal - A waveform that resembles a sine wave i.e. a certain type of monomorphic wave.
- Transient - An isolated, sudden change in amplitude that is different from the background. This may be either a ‘spike’, which is a transient peak with a duration of 20 – 70 ms, or a ‘sharp wave’ that is a transient pointed peak of 70-200 ms.

Synchrony: This refers to the relationship between two events occurring simultaneously,

but at different locations over the head. An example would be the phase relationship between activity measured between the two hemispheres of the brain.

Periodicity: Is a reference to the distribution of patterns within the EEG trace over time i.e. how regularly an event occurs; usually defined as generalised, focal or lateralised.

2.2.7 EEG Morphology

Traditional methods of EEG interpretation consist of visually identifying key factors and attaching significance to this. Frequency content of the EEG for a neonate usually lies between 0.5 and 40 Hz, with each frequency being categorised into four major bands as shown in Figure 8.

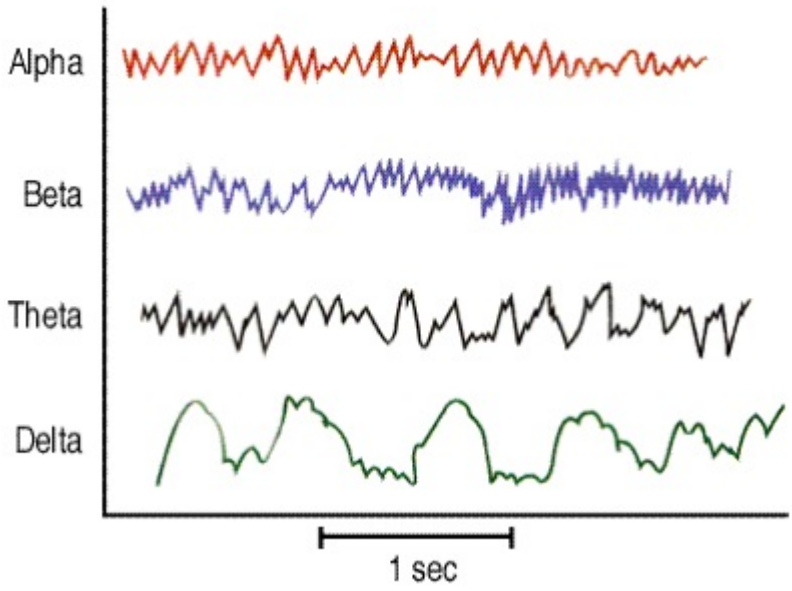

Figure 8: Basic EEG frequency characteristics. Beta (β) 12-30 Hz; Alpha (α) 8-12 Hz; Theta (θ) 4-8 Hz; Delta (δ) 0-4 Hz

Higher frequencies above 40 Hz constitute the gamma band; the exact width of this band has still to be defined. Gamma activity is not usually included as part of a clinical assessment of the neonate as the EEG is predominantly made up of low frequency activity in the 0.5 – 12 Hz range. Another consideration is that of recording EEG in an electrically noisy clinical environment. Although not best practice, it may be necessary

to employ band-pass filtering between 0.5 and 40 Hz to minimise the effect of mains 50 Hz interference.

2.2.8 Artefacts

Artefacts are unwanted signals that distort the original signal. They should be avoided or at least highlighted to avoid misinterpretation. Artefacts are generally of higher amplitude, and have a different wave shape in comparison to the signal sequence (Teplan, 2002). The source of the artefact may be either patient-related or technical. Patient-related artefacts are often unwanted physiological signals, such as coughing, whilst technical artefacts may be reduced by improving electrode impedance or using shorter wires to reduce conductive artefact.

The common artefacts found in EEG recordings are shown below (adapted from Teplan, (2002)):

Patient-related (biological source)

- Body movements, muscle movements, heart-rate, eye movements such as blink artefact, sweating and respiration.

Equipment related (non-biological source)

- Mains interference (50 Hz), variations in impedance, cable movements, broken wires and poor connections to pre-amplifier, poor contact with scalp due to dried or excessive electrode paste.

During sleep monitoring, recording the electrooculogram (EOG) (eye movement), electromyogram (EMG) (muscle contraction) and electrocardiogram (ECG) aids identification of artefact from the EEG signal. For example, a spike that appears on the EEG trace may confidently be interpreted as a blink artefact using video if the corresponding EOG also shows the spike.

2.3 Sleep Monitoring

2.3.1 Polysomnography (PSG)

PSG is an comprehensive assessment of sleep, comprising multichannel EEG, EOG, EMG, ECG & respiratory monitoring as well as real time video recording. The EEG alone is insufficient to be conclusive regarding a neonates sleep state.

EOG records the potential difference between the cornea and the retina (the cornea being positively charged with respect to the retina) using electrodes placed 1 cm above and below the outer canthi of the right and left eyes respectively. It is particularly useful in recognising rapid eye movement (REM) during sleep. Although the importance of REM sleep in the neonate is unclear, it is thought to play an important role in early neurological development (Mirmiran, 1995).

The EMG records facial muscular activity and is measured using two electrodes placed under the neonates chin, above and below the jaw line. EMG is an indicator of sleep state because muscle tension is reduced as the infant becomes more relaxed and enters deeper sleep states. The EMG is also important in identifying the onset of REM sleep as muscle activity measured below the chin is an indicator of active sleep and is not present during quiet sleep.

ECG measures heart activity and uses two electrodes placed under the clavicles on either side of the chest to record the QRS complex and the T wave. Recording the ECG enables removal of cardiac artefacts from the EEG trace.

Detailed annotations are also made during the recording highlighting information such as the observed clinical state of the patient e.g. awake, asleep, movement etc, and the time that these events occurred (De Weerd et al., 1999). Only by unifying all aspects of the recording can an accurate interpretation be made.

2.3.2 Sleep Scoring in Adults

In adults there are five sleep stages, as established and standardised by Rechtschaffen and Kales, (1968). These are four stages of progressively deeper non rapid eye movement (NREM) sleep and one stage of REM sleep. The sleep stages are only applicable to adult recordings as the neonates sleep architecture differs from that of an adult.

2.3.3 Neonatal Sleep Scoring

Sleep scoring in neonate is a more complex procedure than in adults due to the immature brain and changing neural development. Numerous protocols for defining sleep stages in the neonate have been proposed (Anders, 1982; Crowell and Group, 2003; Grigg-Damberger et al., 2007; Hoppenbrouwers et al., 1978). Essentially the neonate can be categorised as being awake or in one of three sleep states: active sleep (AS), quiet sleep (QS) and indeterminate sleep (IS) (De Weerd et al., 1999).

The awake stage can be subdivided into: crying, active awake or quiet awake. In quiet sleep EEG may show either tracé alternant (TA) or high voltage slow (HVS) patterns. In active sleep EEG may show either low voltage irregular (LVI) or mixed (M) patterns (Grigg-Damberger et al., 2007). It should be noted that these criteria are for term infants and should not be applied to preterm infants.

As previously noted, age and maturity are important factors in establishing the stage of sleep since considerable neurological changes occur in late pregnancy and in the early weeks of life. For a neonate, maturity can be defined in a number of different ways (Table 2):

Gestational Age	(weeks): time elapsed between the first day of the last menstrual period and the date of delivery.
Chronological Age	(days, weeks, months, or years): time elapsed from birth.
Postmenstrual Age (PMA)	(weeks): gestational age plus chronological age. Note that in UK literature the term post conceptional age may be used synonymously (but erroneously).
Corrected age	(weeks or months): chronological age reduced by the number of weeks born before 40 weeks of gestation; the term should be used only for children up to 3 years of age who were born preterm.
Conceptional Age (CA)	An historic term, used in early US literature (weeks): time elapsed between the date of conception and the date of delivery. This will be two weeks less than equivalent postmenstrual age.

Table 2: Neonatal age terminology as defined by Engle *et al.*, (2004).

The most accurate term is postmenstrual age (PMA) – for a neonate, full term infant this will be 40 weeks. However, although the American Academy of Pediatrics (AAP) has recommended abandoning the term conceptional age (CA) due to the difficulty involved in accurately establishing the day of conception, much of the existing EEG evidence defines age-appropriate EEG patterns in neonates by conceptional age (Grigg-Damberger et al., 2007). One must therefore consider if a correction factor of two weeks should be applied to conceptional age.

2.3.4 Physical Observations in Neonatal Sleep Scoring

One of the more commonly used methods for physical observations was proposed by (Prechtl, 1974) and is summarised in Table 3.

Stage	Description
Stage 1: Quiet Sleep (QS)	Closed eyes without rapid eye movement (REM). No body movements. Heart and breath rate regular. Very rarely micro-awakening.
Stage 2: Active Sleep (AS)	Closed eyes with REM. Body movements, various motility types. Heart and breath rate irregular. Many micro-awakenings.
Stage 3: Quiet Wakefulness	Open eyes. Few body movements, harmonious. Heart and breath rate regular.
Stage 4: Active Wakefulness	Open eyes. Generalised body and eye movements. Heart and breath rate irregular.
Stage 5: Crying	Generalised body movements. Vocalisation and crying.

Table 3: Prechtl's criteria for sleep/awake state identification (Prechtl, 1974).

The following generalised (table 3) is applicable for scoring PSG for subjects up to 6 months of age. Each epoch would fall into one of the following states.

State	EEG	EOG	EMG	Respiratory & body movements
Active Sleep (AS) - REM	Amplitude Low voltage irregular (LVI) 14µV – 35 µV. High Voltage Slow (HVS) - 50µV – 150 µV. Mixed (M) – a mixture of the above. Frequency Fast theta activity (4 to 8 Hz) dominant with significant amounts of delta (1-5 Hz)	Positive for rapid eye movements (REM)	Low or suppressed.	Irregular. Gross body movements, sucking, grimaces, smiles and vocalisations.
Quiet Sleep (QS) - NREM	High Voltage Slow (HSV) tracé alternant (TA) – a mixture of high voltage slow waves (0.5-3Hz) with rapid low voltage superimposed and sharp waves of 2-4 Hz between slow waves. Mixed (M).	Negative for REM	High	Regular Some mouth movements and occasional startling (*myoclonus*)
Intermediate (IS)	Intermediate is defined when none of the above criteria is met for either active or quiet sleep.			
Awake	Active awake: Eyes open and gross body movements. Possible vocalisations without crying.			
	Quiet awake: relative inactivity with eyes open.			
	Crying: Vocalisations and vigorous activity, with eyes open or closed.			

Table 4: Neonatal sleep scoring criteria, adapted from Lindquist, (2007).

2.3.5 Active Sleep (REM Sleep)

The example below Figure 9 shows an epoch of active sleep. The EEG shows a mixture of low voltage irregular patterns and high voltage slow waves. Faster theta activity is also present, within segments of slow wave delta. The respiratory trace is irregular, and the EOG (the bottom trace) shows some activity.

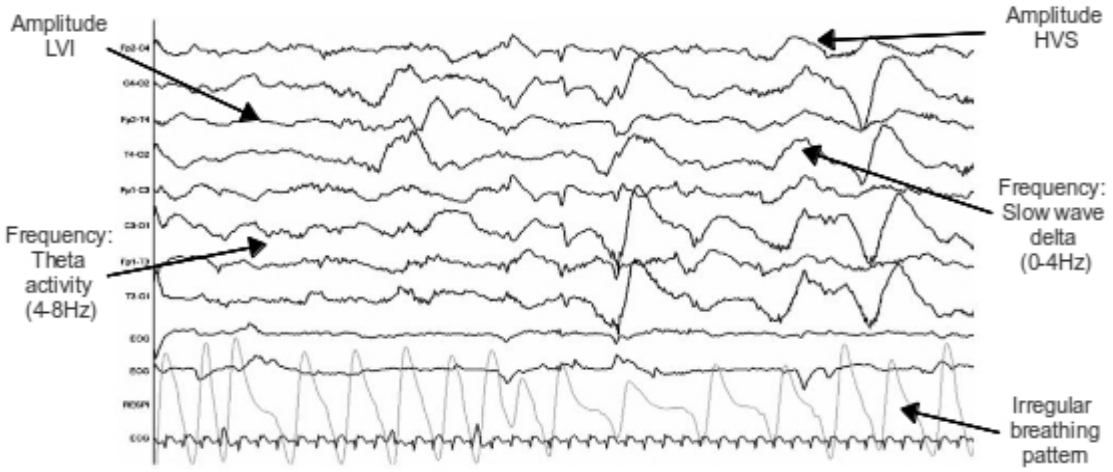

Figure 9: Active sleep in a healthy term infant. The PSG includes multiple EEG channels, where the dominant pattern indicates active sleep. The EEG consists of a mixture of low voltage irregular, and high voltage slow waves. Faster theta activity can also be seen. An irregular breathing pattern is also shown (Crowell and Group, 2003)

2.3.6 Quiet Sleep (Non REM Sleep)

The example below Figure 10 shows a tracé alternant pattern indicative of a quiet sleep where the EEG is a mixture of low voltage signals followed by bursts of high voltage slow waves, with a frequency of 2-4 Hz. The respiratory pattern is regular and smooth, and there is no REM activity shown on the EOG.

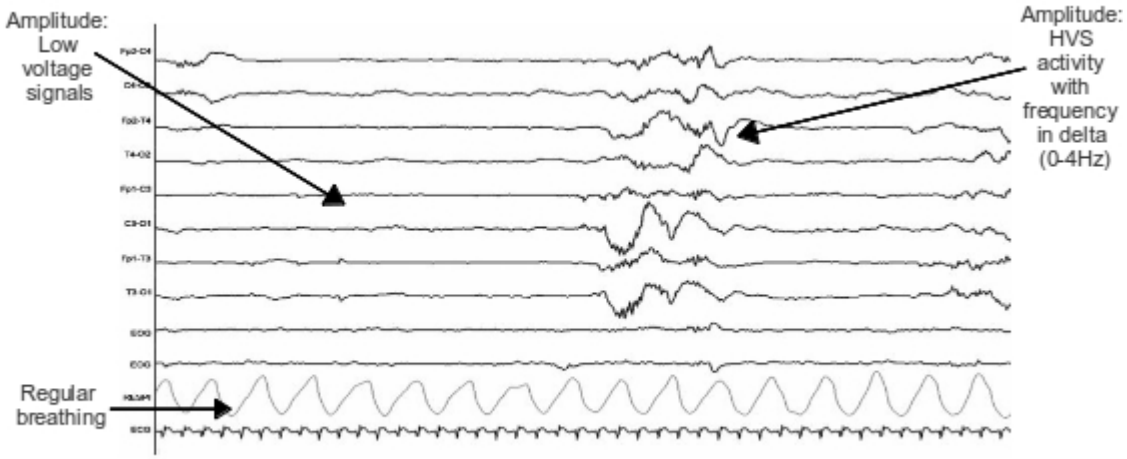

Figure 10: Quiet sleep in a healthy term infant. Here the PSG includes multiple EEG channels, where the dominant pattern indicates quiet sleep. In the EEG, prolonged periods of low amplitude activity are broken up by bursts of high voltage slow frequency waves. Regular, and cyclical breathing are also shown on the respiratory channel (Crowell and Group, 2003).

2.3.7 Indeterminate Sleep

When an epoch has elements of both quiet and active sleep, or it does not contain more than 50% of one type of sleep or the other, it is described as indeterminate sleep.

2.3.8 Hypnograms

Once the PSG has been interpreted by classifying each epoch as a type of sleep, it can be summarised on a hypnogram, which is a graphical representation of sleep activity either throughout one sleep cycle (1 hour), or as an all night recording. Although time consuming to generate, a hypnogram gives a clear picture of whether the sleep patterns are normal, and can highlight periods of abnormality. The task of classifying the sleep stages is generally performed either by a neurophysiology neurologist, or a suitably qualified PSG technologist.

Figure 11 shows an example of a hypnogram over a 40 minute period where the neonate has had periods of active and intermediate sleep between being awake.

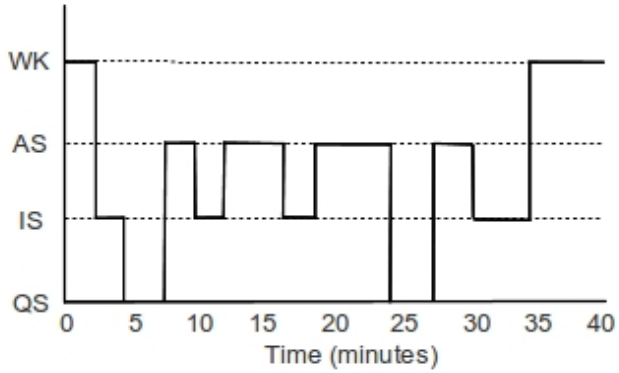

Figure 11: A 40 minute segment of a neonatal hypnogram analysed in 2 minute segments. WK – awake, AS - active Sleep, IS – indeterminate sleep and QS – quiet sleep

Descriptive statistics can be used to highlight patterns and trends between the stages. This approach gives an overall picture of the sleep session and allows for comparison between the sessions/subjects.

2.4 EEG and Quantitative Polysomnography

The methods described above are commonly used for interpreting EEGs. Since interpretation is based on the skill and experience of the viewer, its accuracy is dependent upon availability of highly-trained neurologists, and a degree of subjectivity cannot be eliminated. For this reason, more objective methods have been developed to aid in interpretation of the EEG. These are covered in the chapter on signal processing (Chapter 4).

3 Electrocardiography and Cardiac Vagal Tone

This chapter describes the techniques of recording the electrocardiogram (ECG), extracting the heart rate variability data, and analysing these data in both time and frequency domains. The first sections are an overview of the anatomy and physiology of the heart, and have been sourced from the following references: (Marieb and Hoehn, 2007; Nokes et al., 1995).

3.1 Cardiac Anatomy

The heart is one of the principal organs of the cardiovascular system. In the most general terms, its purpose is to receive oxygen-deficient blood from around the body, send it to the lungs for oxygenation, and then pump oxygen-rich blood around the body. In an adult, the heart is approximately the size of a clenched fist, weighs between 200 and 400 grams, and is located within the centre of the chest, with a third of its body to the right of the midline. The heart pumps at a rate of approximately 60-100 times a minute in a resting healthy adult, and the rate is expressed in beats per minute (bpm).

The heart consists of four main chambers, two atria, and two ventricles (Figure 12). The upper chambers or atria collect blood from the body and from the lungs and the lower chambers or ventricles prove the main pumping force to move blood throughout the body. Consequently the ventricles are larger and are more muscular than the atria.

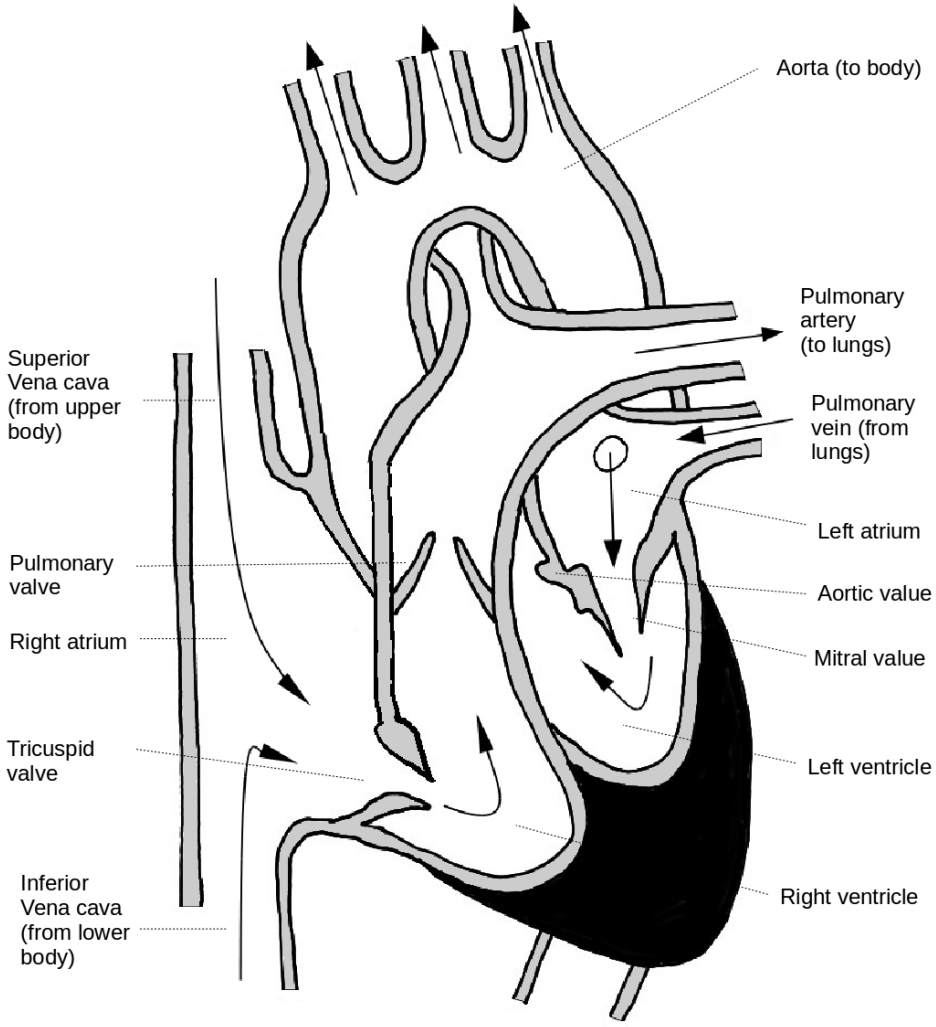

Figure 12: The major sections of the heart.

Separating the chambers are the two atrioventricular (AV) valves (mitral and tricuspid). These prevent back flow from the ventricles into the atria. The two semilunar valves, aortic and pulmonary, control the flow of blood from the heart to the aorta and the pulmonary arteries respectively. The aorta is the main artery of the body while the pulmonary artery is responsible for carrying oxygenated blood from the heart (Figure 12).

The sinoatrial (SA) node is a bundle of highly specialised neurons located in the right atrium. Its role is to send out electrical signals to control the rate at which the heart beats (sinus rhythm); the SA node is thus the heart's natural pacemaker. The electrical impulse from the SA node fires a series of electrical events transmitted through a specialised

conductivity system which controls contraction of the atria and ventricles.

Because the right atrium is closer to the SA node, the right atrium depolarises first, and thus the pumping action in the right atrium precedes that of the left. The electrical impulse is subsequently delayed at the AV node, allowing the ventricles to fill with blood before a further impulse is sent via the Bundle of His and the Purkinje fibres, triggering the muscle contraction required to send blood out of the heart.

3.1.1 Cardiac Electrophysiology

The interior of a cardiac muscle cell is negatively charged in relation to the exterior (the resting potential). When these muscle cells are electrically stimulated from the SA or AV node, they depolarise, the resting potential changes from negative to positive, and a contraction occurs.

The three stages of cardiac action potential are as follows:

- Depolarisation due to an influx of Na^{+} ions into the cell, reversing the membrane potential from negative (-70 mV) to positive (+20 mV).
- The plateau phase, due to the influx of Ca^{++} ions.
- Repolarisation where K^{+} ions leave the cell via the ion channels, and the membrane potential is returned to its resting potential.

The process is shown in Figure 13.

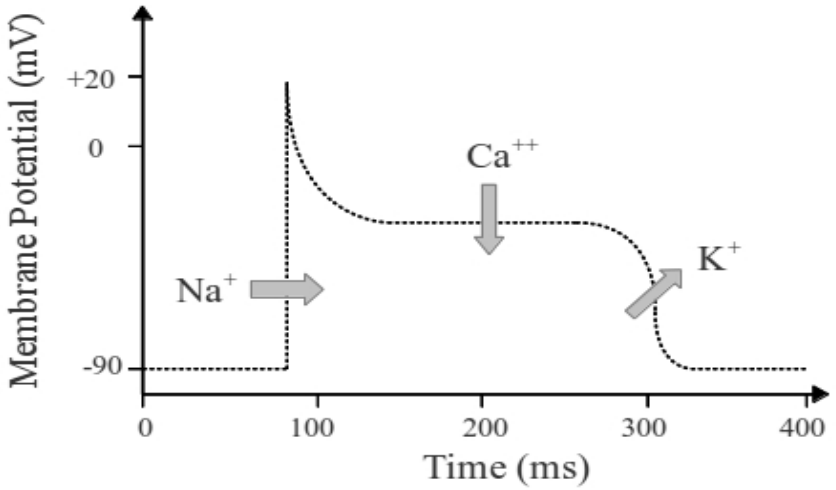

Figure 13: Action potential of cardiac cells.

As electrical impulses spread throughout the heart, the heart's electric field changes in both magnitude and direction, creating the electrical output of the cardiac cycle as observed on an ECG. The cardiac cycle on an ECG has three major phases, namely P; QRS; and T.

Normally the cardiac cycle originates in the SA node, sending a pulse across the atria which initialises the atrial depolarisation and produces the P wave. This impulse then activates the AV node before the impulse is carried over the entire endocardial surface, travelling in multiple directions simultaneously. This stage corresponds to the QRS complex. The final stage is where the ventricular repolarisation occurs, resulting in the T wave.

3.1.2 Heart Rate

The heart rate is determined by the heart itself as well as by regulatory pathways from the brain and hormonal signals from the adrenal gland. Cardiac output is a product of heart rate and stroke volume and is normally dependent on physiological need. Exercise and stress both require an increase in cardiac function, with a greater need for blood

borne nutrients such as glucose and oxygen. Conversely, sleep reduces the need for both oxygen and nutrients. Increased or decreased demands for cardiac output are met in part by regulating the heart rate, mediated via the autonomic nervous system, both sympathetic and parasympathetic.

For an increase in heart rate, the neurotransmitters norepinephrine and epinephrine (adrenaline) are released from the adrenal gland via the sympathetic nervous system, whilst a reduction in heart rate is achieved by the neurotransmitter acetycholine, via the vagus nerve and the parasympathetic nervous system.

Changes in the heart rate, also known as the analysis of the variation of the beat to beat interval, is called heart rate variability (HRV). Using analytical techniques in the time and frequency domain, HRV can be used to separate frequency components. High frequency (HF) oscillations (0.15 – 0.40 Hz) are associated with heart rate and changes in blood pressure, induced by respiratory activity, and are controlled by the vagal branch of the autonomic nervous system. The low frequency (LF) component (0.04 – 0.15 Hz) is related to the baroreflex (the process for maintaining blood pressure) and is associated with sympathetic activity (Villa et al., 2000). Consequently, analysis of the frequency components of heart rate can be used to understand the relative inputs of the sympathetic and parasympathetic at any point in time.

3.1.3 Respiratory Sinus Arrhythmia and Vagal Tone

Respiratory sinus arrhythmia (RSA) is a naturally occurring fluctuation in heart rate associated with the breathing cycle. It is an indirect measure of the parasympathetic nervous system (Katona and Jih, 1975). With each respiratory cycle, the heart rate rises and falls; inspiration results in increased negative intrathoracic pressure and reduced cardiac filling so the heart rate increases to maintain cardiac output. The opposite occurs in expiration, with a consequent reduction in heart rate.

Vagal tone is a measurement of the activity of the tenth cranial nerve, commonly known as the vagal nerve. The vagus nerve is part of the peripheral nervous system and is important in homoeostasis. There are no non-invasive methods of measuring vagal tone

directly but other physiological mechanisms such as heart rate can give an indication of vagal tone.

Vagal tone is temporarily suppressed during inspiration, resulting in an increase in heart rate. Exhalation is associated with resumption of vagal activity and a reduction in heart rate.

3.2 Electrocardiology

Electrocardiology is the measurement of the potentials produced by the mass cellular depolarization and repolarization of cardiac muscle tissue. An ECG is performed by attaching surface electrodes to the patient, and recording the electrical potentials between these points; analysis of ECG signals gives a picture of cardiac electrical and muscle function.

3.2.1 ECG Equipment

A simple, single channel ECG system is made up of three electrodes applied to the chest, an amplifier to magnify the signals (usually measured in mV), a method of applying filters to minimise the effect of unwanted interference, a data storage facility, and a method of representing the waveform either on screen or on paper. .

More comprehensive ECG investigations can be made using additional electrodes, i.e. 12 for the ‘12 lead’ (10 channel) ECG, but this is not necessary for simply monitoring heart rate.

3.2.2 Electrode Positions

The propagation of impulses through the heart creates a vector whose orientation and magnitude varies according to the location of electrodes on the chest. This vector also changes as a function of time. The differential potential is measured between three

positions, the right arm (R), the left arm (L), and the left leg (F). Using the notation of the International Electrotechnical Commission, this configuration gives three channels of data, referred to as lead I (L–R), lead II (F–R) and lead III (F–L). The configuration is called the *Einthoven* triangle, after Willem Einthoven who developed the ECG in 1901. Although the Einthoven triangle is the most basic form of ECG lead placement, various features of the heart's depolarisation can be still established.

For a neonatal sleep study, a three electrode system is considered sufficient, with the electrode placement following the 'modified three electrode bipolar system' (Crowell and Group, 2003). Bipolar refers to the fact that the ECG is the differential between two electrodes, with the third acting as the ground. This configuration produces maximal the P-wave height. The three electrode system detects R waves accurately so that RR investigations are possible.

The normal location of the electrodes for a modified three electrode bipolar recording are the right arm (RA), the left arm (LA) and left leg (LL). This system shows the R wave deflection in an upward direction (Crowell and Group, 2003).

3.2.3 ECG Recording Standards

Different recording standards are recommended depending on the primary purpose of the ECG . The European Society of Cardiology (ESC) developed guidelines for the recording and interpretation of neonatal ECG (Schwartz et al., 2002), and the use of heart rate variability (Force, 1996). The task force report, entitled 'Guidelines for the interpretation of the neonatal electrocardiogram', advises the use of a 12 lead ECG and the American Heart Association (Bailey et al., 1990) recommends a 150 Hz minimum high frequency cut off and 500 Hz as a minimum sampling rate for detailed ECG analysis. However, these standards are for the identification of cardiac abnormalities using ECG.

The American Academy of Sleep Medicine (AASM) has more relaxed standards for heart rate monitoring for the purpose of polysomnography. The AASM Manual for the Scoring of Sleep and Associated Events (Iber, 2007), sets out comprehensive guidelines

for polysomnography, stating the following key recommendations:

- A 3 lead ECG recording.
- A sampling frequency of 500 Hz is desirable, but 200 Hz is a permissible minimal frequency for recording, as long as complex waveform analysis is not undertaken.
- Filter settings for ECG should be 0.3 Hz for low frequency (high pass filter) and 70 Hz for high frequency (low pass filter).
- There should be the capacity for 50/60Hz filter for each channel.
- The digital resolution should be equal to or greater than 12 bits per sample.

Since this study focussed on sleep architecture, as opposed to a complex ECG wave form analysis, the AASM guidelines for recording ECG were used.

3.2.4 ECG Artefacts and Ectopy

An artefact is a distortion of a desired signal due to an unwanted external source. Such artefacts are common in neonatal ECG recording and must be removed from any analysis. The main sources of artefacts for neonatal ECG are electrical noise contamination, patient movement and muscle activity, and baseline drift. They are often due to incorrect application of electrodes.

Although modern ECG electrodes are disposable, pre-gelled and maintain good skin contact with little skin preparation, care must be taken with the correct application of the electrodes to the correct locations limb lead reversal (where the +ve and –ve amplifier inputs have been inadvertently swapped) and incorrect chest lead positioning are both common sources of error (Schwartz et al., 2002). Electrical interference, or 50Hz mains interference, is common particularly in a hospital environment. Modern ECG recorders have the capacity to remove unwanted signals using digital filters but care must be taken to make sure that such filtering does not remove or distort the signal being investigated. Movement and muscle artefacts are common and result in a large

distortion of the trace. Similarly, movements during sleep such as hiccups must be excluded. Baseline drift can occur when electrodes become loose and contact with the skin deteriorates. The main method for dealing with such artefact is to improve electrode contact. To aid with interpretation, recordings should be monitored whilst the trace is being made, and the trace annotated accordingly.

Ectopic beats are disturbances of the cardiac rhythm arising from outside the SA node. They may be classified as either premature ventricular contraction or premature atrial contraction and are most common under periods of stress. The morphology and timing of the ECG signals produced by the ectopic beats will vary according to the site of initiation and the contraction.

3.3 Heart Rate Variability

HRV describes the amount of variability in time between consecutive heartbeats and can be measured from the R wave of each QRS complex. Before any analysis can be performed it is necessary to prepare the ECG dataset:

- Obtain a suitable ECG recording that satisfies the minimum requirements for HRV analysis, as laid out by Force, (1996).
- Identify each R wave which acts as a point of reference, and is defined by its amplitude and time. The R wave peak can be located by hand, but is more commonly located by employing a suitable algorithm.
- Locate and remove any artefacts from the RR interval series.

The output of the previous stage will produce the instantaneous heart rate series, with one data point for each R wave peak identified within the QRS complex in an array of time values. Once this has been done, the data must be re-sampled at selected irregular intervals. This is because RR intervals are not evenly sampled in time. However it is this variation that HRV attempts to capture. Spectral analysis based of discrete Fourier transforms operate on time series with uniform intervals, so it is necessary to resample at uniform intervals.

Variability in heart rate may be evaluated by a number of methods including time domain, non-linear and frequency domain techniques. Each approach has strengths and weaknesses, and will be covered in the further sections.

3.3.1 ECG RR Estimation

The RR interval is the measurement of time, usually in milliseconds, between successive R waves. Mean RR is the average of many RR intervals measured over a set period of time. Heart rate is usually expressed as the number of beats per minute (bpm).

The challenge with automated RR extraction is the correct identification of the R wave when there is variation in the baseline. The algorithm used in this study is an adaptive technique employing a moving average filter, combined with an adaptive 50 Hz mains filter set to exclude 50 Hz noise. R wave peak detection corrected the slope from each Q trough to R wave peak and was therefore independent of sampling frequency. The algorithm was insensitive to EMG and high frequency noise and had RR detection sensitivity and specificity both greater than 99.6% (Christov, 2004).

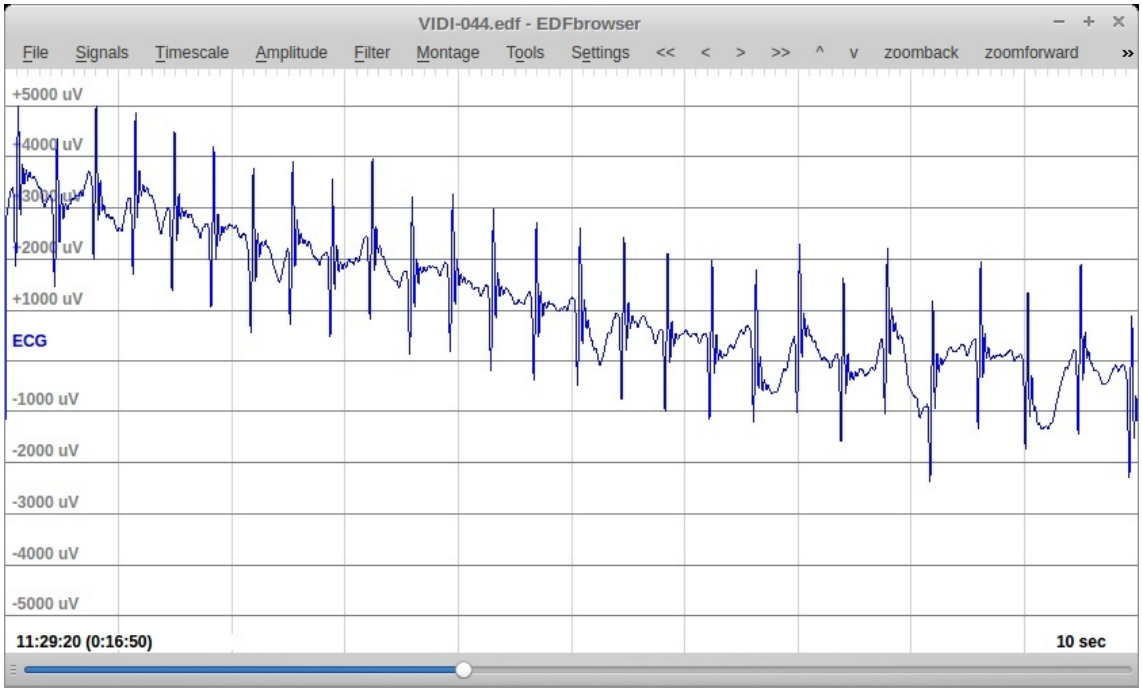

Figure 14: This example shows baseline drift affecting the ECG trace of a 10 second epoch from infant VIDI-044. The EDF browser software is used.

3.3.2 Time Domain HRV Methods

These methods are based on the time between two adjacent R waves. When beats are judged to originate in the sinoatrial node, they are considered normal, and the term "NN" is used in place of RR.

Mean Heart Rate and Mean NN interval

The mean heart rate is the average (mean) number of beats per minute during the recording. The mean NN interval is the average (mean) time in milliseconds between normal (sinoatrial node) RR peaks, i.e. the sinus rhythm. Ectopic beats are excluded from RR interval records to produce NN interval data.

Standard Deviation of the NN interval (SDNN)

As NN intervals naturally vary with time (for example due to respiratory sinus arrhythmia) it is useful to quantify this variability. Standard deviation, the square root of variance, is a commonly used measure of dispersion and can be applied to NN intervals (equation 1):

$$\mathrm{SDNN}=\sqrt{\frac{1}{N-1}\sum_{j=1}^{n}\left(\mathrm{RR}_j-\overline{\mathrm{RR}}\right)^2} \quad (1)$$

where N is the number of intervals, RR_j is the NN interval of interest, and $\overline{RR}$ is the mean NN interval over the duration of the recording. SDNN is expressed in ms and captures all those frequencies responsible for the observed variability over the duration of recording, i.e. from single beat variability to much longer-term variability. The duration over which SDNN is calculated must be stated: longer recording times are likely to give higher SDNN, as they incorporate variability from cycles as long as the recording (Force, 1996).

Root Mean Square of Successive Differences (RMSSD)

Interval differences (rather than intervals themselves) can be used to express heart rate variability. RMSSD (equation 2) is the square root of the mean squared differences of successive NN intervals:

$$\mathrm{RMSSD}=\sqrt{\frac{1}{N-1}\sum_{j=1}^{N-1}\left(\mathrm{RR}_{j+1}-\mathrm{RR}_j\right)^2} \quad (2)$$

where N is the total number of intervals, RR_j is the NN interval of interest, and RR_{j+1} is the next NN interval. RMSSD is expressed in ms. It is a statistical measure of the magnitude of interval differences between normal (sinoatrial node) RR beats, and thus a

measure of short-term heart rate variability.

3.3.3 Non Linear HRV Methods – Poincaré Plots

Processes with recurrent behaviour but also irregularities, such as heart rate, can have both aspects visualised using a Poincaré plot. Axes are identical in scale, and each data point represents two successive RR intervals: the RR interval of interest (RR_i) is mapped to the x-axis, while the previous interval (RR_{i-1}) is mapped to the y-axis. The resulting scatter plot shows beat-to-beat variability of a set of RR intervals (Figure 15).

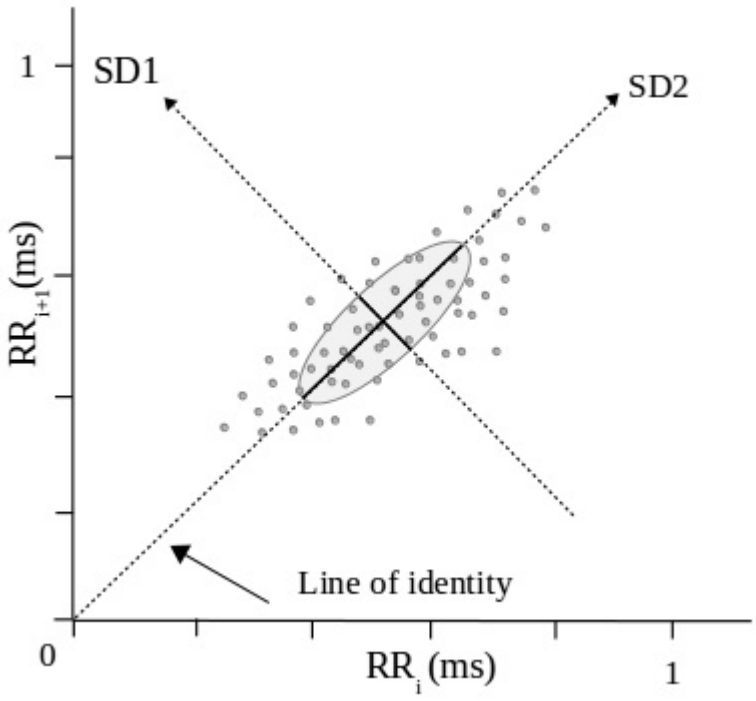

Figure 15: An ECG Poincaré plot. The dispersion of points perpendicular to the line of identity are an indication of short term variability, also defined by SD1. The dispersion of points along the line of identity, defined by SD2, indicates the long term variability. The x-axis is the current RR interval, while the y-axis is the consecutive RR interval.

If all RR intervals were equal throughout the recording, all data points would superimpose at one point. Real data points cluster around the line of identity. If RR intervals changed slowly (successive intervals remaining similar), the points would disperse approximately along, but close to, the line of identity. If RR intervals changed rapidly (successive intervals differing substantially), the points would disperse further

from the line of identity (Brennan et al., 2001).

The shape of an ellipse enclosing the data characterises its distribution. The ellipse width is the standard deviation of the data perpendicular to the line of identity (SD1 on the graph) and represents short-term heart rate variability, i.e. a large number of rapid changes. It is closely related to the time-domain RMSSD described above, both measuring variability over a single beat. SD2 represents only long-term variability, highlighting gradual changes in variability.

3.3.4 Frequency Domain HRV Methods

Frequency domain analysis examines how often events happen, i.e. the frequency of occurrence. This type of analysis shows the variation of RR intervals in relation to their frequency, typically as a frequency spectrum. A hypothetical ECG trace with two sections of equal length, with constant heart rates of 60 bpm (1 Hz) and 90 bpm (1.5 Hz) respectively, would have a frequency spectrum with two peaks, one at 1 Hz, and the second at 1.5 Hz.

As with EEG spectra, the spectra derived from RR intervals can be broken down into frequency bands, and the power and relative power (relative to total bandwidth power) calculated. The frequency bands are listed in Table 5.

Frequency Band	Frequency (Hz)
High Frequency (HF)	0.15 – 0.4 Hz
Low Frequency (LF)	0.04 – 0.15 Hz
Very Low Frequency (VLF)	≤ 0.04 Hz

Table 5: Recommended frequency bands for frequency analysis of adult HRV data (Force, 1996).

3.4 Heart Rate in the Newborn

The heart rate of a newborn infant can range normally from approximately 90 to 180 beats per minute and is generally higher when the infant is crying or agitated (Schwartz *et al.,* 2002). Details from two studies involving sleep are shown in Table 6: Mehta *et al.,* (2002) study involved a 24 hour recording, and included a mixture of awake and sleep states, whilst Doyle et al., (2009) focused on HRV values during quiet and active sleep.

Variable	24 hour	Quiet Sleep	Active Sleep
	Mean (SD)	Mean (SD)	Mean
Mehta *et al.,* (2002)			
HR (bpm)	130 (8)	-	-
SDNN (ms)	47 (12)	-	-
RMSSD (ms)	22 (7)	-	-
Doyle *et al.,* (2009)			
HR (bpm)	-	110 (7)	114 (7)
SDNN (ms)	-	15 (6)	24 (8)
RMSSD (ms)	-	12 (5)	11 (5)

Table 6: Heart rate and HRV in the neonate from sleep studies by Mehta et al., (2002) and Doyle et al., (2009). Heart rate is shown in the first row, whilst HRV is defined by SDNN and RMSSD. The values in brackets are standard deviations.

The first three rows show the results of a time domain analysis.. It is clear that HR is slower during sleep than over a 24 hour period which will include wakeful periods, and is slower in quiet sleep than active sleep. The SDNN, which is a measure of HRV is higher over 24 hours than during sleep, both because of the longer duration of recording and the likelihood of more variability in wakeful periods. RMSSD, which captures short term variability, is also higher over 24 hours than in sleep.

3.5 Variations in Neonatal Study Analysis Parameters

Previous studies of HRV (in the newborn) have used a range of different recording conditions making comparison between studies difficult, and normative values hard to identify. Differences in recording methods include use of the Holter method of 24 hour ambulatory recordings, or extraction of ECG data from the PSG. In general, for 24 hour studies, identification of sleep state has not been made; this is important as heart rate tends to slow during sleep. There is also considerable variation between studies with the epoch size for analysis ranging from from 64 seconds to 300 seconds. Subtle changes occurring over short periods of time may be lost in the analysis of longer epochs. Table 7 summarises studies published to date showing the variation in techniques used and highlighting the problems due to a lack of normative values.

Study	Study group	Mean GA (weeks)	Mean birth-weight (g)	ECG type	Recording length	fs (Hz)	PSD type	Epoch/ window size
Mehta *et al.* (2002)	Term Newborns	39.4	3,250	3 channel Holter	24 hours	125	FFT ?	300 sec.
Schäffer *et al.* (2008)	Term Newborns	38.6	3,245	3 channel Holter	24 hours	?	FFT + (Hamming window)	300 sec.
Longin *et al.* (2005)	Term Newborns	39.1	3,448	1 channel ECG	10 mins.	256	FFT	64 sec.
Spassov *et al.* (1994)	Term Newborns	37-41	3,142	PSG	4 hours	286	STFT	512 heart beats (225 sec.) *
Doyle *et al.* (2009)	Term Newborns	>37	<2,500	EEG & ECG	1-2 hours	256	Lomb	120 sec
Vandeput *et al.* (2009)	Preterms with respiratory problems	32.3	2,240	ECG	8 hours	100	FFT ?	300 sec.
Selig *et al.* (2011)	Term Newborns	>37	3,085	ECG	26 mins.	?	FFT	?
* Assuming a neonatal HR of 120 – 160 bpm, the epoch size would be 4.3 – 3.2 minutes, or an average of 3.75 minutes, although this assumes linear spacing between RR intervals.								

Table 7: A summary of ECG studies involving neonates. Each of the studies has included a spectral analysis based on a recording varying from 10 minutes to 24 hours. Depending on the type of recording, epoch length varied between 64 seconds and 300 seconds. The table shows the variation in analysis methodology when performing spectral analysis on neonatal ECG data. GA – gestational age; PSD – power spectral density; FFT – fast Fourier transform; STFT – short time Fourier transformation.

3.6 Cardiac Vagal Tone (CVT)

Vagal tone is a measurement of the activity of the vagus nerve (or tenth cranial nerve), which originates in the medulla oblongata in the brainstem. The vagus nerve is part of the parasympathetic nervous system and plays an important role in homoeostasis. Vagal tone can be measured directly by inserting electrodes into the nerve and indirectly by observing its effects upon organs such as the heart. By inhibiting the firing of the SA node, increased vagal activity results in a decrease in heart rate and so heart rate and its variability can be used to estimate vagal tone.

3.6.1 Estimating Vagal Tone

There are two main time domain methods of estimating vagal tone from heart rate, one proposed by Porges (1985) and the other by Julu and Little (1998). Both have been patented and the algorithms built into commercial software, called Mxedit and Neuroscope respectively. Although the Porges (1985) method has been more widely used, the method of Julu and Little (1998) has distinct advantages over its predecessor.

Porges (1985) – The Mxedit Software

The ECG signal is used to extract the RR interval and a 21-point moving polynomial detrending algorithm applied to remove linear and higher order trends such as episodes of bradycardia. The signal is bandpass filtered (0.3-1.3 Hz) and the variance of the heart period extracted. An estimate of cardiac vagal tone is then based on the natural logarithm of the variance. A typical value for a healthy term (36-42 weeks gestation) neonate is approximately 3.0 (SD 1), and for a premature neonate (27-35 weeks gestation) 2.2 (SD 0.6) (Lee, 2009).

Julu and Little (1998) – The Neuroscope Software

The approach taken by Julu and Little (1998) in the Neuroscope™ (Pontoppidan, Copenhagen, Denmark) is based on an RR interval ECG input. The signal is sampled at 5 kHz and each QRS complex compared with a template generated from the initial stages of the recording. If the QRS complex of interest is sufficiently similar to the template, a fixed duration 1 mV pulse is generated. A pulse train is thus created, with pulse separation matching the RR intervals of the ECG. The pulse train thus carries all the RR interval data in a much simpler signal which is easier to process. It is integrated with a time constant of 2 seconds and the output passed in parallel into two limbs (high and low pass) of the algorithm.

The high pass limb first contains a high-pass (0.2Hz) filter which produces an AC voltage synchronised with the variation in RR intervals. An integrator then produces a DC voltage proportional to the peak-to-peak amplitude of the AC signal. A voltage controlled oscillator (VCO) then generates a pulse train whose frequency depends on the DC voltage, i.e. the higher the DC voltage, the higher the frequency of the pulses. The low pass limb first contains a low-pass (0.015 Hz) filter with a time constant of 10.6 s and then a VCO. Signals from each limb are passed through a phase comparator, whose output is proportional to the difference in frequency between the two VCO outputs. The phase comparator output is integrated and a DC component added, before comparing with an experimentally established linear scale, called the linear vagal scale (LVS). The process is shown in Figure 16.

A value of zero on the LVS indicates no nerve impulses in the cardiac vagus nerve, whilst an increase in LVS indicates increased cardiac vagus nerve activity.

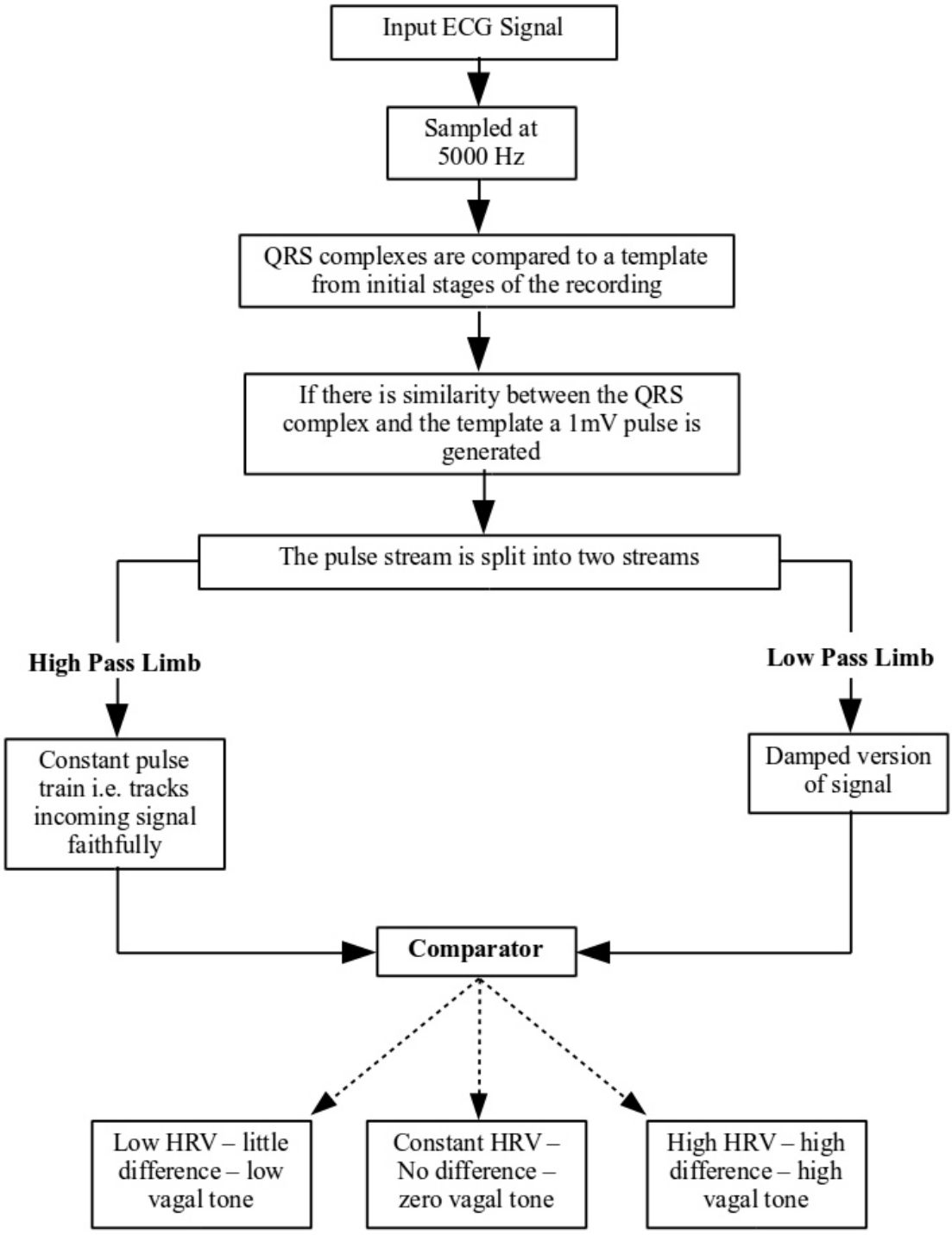

Figure 16: A flowchart describing the method used by the Neuroscope in estimating vagal tone. HRV - heart rate variability; QRS – components of a heart beat; ECG – electrocardiogram.

Vagal Tone and HRV Frequency Domain Analysis

The two methods described above are both time domain techniques but HRV frequency domain analysis can also be used as an indicator of autonomic nervous activity. The low frequency (LF) band of the HRV power spectrum is related to vagal activity, as LF increases with sympathetic stimulation. The high frequency (HF) band may also be connected to vagal activity. Thus the LF/HF ratio is an important marker of sympathetic/vagal balance on heart rate control (Acharya et al., 2004).

3.6.2 Polyvagal Theory

As an extension of his work on monitoring vagal tone, Porges proposed the polyvagal theory (Porges, 2001). This states that the vagus nerve has two distinct branches that dictate physiological state in relation to psychological experience. The first, more primitive branch is called the dorsal vagal complex (DVC), also described as the 'vegetative vagus', and is found in mammals, vertebrates, reptiles and amphibians. Its purpose is to elicit immobilisation behaviours such as feigning death, allowing animals under great stress to conserve their metabolic resources. The DVC provides control and regulation of organs such as the digestive tract, but under prolonged disinhibition lethal apnoea and bradycardia can occur. This branch of the vagus nerve is unmyelinated.

The second branch is called the ventral vagal complex (VVC), or the 'smart vagus', because it is associated with 'fight or flight' behaviours such as self-soothing and calming. Importantly, the VVC also influences heart rate: when vagal tone is high, a resting, or slower, heart rate is produced. The vagus nerve thus acts as a brake or restraint, without which the sympathetic-adrenal system would be activated. The VVC is myelinated so that it can respond quickly to activation. It is the evolutionary development of this second branch that dictates psychological behaviour, and consequently has been related to the study of stress, emotion and social behaviour. When the more evolved branch fails, the primitive systems are activated.

Using Porges, (1985) method of vagal tone estimation described above, Reed et al., (1999) linked the high heart rate variability found in the healthy human foetus with regulation of the vagus nerve. Heart rate decelerations, also mediated by the vagus nerve, are a sign of foetal distress. When the influence of the vagal nerve is increased, the heart becomes more vulnerable to the influence of the more primitive DVC, which can lead to a markedly slower heart rate.

3.6.3 Neonatal Vagal Tone Studies

In a study using the Mxedit software, Lee (2009), described CVT in 72 healthy term and 62 premature infants. They showed that healthy term infants had significantly higher CVT than then premature infants, although there were no significant differences in heart rate (mean RR intervals).

In a study involving behavioural states and heart rate patterns in infants, di Pietro et al. (1987) described how breast-fed neonates had significantly slower heart rate, elevated heart rate variability and higher CVT than the bottle-fed neonates. The breast-fed group was also more irritable and difficult to console. The authors concluded that “Results indicate that breast-fed infants had significantly longer heart periods, elevated heart period variability, and higher vagal tone than bottle-fed infants. Behaviourally, breast-fed infants were significantly more irritable, more difficult to console, and more often unable to complete the alert orientation portion of the assessment.”

A further study investigating the effects of sponge bathing on vagal tone in premature infants. Lee, (2002) showed that a sample of 40 premature infants born between 27 and 36 weeks gestation, reacted during bathing with a reduction in CVT and increase in heart rate, compared with before and after bathing, although there were no significant differences in behavioural distress. This indicates that vagal tone can be used to monitor subtle physiological states which heart monitoring may miss.

Examining the effect of neonatal cries and vagal tone on the neonatal during

circumcision, Porter et al., (1988) showed that the vagal tone was significantly reduced as the pitch of the infant's cry increased and they became more stressed.

The body of literature covering vagal tone and healthy neonates suggests that increased vagal tone results in more regulation of the heart to stressful external stimuli and may thus be advantageous in the infant's development. However, in older infants (8-11 months) with regulatory disorders, DeGangi et al., (1991) found higher baseline vagal tone was associated with disturbances in sleep, feeding, self-calming and mood regulation.

Many of the characteristics described in "regularity disordered" older infants are found in the neonate with signs of NAS, indicating that vagal tone could be a useful tool in monitoring these infants. Jansson *et al.,* (2007) found that maternal vagal tone might be a useful marker for the predisposition of NAS in the newborn infant (as described in section 1.4.2). In a study of 50 methadone-maintained pregnant women, vagal tone was estimated and compared with the severity of NAS in the newborn infant. They found that the extent of NAS in the infant was related to the vagal response of the mother, and concluded that NAS is "essentially attributable to disruption or dysregulation of the autonomic nervous system".

It is the monitoring of this disruption or dysregulation of the autonomic nervous system in the NAS infant, with its effects on both the nervous and cardiovascular system that is the basis of this thesis.

4 Electrophysiological Signal Processing

4.1 Introduction

This chapter describes the theoretical background to the techniques used to prepare and analyse the recorded electrophysiological signals. It covers acquisition of biosignals, filtering techniques, methods of EEG and ECG analysis and practical considerations.

4.2 Acquisition of Biosignals

The biosignals recorded from the body in this study are continuous voltage signals that vary over time. These can give an insight into the physiological processes creating them. Before processing, these analogue signals are converted into a digital signal, i.e. a sequence of discrete values.

Conversion is performed using an analogue to digital converter (ADC). An ADC converts the amplitude of a continuous analogue signal, into an equivalent digital signal in a process called quantization, occurring multiple times a second (the sampling rate). The output of this process is a digital representation of the analogue signal. The number of discrete voltage values produced over the amplitude range of the analogue signal is defined by the resolution of the ADC. Resolution is expressed in bits (the basic unit in computing with two states, one and zero), and consequently is expressed as a power of two: an ADC with an 8 bit resolution can digitise an analogue signal into 256 different levels ($2^8 = 256$), and can be represented as a range from 0-255, or -128 to 127 if the signal contains negative values.

The (time) sampling rate defines the number of times sampling occurs within a set time period, with the sampling frequency (fs) being the number of samples acquired in one second. For example, an fs of 256 Hz indicates that the process of quantization occurs 256 times in one second.

Slowly changing input analogue signals can be adequately represented with lower sampling rates, but if the input analogue signal varies rapidly, the sampling rate must be fast enough to capture all of the frequencies that make up the input signal.

Aliasing occurs when the analogue signal changes faster than the sampling frequency, creating anomalous signals called aliases in the output of the DAC.

Digital to analogue conversion (DAC) can be used to check for aliasing: for example, if the analogue input was a 200 Hz sinusoid and the sampling frequency was 128 Hz, the ADC would misrepresent the true signal, and the DAC would show a 72 Hz signal. An example of aliasing is shown in Figure 17.

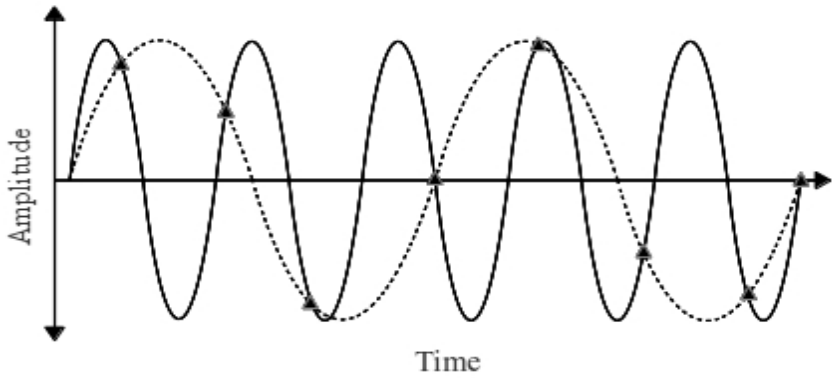

Figure 17: An example of aliasing. This example shows an input signal of 200 Hz, being sampled at 128 Hz. If digital to analogue conversion was performed, the reconstructed signal would be 72 Hz, showing that the resulting signal is a poor representation of the input signal.

The Nyquist-Shannon sampling theorem states that to reconstruct the original signal accurately, the sampling frequency should be greater than twice that of the maximum frequency content of the signal being sampled. This sampling frequency is known as the Nyquist frequency.

4.3 Filters

Filters are often required to remove unwanted noise or artefacts from a signal. This process should remove all unwanted elements without unduly affecting the component of interest.

Analogue filters consist of a set of components with fixed value in an electronic circuit.

Digital filters are more flexible, as they are implemented computationally and consequently can be altered by changing their parameters. This section will focus on the use of digital filters as opposed to analogue filters.

Filters fall into three main categories:

- High pass filters allow signals above a defined frequency, blocking lower frequencies.
- Low pass filters allow signals below a predefined frequency and block higher frequencies.
- Notch or band-stop filters block frequencies between two predefined frequencies, and pass frequencies either side of this value. A commonly used notch filter is a 50 Hz filter for removing mains electricity interference.

For biosignal acquisition, filters are often applied in pairs to create a bandpass: for example, the recommended filter settings for ECG recordings (Iber, 2007) are a low pass filter of 0.3 Hz and a high pass filter of 70 Hz. The transfer function is the ratio of the output of a system to the input of a system and is defined below (equation 1) where X(s) is the input, and Y(s) is the output, and H(s) is the transfer function.

$$H(s)=\frac{Y(s)}{X(s)} \tag{1}$$

A graph, known as a Bode plot, shows a filter's transfer function, i.e. how the output of a filter changes with frequency (logarithmic frequency axis) and is shown in Figure 18.

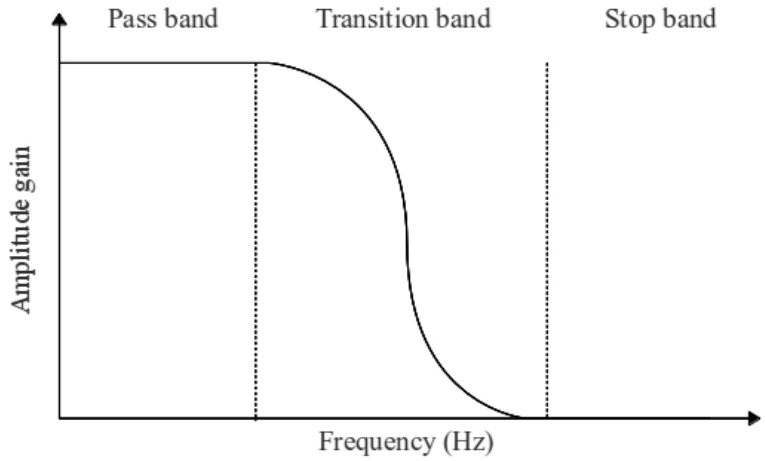

Figure 18: An example of a Bode plot for a low pass filter, attenuating low frequency components in the pass band. Frequencies in the pass band will be allowed, the stop band blocked, and attenuation in the transition band dependant on the input frequency.

A Bode plot illustrates the pass band, i.e. the frequencies that the filter passes without significant attenuation; the stop band, i.e. those frequencies where little or no energy from the input signal is passed; and the transition band, i.e. the frequencies where there is a frequency-dependent level of attenuation. In an ideal filter, the transition band is narrow, and the transition from pass to stop bands has the steepest slope.

Further characteristics include:

- The cut off frequency (corner frequency, f_0) – the frequency where the output from a filter has fallen to a specific proportion. This proportion is defined as half of the passband power, also called the 3dB point since a drop of 3dB is equivalent to halving the power. It is $0.5^{1/2} \approx 0.707$ of the passband voltage.
- Roll off – the slope of the transition band, and is the rate at which attenuation increases beyond f_o.
- Ripple – the unwanted residual variations that characterise the filter's capability to attenuate signal in a linear manner.

For biosignal filtering, narrower bandpass filters are required because the signal of

interest is often close to the frequencies of signals that need to be removed. For example, when separating adjacent frequency bands from an EEG signal for spectral analysis, delta, theta, alpha and beta bands need to be separated from the overall EEG spectrum. The high frequency end of the delta band is 3.99 Hz, while the low frequency end of the theta band starts at 4 Hz, so it is necessary to have a sufficiently narrow transmission band that this boundary can be distinguished.

An ideal (theoretical) filter removes all frequency components outwith the desired bandwidth, has a vertical transition band, and has no effect on the phase of the output signal. In reality, it is not possible to produce a filter with these characteristics, but it is possible to design one that satisfies some of the properties of an idealised filter.

Digital filters fall into two categories, depending on how they respond to an impulse as input signal (their impulse response):

- Finite Impulse Response (FIR) filter - the impulse response has finite duration, i.e. settles to zero after a finite length of time.
- Infinite Impulse Response (IIR) - the impulse response is non-zero indefinitely, although its response usually decays over time.

IIR filters require fewer computations than the equivalent FIR filter, thus reducing processing time. They can be designed to emulate the responses of analogue filters such as the commonly used Butterworth or Chebychev filters.

The phase response of a filter is the change, in degrees or radians, of the phase of the output signal relative to the phase of the input signal to the filter. If the phase of a sinusoidal input to a filter is identical to the phase of the output, the filter has zero phase response to that signal. Phase response can be linear or non-linear depending on the filter characteristics, and can accumulate over multiple cycles, i.e. exceed 360°.

4.3.1 Common Filter Designs

The Butterworth filter is characterised by a nearly flat passband with no ripple. Transition band roll off is smooth, with a roll off rate of 20 dB/decade (or 6 db/octave).

The Chebyshev filter has a faster roll off than the Butterworth, but at the cost of having ripples; the type 1 Chebyshev filter has ripple in the passband, while type 2 Chebyshev has ripple in the stop band. Chebyshev filters also introduce greater phase distortions than the Butterworth filter.

The elliptic filter has a sharper transition than the other two filter types, but introduces ripple in both the pass band and the stop band, as well as non-linear phase distortions. This type of filter would be best suited to rejecting frequencies in the stop bands, and can perform at low-orders, minimising the number of computations required Figure 19.

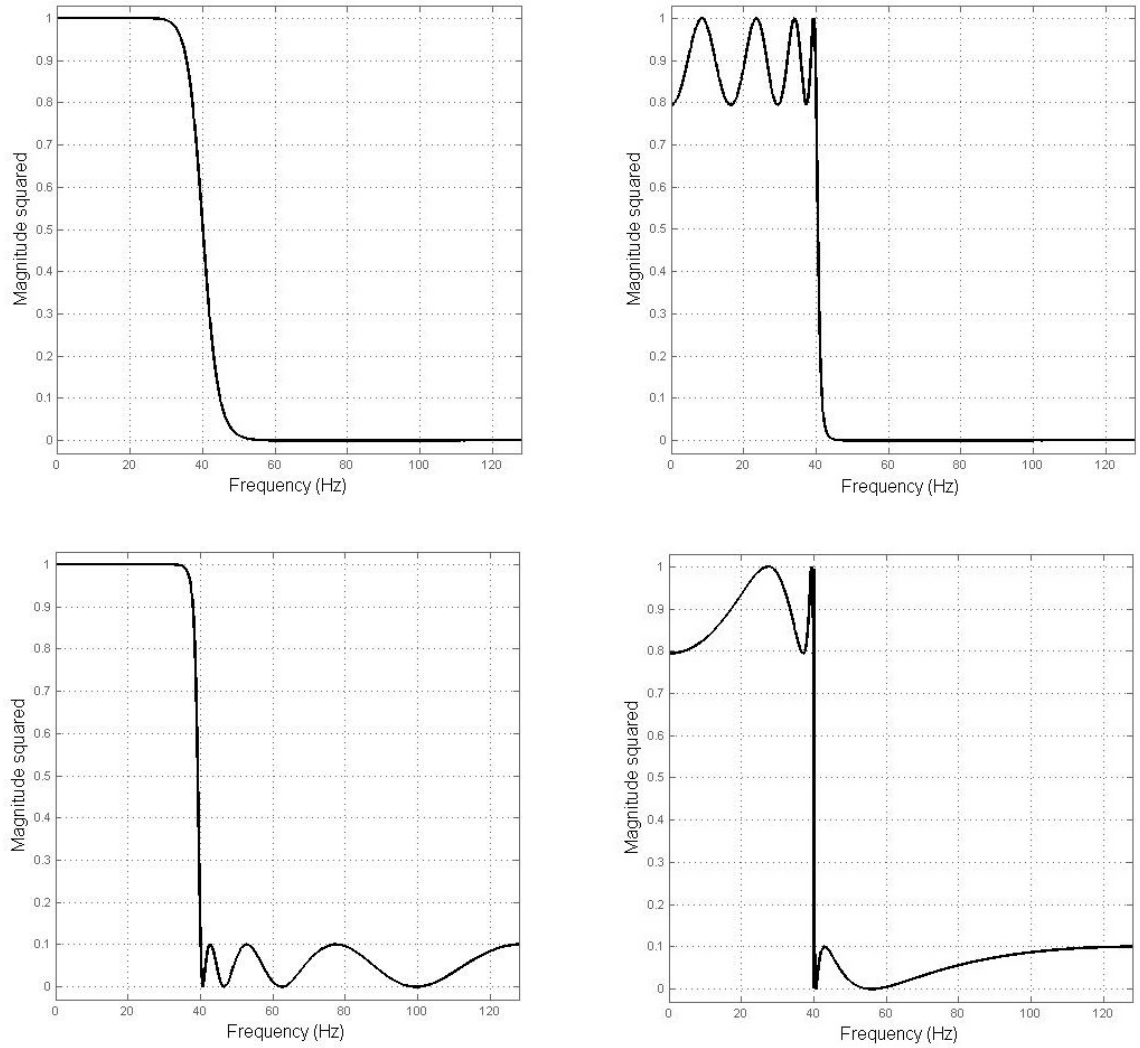

Figure 19: A comparison of the frequency response for four types of IIR filters. Each graph is for a low pass, 8th order filter with a sampling frequency of 256 Hz, and a cut off of 40 Hz and was generated using Matlab's filter design software, fdatool. The top left shows a Butterworth filter with a nearly flat passband and no ripple. Top right shows a type 1 Chebyshev filter, with ripple in the passband. Bottom left, a type 2 Chebyshev filter with ripple in the stop band, and bottom right showing an elliptic filter with a very steep transition band, but ripple in both the pass and stop bands.

A notch filter passes all frequencies apart from those defined in the stop band, and is centred around the required frequency, usually mains at 50 or 60Hz. The shape of the frequency response plot is a 'notch', wider at the top and narrower at the base (Figure 20). Notch filters can introduce significant phase distortions and therefore are not suitable when acquiring biosignals where timing is critical, e.g. evoked potentials. They will also affect amplitude in nearby frequencies, i.e. the upper range of the EEG for a 50 or 60 Hz filter.

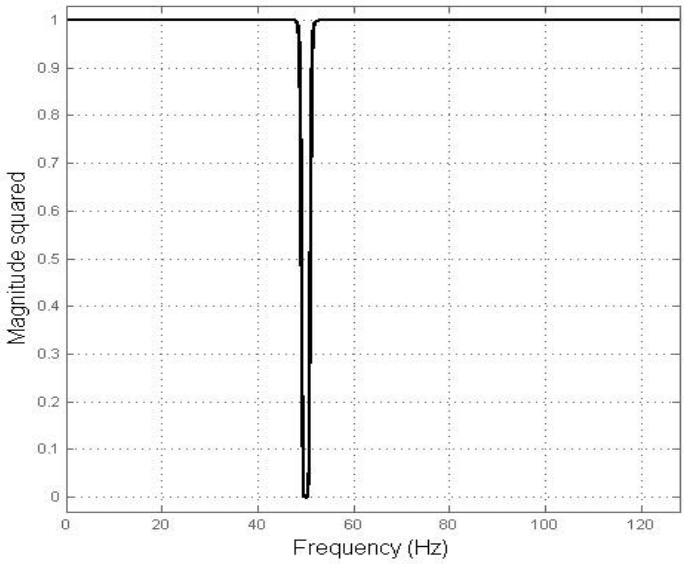

Figure 20: A frequency response curve for a Butterworth 8th order 50 Hz notch filter. Here the frequencies either side of the stop band (48-52 Hz) are passed, whilst the frequencies around the filtered frequency are blocked. The graph was generated using Matlab's filter design software, fdatool.

4.4 Analysis of Biosignals

Visual inspection of the trends and patterns of signals can elicit useful deductions about the underlying physiological system, but requires an expert viewer to be clinically useful: this approach is commonly used for EEG interpretation. More objective interpretation uses measurements of signal amplitude and time, for example by measuring the time between two R peaks of an ECG. This analysis of signals in the time domain is widely used in ECG and many other biosignal fields.

An alternative, objective approach is to examine data in the frequency domain.

The information in this section is sourced from the following references: Lessard, (2006); Peters et al., (1998); Sanei and Chambers, (2007); Semmlow, (2004); Tong and Thakor, (2009); van Drongelen, (2006).

4.4.1 Spectral Analysis

Spectral analysis is a method for estimating the energy content of a time-varying signal as a function of frequency. In the time domain, it is normal to plot data with the y-axis representing energy, and the x-axis time, whilst for the frequency domain, the x-axis shows frequency. Spectral analysis is based on the result of techniques such as the discrete Fourier transform (DFT), where the spectrum produced represents energy at a range of frequency bins. If a signal contains little diversity of frequency content, it will closely resembles a sinusoid in the time domain, and its frequency spectrum will be similar to a single line at the frequency of the signal. As the signal increases in complexity, and thus is made up of more sinusoids, the frequency spectrum will become more complex, containing multiple lines representing the various frequencies present.

Spectral analysis is a powerful tool in the analysis of biosignals and is used extensively in EEG and ECG analysis.

Non-stationarity of Biosignals

A stationary process is defined as continuous and would therefore repeat itself indefinitely. Spectral analysis is based on the Fourier series, which repeats itself infinitely and assumes stationarity of a signal. However, biosignals in their raw form are rarely stationary, and require a degree of manipulation before spectral analysis can be performed. As an example, consider one hour of ECG recording, which is not stationary. However, smaller epochs of the ECG approximate to a stationary signal, and spectral analysis may be performed (Dumermuth and Molinari, 1987).

Fourier Analysis

The Fourier series can be used to describe a periodic time domain signal as the sum of an infinite series of sinusoids: a fundamental frequency component and its harmonics.

If a periodic signal is defined as $f(t)$, and has a period of T, then $f(t)=f(t+T)$ for all

values of t. Consequently a Fourier series representation of the function $f(t)$ can be expressed as in equation (2).

$$f(t)=a_0+a_1\cos(\omega_0 t)+a_2\cos 2(\omega_0 t)+\ldots a_n\cos(n\omega_0 t)\ldots \\ +b_1\sin(\omega_0)t+b_2\sin(2\omega_0)t+\ldots\ b_n\sin(n\omega_0)t+\ldots\ n-1,2,3,\ldots\ \infty-1 \quad (2)$$

where $\omega_0=\frac{2n\pi}{T}$, period T = 1/f, n is the nth harmonic of the fundamental frequency ω0, and a_i and b_i are the Fourier coefficients which govern the amplitudes of the sinusoids.

It can be seen from equation (2) that the signal $f(t)$ can be represented by an infinite number of sinusoids of harmonically related frequencies, in addition to the fundamental frequency ω_0. Fourier analysis calculates the values of the coefficients a_i and b_i, and determines the number of coefficients required to describe the input signal with adequate accuracy.

The Fourier series shown in equation (2), may be simplified as the more general equation (3):

$$v(t)=a_0+\sum_{1}^{\infty}\left(a_n\cos(n\omega t)+b_n\sin(n\omega t)\right) \quad (3)$$

where $\omega=2\pi f$.

The complex Fourier coefficients a_i and b_i are determined as in equations (4), (5) and (6):

$$a_0=\frac{1}{2T}\int v(t)\,dt \quad (4)$$

$$a_n=\frac{1}{2T}\int_0^T v(t)\cos(n\omega_0 t)\,dt \quad (5)$$

$$b_n = \frac{1}{2T} \int_0^T v(t) \sin\left(n\omega_0 t\right) dt \tag{6}$$

The process of satisfying these coefficient requirements is called the Fourier transform. The output of this transformation gives a set of sinusoids with amplitudes and phases such that when added together, they recreate the original signal.

The Discrete Fourier Transform (DFT) is a mathematical variant of the Fourier transform used for a finite array of equally spaced, discrete samples. The discrete time function is transformed into an array of coefficients of a finite combination of complex sinusoids, ranked by their frequency. The Fast Fourier Transform (FFT) is one algorithm commonly used to implement the DFT and is optimised for fast computation.

The Power Spectrum

A power spectrum (or periodogram) is the squared magnitude of the amplitude-frequency spectrum, and shows the contribution (power) made by a frequency per unit frequency.

The magnitude of the coefficients can be established using equation (7) and has units of V/Hz.

$$c_n = \sqrt{\left(a_n + b_n\right)\left(a_n - b_n\right)} \tag{7}$$

where $_a$ and $_b$ are the Fourier coefficients.

Parseval's theorem (equation 8) states that the square of a function in the time domain equals the square of the transformed function, i.e. in the frequency domain. Therefore, the power spectrum can be obtained using equation (9):

$$\int_{-\infty}^{+\infty} |v(t)|^2 dt = \frac{1}{2\pi} |X(\omega)|^2 d\omega \tag{8}$$

where v(t) is the time domain, and the frequency domain is represented by X(ω).

The coefficients in equation (9) are squared magnitude of the complex coefficients, and therefore have units of V^2/Hz.

$$c_n^2 = a_n^2 + b_n^2 \tag{9}$$

The FFT algorithm requires 2^n data points. For example, using a sampling frequency of 256 Hz and a four second window or epoch results in a signal with 1024 (2^{10}) data points. Longer epochs, for example 30 s, could result in loss of time-domain information such as specific events. Padding the signal with zeros in the time domain can prospectively achieve the required number of data points in the frequency domain.

When discontinuities are introduced into a signal, usually due to truncation, rectangular windowing, or zero-padding, the effect on the power spectrum is spectral leakage. For example, the sine function shown in Figure 21a does not fit within the time window exactly, and thus has a non-integer number of cycles. The end of the previous cycle does not match the beginning of the next cycle, so a discontinuity is introduced. The spectral leakage reduces the line spectrum at the sinusoid frequency, and increases its representation in adjacent bins (Figure 21b).

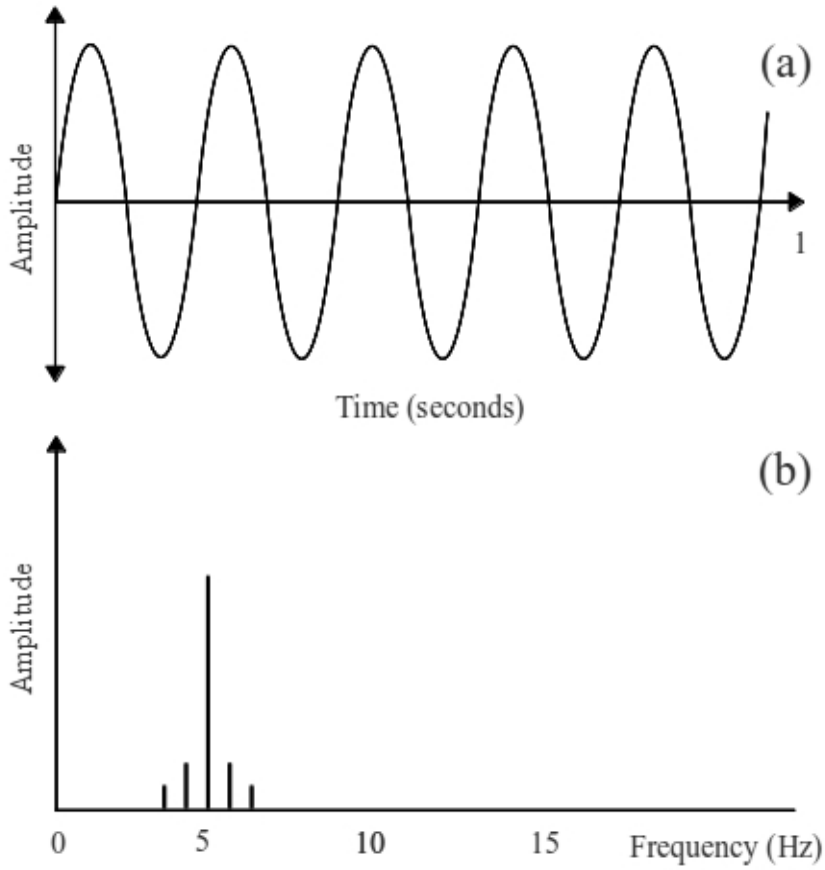

Figure 21: Spectral leakage caused by a non-integer number of sinusoids within a set epoch. The top graph (a) shows a sinusoid in the time domain, and the bottom (b), its frequency domain equivalent. As the signal in (a) does not contain an integer number of cycles, spectral leakage in the frequency domain (b) can be seen in adjacent bins.

4.4.2 Windowing

To reduce the effect of leakage, a window function, or weighting function, can be applied to the time domain signal before it undergoes a frequency transform. Windowing tapers the signal amplitude to avoid discontinuities and therefore avoids spectral leakage. However, windowing leads to a loss in energy of the system, as signal amplitude is lost. An example of the tapering effect of windowing for a sinusoid is shown in Figure 22.

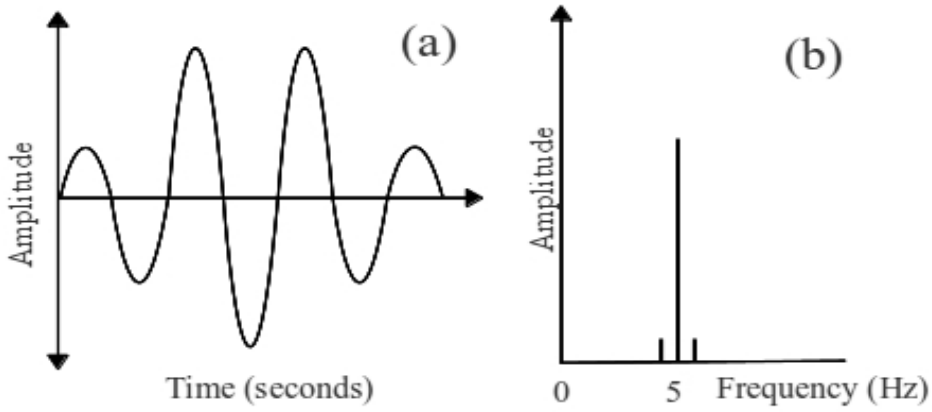

Figure 22: Windowing used to reduce the effects of spectral leakage. (a) shows a tapered sinusoid, with the start and end of the signal having zero amplitude. Its frequency transformation is shown in (b).

Four of the most common types of windowing function are described below (Figure 23):

Rectangle window : The simplest form of window is the rectangular or boxcar window. This replaces all but a predefined set of values at the start and end of the signal with zeros. This gives the appearance of the waveform abruptly turning on and off. This process is simple to implement, but creates discontinuities and so leads to spectral leakage in the frequency domain.

Welch window : The Welch window consists of a single parabolic section which tapers the beginning and end of the signal more slowly than the rectangular window.

Hanning window : The Hanning window consists of a polynomial closer to a sine wave, with more gentle side lobes, so the transitions are less abrupt than other windows.

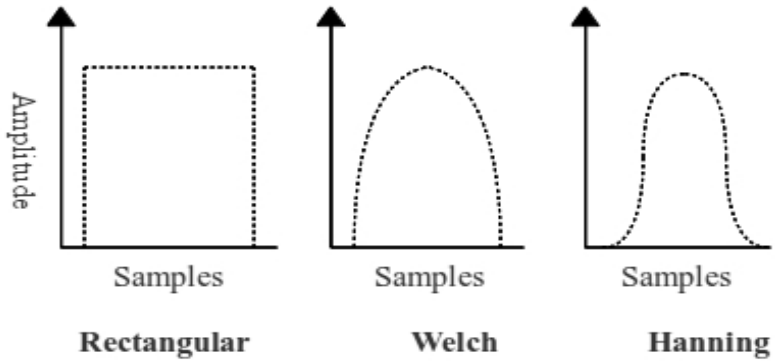

Figure 23: The generalised window shapes of the rectangular, Welch and Hanning window functions.

4.4.3 The Welch Periodogram

As windowing reduces the energy in the system, one method of minimising this loss is to overlap adjacent, windowed sections of the signal. A commonly used technique of applying windowing and overlapping is known as the Welch periodogram (Welch, 1967). If the overlap is half the window length, then each sample will make approximately the same contribution to the overall spectrum, as windowing emphasises data from the centre of a segment at the expense of data at its edges. The epoch is split into multiple segments of equal length with 50% overlap between adjacent segments. Hanning windows are applied to each segment, and their periodograms computed using the DFT (Figure 24).

All periodograms are then time-averaged. This has the effect of averaging each epoch's frequency output, thus reducing noise, but at the cost of frequency resolution (Semmlow, 2004). It is a commonly used tool in EEG and ECG spectral analysis because of its noise reduction capabilities and its relatively low computational overheads. This approach is suitable for examining the underlying trends in the EEG signals, but is not suitable for evoked potential analysis, as the averaging effect smooths out important components: "A smeared spectral estimate is a consequence of the windowing" (Kay and Marple, 1981).

By introducing smearing across the bins, power at the band power boundaries is altered: for example, power close to the 4 Hz delta/theta boundary may be smeared across the adjacent frequency bins, giving misleading values for band power.

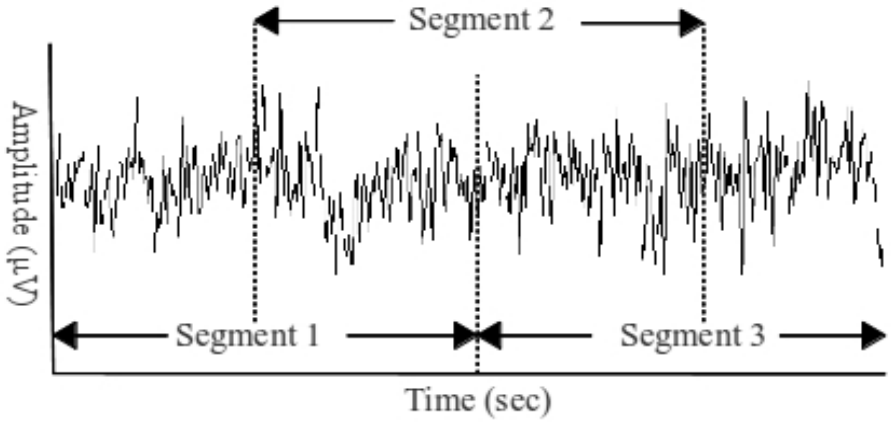

Figure 24: The Welch periodogram showing the epoch separated into three segments with 50% overlap between each. Each segment is then windowed. In this example, the latter 50% of segment 1 overlaps the first 50% of segment 2.

4.4.4 The Short Time Fourier Transformation (STFT) – Spectrogram

A limitation of the Fourier transform is that all time information is lost when data is transformed from the time domain to the frequency domain, so although the frequency of events is known, the timing of an event is not.

To overcome this, a spectrogram can be employed. The spectrogram is an array of epochs 'stacked up' on each other in layers, so that each layer represents a further epoch in time. For example, for a 1 second epoch, if an event was evident in the third epoch/layer, then it can be assumed that the event occurred during the third second. However, temporal resolution is limited: if the epochs are too short, spectral leakage diminishes the reliability of the spectral analysis.

An example of a spectrogram is shown in Figure 25. The spectrogram is built up by layers of epochs from the left of the figure. The power is represented by the colour, with lower values being darker, such as blue, whilst high values of power are represented in red. The figure shows that, over the period of 1 second, the signal changes frequency from 1000 Hz to 3000 Hz. It gives an indication of not only the frequency of the signals, but the time at which they occur.

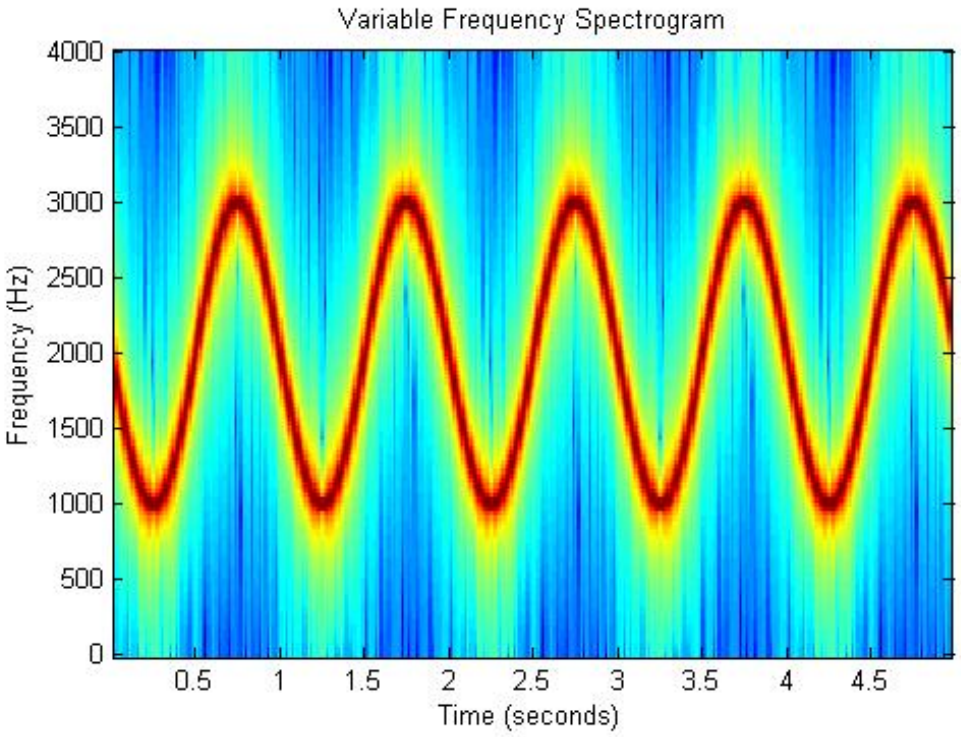

Figure 25: The spectrogram. In this example the frequency of the input signal varies between 1000 and 3000 Hz. The amplitude of the signal also varies with darker colours indicating low amplitude, and higher colours high frequency. The frequency of the signal varies with time being at a minimum of 1000 Hz at 0.5 seconds, and a maximum of 3000 Hz at 1 second, before repeating itself.

4.5 EEG Signal Processing

4.5.1 Absolute and Relative Band Power

A spectrum can be split into bands and the power within each band can be calculated as an absolute value, or relative to the power of the entire spectrum (Figure 26). These bands are: delta (0-4 Hz), theta (4-8 Hz), alpha (8-12 Hz) and beta (12-30 Hz). Although gamma (30 Hz upwards) is used in adult EEG spectral analysis, it is not used in neonatal analysis and so is not discussed further here.

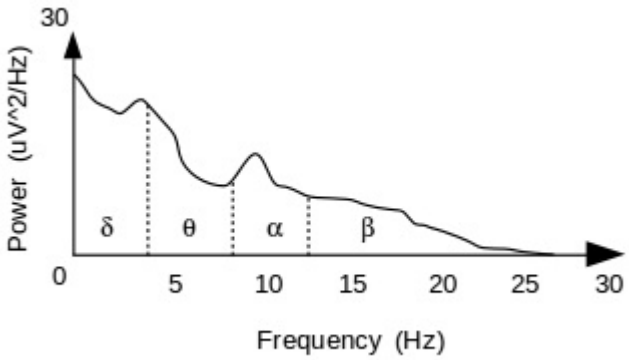

Figure 26: EEG band power. The four bands shown are delta (0-4 Hz), theta (4-8 Hz), alpha (8-12 Hz) and beta (12-30 Hz).

The total power is the area under the entire curve between two frequencies, usually 0 and 30 Hz (equation 10):

$$\mathrm{TotalPower}(\mathrm{TP}) = \sum_{0\mathrm{Hz}}^{30\mathrm{Hz}} \left(X(f)^2 \right) \tag{10}$$

where X(f) is the power function. Absolute band power is the sum of the power under the curve between the band frequency boundaries. Relative band power is the percentage of band power relative to total power, and an example for delta power is described in equation (11):

$$Relativepower(delta) = \frac{deltabandpower(0-4\ Hz)}{Totalpower(0-30\ Hz)} x\,100 \quad (11)$$

4.5.2 Spectral Edge Frequency

The spectral edge is defined as that frequency below which 95% of the total power (cut off frequency = 30Hz) is accumulated (Fell et al., 1996). Spectral edge measurements have a long history of use in adult EEG, for example in assessing depth of anaesthesia, and have also been shown to correlate with gestational age in healthy neonates, suggesting a role for measuring cerebral maturation or stress levels (Bell et al., 1991).

4.6 ECG Signal Processing

As with EEG spectra, the frequency spectrum of HRV can be broken down into bands (Table 8), and the power within each band can be calculated.

Band	Frequency (Hz)
High Frequency (HF)	0.15 – 0.4 Hz
Low Frequency (LF)	0.15 – 0.4 Hz
Very Low Frequency (VLF)	0.0033 – 0.04 Hz
Ultra Low Frequency (ULF)	0 – 0.003 Hz

Table 8: Frequency ranges of each ECG band power (Mehta et al., 2002).

4.7 Summary

This chapter has summarised the key elements of signal processing, starting with the methods of acquiring biosignals and methods of removing unwanted noise by the application of filters. The use of the Fourier transform as the basis of frequency analysis, with sections on spectral leakage, and methods of limiting its effect with the application of windowing techniques, were then described. The short-time Fourier transformation was introduced as a tool for identifying when event occurs within a series of epochs, without losing the frequency information from the spectral analysis. Finally applications and quantifiable variables were described with the application of spectral analysis to both EEG and ECG.

5 Software

5.1 Introduction

This chapter describes the custom software developed for EEG analysis, and the open source and proprietary software used for ECG analysis, for all data acquisition and for all data storage.

Open source means the source code is available to view, modify and distribute. Proprietary (closed source) means the source code is owned by the distributing organisation or author, and is not available. For this project no single proprietary software solution that satisfied all of the requirements was available.

A major part of the work I undertook for this thesis was the development of the custom software for EEG analysis. The work comprised specification, design, writing of code and testing. I also wrote the custom databases for the study.

5.2 Data Acquisition

All data were acquired using Xltek Neuroworks system (Nautus Medical, Oakville, Ontario, Canada), software version 5.4.0 (build 503), running on a Microsoft Windows XP platform, a proprietary hardware/software combination. It consists of a small hardware box connected to a laptop. It collected all the electrophysiological signals recorded in this study, i.e. 12-channel EEG, ECG, EMG, respiratory variations and EOG. It was also used to record simultaneous video, which was required for identifying sleep states and recording any unusual movements.

The Xltek system is used in the EEG department at the Royal Hospital for Sick Children, Glasgow for all routine, clinical work. The same system was selected for the

study to provide maximum consistency with routine, clinical practice of the consultant paediatric neurologist (Dr Mary O'Regan) who interpreted the EEGs of the study infants.

The Xltek Wave viewer software is part of the Xltek EEG system, and allowed inspection of multiple channels of electrophysiological data with real time video. It also displayed time-labelled annotations recorded manually during the recording which allowed post-hoc identification of artefacts (Figure 27).

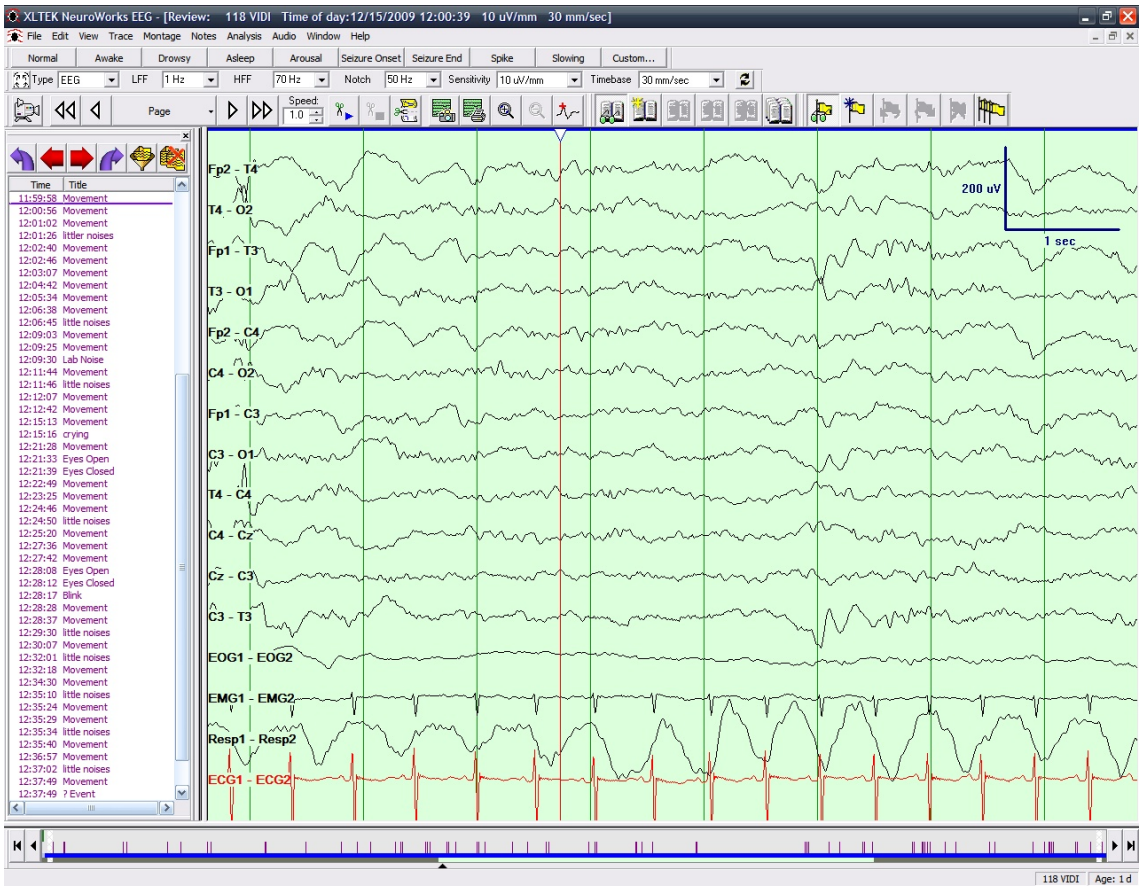

Figure 27: Xltek Wave viewer software. The data shown are from VIDI study infant #118, recorded at age 23 hours. Annotations and comments made during the recording are listed in the left hand window. The main electrophysiological data are shown in the central (green) window; EEG channels are at the top, EOG, EMG and respiratory follow, and the ECG is at the bottom in red. The video channel has not been included to maintain patient anonymity, but was also viewed when the neurologist interpreted the PSG.

5.3 Data Storage

For uniformity of electrophysiology data file format and ease of transfer between systems, all data required for PSG (EEG, ECG, EOG, EMG and respiratory) were stored in the open source European data format (EDF) file format proposed by Kemp et al., (1992). This format has a header containing general information, such as patient identification, recording start/end time, duration of recording, as well as the technical specifications of each signal, including calibration details, sampling rate and filter settings. Because EDF files are coded as 16-bit integer ASCII (American Standard Code for Information Interchange) characters, the data are viewable without encoding using a standard text editor. The Xltek Wave viewer software was used to create EDF format data output rather than its propriety, closed source format.

EDF files were imported using the cross platform (Microsoft Windows XP Professional Service Pack 3 & Linux) BioSig software toolbox 2.61 (Schlogl and Brunner, 2008) as a parser. An example of the output from the Biosig header file is shown below (Table 9).

Variable	Function
HDR.FileName	File name
HDR.SampleRate	Sampling frequency, fs (Hz)
HDR.FILE.size	File Size
HDR.NS	Number of channels
HDR.NRec*HDR.SPR	Number of samples
HDR.PatientName	Patient name
HDR.Manufacturer.Model	Manufacturer make and model of the bio-amplifier used.

Table 9: Examples of Biosig header file variables. HDR – Header; Fs – sampling frequency; NS – number of channels; Nrec - number of records; SPR – sampling rate (Hz).

5.4 Data Analysis

5.4.1 EEG

No proprietary analysis system satisfied all of the EEG analysis requirements. I therefore developed a custom application, written to be used in conjunction with the manually scored, classical PSG analysis.

Specification and design In general, the purpose of the software was to import files from the Xltek Neuroworks system, perform a series of computational procedures, and output the results both graphically and as a text file for importing into the PSG database. The specific requirements were:

- Import EDF files, extract header information and information concerning the montage configuration.
- Extract user-definable epochs for analysis
- Allow selection of individual epochs using a graphical user interface (GUI)
- Apply the following digital signal processing (DSP) methods:
  - Optional filters (notch, high and low pass), both based on Butterworth filters with user selectable parameters e.g. filter order, high and low pass cutoffs. See chapter 4.3.
  - Linear de-trending of the signal in the time domain by removing the epoch average value from each data point.
  - If required to apply a Hamming window to the epoch, the parameters defined by the user. See chapter 4.4.2.
- Perform time domain analysis and extract maximum signal amplitude, mean amplitude and epoch variance.
- Perform frequency domain analysis using power spectra, and extract the following features: SEF 95% (0-30 Hz and 2-20 Hz), absolute and relative

band powers; delta (0-4 Hz), delta low (0-2 Hz), delta high (2-4 Hz), theta (4-8 Hz), alpha (8-12 Hz), beta (12-30Hz). See chapter 4.5.1.

- Plot time domain graphs, frequency domain graphs and and a histogram of the distribution of the amplitude data.
- Plot 2D/3D colour density spectral array, based on the results of the output of combining the power spectra for all epochs analysed.
- Output numerical data to a text file for importing into the PSG database and into a summary report for printing.

Initially a proprietary solution was sought to satisfy these requirements, as this would mean development time for the analysis phase of the project would be kept to a minimum. Two packages were investigated; Prana Software Suite[1] (PhiTools, 1, rue du Général de Castelnau, 67000 Strasbourg, France), and g.Bsanalyze[2] (g.Tec, Guger Technologies OG, zH Frau Mag. Barbara Vogt, Sierningstraße 14, 4521 Schiedlberg).

The Prana software was available as a demonstration version that had limited functionality for testing purposes. When installed on the test machine (Intel P4 3 gigahertz CPU with 1 gigabytes of memory – later upgraded to 2 gigabytes) it ran too slowly to be usable due to the PC's limited memory, and the large video files to be imported. The g.Tec software, at that time, could not output variables such as spectral edge, which were considered essential for the analysis.

Consequently a bespoke solution was required. For this reason, an agile approach was used for the development of the EEG software, where the project is broken down into small tasks, and each task was completed before moving on to the next: the process is iterative as requirements can be modified before the start of the next task. This evolutionary approach was suitable as the precise outcomes of the project were not always clear at the outset, and was preferred to the more rigid waterfall design method where the design specifications cannot easily be adjusted during the coding phase (Figure 28).

The agile approach suited the pragmatic requirements of the study, where EEG

[1] http://www.phitools.com/

[2] http://www.gtec.at/Products/Software/g.BSanalyze-Specs-Features

quantitative analysis techniques were researched in parallel with designing the software requirements. Requirements could be modified to match my improving understanding of EEG analysis, improving programming skills, and to accommodate unforeseen difficulties.

An agile approach was chosen for the development of the EEG software for the

following reasons:

1. To avoid delay in software development, EEG quantitative techniques were researched in parallel with requirement design, requiring an agile approach to flexibly develop software in response to improved EEG analysis understanding. Use of the waterfall method would have necessitated completion of the research prior to software development and thus delayed the start of writing the code.
2. Many small pilot modules of code had to be developed, and not all of them were included in the final application. The agile approach gave the flexibility to include or exclude modules accordingly.
3. The MATLAB® programming language was learned at the same time as the requirements were established. As better methods of algorithm design were learnt and understood, they could be more easily incorporated into the main program (code base).

The agile approach gave the flexibility to include or exclude modules accordingly.

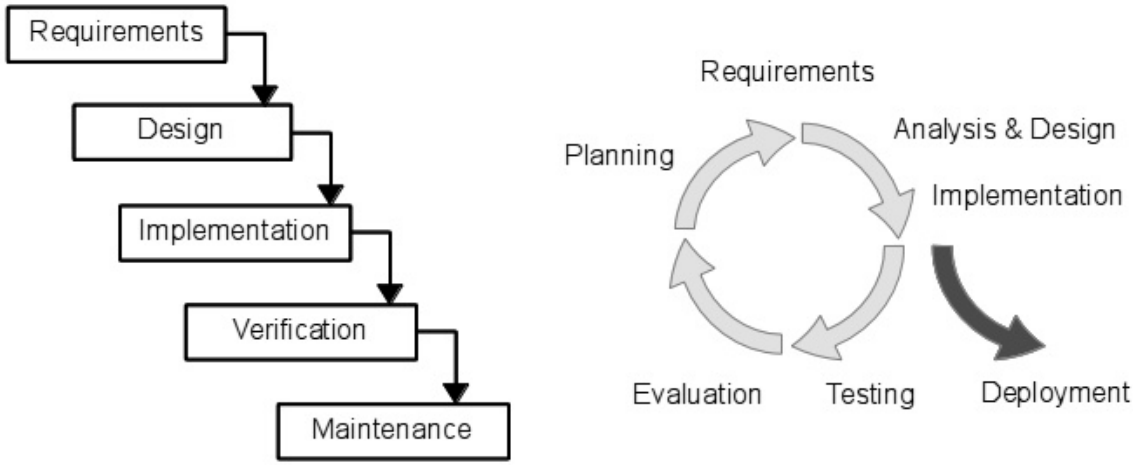

Figure 28: Software design methodologies. On the left, the waterfall method showing each stage that needs completion before progression to the next, and on the right, the agile approach, that updates the requirements in relation to changing user needs.

Legislation and version control: Although the project did not aim to develop software for sale in the European Union, the processes laid down in the relevant standard (IEC 62304) for medical device software were followed: requirement establishment; architecture and design of the system; implementation (coding); testing and deployment. IEC 62304 is the international standard, harmonised by the European Union and a benchmark for compliance with the regulatory requirements of the Medical Device Directive MDD 93/42/EEC. It establishes a framework for developing safety critical and highly reliable software via the software design process.

The open-source version control system Fossil[3] was used to monitor changes during software development. The nature of each change and its reason were documented so that if a problem occurred, it was possible to track back to find errors in the source code. Fossil was chosen for its small size and built-in bug tracking.

Language: The analysis software was written in the proprietary mathematical programming language Matlab® (MathWorks, Natick, MA, USA). This software was suitable for the purposes of the study as it allowed manipulation of matrices, plotting of functions and data, algorithm implementation, and generation of GUIs. It was also suitable for transfer of software across systems (i.e. Microsoft Windows and Linux). Matlab® includes a Signal Processing Toolbox, which allowed development of off-line

[3] http://www.fossil-scm.org/index.html/doc/trunk/www/index.wiki

(that is, not in real-time) spectral analysis software. Although other open-source programming languages such as Python[4] (using the scientific add on library SciPy[5]) or R[6] (statistical programming language), were also considered, Matlab® was preferred because of its excellent reference material available for signal processing, and the numerous, freely available sections of code (Matlab Central)[7] available for testing.

Minimum hardware and software requirements: The primary development platform was a Hewlett Packard / Compaq desktop PC with a 3GHz Intel P4 central processing unit (CPU), and 2 gigabytes of internal Random Access Memory (RAM). The operating system was Microsoft Windows XP SP3[8]. The software was also developed in part on a Hewlett Packard 2730p laptop, with a 1.83 GHz Intel Dual Core 2 CPU and 2 gigabytes of RAM, but running Cannonical's Lubuntu[9] version 12.04 with version 3.2+ of the Linux kernel. The software was developed on two platforms to take advantage of portability, and Linux's lower resource requirements.

Overview of system: The flow diagram (Figure 29) summarises the processes for the EEG analysis software. The user selects a suitable EDF file, and the software reads in its header, presenting the user with the details such as patient information and recording details. The user then selects the individual channels for analysis to reduce the computational load; only the data being analysed was ever held in memory, as opposed to reading in the entire dataset. The channels of data from the requested pairs of electrodes (e.g. C3-O1) were then extracted from the dataset. The user then selected options of digital filtering, windowing and/or linear de-trending of each epoch. The main analysis loop was then initiated, performing power spectrum estimation on the selected epoch. Spectral results from each epoch were added to an ongoing array, then exported to a text file. The GUI was then shown (Figure 32) and the user could inspect any individual epoch, or look at overall trends.

4 www.python.org
5 www.scipy.org
6 www.r-project.org
7 www.MathWorks.co.uk/matlabcentral/g
8 http://windows.microsoft.com/en-US/windows/products/windows-xp
9 http://lubuntu.net/

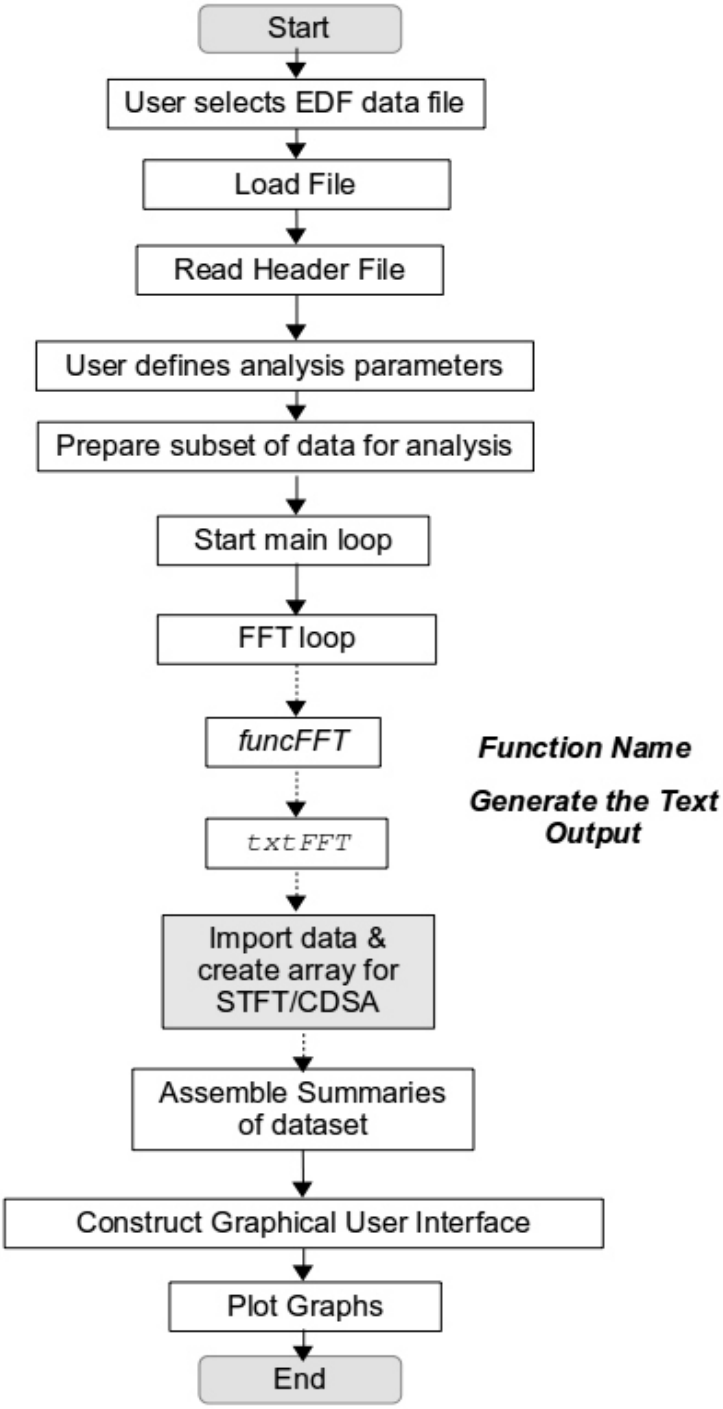

Figure 29: The EEG analysis software systems flowchart showing each stage necessary for the analysis.

EDF header extraction Figure 30 is an example of the header file from an EDF file read by the BioSig parser, highlighting all the key variables for the analysis software. Information contained within the header file about sampling rate, channel labels and amplitude were used during spectral analysis.

```
Version=0.10
generated=2012-06-18 16:36:11.7
[Fixed Header]
Filename      = C:\PilotNIRSedf\PRANA_reduced_data.edf
Format        = EDF

SizeOfFile    = 393472
NumberOfChannels     = 3
SamplingRate         = 128
Number_of_Samples    = 65408
RecordingDateTime    = 2011-02-01 15:40:01.000

Patient.
       Name          =
       Id            = PRANA
       Gender        = unknown

[Channel Header]
#No Label     fs [Hz]       GDFTYP TH-    TH+    PhysDim
 1 Time        128.0 3      -32768 32767  s
 2 channel 1   128.0 3      -32768 32767  uV^2/Hz
 3 channel 2   128.0 3      -32768 32767  uV^2/Hz

[Event Table]
NumberOfEvents=0 SampleRate=128.000000

Sampling Header information
===========================

Sampling Frequency: 128
Number of data points: 65408
Duration of recording: 511 seconds or 00:08:31 hrs:mins:sec
Frequency: 128 Hz
Number of data points: 65408

Basic Header information
========================

Sampling Frequency: 128
Number of data points: 65408
Duration of recording: 511 seconds or 00:08:31 hrs:mins:sec
```

Figure 30: BioSig EDF file header output.

Epoch selection An initial design requirement was that the software could read in a user-defined sample from one channel of data, and run all the analytical procedures on this data. One hour of multichannel PSG data with video is typically 400-600 Mb, which is a large dataset for a low specification PC (2 Gb RAM, Intel P4 3.0GHz), so the final software allowed analysis of short epochs (user definable, but for this study four seconds), repeated to cover the entire hour's worth of data, one channel at a time. The software allowed the user to select the required channel, the start position of the epoch (in seconds), the number of epochs and the duration of the epochs. The software then ran an iterative process, extracting the epoch under investigation [epochData] by defining the start [posStart] and end [posEnd] positions within the array [allData] (Figure 31). Epoch lengths are rarely longer than 1 minute: at a sampling frequency of 256 Hz, this created 15,360 data points per epoch which was manageable by the computers used.

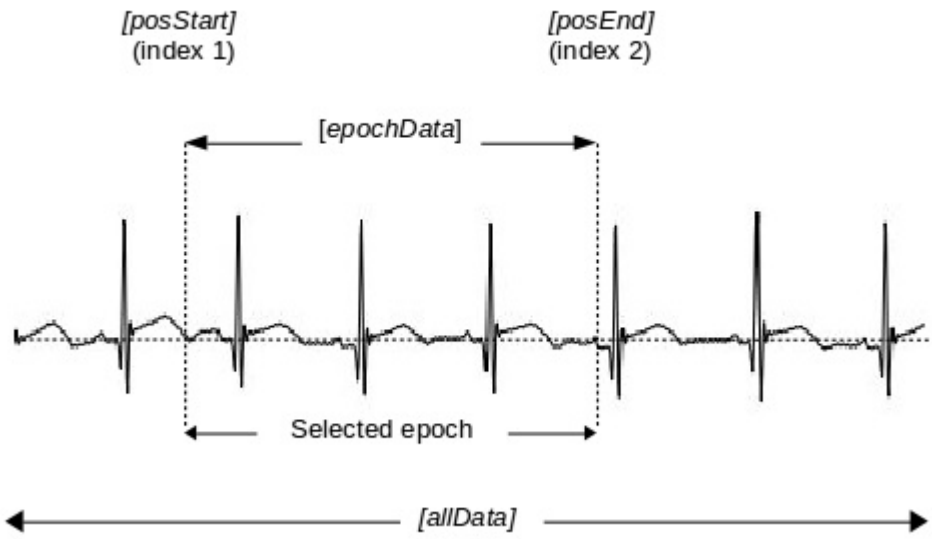

Figure 31: The epoch selection method. The image above is of artificially created data to demonstrate the epoch selection process used by the analysis software. The user defines the epoch length, the number of epochs required and the time position of the start of the first epoch. Each subsequent epoch is then analysed.

Following analysis (see below), the output array of parameters were stored in a text file for reconstruction as graphs or tables, minimising CPU and memory overheads and allowing a large dataset to be analysed in sections.

Numerical analyses Briefly, data epochs were transformed into the frequency domain using the discrete Fourier transform (DFT) (see section 4.4.1), squared to produce a power spectrum, as per the method[10] described by van Drongelen, (2006). The software output was a three column array containing respectively an index number, the bin frequency (Hz); and power at that frequency (μV^2/Hz).

Absolute and relative powers were calculated from this output. Frequency values corresponding to EEG band boundaries (see Table 13) were stored, and power was calculated by adding the power in all bins between (and including) the two boundaries. If the boundary did not correspond to an exact bin frequency, for example where the frequency resolution did not exactly match the boundary value, the nearest lower value was stored. Relative band powers were computed as percentages of the total band power.

Spectral edge frequencies were calculated in a similar manner. The area under the curve was calculated between two frequency ranges (0-30Hz or 2-20Hz). This represents 100% of the power. 95% of this power was then calculated and then the frequency at which this value occurred noted as the spectral edge frequency (see section 4.5.2).

The main GUI This has five sections (Figure 32). 1 (left): file/epoch information and signal processing details. Any processing applied by the user from the command line was summarised here (filtering; windowing or de-trending). 2 (top, centre): the main graph window plotted the current epoch in the time domain (top) and frequency domain (bottom), showing amplitude and power spectra (these graphs were derived from the results of the DFT, with the power spectrum being created from the DFT). An amplitude histogram was also plotted. Cursor functionality allowed amplitude measurements to be made directly from the time domain graphs, although in the final analysis this function was not used, as it was more applicable to evoked potential analysis not time series analysis. 3 (centre): the epoch selector panel was used to navigate between epochs and to highlight obvious artefacts. An ‘artefact’ button was used to flag the epoch as unsuitable for analysis, and the user could exclude it from the final analysis. 4 (bottom): displays user selectable graphs showing the output from the frequency analysis of the entire dataset ([allData], or the entire data range selected by

[10] https://books.google.co.uk/books?id=Oa7OtAqJk5wC&lpg=PP1&dq=signal%20processing%20for%20neuroscientists&pg=PA107#v=onepage&q&f=false

the user). The graph options were colour density spectral array (CDSA), or graphs of delta power, total power, band power (delta, theta, alpha and beta all plotted on the same graph), or spectral edge (95%) frequency. The purpose was to show how different parameters varied over the entire recording, but the final analysis only showed user defined pre-selected epochs that were deemed artefact free. 5. (right): the analysis output panel showed the parameters for each epoch from both time domain (maximum amplitude, epoch variance and mean amplitude) and frequency domains (both absolute ($\mu V^2/Hz$) and relative (%) delta, theta, alpha and beta power values; total power ($\mu V^2/Hz$); SEF 95% frequency for the following ranges of 0-30Hz and 2-20Hz, and measured in Hertz). It is these values that were written to the text file output, and used for the final statistical analysis. Each epoch was examined using the GUI, highlighting artefacts or problems where necessary. Annotations were exported in a separate text file.

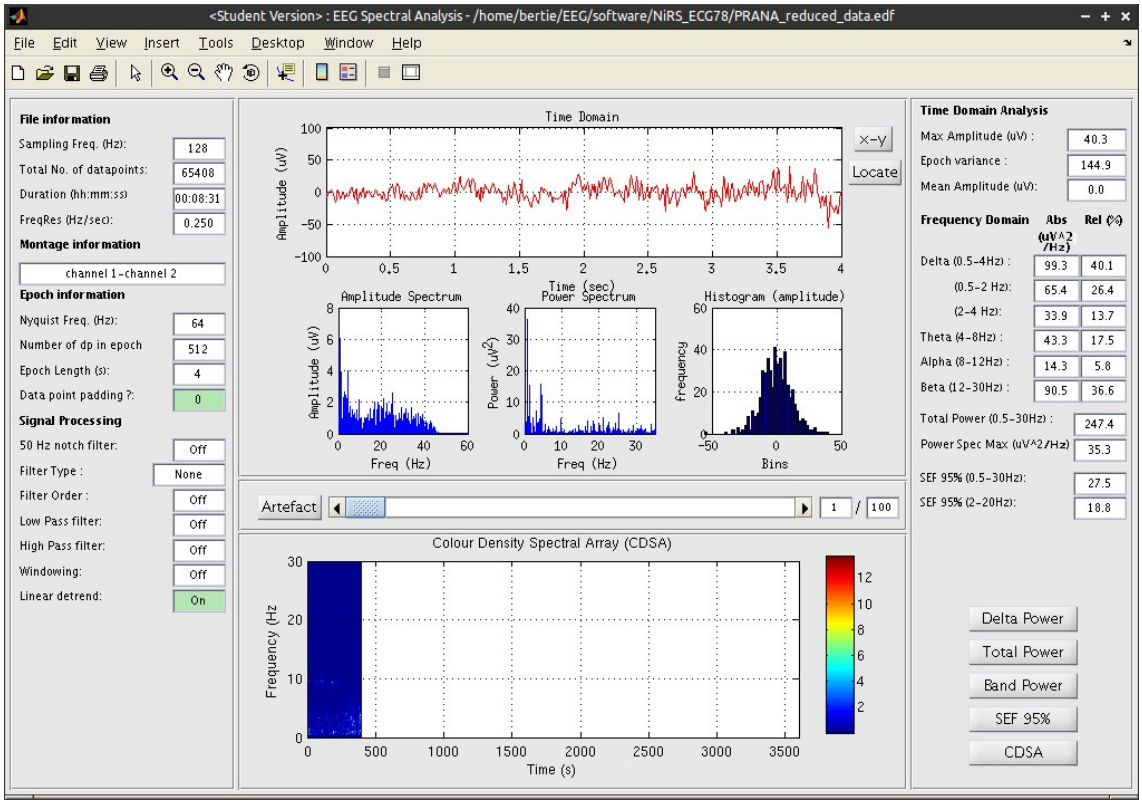

Figure 32: The EEG analysis software main window. The left hand panel shows the file header information, the user selected epoch details, and any signal processing options selected initially. The central panel shows the frequency and time domain graphs, with the colour density spectral array (CDSA) below. The right hand panel shows the results of the analysis for that epoch.

Text file output The output text files were in the comma separated value (*.csv) format, and were imported into the PSG database (Microsoft Access, see section 5.5.2) and into the relevant EEG or ECG analysis software. The files were called output.csv, and were stored in the analysis folder for each infant. Each epoch was identified by subject study number, epoch times and epoch details, so that each channel of data could be identified. This allowed comparison of all channels of the PSG montage in both time and space (electrode position). A truncated example of the text file output looks like:

```
Filename,fs,Channel,posStart,posEnd,epochNo,RMS, ...
VIDI_46_output.edf,128,channel 1-channel 2,0,4,1,1.0754,...
VIDI_46_output.edf,128,channel 1-channel 2,4,8,2,2.4213,...
```

where the top line defines the entries in the subsequent lines, and entries are separated by commas. In this example, the second line contains data from the file (filename) VIDI_46_output.edf, sampling frequency (fs) is 128 Hz, electrode montage (Channel) is channel 1-channel 2, the epoch start (posStart) is at 0 seconds, the epoch end (posEnd) is at 4 seconds, the sequential index number called the epoch number (epochNo) is 1 and the RMS voltage of the epoch is 1.0754 μV.

Testing The EEG analysis software was tested using a text file, converted into the EDF format using EDFbrowser. The 16 different test signals were: a square wave, two sawtooths, a reversing, periodic impulse function, a noise signal, seven sinusoids with different frequencies, a flattened sinusoid and three DC signals (Figure 34). All signals had a constant amplitude except the noise signal.

The sinusoids, DC offset, and pulse signals were generated in LibreOffice Calc and a screen shot of the spreadsheet developed to create the test signals shown in Figure 33. The square wave, sawtooth and noise functions were written in MATLAB® using short programs.

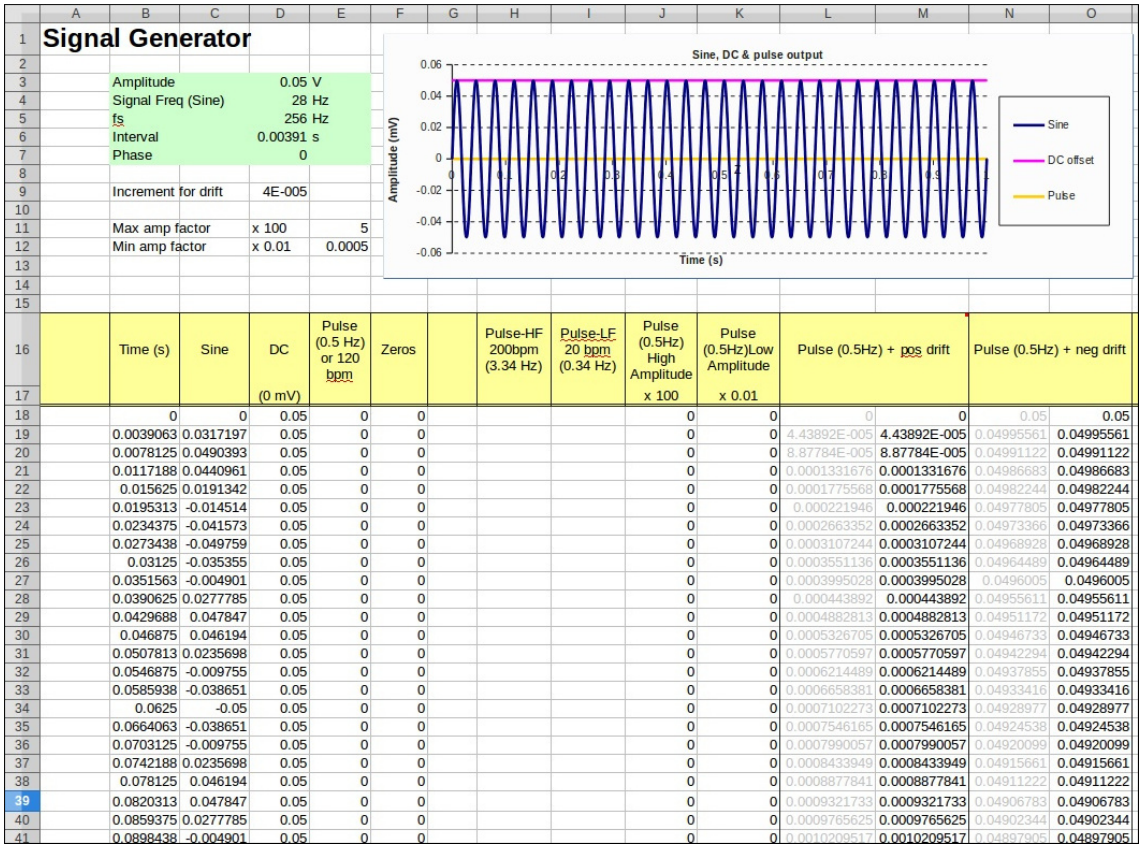

	Time (s)	Sine	DC (0 mV)	Pulse (0.5 Hz) or 120 bpm	Zeros		Pulse-HF 200bpm (3.34 Hz)	Pulse-LF 20 bpm (0.34 Hz)	Pulse (0.5Hz) High Amplitude x 100	Pulse (0.5Hz)Low Amplitude x 0.01	Pulse (0.5Hz) + pos drift		Pulse (0.5Hz) + neg drift	
18	0	0	0.05	0	0				0	0	0	0	0.05	0.05
19	0.0039063	0.0317197	0.05	0	0				0	0	4.43892E-005	4.43892E-005	0.04995561	0.04995561
20	0.0078125	0.0490393	0.05	0	0				0	0	8.87784E-005	8.87784E-005	0.04991122	0.04991122
21	0.0117188	0.0440961	0.05	0	0				0	0	0.0001331676	0.0001331676	0.04986683	0.04986683
22	0.015625	0.0191342	0.05	0	0				0	0	0.0001775568	0.0001775568	0.04982244	0.04982244
23	0.0195313	-0.014514	0.05	0	0				0	0	0.000221946	0.000221946	0.04977805	0.04977805
24	0.0234375	-0.041573	0.05	0	0				0	0	0.0002663352	0.0002663352	0.04973366	0.04973366
25	0.0273438	-0.049759	0.05	0	0				0	0	0.0003107244	0.0003107244	0.04968928	0.04968928
26	0.03125	-0.035355	0.05	0	0				0	0	0.0003551136	0.0003551136	0.04964489	0.04964489
27	0.0351563	-0.004901	0.05	0	0				0	0	0.0003995028	0.0003995028	0.0496005	0.0496005
28	0.0390625	0.0277785	0.05	0	0				0	0	0.000443892	0.000443892	0.04955611	0.04955611
29	0.0429688	0.047847	0.05	0	0				0	0	0.0004882813	0.0004882813	0.04951172	0.04951172
30	0.046875	0.046194	0.05	0	0				0	0	0.0005326705	0.0005326705	0.04946733	0.04946733
31	0.0507813	0.0235698	0.05	0	0				0	0	0.0005770597	0.0005770597	0.04942294	0.04942294
32	0.0546875	-0.009755	0.05	0	0				0	0	0.0006214489	0.0006214489	0.04937855	0.04937855
33	0.0585938	-0.038651	0.05	0	0				0	0	0.0006658381	0.0006658381	0.04933416	0.04933416
34	0.0625	-0.05	0.05	0	0				0	0	0.0007102273	0.0007102273	0.04928977	0.04928977
35	0.0664063	-0.038651	0.05	0	0				0	0	0.0007546165	0.0007546165	0.04924538	0.04924538
36	0.0703125	-0.009755	0.05	0	0				0	0	0.0007990057	0.0007990057	0.04920099	0.04920099
37	0.0742188	0.0235698	0.05	0	0				0	0	0.0008433949	0.0008433949	0.04915661	0.04915661
38	0.078125	0.046194	0.05	0	0				0	0	0.0008877841	0.0008877841	0.04911222	0.04911222
39	0.0820313	0.047847	0.05	0	0				0	0	0.0009321733	0.0009321733	0.04906783	0.04906783
40	0.0859375	0.0277785	0.05	0	0				0	0	0.0009765625	0.0009765625	0.04902344	0.04902344
41	0.0898438	-0.004901	0.05	0	0				0	0	0.0010209517	0.0010209517	0.04897905	0.04897905

Figure 33: A screenshot of the spreadsheet used to create the test signals. This example shows three test signals (sine, DC offset and pulse) for testing the HRV/ECG software. In the top left corner, the user enters the amplitude of the signal, frequency in Hz, the sampling frequency, and phase change (if desired). Each column was then populated automatically and the resulting signals plotted in the graph at the top left. The output of the spreadsheet was then copied to a separate worksheet, exported to text file, and converted to an EDF file using EDF browser.

When all the test signals had been produced they were merged into a single spreadsheet (LibreOffice Calc) and imported into EDF browser to generate the EDF compatible file for testing the EEG analysis software, the Kubios HRV software and the Neuroscope CVT software. A screen shot of the final file is shown in Figure 34.

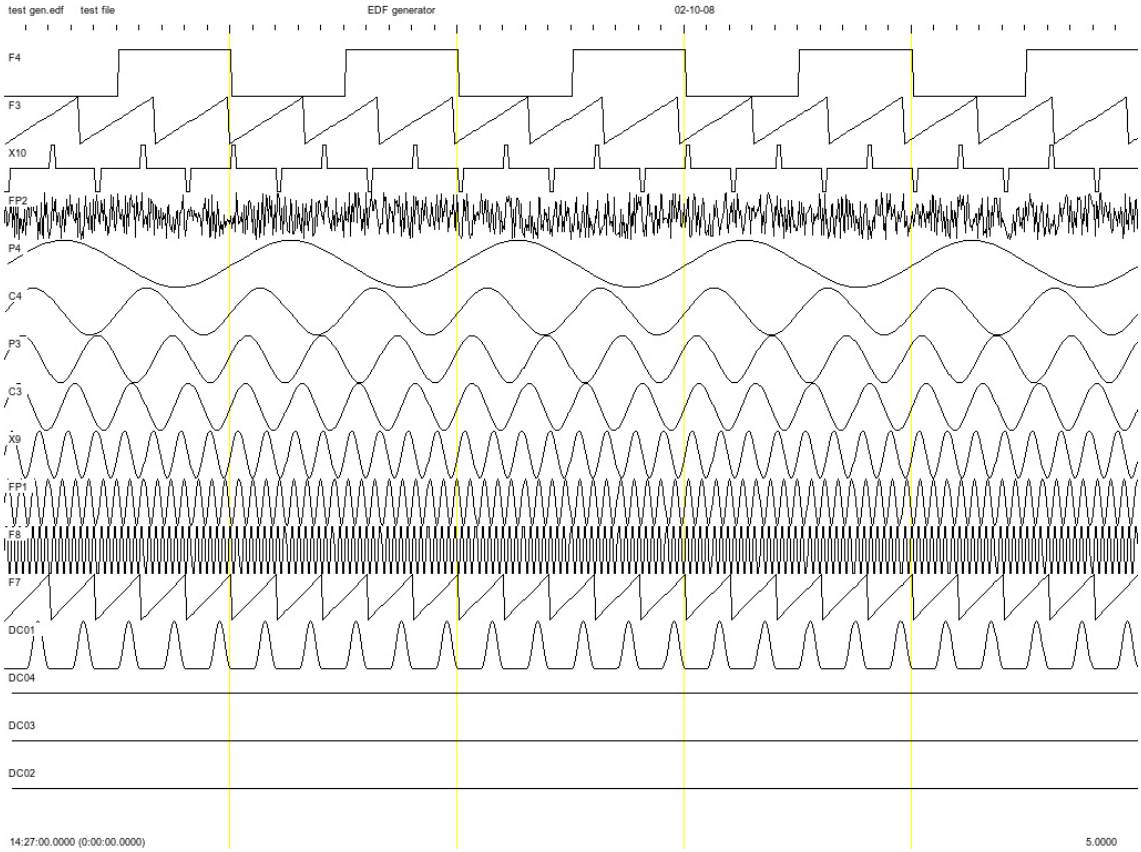

Figure 34: Graphical output of the EDF test file illustrating the 16 test signals used. The signals are as follows; a square wave, two sawtooths, a reversing, periodic impulse function, a noise signal, seven sinusoids with different frequencies, a flattened sinusoid and three DC signals. All the signals had a constant amplitude except the noise signal.

Signals were chosen to create precisely predictable spectra, and were used to look for any errors causing (for example) leakage into adjacent bins. Signals had at least 1024 data points to emulate a 4 second epoch with a sampling frequency of 256 Hz.

When testing the EEG analysis software, a number of errors were found in the EEG analysis software. Spectral leakage was identified when using a fixed amplitude sinusoid. This was due to a very small error in the test signal where the sinusoid generated as the test signal did not contain an integer number of cycles. The signal was recreated to have an exact integer number of cycles, and the error was eliminated. Also, the amplitude of the signal in the frequency domain was lower than expected when tested with the DC offset signal. This was because the power spectrum had not been normalised beforehand, and when corrected, the problem was resolved.

The band power algorithm was tested using a 4 second vector (the same length as a typical epoch, and therefore with a frequency resolution of 0.25 Hz) and containing only 'ones'. This was designed to produce bins each with power of $1\mu V^2/Hz$, and tested frequencies up to the Nyquist frequency 128 Hz (Figure 35).

Index	Frequency (Hz)	Power ($\mu V^2/Hz$)	Boundary
1	0.00	1	
2	0.25	1	
3	0.50	1	Delta lower
4	0.75	1	
...	...		
16	3.75	1	
17	4.00	1	Delta upper
18	4.25	1	
...	...	...	
n	Nyquist Frequency	1	

Figure 35: The band power test array, illustrating the boundaries of the EEG delta band at 0.5 and 4 Hz corresponding to index values of 3 and 17. Band power is therefore 15 $\mu V^2/Hz$, the sum of power in bins 3–17 inclusive (n=15 bins), each of 1 $\mu V^2/Hz$.

The same process was repeated for the other bands, theta, alpha and beta. The output from the software is shown below (Figure 36). No errors were found using this process.

```
Please enter the epoch length in seconds: 4
Each bin will represent 0.25 Hz.

Results
=======
Length of epoch: 4 sec
Sampling Frequency: 256 Hz
Number of data points in epoch: 1024
Minimum Resolvable Frequency: 0.25Hz

absDeltaPower (0.5-4Hz): 15 uV^2/Hz
absThetaPower (4.25-8Hz): 16 uV^2/Hz
absAlphaPower (8.25-12Hz): 16 uV^2/Hz
absBetaPower (12.25-30Hz): 72 uV^2/Hz

absTotalPower: 119 uV^2/Hz

relDeltaPower: 12.605 %
relThetaPower: 13.4454 %
relAlphaPower: 13.4454 %
relBetaPower: 60.5042 %

relTotalPower 0.5-4: 100 %
```

Figure 36: Example of band power testing results.

The spectral edge algorithm was tested by using the same array as the band power. As the total power had already been established from the band power testing (119 $\mu V^2/Hz$), the SEF is 95% of the total power (113.05 $\mu V^2/Hz$). The index value that corresponds to this frequency in the array is position 113, which corresponds to 28 Hz. The process is shown in (Figure 37).

```
absTotalPower: 119 uV^2/Hz

SEF95 totalpower (0.5-30 Hz): 113.05 uV^2/Hz

SEF95 index position: 113

SEF95: 28 Hz
```

Figure 37: Example of spectral edge frequency testing. If the absolute total power between two frequency boundaries is 119 $\mu V^2/Hz$, 95% of this value is 113.05 $\mu V^2/Hz$. The array index value that is closest to 113.05 $\mu V^2/Hz$ is 113, which represents a frequency of 28 Hz.

5.4.2 ECG

The requirements for ECG analysis software were: ability to estimate the RR interval; ability to derive standard ECG HRV parameters in both time and frequency domains, and ability to derive CVT parameters as a proxy measurement of parasympathetic nervous system function. These requirements could be met using existing software, so the process of specification, design and implementation of custom software was not required for ECG data analysis. The data was acquired using the Xltek Neuroworks system.

Data preparation Each 60 second epoch of ECG was visually inspected; if major artefact was present, the epoch was discarded. Manually marked comments and artefacts were then exported via comma separated text file and imported into the PSG database, so that the artefacts can be excluded from the final analysis. Inspection was undertaken using the EDF browser[11] software version 1.48, written by Teunis van Beelen, and covered by the GPL version 2 software license which allows free use providing the author is suitably acknowledged. EDF browser allows viewing and some analysis of electrophysiological signals in EDF format.

RR interval EDF browser was also used for automated measurement and extraction of the RR time intervals (time between each heart beat) of the ECG. The method used in EDF browser was proposed by Christov (2004). A screen shot of the software is shown in Figure 38. The RR intervals were exported in ASCII text file format.

[11] *www.teuniz.net/edfbrowser/*

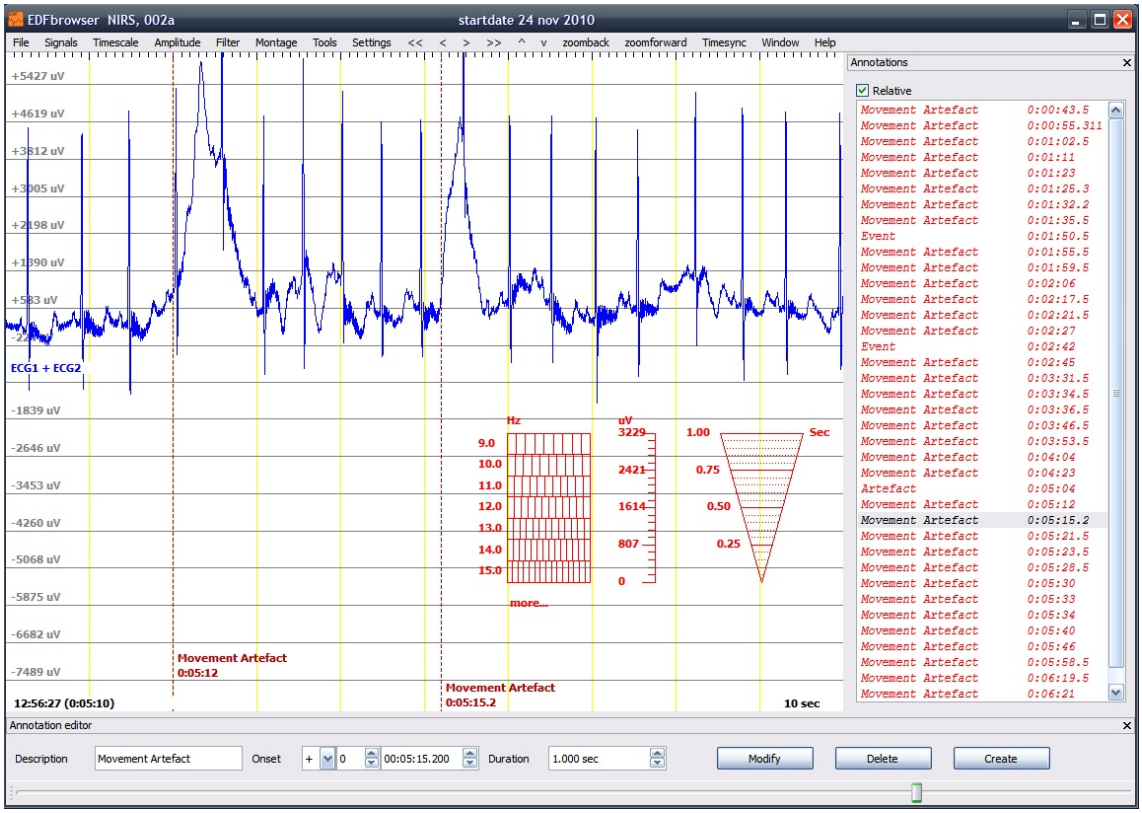

Figure 38: A screenshot of EDF browser main window, showing the ECG recorded from an infant from another study for illustrative purposes. Positions of movement artefacts are manually highlighted with time stamps. The 'rulers' allow measurement of the amplitude, timing and frequency of sections of the ECG. The right hand window shows all the manually marked annotations, and comments that the user has applied.

The Kubios HRV software version 2.0 (Tarvainen and Niskanen, 2008) was used to analyse the RR interval data. It was written by the Biosignal Analysis and Medical Imaging Group (BSAMIG) at the Department of Physics, University of Kuopio, Kupio, Finland. The software was developed in MATLAB® 2008a (The MathWorks, Inc) and was compiled to a deployable standalone application with the MATLAB® Complier 4.8. Its use was covered by the University of Kupio software license.

Parametric methods of spectral density estimation (e.g. autoregression) were available in the Kubios HRV software, but were not used for the final analysis, as the technique assumes the signal is stationary, stochastic and can be described using a small (known) number of parameters (Akaike, 1969), prior knowledge not available in this case. It was decided to use the non-parametric Fourier analysis based methods, as they do not require prior knowledge about the signal to be analysed. Fourier analysis has been used

in many other similar neonatal studies, making comparison easier (Bell et al., 1991; Doyle et al., 2007; Scher, 2004).

ASCII text files were imported into the analysis software. The output was in a comma separated value text file format.

The main window has three panels (Figure 39): one for header data and analysis parameters; one for a time domain plot of the ECG which can be cursored; and one for the results of analyses.

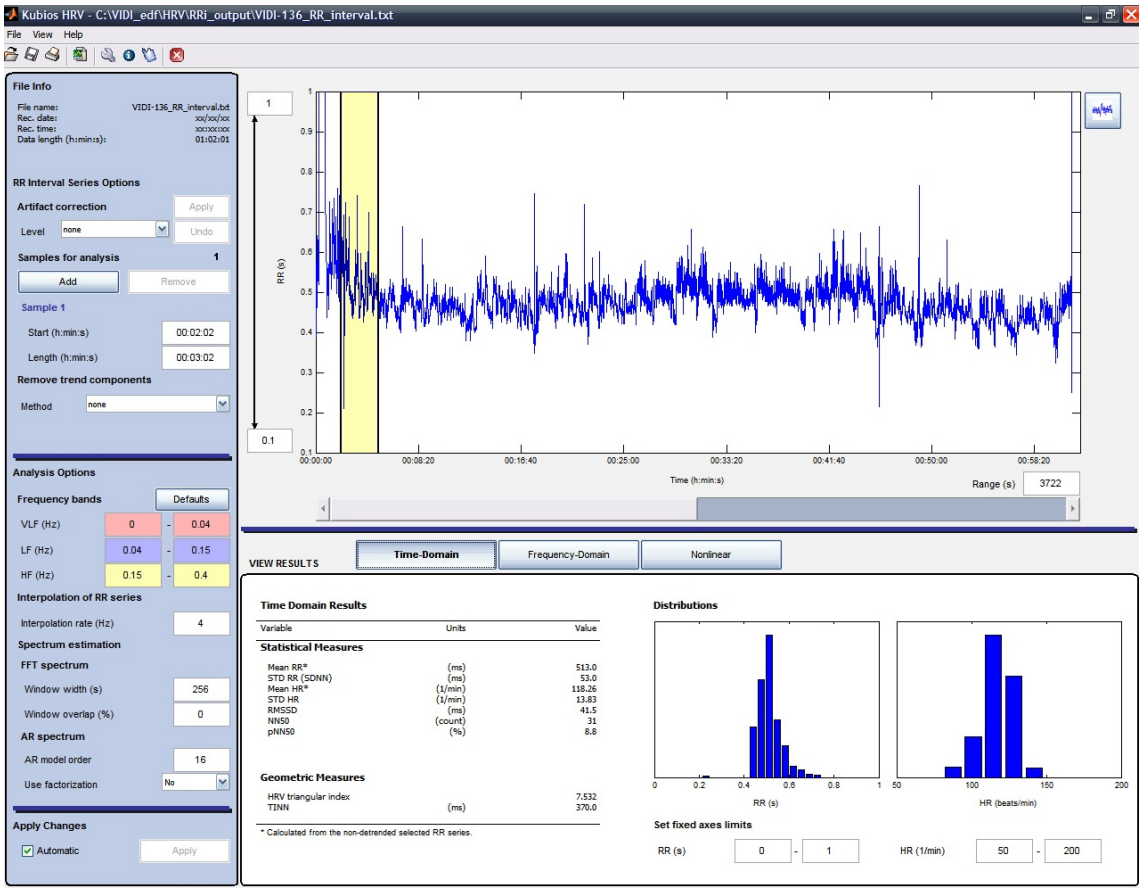

Figure 39: The Kubios HRV software main window. This analysis was from VIDI subject #136, and the epoch analysed was scored as active sleep. The top left section shows file details, any pre-processing smoothing parameters and analysis parameters. The main window shows 60 minutes of RR interval data. Data cursors can select regions to be analysed. The lower panel shows the results of analyses, either time domain, frequency domain or non-linear. In this example, time-domain analysis results are visible.

Time-domain analysis Time domain analyses calculated the mean heart rate (HR, beats per minute, bpm), mean RR interval (ms) standard deviation of mean HR (normal RR peaks, NN intervals) (SDNN, ms) and the square root of the mean of the squares of successive NN interval differences (RMSSD, ms). Histograms of the parameter distributions were plotted (Figure 40).

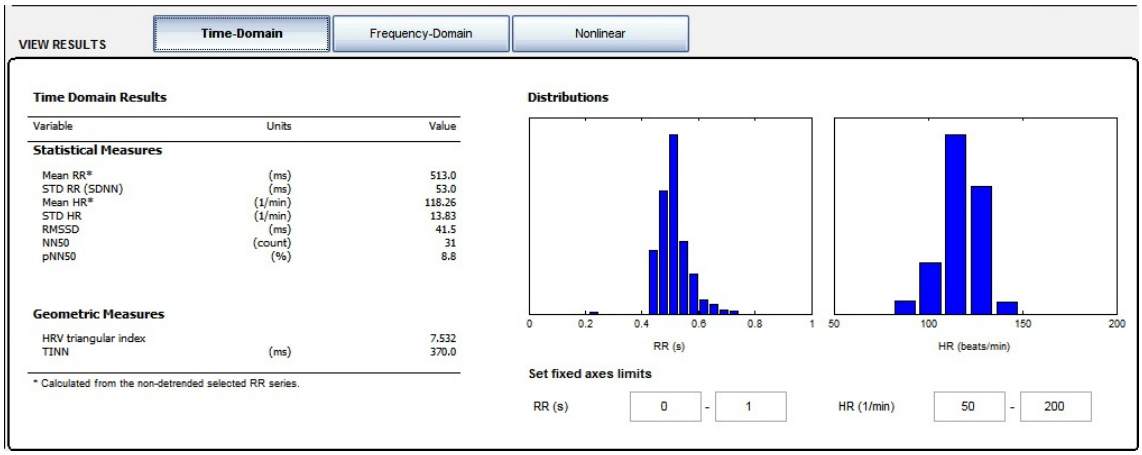

Figure 40: The Kubios HRV time-domain analysis window. This analysis was from VIDI subject #136, and the epoch analysed was scored as active sleep. SDNN – standard deviation of the NN (RR) intervals; HR – heart rate; STD HR – standard deviation of the heart rate; RMSSD – root mean squared standard deviation, NN50 – the number of pairs of successive NNs that differ by more than 50ms (not used for newborns as NN (mean RR) is often much greater than 50ms); TINN - triangular index evaluated through triangular interpolation.

Frequency domain analysis FFT spectrum estimation analysis was conducted, with band power calculated and given numerically and shown in colour plots (Figure 41). The relative power (to total power) of very low frequency, low frequency and high frequency signals (VLF, LF, HF) and the LF/HF power ratio were calculated (see section 3.3.4).

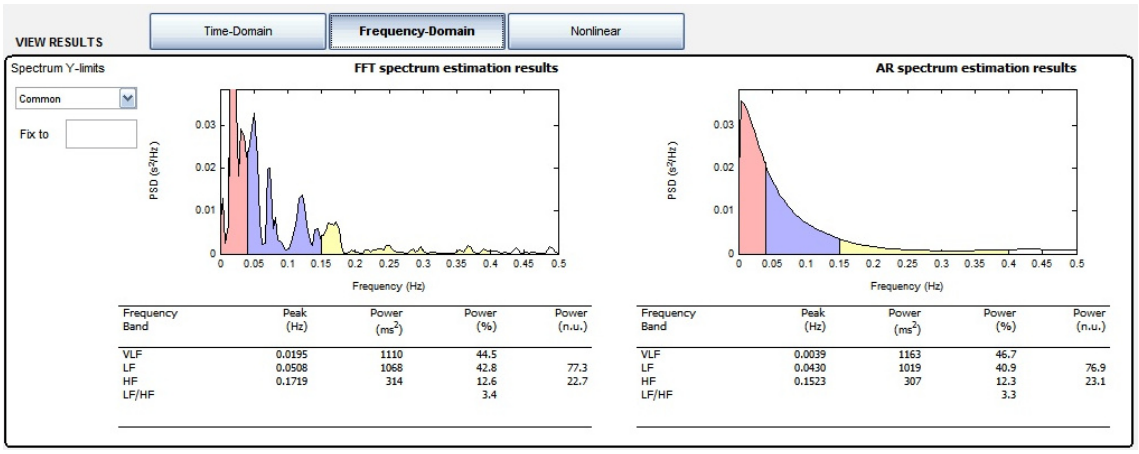

Figure 41: The Kubios HRV frequency-domain analysis window. This analysis was from subject #136, and the epoch analysed was scored as active sleep. The power spectrum estimated using the fast Fourier transform is shown on the left showing the following outcome parameters used this technique (VLF – very low frequency; LF – low frequency; HF – high frequency; LF/HF low frequency/high frequency ratio). A plot of the autoregressive parametric technique is shown on the right for illustrative purposes, but was not used for further analysis.

Nonlinear analysis Poincaré plots were made, giving SD1 and SD2, measures of short- and longer term variability. Figure 42 shows the output of the non-linear analysis, both graphically and numerically, with the Poincaré plot highlighting the cluster of data around the diagonal axis. The last section of the report includes the non-linear Poincaré plots, with the SD1 and SD2 measurements, showing the variation of RR intervals graphically (section 3.3.3).

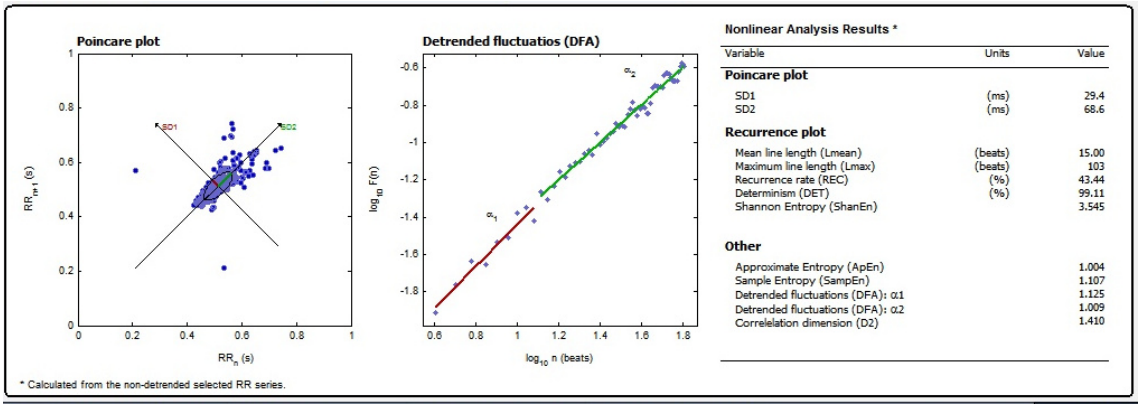

Figure 42: Kubios non-linear analysis window. This analysis was from subject #136, and the epoch analysed was scored as active sleep. SD1 and SD2 are the standard deviations of the Poincaré plot.

5.4.3 CVT

The Neuroscope™ TONE software[12] version 3.14f (Medifit Instruments Ltd, Enfield, England, was used to calculate vagal tone measurements, based on the method proposed by (Julu, 1992). Neuroscope™ is proprietary software, and was made available for use by Dr Stig Hansen, Department of Clinical Physics and Bioengineering, Institute of Neurology, Southern General Hospital, Glasgow.

The software works on the principle that heart rate can be predicted from measurements of parasympathetic activity from the vagus nerve (Katona et al., 1970), and is done by analysing the RR intervals from the ECG. By comparing QRS complexes to a template generated from the initial stages of a recording, if such complexes are similar enough to this template a 1 mV pulse is generated. The time between these pulses is equivalent to the RR interval. These pulses are then sent into two circuits, a high pass limb and a low pass limb. The high pass tracks the incoming signal faithfully, whilst the low pass produces a damped version of the signal. If variability is low, there is only minor damping so the signals in each limb are similar, and the Neuroscope™ output is small, or zero. If variability is high, then more damping occurs, and the difference between the two limbs is greater, and the CVT score higher. A constant heart rate, with no variability would give an output of zero. The measured output is then compared with experimentally derived data, and a score for vagal tone presented (Julu and Little, 1998). A more detailed description of the methods of CVT estimation can be found in section 3.6.1.

To use the Neuroscope™ software, ECG data was exported from the Xltek software in EDF format. To make these files directly compatible with the Neuroscope™ software, a custom made conversion program, written and applied by Dr Stig Hansen, was used. Although I did not have access to this code, the program performed two operations, removal of DC shift (a baseline removed from each sample point) and application of a simple five point smoothing algorithm (all points having equal weight). The output file was then be loaded into the Neuroscope™ software.

[12]www.medifitgroup.com/Neurology.htm

As the software was originally designed to run on a standard PC running Microsoft MS-DOS and was not Microsoft Windows XP compatible, it was run within the DOSBox[13] emulation application. A screenshot of the software can be seen in Figure 43.

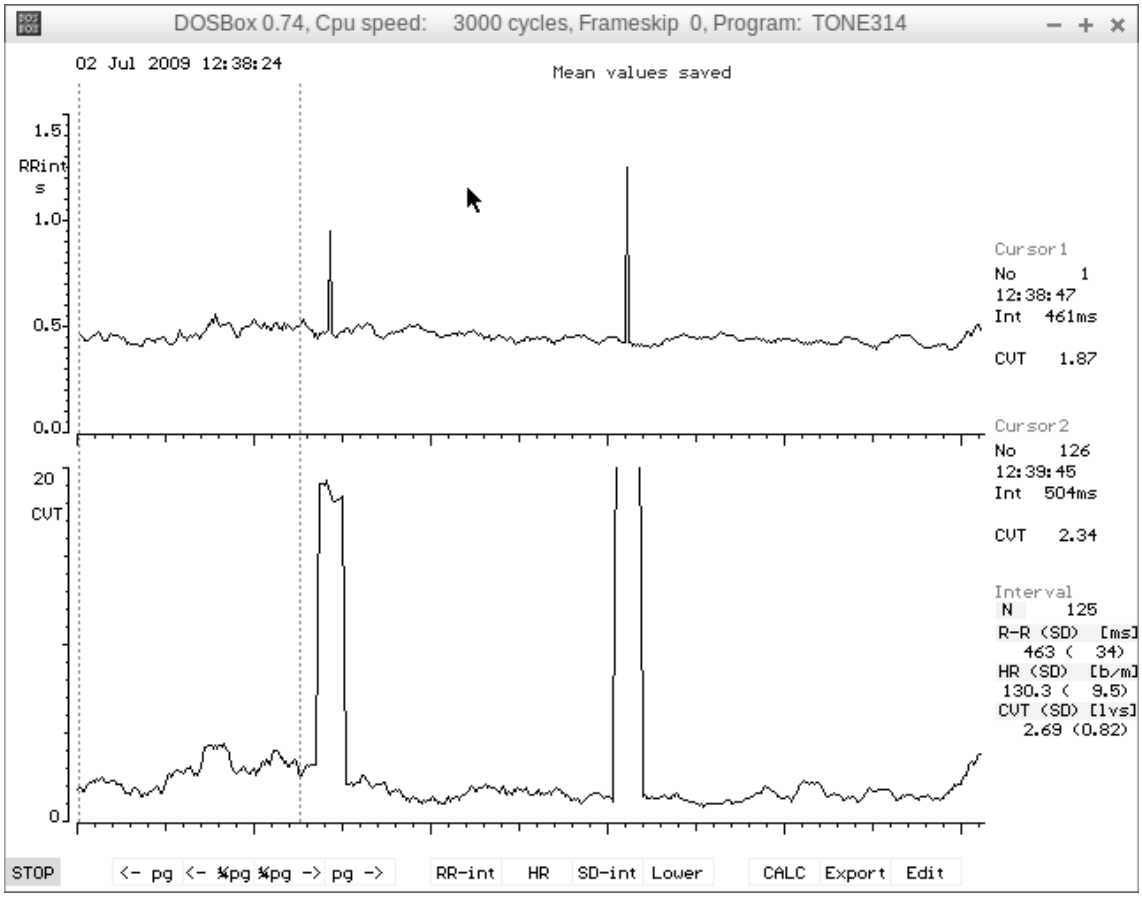

Figure 43: The Neuroscope™ software running in DOSbox showing data from VIDI study number #136, during active sleep. The top graph shows the changes in RR interval. As the software measures the changes in RR variability to produce an estimate of CVT, the bottom graph mirrors this but matches the output with an experimentally derived linear scale. Here the user has selected an epoch, shown as the two dotted lines, and the CVT estimates are shown on the right hand side. The CVT values for both cursor positions and the average CVT between the two cursors are shown below this.

Testing The CVT Neuroscope™ software was tested using a series of pulses generated using the function generator spreadsheet described above (Figure 33). The first signal was designed to test whether the filters could distinguish higher or lower than normal frequencies: this was important as the neonates heart rate is normally up to twice that of an adult. The low frequency pulse train was equivalent to a frequency of

[13] www.dosbox.com

0.34Hz or approximately 20 bpm, and the high frequency pulse train was 3.34Hz or approximately 200 bpm (Figure 44). This testing highlighted a limitation in the software at high frequencies, and Dr Hansen accordingly amended his conversion software.

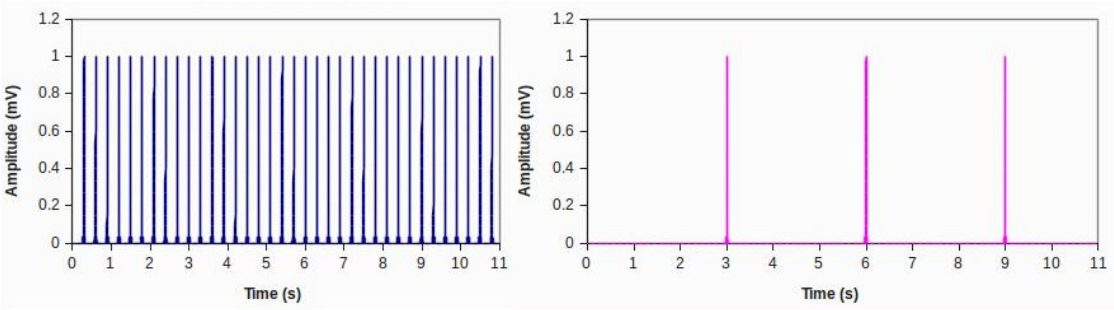

Figure 44: Pulse trains for testing the CVT software. The left hand figure shows the high frequency pulses (200 bpm), whilst the right shows the low frequency signal (20 bpm). Both frequencies were chosen to match extremes of heart rate of a newborn infant.

The second test signal (Figure 45) was designed to test whether the software could still identify the pulse train (frequency 0.5Hz, or 120 bpm) when there was significant positive or negative drift on the signal as was sometimes the case with the subjects in this study. In both cases, the software accurately identified the correct location of the pulses i.e. the simulated R wave.

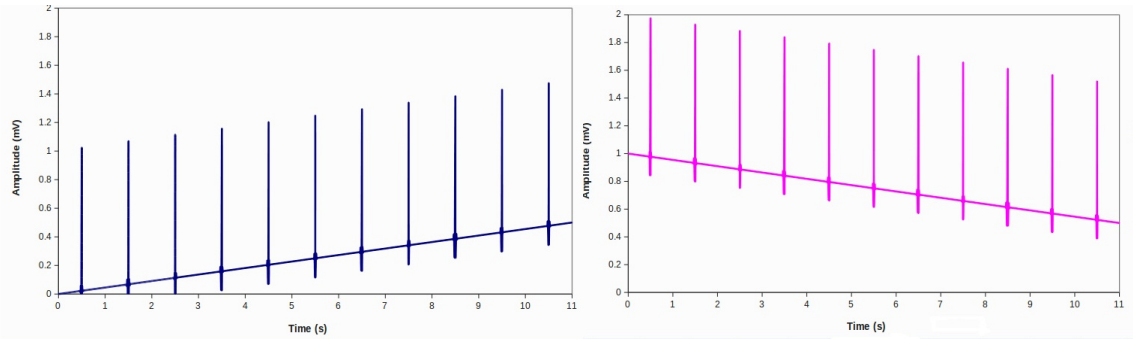

Figure 45: Pulse trains to test how the Neuroscope™ software deals with drift. The left hand figure shows a low frequency signal (~20 bpm) with a growing baseline. The right hand figure shows the same frequency signal with a decaying baseline.

5.5 Databases

5.5.1 VIDI Study Database

The VIDI study database was necessary for four reasons. Firstly, there were around 75,000 data items associated with the study: 155 patient records with up to 500 variables per patient. Secondly, to minimise the level of data management, and reduce the amount of work required before the dataset could be closed, a means of error checking on the front end interface was required. Thirdly, the database had to be accessible on multiple NHS Greater Glasgow & Clyde PCs, but still include security features and comply with the Data Protection Act. Patient identifiers were not stored and the dataset was not used outside the realm of the health board. It was written in Microsoft Access 2003.

The main purposes were to help in the collection of case report form (CRF) data, ease the transfer of data to an electronic format, help deal with any data management issues, and finally to output the corrected datasets for statistical analysis.

Its structure was relational, i.e. the dataset was split over a number of tables linked by the unique identifier, or primary key (study number), thus avoiding duplication, and giving faster access as not all the data is needed at one time. A dual data entry system was employed so that the same infant could not be registered twice into the system. This involved entering the study number twice on the recruitment screen, where the system checked the uniqueness of the number entered. This can be seen in Figure 46.

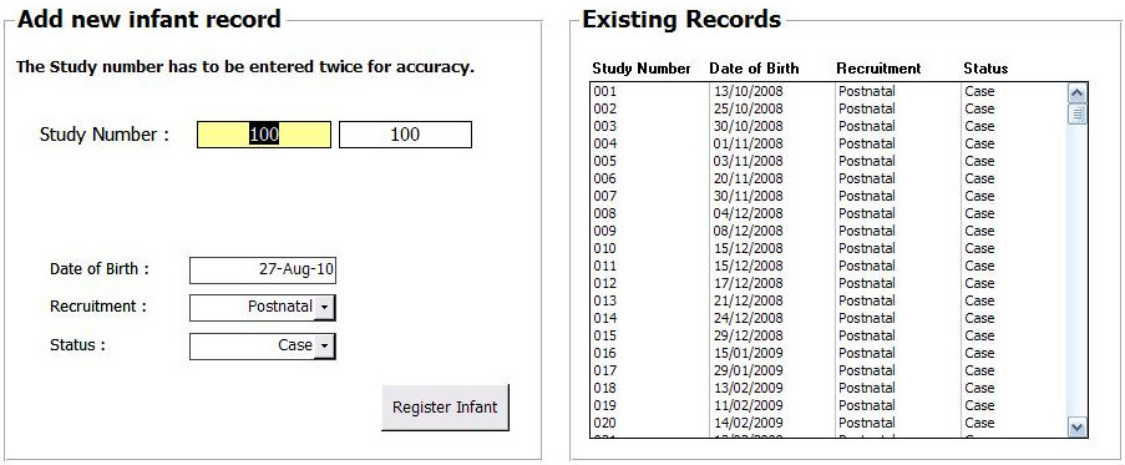

Figure 46: The registration screen for the VIDI database. The user enters the study number to be registered twice (the first cell being highlighted in yellow), enters the date of birth, recruitment type and the exposure status. The system then checks if the study number has been registered already, and allows the user to continue if not.

Correct registration of the study number is important to maintain referential integrity in the database. To avoid using an inefficient flat file approach, where all the data is stored in a large table and where there is likely duplication of information, the entire dataset was broken down into a number of smaller tables, and linked via a key. A key is a unique identifier (usually a number) that links one or more tables together. In this database, the study number was a primary key, in that it was a unique identifier of a infants record. Other tables called 'child' tables were then linked to this primary key with foreign keys (a field in a sub-table that matches the primary key) so that each study number could have numerous sub-tables. An example of this linking via keys is shown in Figure 47.

This gives the database flexibility in that once a infant has been registered it can have many linked tables associated with it. An important factor is referential integrity between these tables, in that a study number cannot be removed without first removing the child tables so a record could not exist in a sub table without a link to its primary key.

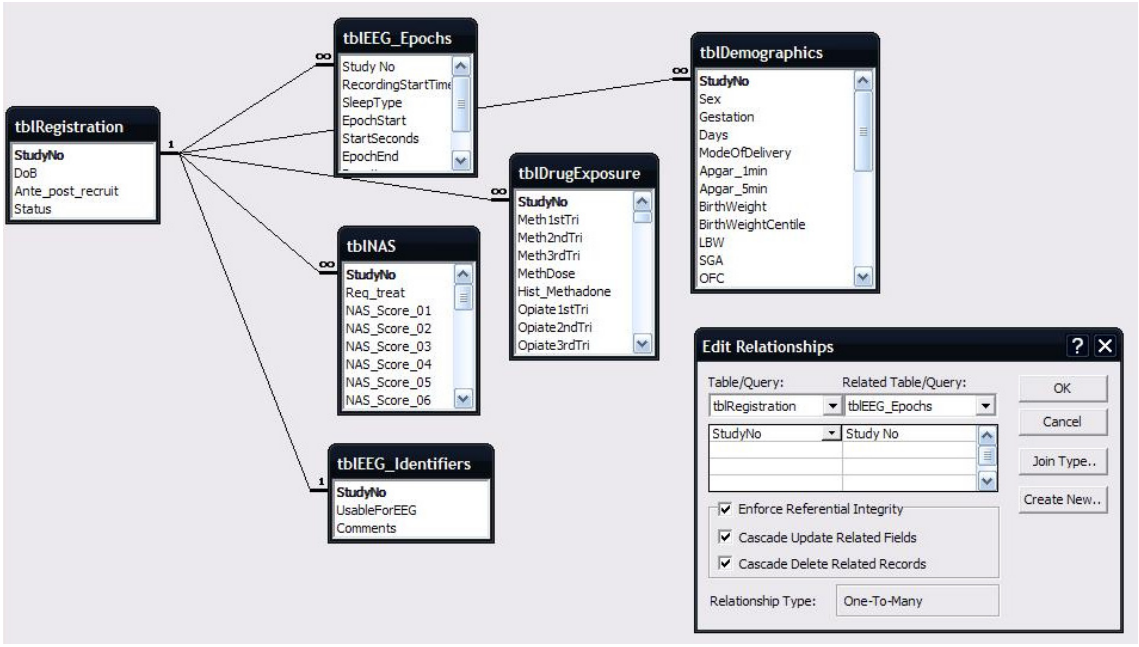

Figure 47: The relationship diagram of the VIDI database showing the linking between the primary key in [tblRegistration] and the sub-tables. Note that referential integrity was enforced so that child tables cannot be removed without first removing the record from [tblRegistration]. The window in the bottom right hand corner shows the details of the relationship between [tblRegistration] and [tblEEG_Epochs], in that they are linked by the primary key [StudyNo], and have a one to many relationship i.e. a study number can have many EEG epoch records.

One of the requirements of the system was that it had to be accessible to multiple users concurrently. For this a server-client model with a separate user interface (stored on the client machine) from the back-end database (stored on a file server) was employed. Although Microsoft Access is not designed for large numbers of concurrent users, it can handle small numbers (up to 5) using this client server model. Record locking was enforced so that users could not work on the same record at the same time, so it did not have the power of a full transaction server like Microsoft's SQL Server.

The user interface was designed for easy navigation between patient records and also to restrict what the user could enter in order to keep the underlying data accurate and consistent. The interface was constructed in Visual Basic for Applications 6.3.8863 (Microsoft Corporation, Redmond, Washington, USA), and linked with the back-end database using Object Database Connectivity (ODBC, Microsoft Corporation, Redmond, Washington, USA). Although ODBC is old compared to object linking embedding (OLE), it is compatible with many analysis systems, for easy data transfer

across different operating systems i.e. Windows to Linux.

Paper case report forms (CRFs) were used to collect data from the medical records, and were transferred into the database. This was done as paper is more convenient for collecting data when no computer is to hand, and it also gives a hard copy of the information in case of electronic data loss.

The paper CRF was designed to mirror the database user interface, and a combination of drop down lists and restricted text input boxes, supported an interface that was easy to use, but adequately protected from data entry mistakes. Free text could be stored in cases where the input options were not applicable so entries could still be successfully coded but flagged up during the data management process. An example screen shot from the database is shown in Figure 48.

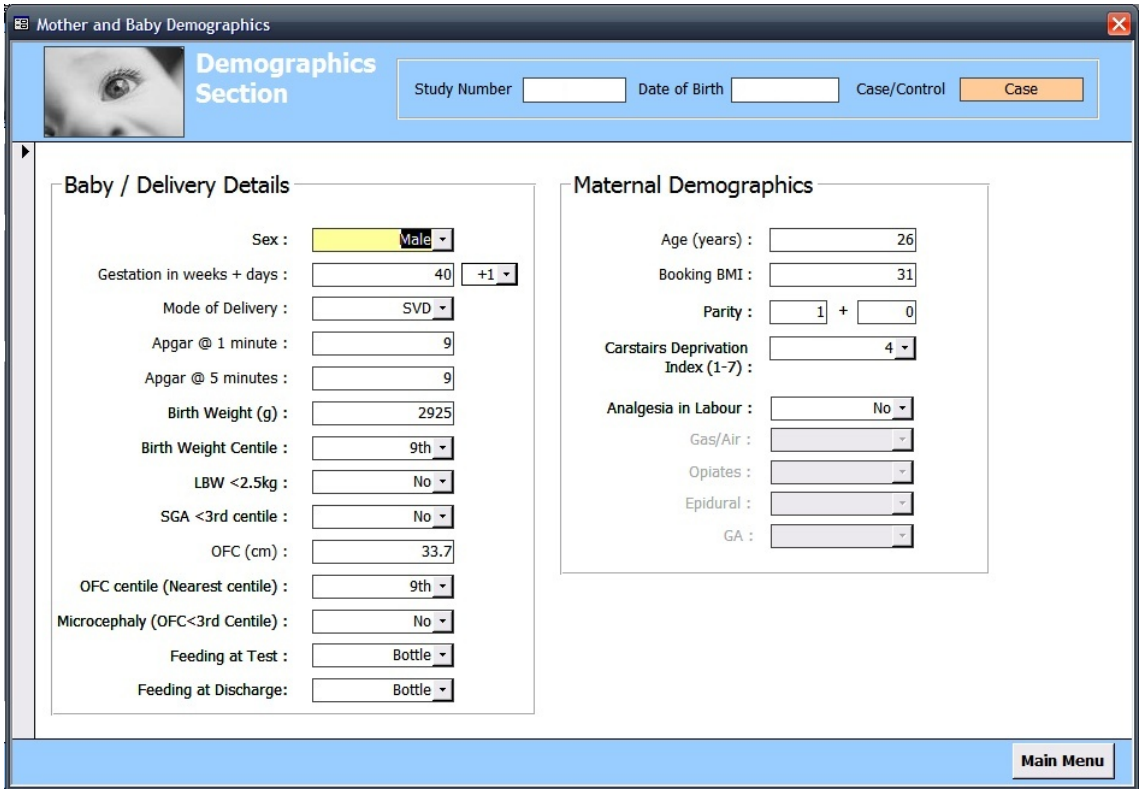

Figure 48: The VIDI database. This section shows the demographics form. Drop down menus were used to avoid typographic errors during data entry. LBW – low birth weight; SGA – small for gestational age; OFC – occipital frontal circumference; BMI – body mass index

On completing the study, there were very few corrections required before closing and locking the dataset to start the statistical analysis; this highlights the adequately

controlled nature of the data entry. Corrections required were usually missing data fields, as the GUI stopped the entry of unformatted data.

5.5.2 PSG Study Database

A second database was written in Microsoft Access 2003 to hold the PSG data for those VIDI study infants from whom PSGs were recorded.

A folder was created for each patient containing the results of analysis for each channel and the results stored as individual text files. Each file corresponded to a channel in the EEG montage, and was imported into the database to allow cross channel averaging and analysis. Each channel was merged to create one large record for each patient.

This database held output parameters from the EEG analysis and the results of the sleep state scoring, bringing both the classical EEG analysis and the spectral analysis together. Highlighted artefacts were also stored, with their time locations, giving an overall picture of the individual patients' results. It is from this database that both the entire dataset for each patient was analysed, as well as the in-depth spectral analysis for each individual patient.

5.6 Summary

Software development was a major element of this project. Initial research of available software led to the decision to develop custom software, or to use proprietary applications. Where custom software was developed, recognised software engineering processes - planning, requirements, development, testing and distribution - were followed wherever possible, so that the output was of an acceptably high standard with optimal reliability.

By writing custom software, I gained a comprehensive understanding of the tools, programming infrastructures, and software methodologies. This in turn led to a better understanding of the strengths and weaknesses of analytical tools used elsewhere, as well as a greater appreciation of the limitations of the commercially available packages.

The combination of software solutions employed enabled the appropriate acquisition, processing, storage and analysis of the very large dataset used in this study.

6 Study Design

6.1 Introduction

This chapter introduces all aspects of the study not covered in more detail in the later chapters on ECG or EEG. It includes the study protocol and description of the recruitment, patient demographics and toxicology results. This study was run as part of a larger study, entitled 'Vision in Drug dependent Infants' (VIDI), examining the effects of methadone exposure upon visual development in infancy. The study described in this thesis incorporated a subset of subjects from the VIDI study population who additionally underwent polysomnography. Collaboration proved highly beneficial for both studies; patient recruitment, collection of urine and meconium samples, and medical history were performed by Dr Laura McGlone (neonatal trainee who undertook the VIDI study) and database design and development of custom analysis software for the VIDI study were carried out by myself.

6.1.1 Study Protocol

The study was undertaken in the neonatal unit at the Princess Royal Maternity (PRM) in Glasgow. The hospital provides support for the majority of drug misusing women in the area. Drug-misusing mothers who had been prescribed substitute methadone in pregnancy were approached, and asked for consent for inclusion in this study. Exclusion criteria included significant prematurity (>36 weeks gestation), congenital abnormalities and/or neonatal illness.

The investigation followed the format of a case/control study where drug-exposed neonates were compared with matched unexposed neonates, following the same exclusion criteria. To minimise the confounding effects of birth weight (±250 grams), socio-economic status (socio-economic DEPCAT group ±1; (McLoone P. 2004) and

gestation (completed week of gestation) revealed in a pilot study, control infants were selected by these criteria.

Ethics approval was obtained from the Glasgow Royal Infirmary Research Ethics Committee prior to the start of the study (REC reference number 08.S0704.40), and approved by the Greater Glasgow and Clyde Health Board (Project number YN 08 NN 325). The study was conducted in compliance with the principles of 'Good Clinical Practice' (GCP). Recruitment started on the 15th October 2008, and ended on 30th March 2010.

6.1.2 Recruitment of Subjects

Mothers of infants suitable for entry into the study were identified by Dr McGlone in conjunction with the midwifery staff on the postnatal wards of the PRM. Interviews were conducted with the attending midwife, and after a discussion describing the study, mothers were given verbal and written details to consider if they wished to be enrolled. If in agreement, a copy of the consent forms for both the mother and the study records were signed, and a patient information sheet given. Copies of these consent sheets were stored in the infants' notes, and kept as part of the study documentation. The mothers' general practitioners were also informed that they had been enrolled in the study.

6.1.3 Data Collection

Infant drug exposure during pregnancy was determined from a combination of confidential interview with the mother (all conducted by Dr McGlone), and review of the maternal records including urine toxicology obtained during pregnancy (see below). Details concerning smoking and alcohol use during pregnancy were also collected. Socioeconomic group was defined using the Carstairs DEPCAT scoring system (McLoone P *et al*, 2004). This system uses data from the national 2001 census to define geographical areas in relation to socio-economic groups. DEPCAT scores are based on postcode, and defined by factors such as the presence of overcrowding, unemployment,

car ownership, social class (based on occupation). The most affluent area has a score of one, whereas the most socially deprived regions score seven.

Neonatal data collected included birth weight, gestation, sex, head size (occipito-frontal circumference – OFC), Apgar scores at birth, method of delivery and method of feeding. OFC was measured at the time of recording of electrophysiological data.

6.1.4 Assessment of NAS

NAS severity was measured during the neonates stay in hospital, including any necessary pharmacological treatment. NAS severity was assessed using the modified Lipstiz scoring method which is routine practice at the PRM (Lipsitz, 1975). Twice daily scoring by midwifery staff on the postnatal ward was undertaken with two consecutive scores determining a need for pharmacological treatment (see section 1.2). All treatment was recorded as well as the duration of the neonates stay in hospital.

6.1.5 Confidentiality

To comply with both the NHS Greater Glasgow and Clyde policy on data protection and the principles of GCP, study data was stored in a password protected database (see section 5.5.1). Enrolled subjects were given unique study numbers, with the look up table of numbers to names being stored on paper in a locked filing cabinet at the PRM. Access to the database was restricted to the users only.

6.1.6 Toxicology Assessment

In addition to maternal urine toxicology at 36 weeks' gestation, neonatal toxicology was undertaken by analysis of urine and meconium (the neonates earliest stool). These samples were collected during the electrophysiology recording session, and sent to the appropriate laboratory for analysis. The urine samples were analysed by the regional toxicology laboratory based at Gartnavel General Hospital in Glasgow. The Abbot

enzyme multiplied immunoassay technique (EMIT) was used. The meconium samples were analysed under the supervision of Dr Gail Cooper, based at the Department of Forensic Medicine and Science at the University of Glasgow. Enzyme-linked immunosorbent assay screening plus phase and liquid-liquid extraction were used in conjunction with gas chromatography-mass spectroscopy to detect the major drug groups including methadone exposure. This method also included detection of elevated acid ethyl esters, indicative of prenatal alcohol exposure. A level greater than or equal to 10,000 nanograms/gram was used to indicate excessive alcohol consumption during pregnancy (Gareri et al., 2008).

6.1.7 Combined Drug Exposure

The results of the toxicology assessment for both the mother and the neonate as well as maternal medical case note review and confidential maternal interview were used to establish an accurate picture of *in utero* drug exposure. Positive exposure was defined as a positive result from any of the toxicology samples, or the maternal history. Prescribed maternal methadone dose at delivery was also recorded.

6.1.8 Electrophysiology Recording

Recordings were made within the first 48 hours of life including PSG and visual evoked potentials. This is described in detail in section 7.2.1. Following completion of the recording the neonate was returned to his or her mother in the post natal ward, and the mother thanked for their participation in the study. No payment was made to any participant.

6.2 Results

6.2.1 Excluded Data

Although 55 subjects were recruited into this study, only 45 were included in the final analysis. 6 cases and 4 controls were excluded as polysomnography was not possible. A more detailed account of the reasons why this is the case can be found in EEG results section 7.3.1.

6.2.2 Neonatal and Maternal Demographics

A summary of the data collected for the neonate and maternal demographics is shown in Table 10 and statistical comparisons between groups are also shown where necessary. During recruitment, the neonates were frequency matched on birth weight (+/- 250g), gestation and the maternal socio-economic status (DEPCAT score).

The other variables, when related to exposure, and a source of possible confounding were tested using either Mann Whitney U tests, or Fischer exact tests depending on the data type. As long as unmatched variables were similar they cannot be confounders.

	Cases median (n=20)	Controls median (n=25)	p-value	CI (95%)
Neonatal Details				
Sex (male/female)	9 (45%) / 11 (55%)	12 (48%) / 13 (52%)	0.84	(0.23, 3.63)
Birth weight (grams)	**3078**	**3125**	**0.08**	**(-395, 318)**
Gestation (weeks)	**39.5**	**39.1**	**0.36**	**(-3.4, 1.0)**
Head circumference – OFC (cm)	34.3	34.5	0.44	(-1.3,0.5)
5-min Apgar score	9	9	0.37	(-1,0)
Mode of Delivery				
Spontaneous Vertex Delivery (SVD)	15 (75%)	17 (68%)	Not related to exposure	
Ventouse	2 (10%)	1 (4%)	Not related to exposure	
Lower Uterine Segment Caesarean Section (LUSCS) - Elective	1 (5%)	5 (20%)	Not related to exposure	
LUSCS - Emergency	1 (5%)	2 (8%)	Not related to exposure	
Other	1 (5%)	0 (0%)	Not related to exposure	
Feeding & Neonatal Length of Stay				
Bottle/Formula	4 (20%)	3 (12%)	Not related to exposure	
Breast	14 (70%)	21 (84%)	Not related to exposure	
Mixed	2 (10%)	1 (4%)	Not related to exposure	
Length of Hospital Stay (days)	8.6	2.6	Not related to exposure	
Maternal Details				
Maternal Age	30	24	0.11	(-1.0,8.0)
Maternal Smoking	19 (95%)	14 (56%)	0.003	(5, 50)
Maternal BMI	24	25	0.39	(-6,2)
Maternal DEPCAT	**7**	**5**	**0.31**	**(0, 2)**
Maternal Alcohol consumption	2 (10%)	1 (4%)	0.16	(0.7, 12.0)

Table 10: Neonate and maternal demographic data. The table shows median values for the neonate, covering delivery and maternal information. Birth weight, gestation and socio-economic status were all matched during recruitment (highlighted in bold). Other factors such as mode of delivery and feeding were not related to the exposure. Where factors could be potential confounders, statistical tests were performed comparing the two groups.

Comparison of the two neonatal groups on the matched variables showed no statistical difference for birth weight (cases 3078g vs controls 3125g; Mann-Whitney p=0.08), gestation (cases 39.5 weeks vs controls 39.1 weeks; Mann-Whitney p=0.36) and maternal socio-economic status (DEPCAT score), (cases 7 vs controls 5; Fischer exact p=0.31).

For the unmatched variables, no significant difference was shown for head circumference (OFC), although the cases had marginally smaller heads (cases 34.3 cm versus controls 34.5 cm; Mann-Whitney p=0.44) or Apgar scores (cases 9 vs controls 9; Fischer exact p=0.37). Although not related to exposure, noticeable was that most of the neonates, cases 70% (14/20) vs controls 84% (21/25), were bottle fed, not the recommended breast fed.

A higher proportion of drug exposed mothers smoked during pregnancy (cases 19/20 95% verses controls 14/25 56 %). Although this may be indicative of lower birth weights (Abel, 1980), this was not evident in this dataset.

Maternal BMI was marginally lower in the cases (24) vs controls (25); Mann-Whitney p=0.39). Alcohol consumption during pregnancy was higher in the cases (10% 2/20) vs controls (4% 1/25).

Length of stay of the cases was over three times greater (cases 8.6 days vs controls 2.6 days) indicating the significant increased clinical time required to manage these neonates.

For a frequency matched case control study like this, there is no need to use matched-pair analysis such as conditional logistic regression as there is no need to control for the matching variables when they are not associated to the exposure, as they could not be potential confounders. For this reason, conditional logistic regression was not performed including any of the matched variables. However, Table 10 shows that none of the unmatched variables, that were related to exposure, were statistically different, apart from smoking. Consequently a comprehensive logistic regression would be performed for any future publication of results, exploring the role of smoking in the analysis.

6.2.3 Drug Exposure Results

Details of drug exposure are shown in Table 11. All the neonates defined as cases had been exposed to methadone *in utero*. Other opioids (60%) and cannabis (55%) were found in over half of the study subjects. Of the total number of cases, 5 (25%) were exposed to methadone only, that is no trace of other exposure was found.

Exposure Type	Number	% of total (20)
Methadone	20	100
Other opioids	12	60
Benzodiazepines	11	55
Amphetamines	5	25
Cocaine	2	10
Cannabis	11	55

Table 11: Other drug exposure amongst the methadone-exposed group. All the cases had been exposed to methadone.

6.2.4 NAS Assessment Results

NAS scores for the cases are shown in Table 12. 4 (20%) of these neonates went on to require pharmacological treatment for symptoms of withdrawal. This value is lower than expected as it is more normal for around half of neonates exposed to methadone *in utero* (Dryden et al., 2009) to show signs of NAS. None of the neonates showed evidence of seizure activity.

Maximum NAS Score	Number (n=20)
1-4	14
5	3
6-10	3

Table 12: Number of cases grouped by their NAS scores.

6.3 Summary

The purpose of this chapter was to describe the study and the factors that potentially affect the electrophysiology that will be covered in greater depth in the following chapters. Of note, it is important to highlight that the two groups have been matched on a number of factors making them comparable. Methadone is the common exposure to all of the cases, and none of the controls. Even though multi-drug exposure was common amongst the cases, 25% had been exposed to methadone only, and no trace of other drugs found.

7 EEG Experiments

7.1 Introduction

This chapter covers the methods of recording, interpreting and analysing the EEG data then presents the findings.

7.2 Methods

7.2.1 PSG Experimental Set-up

The recordings were made within the Neonatal Unit at the Princess Royal Maternity Unit, in Glasgow. The room used was small and windowless, with only minimal outside noise, thus making it suitable for sleep studies. The room temperature was warm, to aid the neonate sleeping, and kept at a constant level. As well as the neonate under investigation, present during the recordings were medical physicist (Richard Boulton – RB) and neonatologist (Dr Laura McGlone - LMcG), and if they requested, the parents/guardians. The study status of the neonate i.e. methadone-exposed / unexposed, was known prior to the recording. The neonate was then fed (if this had not happened prior to the recording). A urine bag was attached to the neonate (by LMcG) so that a sample could be collected after the recording for analysis. Finally, the neonate was swaddled, and helped to settle in the cot, in the supine position.

As the VIDI study involved two branches, visual and neurological, the visual part would take place first, with the application of three scalp electrodes, followed by recirding of flash and flicker visual evoked potentials (VEPs). On completion, the neonate was then be prepared for one hour of polysomnography (by RB). This involved the application of a full set of electrodes (as described below), necessary for a sleep study. Impedance

measurements were made at the beginning and end of each recording, and the results were embedded into the PSG recording.

The lights were dimmed, and when the neonate was suitably settled, recording of the PSG began. The neonate was videoed for the duration of the recording to aid in the visual interpretation of the sleep states at a later date. Frequent notes were also made, highlighting any significant factors such as movement or artefacts, that may affect interpretation.

On completion of the recording, the lights were switched on again, and the electrodes removed. Any urine sample collected, and meconium gathered beforehand was sent for toxicological analysis, and the neonate was returned to its mother. The neonates were given no medication prior to or during the recording.

The equipment used for the polysomnography was the Xltek HD Ambulatory system (model EMU128FS head box). This is a portable system that integrates up to 24 channels for data acquisition with video capability. It was used to record 12 channels of EEG plus EOG, EMG, ECG and changes in respiration. EMG was included to measure muscle activity under the jaw to indicate any sucking movement that is important in sleep state identification. Respiratory measurements were performed using a piezoelectric stress gauge wrapped around the neonates chest, and were used in sleep state identification. An example of a neonatal set up for polysomnography is shown in Figure 49.

The Xltek HD system was attached to a standard laptop PC running Microsoft Windows XP as the operating system, and the Neuroworks™ software for recording. A more comprehensive description of the Neuroworks™ software can be found in section 5.2.

Considering that the recordings included video, the sampling frequency was set to 256 Hz, giving a reasonable balance between resolution and file size. As each PSG was approximately one hour in duration (including calibration and impedance testing), the resulting file size was approximately 600 mega bytes (Mb) per recording session.

Figure 49: A settled infant during a PSG, showing the recording headbox (top left corner), multiple electrodes, and a scalp net to hold the electrodes in place.

EEG Electrodes

The montage used was a standard neonatal montage, recommended by the American Clinical Neurophysiology Societies guidelines for continuous EEG monitoring in neonates (Shellhaas et al., 2011). The montage details are shown in Figure 50.

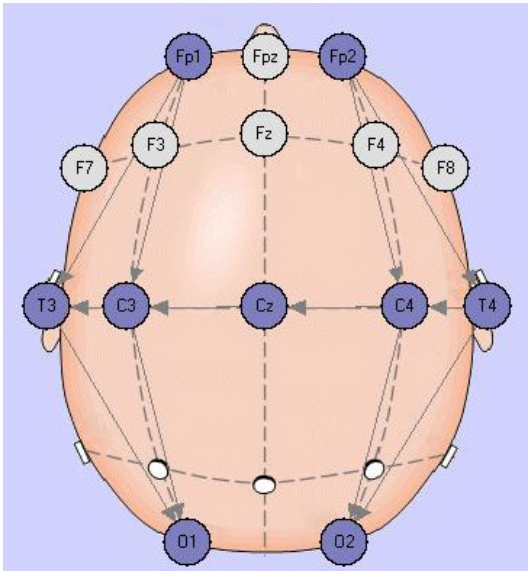

Figure 50: Montage details for neonatal PSG (from the Neuroworks™ software), in accordance with the international 10-20 system.

Firstly, the site for each electrode was cleaned using an alcohol swab and abraded with NuPrep. Silver-silver chloride electrodes with Ten20 conduction paste were then attached to the scalp and held in place with a gauze material. When all the EEG electrodes had been applied, and impedances tested, a scalp net was used to hold them in place during the recording.

Other electrodes

The ECG was recorded from three leads, attached in accordance with the modified three electrode biopolar system, as described in section 3.2.2. They were attached on the right (R) and left arms (L), and the left side of the abdomen (F) respectively. The resulting R wave deflection was upwards. Using two disposable stick-on electrodes, muscle activity (EMG) was recorded under the chin. Ocular activity (EOG) was recorded to identify blink activity with the left electrode being placed above the outer canthus of the left eye, and the right, below the outer canthus of the right eye. Finally, the respiratory band was placed around the rib cage and above the nipple line.

Pre-recording Filters

The Xltek trex headbox comes with a built in anti-aliasing filter. The filter cut-off is 40% of the sampling frequency (fs), or 80% of the Nyquist frequency. For a 256 Hz sampling frequency, signals of frequencies higher than approximately 100 Hz would have some degree of aliasing. The manufacturer's documentation shows that this was the only filtering that occurs during the recording. Digital filtering was available whilst viewing the recording e.g. notch, high and low pass filters.

Signal Quality and Recording Practicalities

The Xltek headbox was calibrated prior to each recording session using the inbuilt test signal module, which applied a predefined set of test signals to the amplifiers, and examining the output for noise and drift.

Impedance measurements were made using the Neuroworks™ software prior to the onset of recording, and electrodes would be reapplied/altered if levels were greater than 10 kΩ.

Recording EEG in the neonates is difficult, and when they show the early signs of NAS even more so. It was not unusual for sudden jerky movements (myoclonus) from the neonate to detach an electrode whilst the neonate slept, requiring reapplication with the potential for disturbance. To be able to capture all three sleep stages within one hour it was necessary for the neonate to be settled throughout; any interference with the recording could end the PSG.

With this in mind it was common for impedance levels to change throughout a recording. Wherever possible, the electrode would be reattached and the impedance lowered, but at the risk of waking up the sleeping neonate. If levels could not be lowered without disturbing the neonate significantly, the high impedance would be noted and excluded from the later analysis. On a small number of occasions the reapplication of electrodes woke the already agitated neonate so that no further sleep measurements were possible.

There were also a small number of instances when a neonate did not sleep at all throughout the recording session, thus making the data recorded unsuitable for analysis.

7.2.2 PSG Classical Interpretation

The classical interpretation was performed by inspection by paediatric consultant neurologist, Dr Mary O'Regan (Fraser of Allander Paediatric Neurosciences Unit, Royal Hospital for Sick Children, Glasgow). The data recorded at the PRM was transferred via an encrypted (Truecrypt – 512 bit - Twofish-Serpent encryption algorithm) portable hard drive, and uploaded to the Xltek server system. The data had no patient identifiers embedded in it, and was only identifiable by the study number, thus Dr O'Regan was unaware (blinded) to the exposure status of the neonate under investigation.

The interpretation involved examining all channels of data in conjunction with the video and notes, and identifying epochs of data for each of the three sleep states (active, quiet

and indeterminate). By using the EEG, ECG and respiratory channels with the physical appearance of the neonate (video), an estimate of the sleep stage was determined. The characteristics of each sleep stage are described in the chapter on EEG (section 2.3.3). These epochs were also deemed as artefact free, and ranged from seconds to minutes in duration. It was these epochs on which the spectral analysis was based.

Although the entire 1 hour of PSG data for each neonate was inspected it was not always possible to identify epochs of suitable quality for analysis. In a small number of recordings (n=10) no sections of sleep were identified because the neonate failed to sleep, or was too agitated throughout the recording.

It was initially intended that the PSG would be scored for sleep stages and a hypnogram constructed showing the sleep architecture of the neonate throughout the 1 hour period. However, due to the challenges of recording as well as the agitated nature of some of the neonates, Dr O'Regan reported that it would not be possible to construct complete hypnograms, as they would contain too many missing segments. These segments would be periods where it was not possible to define accurately what sleep stage that neonate was in. For this reason, the EEG analysis was based on the epochs of artefact free data only.

In total 56 1 hour recordings were interpreted and scored for sleep states.

7.2.3 PSG Spectral Analysis

The output of the classical interpretation discussed above was taken and a spectral analysis performed. This derived frequency information on the nature of the EEG signals under investigation. To do this, a spectral analysis application was written, with a more comprehensive description to be found in section 5.4.1. To be able to perform this analysis, a number of parameters had to be quantified, before each epoch was analysed.

7.2.4 Spectral Analysis Parameters

Below is a summary of the parameters used with the EEG analysis software.

- 4 second epochs, giving a frequency resolution of 0.25 Hz.
- A sampling frequency of 256 Hz, giving 1,024 data points per epoch.
- A power of 2 data points, so the data was not padded.
- No windowing/smoothing.
- No overlap.
- Output Analysis Parameters (Band Power and SEF 95%).

Band Power

As covered in section 4.5.1, the frequency of the signal can be broken down into four or more ranges, categorised as delta, theta, alpha and beta. When the signal is transformed from the time domain to the frequency domain using a discrete Fourier transformation and a power spectrum established, these boundaries still apply. Consequently the band power of the DFT is defined as the summation of the energy between two frequencies, f_1 and f_2 as shown in the Table 13.

Band Power	f1 (Hz)	f2 (Hz)
Delta	0.5	4
Theta	4	8
Alpha	8	12
Beta	12	30
Total Power	0.5	30

Table 13: EEG band power ranges from Tonner and Bein, (2006).

However, the power spectrum is a representation of the power at each frequency bin, which in turn is defined by the frequency resolution of the signal (equation 12).

$$Frequency\ Resolution = \frac{1}{Length\ of\ epoch(s)} \tag{12}$$

For example, if the epoch length was 4 seconds, the frequency resolution would be ¼ or 0.25 Hz. If the frequency resolution was 1 Hz, as would be the case for an example with a 1 second epoch, it would not be possible to accurately resolve the lower boundary of the delta power range, as this is 0.5 Hz. So to be able to resolve the lower delta boundary, an absolute minimum frequency resolution of 0.5 Hz is required.

Other Neonatal Studies Using Band Power

Table 14 shows a summary of a range of studies that all use band power as an output variable. It highlights the lack of standardisation between studies, in that fixed boundaries for band power have not been established. Although most studies 'roughly' follow the generalised version shown in Table 13, many establish their own boundaries to highlight a specific neurological condition e.g. use of delta power in conjunction with sigma power (a sub frequency of beta) for neonatal seizure detection.

Author	Subjects	Year	PSD Type	Windowing	Delta (Hz)	Theta (Hz)	Alpha (Hz)	Beta (Hz)	Total Power (Hz)
Scher *et al.*	Neonates term & Preterm	1997	DFT	Kaiser	0.5-4	4-8	8-13	13-22	0.5-22
Scher *et al.*	Neonates term & Preterm	1994	DFT	Kaiser	0.5-4	4-8	8-13	13-22	0.5-22
Okumura *et al.*	Preterm Neonates	2006	DFT	None	-	4-6 & 6-8	8-13	13-20 & 20-30	-
Paul *et al.*	Neonates	2003	DFT	None	0.5-1.5 & 1.6-3	3.1-5 & 5.1-8	8.1-14	-	-
Bell *et al.*	Neonates	1991	DFT	10% Hanning	0.3-1 & 2-3	4-7	8-13	14-30	0.3-30
Schramm *et al.*	Neonates term & Preterm	2000	DFT	None	0.4-1.5 & 1.5-3.5	3.5-7.5	7.5-12.5	12.5-19.5 & 19.5-25	0.4-25
Ktonas *et al.*	Infants	1995	DFT	Cosine	0.5-1.5	-	-	11.5-15.5	-
Victor *et al.*	Preterm Neonates	2005	DFT	None	0.5-3.5	4-7.5	8-12.5	13-30	0.5-30
Fagioli *et al.*	Infants	1999	DFT	None	0.5-1.5	-	-	11.5-15.5	-
Drummund *et al.*	Adult	1991	DFT	None	0-4	-	8-20 (alpha+beta /delta)		0-20

Table 14: A summary of multiple studies that use spectral band power output. This table compares studies involving preterm, neonates or infants, and highlights the differences in band power ranges used between studies. It also shows if any windowing of the data was performed and the window function used.

Spectral Edge Frequency (SEF)

Table 15 is a summary of a selection of papers that used spectral edge in their analysis. It can be seen that the parameters for SEF vary from study to study, making comparison between studies difficult. The ranges are also dependent on the analogue filter settings (if used) of the study. If a high pass filter was used for example, there would be no reason to have a lower SEF boundary of zero, as the filtering would remove the power at these very low frequencies. However, if no high pass filter is applied, then the trace is at risk of being contaminated by drift and DC offset. If no low pass filter is applied then the trace is at risk of contamination from high frequency artefact such as EMG (Whitham et al., 2007).

A compromise is to have a lower SEF boundary just above the high pass filter setting, so that very low frequency artefacts are removed i.e. 0.3 Hz, and a low pass filter setting of 35 Hz to remove higher frequency contamination. Considering the roll off of the 0.3 Hz high pass filter, a sensible setting for the SEF would be 0.5 Hz. Consequently, the SEF calculations for this study were based on a spectrum of 0.5 – 30 Hz. Also by using this range, results could be compared with the study performed by Bell et al., (1991) which is considered the most comprehensive application of SEF in neonates.

Author	Subject	Year	Epoch Length (sec)	Data Points	Frequency Resolution (Hz)	SEF %	SEF Low (Hz)	SEF High (Hz)
Bell *et al.*	Neonates	1991	4	512	0.25	95	0.3	30
Korotchikova *et al.*	Neonates	2009	4	1024	0.25	90	0.5	32
Doyle *et al.*	Neonates	2007	4	1024	0.25	90	0	1
							1	4
							4	30
							2	20
Drummond *et al.*	Adult	1991	4	Not known	0.25	90	0	20
Greene *et al.*	Neonates	2008	2	512	0.5	90	0.5	20
							0.5	32
							2	20
Fell *et al.*	Adult	1996	Not known	1000	Not known	90	0.5	45
Inder *et al.*	Neonates	2002	4	1024	0.25	90	2	20
Kobayashi *et al.*	Neonates/ Infants	2011	1	500	1	90	0	20
Miyashita *et al.*	Adult	2003	2	256	0.5	50, 90 & 95	?	?
Sleigh *et al.*	Adult	1999	5	Not known	0.2	95	5	30
Thordstein *et al.*	Neonates	2004	Not known	1024	Not known	95	0	30
Victor *et al.*	Preterm Neonates	2005	2	512	0.5	95	0.5	30
Wong *et al.*	Neonate	2006	60	24,000	0.1667	90	2	20
West *et al.*	Preterm Neonates	2006	4	1024	0.25	90	2	20

Table 15: A summary table showing a number of different studies and the variation used in spectral edge parameters. It highlights that there is considerable variation in the spectral edge frequency used (50%-95%), with varying boundaries for total power (0-30Hz), highlighting the difficulty in having a standardised value for comparison with other studies.

7.2.5 Filters

As discussed earlier, the Xltek recording system only applies an anti-aliasing filter (if necessary, and dependent on the sampling frequency) whilst the recording is being made, so no other filters are used. Raw EEG signals have amplitudes in the microvolt range, and can contain frequency information up to 300 Hz. However, it is more normal in the neonatal sleep EEG to examine a much lower frequency range such as 0.1 Hz to 35/70 Hz.

Using high pass filters, the lower boundary is often between 0.3 and 1.0 Hz (Butkov et al., 2007) to eliminate slow frequency artefacts such as those caused by perspiration, breathing or 'popping artefacts' (direct pressure against an electrode). Guidelines on neonatal EEG advise the use of low frequency filters between 0.25 and 0.5 Hz to avoid affecting low frequency signals (Scher, 1996). However, studies by Thordstein et al., (2005) and Vanhatalo et al., (2002) showed that even these settings would remove valuable information about infra-slow EEG activity. For these reasons no high pass filter was applied to the study data, because of the uncertainty of the effect it would have on the low-frequency data. This is the approach used by Doyle et al., (2007) in their EEG investigations.

As the analysis was based on FFTs, if the beginning and the end of the epochs differed in amplitude significantly, the algorithm would introduce a degree of spectral leakage. As it has already been stated, windowing (tapering) was not used in this analysis; de-trending methods were used instead. This involves removing the mean value of the epoch from the vector under analysis, and is commonly used in FFT processing. The result is that very low frequencies, such as drift, are removed from the epoch. Consequently this has a similar effect to the removal of low frequency signals by the application of a high pass filter, but without loss of very low frequencies while minimising discontinuities of the start/end amplitudes within the epoch and therefore introducing spectral leakage. The application of trend removal to an unfiltered signal was considered the least destructive approach, so this was the approach used.

The main spectral output from which other variables were derived (such as band power and SEF) is total power (TP), with a band width of 0.5-30Hz. If a low pass filter had

been used, it would have had to have a very steep roll off close to the 30 Hz boundary, or it may have affected the top end of the total power calculation. This would have meant that large artefacts just above the 30Hz boundary would have negatively affected the TP calculation, but as the epochs selected were identified as being 'artefact' free, a low pass filter was not considered necessary.

7.2.6 Mains Filtering & Notch Filters

Mains interference (50/60 Hz) can contaminate EEG signals. The cause is often a poor connection between the electrode and the scalp, and is usually rectified by the re-application of the electrode. However, in polysomnography where long recordings (1 – 24 hours) are normal, it is not uncommon to have mains interference at some point. It is not recommended to apply a mains filter whilst recording, but it is desirable to have the option to view data without mains interference after the recording when inspecting the data. The standard way of doing this is by using a notch filter, or a bandpass filter with steep roll off before and after the frequency to be removed e.g. 47 Hz and 53 Hz. The application of a notch filter, especially a high order filter, can introduce significant phase distortion between channels, and should be used sparingly.

Since this study was based on spectral analysis, an investigation was made examining the effect of applying a notch filter prior to the recording of the data. The national grid keeps the mains frequency in the UK at approximately 50 Hz, and is a sine wave. The normal operating tolerance is +/- 0.2 Hz (49.8-50.2 Hz), although the national grid is obliged to maintain the tolerance between +/- 0.5 Hz (49.5-50.5 Hz). The daily mains frequency is recorded, and can be found at the following website:

www.nationalgrid.com/uk/Electricity/Data/Realtime

On examining study data where there was mains interference present, the frequency appeared to span a number of frequency bins between 47-53 Hz despite the tolerance for the national grid being at worst +/- 0.5 Hz, giving a spread of only 49.5-50.5 Hz. Consequently, the apparent spread of energy was due to spectral leakage caused by truncating the sine wave, rather than a drift in the mains source frequency.

This study examines data between the range of frequencies 0 to 30 Hz, and for EEG analysis is called Total Power (TP). The application of a 50 Hz notch filter will therefore have no effect on the frequencies that make up the TP band as any effect of leakage does not spread far enough to contaminate the TP band. Experimental evidence showed that unfiltered spectra values do not differ when a zero-phase 50 Hz notch filter is applied.

7.2.7 Data Management and the Processing of Data

The EEG analysis software had two main roles: to analyse individual 4 second epochs, then to average groups of four together in the frequency domain e.g. 4 x 4 second epochs giving 16 second epochs. This was the analysis for each channel, so a short program was written to create 16 second epochs across all 12 EEG channels. This data formed the results for that sleep state and were stored in a spreadsheet. When all the epochs had been analysed, they were then imported into the VIDI database to re-link the results with the demographic and exposure data. Finally the re-linked data was stratified by a user definable variable e.g. case / quiet sleep. Figure 51 shows the process in its entirety.

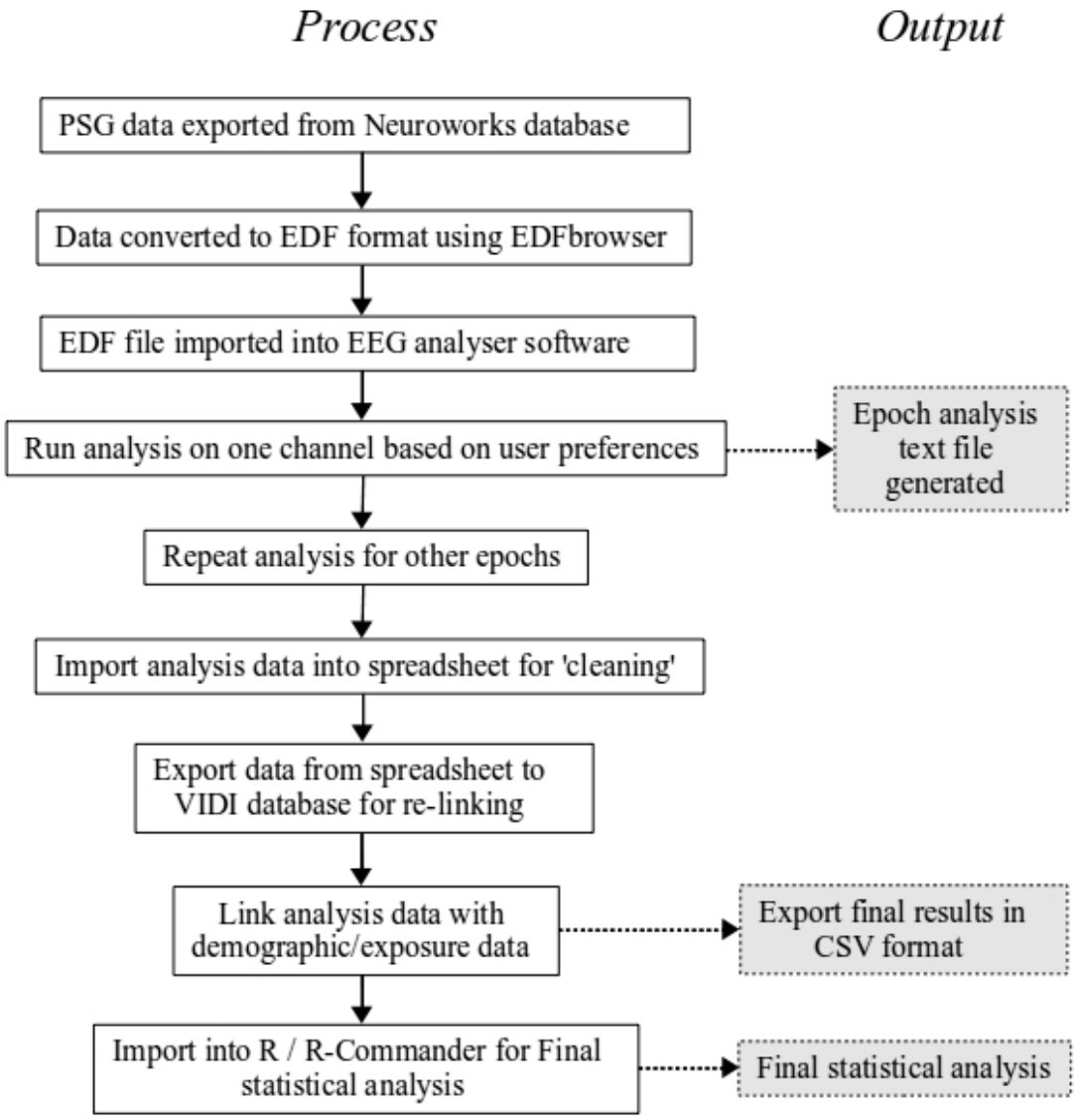

Figure 51: The overall work flow showing the stages from extracting data from the PSG to the final statistical analysis.

The final dataset was prepared using Microsoft Access, and cleaned using a spreadsheet (LibreCalc 4.1) before statistical analysis, performed using the R statistical programming language (R Core Team, 2013) in conjunction with the R-Commander (Fox, 2005) graphical user interface.

7.3 Results and Analysis

7.3.1 Excluded Data

The dataset had 55 subjects consisting of 26 cases and 29 controls. However, as described earlier, a number of the PSGs could not be used for analysis. In total, 10 complete PSGs (6 cases, 4 controls) were excluded from the overall EEG analysis for the reasons shown in Table 16.

Study Number	Status	Reason
42	Case	The neonate was very unsettled, PSG not scored.
43	Case	EEG abandoned. The neonate was very unsettled.
47	Case	Montage problems during the recording.
64	Case	No sleep stages identified. Sleep not achieved.
65	Control	Persistent artefact on T4-O2 and FP1-T3, not suitable for spectral analysis.
68	Case	No sleep stages identified.
74	Case	High level of artefact throughout recording.
79	Control	Persistent artefact on O1, not suitable for spectral analysis, no sleep stages marked.
95	Control	Sleep not achieved.
145	Control	Sleep not achieved, very unsettled neonate.

Table 16: Reasons why certain study neonates were excluded from the analysis.

Sleep Outliers

A small number (n=5) of sections were removed because of artefact on sections that had been scored. The likely reason was artefact of significantly large amplitude on one or two channels which skewed the overall average of the epoch. The sections removed from the final analysis are shown in Table 17.

Study Number	Sleep State	Reason
48	QS	Excessively high power values caused by artefact.
59	IS	Excessively high power values caused by artefact.
82	QS	Excessively high power values caused by artefact.
94	IS	Excessively high power values caused by artefact.
102	AS	Excessively high power values caused by artefact.

Table 17: Sleep epochs removed from the analysis due to artefact.

After removal of these results, the dataset consisted of 45 subjects (20 cases and 25 controls). Although all 45 subjects had an hour of polysomnography it was not possible to identify all three sleep states for any of the subjects. Figure 52 Shows the percentage of identifiable sleep states for each study group. Not one of the 45 neonates achieved all three sleep stages during their PSG.

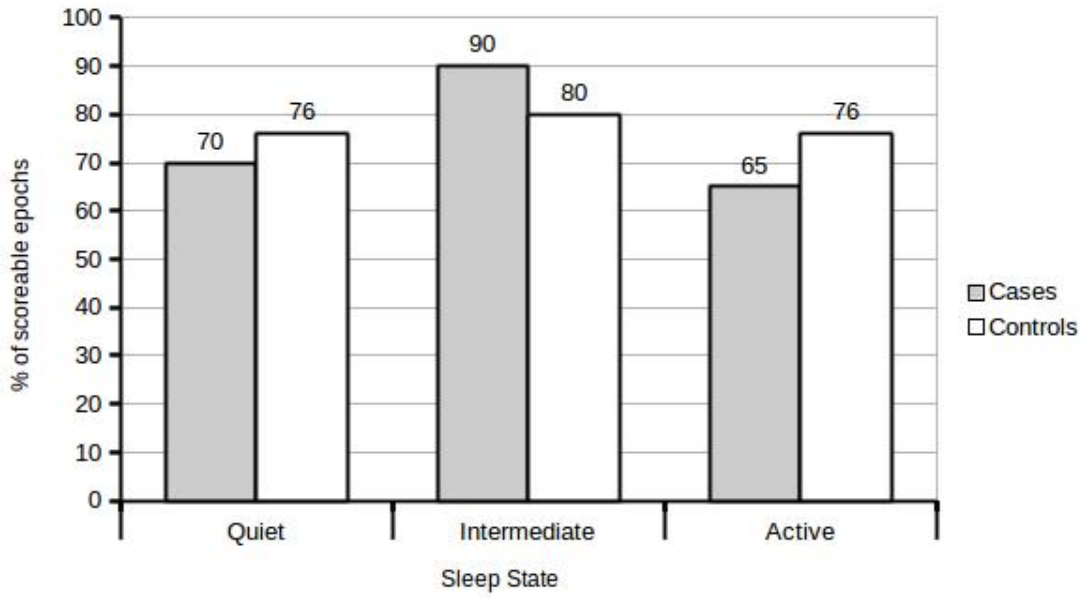

Figure 52: The distribution of epochs by sleep state. This graph shows that for each sleep state it was not possible to identify all three sleep states for each infant, either because such states did not occur during the one hour of PSG, or because they could not be defined with any degree of accuracy. For example, 70% of the cases had at least one epoch of quiet sleep identified during the recording.

7.3.2 Statistical Analysis

The final statistical analysis for the EEG parameters was based on the dataset of 45 neonates. The choice of statistical test was based on two methods, visual inspection of the histograms and the results of the Shapiro-Wilk normality tests (Shapiro and Wilk, 1965). The tests then compared the cases and controls based on the sleep state identified. The Shapiro-Wilk test indicates a degree of normality when the p-value is greater or equal to 0.05. The 'W' score is the test statistic and the results are shown below.

Normality Testing for Controls

	Active Sleep		Quiet Sleep		Indeterminate Sleep	
Variable	W Score	p-value	W Score	p-value	W Score	p-value
Absolute Delta Power ($\mu V^2/Hz$)	0.70	**0.00**	0.87	**0.02**	0.94	0.26
Absolute Theta Power ($\mu V^2/Hz$)	0.63	**0.00**	0.94	0.27	0.56	**0.00**
Absolute Alpha Power ($\mu V^2/Hz$)	0.63	**0.00**	0.92	0.13	0.78	**0.00**
Absolute Beta Power ($\mu V^2/Hz$)	0.67	**0.00**	0.85	**0.01**	0.75	**0.00**
Absolute Total Power ($\mu V^2/Hz$)	0.70	**0.00**	0.88	**0.01**	0.75	**0.00**
Relative Delta Power (%)	0.95	0.45	0.94	0.31	0.57	**0.00**
Relative Theta Power (%)	0.95	0.44	0.97	0.70	0.98	0.97
Relative Alpha Power (%)	0.95	0.45	0.84	**0.00**	0.98	0.94
Relative Beta Power (%)	0.95	0.56	0.90	**0.05**	0.93	0.12
SEF 95% (5-30 Hz)	0.97	0.77	0.88	**0.02**	0.86	**0.01**
SEF 95% (2-20 Hz)	0.94	0.34	0.95	0.35	0.89	**0.03**
Absolute Delta Low Power ($\mu V^2/Hz$)	0.71	**0.00**	0.86	**0.01**	0.94	0.22
Absolute Delta High Power ($\mu V^2/Hz$)	0.63	**0.00**	0.98	0.91	0.56	**0.00**
Relative Delta Low Power (%)	0.96	0.69	0.99	0.98	0.75	**0.00**
Relative Delta High Power (%)	0.93	0.23	0.96	0.56	0.97	0.71

Table 18: Shapiro-Wilk (1965) normality tests of controls for the EEG variables. A p-value greater than 0.05 indicates an adequate normality of the distribution. The table shows that not every variable is normally distributed. Bold text indicates normally distributed data.

Normality Testing for Cases

	Active Sleep		Quiet Sleep		Indeterminate Sleep	
Variable	W Score	p-value	W Score	p-value	W Score	p-value
Absolute Delta Power ($\mu V^2/Hz$)	0.65	**0.00**	0.97	0.89	0.60	**0.00**
Absolute Theta Power ($\mu V^2/Hz$)	0.67	**0.00**	0.91	0.15	0.53	**0.00**
Absolute Alpha Power ($\mu V^2/Hz$)	0.68	**0.00**	0.93	0.29	0.52	**0.00**
Absolute Beta Power ($\mu V^2/Hz$)	0.68	**0.00**	0.90	0.12	0.51	**0.00**
Absolute Total Power ($\mu V^2/Hz$)	0.65	**0.00**	0.97	0.87	0.59	**0.00**
Relative Delta Power (%)	0.93	0.36	0.94	0.38	0.95	0.42
Relative Theta Power (%)	0.95	0.56	0.85	**0.02**	0.98	0.96
Relative Alpha Power (%)	0.94	0.51	0.81	**0.01**	0.96	0.59
Relative Beta Power (%)	0.93	0.38	0.85	**0.02**	0.96	0.55
SEF 95% (5-30 Hz)	0.97	0.91	0.86	**0.03**	0.96	0.65
SEF 95% (2-20 Hz)	0.85	**0.04**	0.95	0.54	0.97	0.73
Absolute Delta Low Power ($\mu V^2/Hz$)	0.65	**0.00**	0.97	0.91	0.60	**0.00**
Absolute Delta High Power ($\mu V^2/Hz$)	0.68	**0.00**	0.93	0.27	0.53	**0.00**
Relative Delta Low Power (%)	0.97	0.77	0.96	0.72	0.95	0.50
Relative Delta High Power (%)	0.91	0.20	0.95	0.61	0.92	0.12

Table 19: Shapiro-Wilk (1965) normality tests of cases for the EEG variables. A p-value greater than 0.05 indicates an adequate normality of the distribution. The table shows that not every variable is normally distributed. Bold text indicates normally distributed data.

The results of the normality tests and the visual inspection of the histograms show there is a combination of both normally distributed and non-normally distributed data. To be able to use statistical tests such as t-tests, an adequate degree of normality is required. Although a number of parametric transformations were tried to normalise the data (logs, square root and squared) there were still problems of skewness, making parametric tests unsuitable.

For these reasons non-parametric tests were used instead. The Mann-Whitney U test

(also called the Wilcoxon rank sum test) is a non-parametric alternative to t-tests, where medians are used as opposed to mean values. Where a statistically significant result was found, Bonferroni corrections were then applied to the Mann-Whitney results to deliver a more conservative estimate of the statistical significance of the difference in the medians.

7.3.3 EEG Frequency Domain Results

The results of the EEG spectral analysis follows. Each variable has been presented graphically for visual comparison using box plots, and also in a table showing the results of the Mann-Whitney test. Although absolute band power results are not usually presented in publications due to the large variability in potential amplitudes, they are presented here for completeness. Also the total power band power estimate, which is a commonly used output variable, is based on these absolute values. Relative band power values are more frequently presented as band power divided by the total band power, and are therefore more suitable when amplitudes vary considerably.

Absolute Delta (0-4 Hz) Band Power

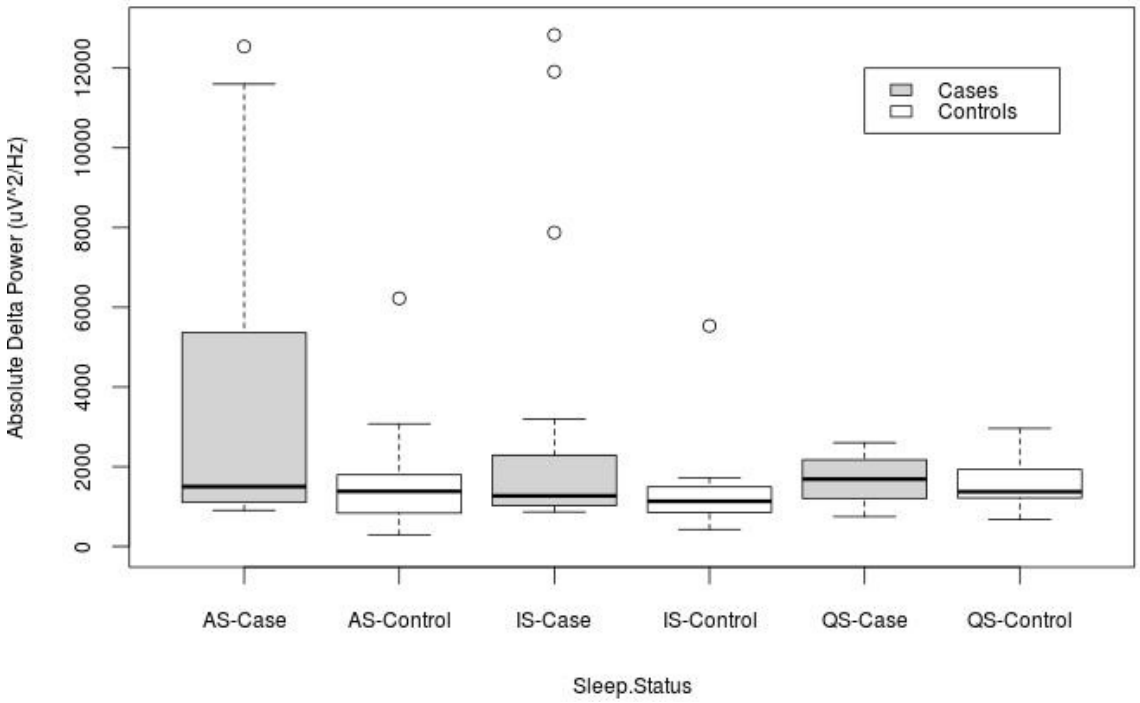

Figure 53: Box plots for absolute delta (0-4 Hz) band power for all three sleep states, with cases shown in grey. The top and bottom of the boxes show the 1st (Q1) and 3rd (Q3) quartile respectively, while the whiskers show Q1 or Q3 ±1.5 of the interquartile range. The black line within the box indicates the median value and outliers are shown by small circles. AS: active sleep; IS: indeterminate sleep; QS: quiet sleep.

	Cases		Controls		p-value	95% Confidence intervals of the
	n	Median (μV^2/Hz)	n	Median (μV^2/Hz)		difference (cases minus controls)
Active	13	1499	18	1382	0.24	(-312, 2141)
Indeterminate	17	1268	20	1132	0.27	(-123, 716)
Quiet	14	1687	19	1370	0.65	(-320, 582)

Table 20: Results of Mann-Whitney U tests comparing absolute delta band power for cases and controls for each sleep state.

No statistical difference was found between the absolute delta power medians for any sleep state, indicating that there was no difference identifiable between the study groups using this statistical methodology.

Absolute Delta (Low: 0-2 Hz) Band Power

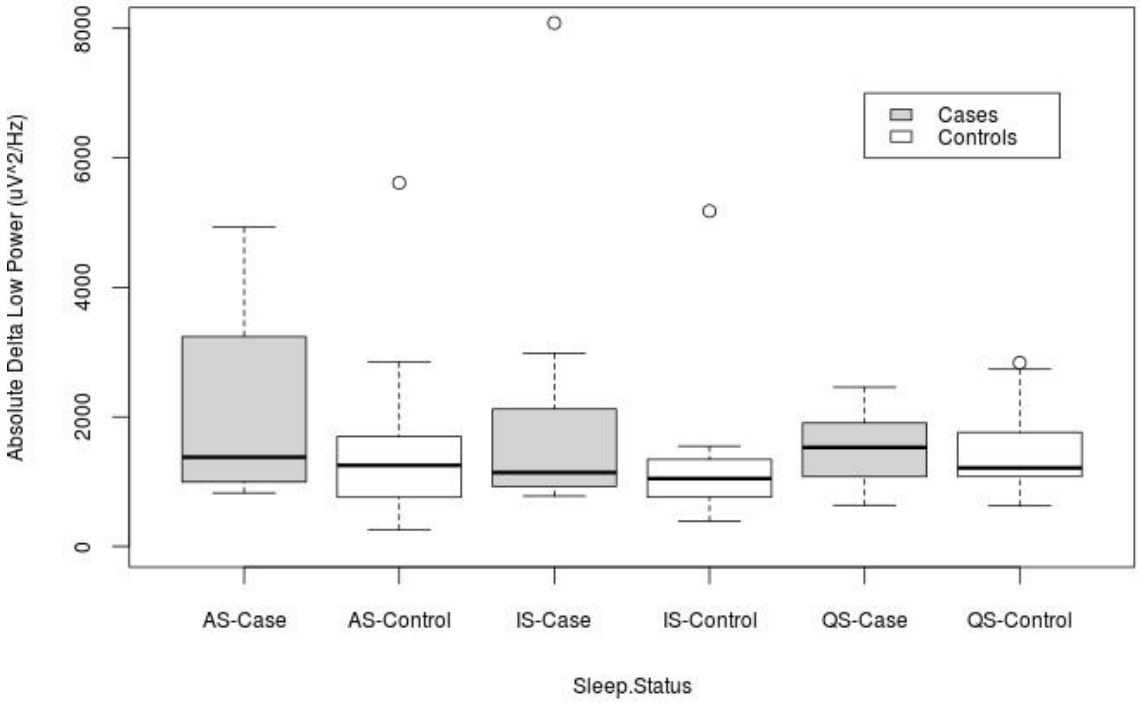

Figure 54: Box plots for absolute delta low (0-2 Hz) band power for all three sleep states, with cases shown in grey. The top and bottom of the boxes show the 1st (Q1) and 3rd (Q3) quartile respectively, while the whiskers show Q1 or Q3 ±1.5 of the interquartile range. The black line within the box indicates the median value and outliers are shown by small circles. AS: active sleep; IS: indeterminate sleep; QS: quiet sleep.

	Cases		Controls		p-value	95% Confidence intervals of the
	n	Median (μV^2/Hz)	n	Median (μV^2/Hz)		difference (cases minus controls)
Active	13	1377	18	1251	0.25	(-319, 1599)
Indeterminate	17	1140	20	1048	0.31	(-143, 674)
Quiet	14	1528	19	1212	0.63	(-285, 534)

Table 21: Results of Mann-Whitney U tests comparing absolute delta low (0-2 Hz) band power for cases and controls for each sleep state.

As for absolute delta power, no statistical difference was found between the absolute delta (low) power medians for any sleep state, again indicating no difference identifiable between the study groups using this methodology.

Absolute Delta (High: 2-4 Hz) Band Power

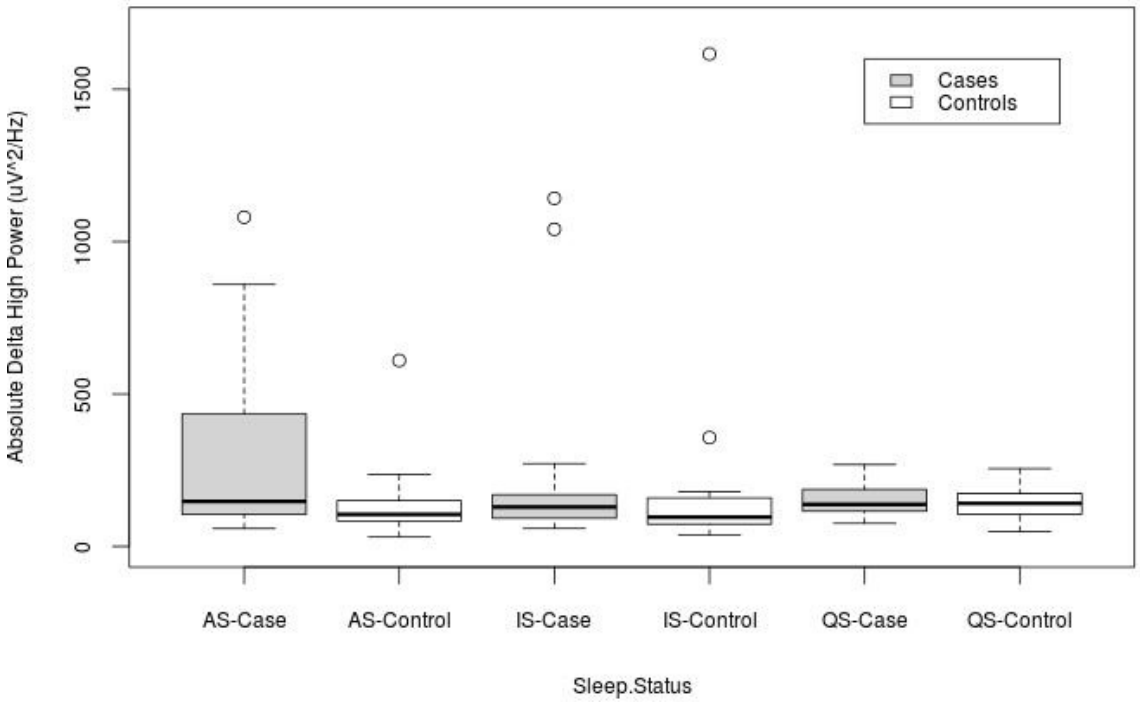

Figure 55: Box plots for absolute delta high (2-4 Hz) band power for all three sleep states, with cases shown in grey. The top and bottom of the boxes show the 1st (Q1) and 3rd (Q3) quartile respectively, while the whiskers show Q1 or Q3 ±1.5 of the interquartile range. The black line within the box indicates the median value and outliers are shown by small circles. AS: active sleep; IS: indeterminate sleep; QS: quiet sleep.

	Cases		Controls		p-value	95% Confidence intervals of the
	n	Median (μV^2/Hz)	n	Median (μV^2/Hz)		difference (cases minus controls)
Active	13	147	18	105	0.13	(-15, 169)
Indeterminate	17	129	20	96	0.17	(-12, 71)
Quiet	14	138	19	141	0.73	(-33, 51)

Table 22: Results of Mann-Whitney U tests comparing absolute delta high (2-4 Hz) band power for cases and controls for each sleep state.

Once again, no statistical difference was found between the absolute delta (high) power medians for any sleep state, indicating that there was no difference identifiable between the study groups using this statistical methodology.

Absolute Theta (4-8 Hz) Band Power

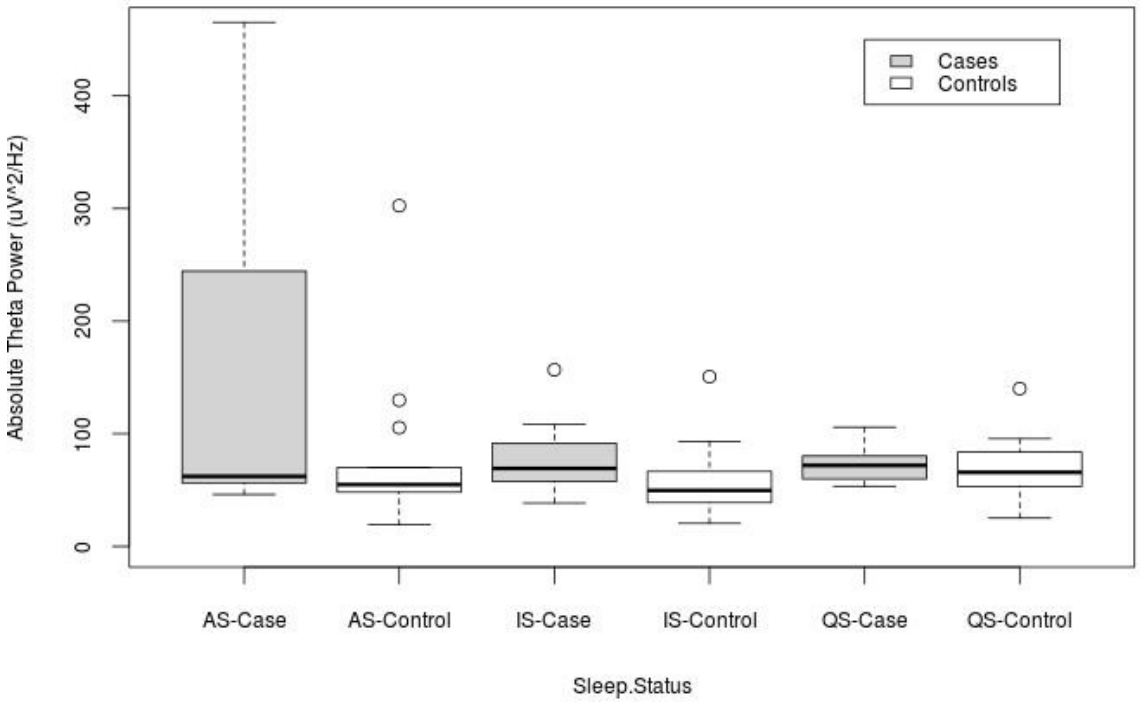

Figure 56: Box plots for absolute theta (4-8 Hz) band power for all three sleep states, with cases shown in grey. The top and bottom of the boxes show the 1st (Q1) and 3rd (Q3) quartile respectively, while the whiskers show Q1 or Q3 ±1.5 of the interquartile range. The black line within the box indicates the median value and outliers are shown by small circles. AS: active sleep; IS: indeterminate sleep; QS: quiet sleep.

	Cases		Controls		p-value	95% Confidence intervals of the
	n	Median (μV^2/Hz)	n	Median (μV^2/Hz)		difference (cases minus controls)
Active	13	62.2	18	54.9	0.18	(-5.7, 131.9)
Indeterminate	**17**	**69.2**	**20**	**49.7**	**0.048**	**(0.1, 40.8)**
Quiet	14	71.9	19	65.8	0.46	(-7.8, 20.9)

Table 23: Results of Mann-Whitney U tests comparing absolute theta band power for cases and controls for each sleep state.

Although a small, statistically significant difference was found between the cases and controls for intermediate sleep, that difference was no longer present when a Bonferroni correction was applied. The other sleep stages were shown to not be statistically significant using this technique.

Absolute Alpha (8-12 Hz) Band Power

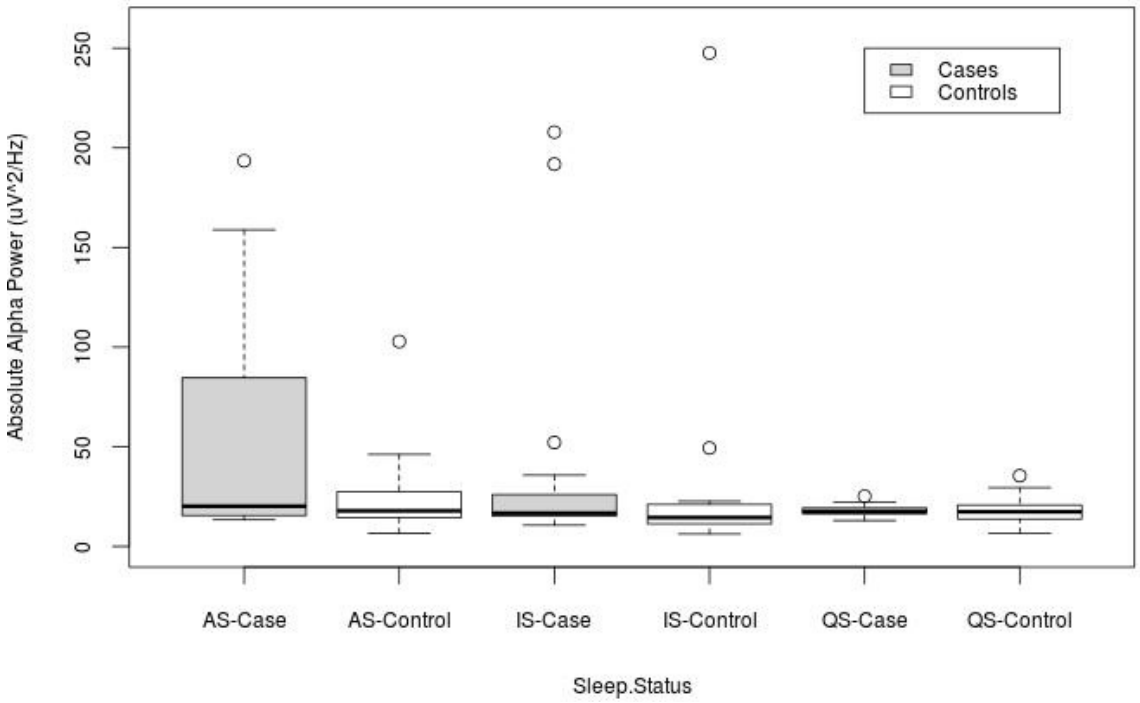

Figure 57: Box plots for absolute alpha (8-12 Hz) band power for all three sleep states, with cases shown in grey. The top and bottom of the boxes show the 1st (Q1) and 3rd (Q3) quartile respectively, while the whiskers show Q1 or Q3 ±1.5 of the interquartile range. The black line within the box indicates the median value and outliers are shown by small circles. AS: active sleep; IS: indeterminate sleep; QS: quiet sleep.

	Cases		Controls		p-value	95% Confidence intervals of the difference (cases minus controls)
	n	Median (μV^2/Hz)	n	Median (μV^2/Hz)		
Active	13	20.1	18	17.9	0.59	(-6.7, 49.1)
Indeterminate	17	16.7	20	14.5	0.60	(-3.7, 6.8)
Quiet	14	17.5	19	17.4	0.74	(-3.6, 5.1)

Table 24: Results of Mann-Whitney U tests comparing absolute alpha band power cases and controls for each sleep state

No statistical difference was found between the absolute alpha power medians for any sleep state. This indicates that there was no difference identifiable between the study groups using this statistical methodology.

Absolute Beta (12-30 Hz) Band Power

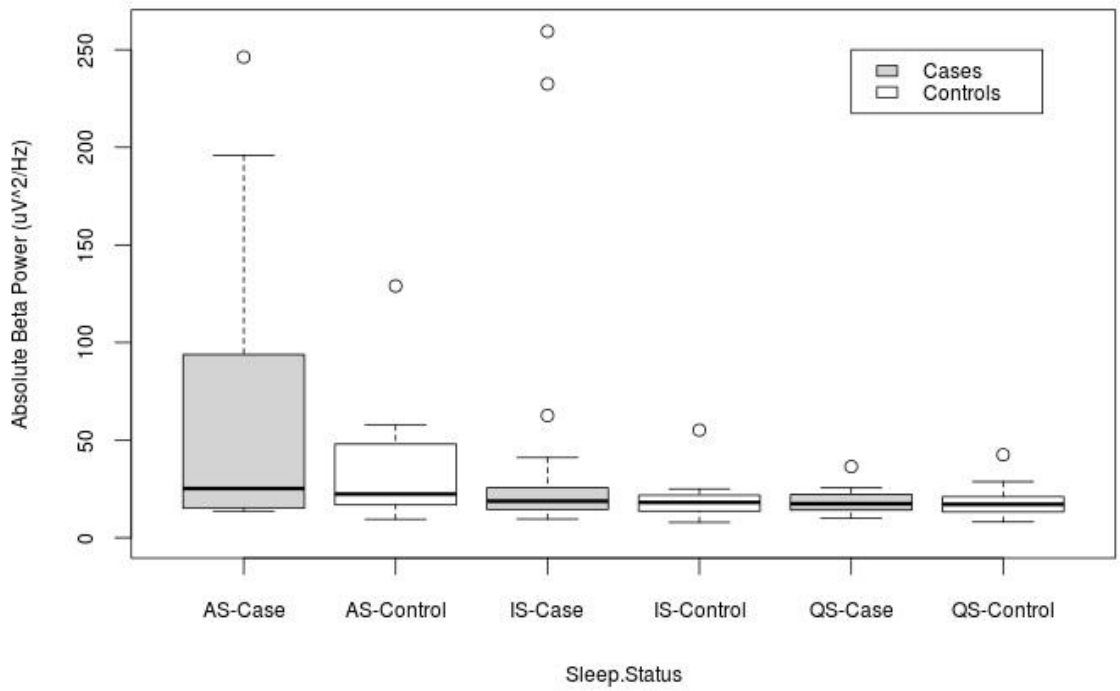

Figure 58: Box plots for absolute beta (12-30 Hz) band power for all three sleep states, with cases shown in grey. The top and bottom of the boxes show the 1st (Q1) and 3rd (Q3) quartile respectively, while the whiskers show Q1 or Q3 ±1.5 of the interquartile range. The black line within the box indicates the median value and outliers are shown by small circles. AS: active sleep; IS: indeterminate sleep; QS: quiet sleep.

	Cases		Controls		p-value	95% Confidence intervals of the difference (cases minus controls)
	n	Median (μV^2/Hz)	n	Median (μV^2/Hz)		
Active	13	20.1	18	17.9	0.24	(-3.3, 45.2)
Indeterminate	17	16.7	20	14.5	0.18	(-2.0, 8.9)
Quiet	14	17.5	19	17.4	0.55	(-2.5, 4.1)

Table 25: Results of Mann-Whitney U tests comparing absolute beta band power cases and controls for each sleep state.

Again, no statistical difference was found between the absolute beta power medians for any sleep state. This indicates that there was no difference identifiable between the study groups using this statistical methodology.

Absolute Total (0-30 Hz) Band Power

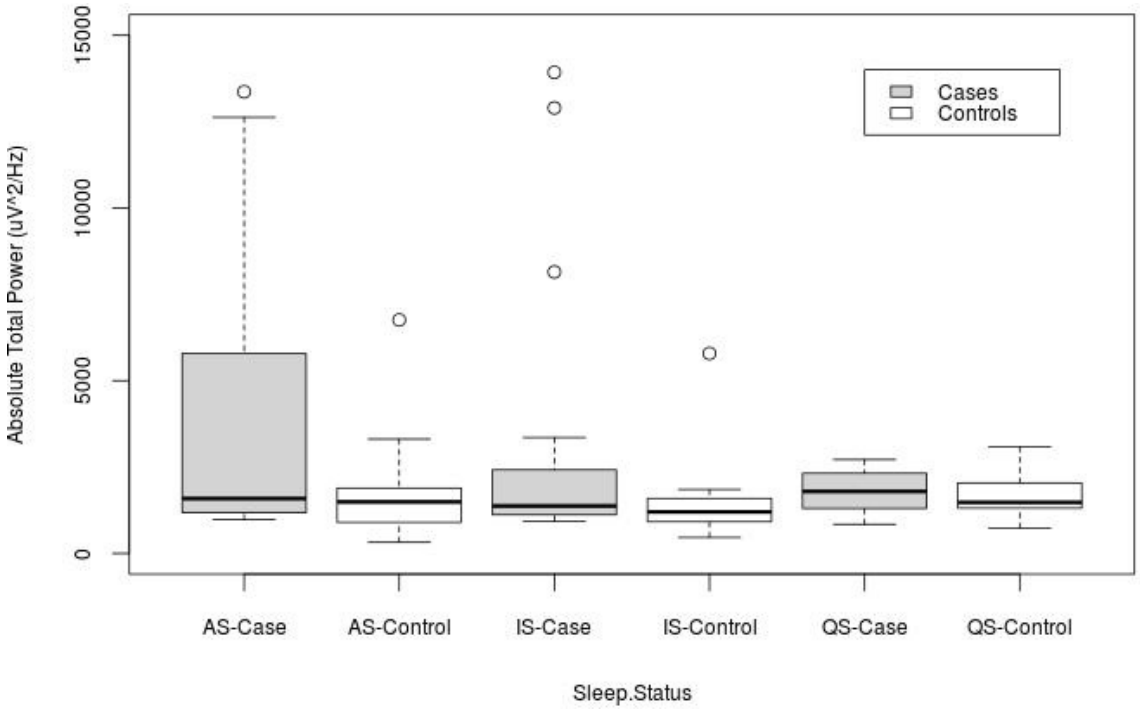

Figure 59: Box plots for absolute total power (0-30 Hz) band power for all three sleep states, with cases shown in grey. The top and bottom of the boxes show the 1st (Q1) and 3rd (Q3) quartile respectively, while the whiskers show Q1 or Q3 ±1.5 of the interquartile range. The black line within the box indicates the median value and outliers are shown by small circles. AS: active sleep; IS: indeterminate sleep; QS: quiet sleep.

	Cases		Controls		p-value	95% Confidence intervals of the difference (cases minus controls)
	n	Median ($\mu V^2/Hz$)	n	Median ($\mu V^2/Hz$)		
Active	13	1587	18	1489	0.24	(-318, 2476)
Indeterminate	17	1372	20	1201	0.23	(-131, 772)
Quiet	14	1794	19	1477	0.65	(-349, 616)

Table 26: Results of Mann-Whitney U tests comparing absolute total (0-30 Hz) band power for cases and controls for each sleep state.

No statistical difference was found between the absolute total power medians for any sleep state again indicating that there was no difference identifiable between the study groups using this statistical methodology.

Relative Delta (0-4 Hz) Band Power

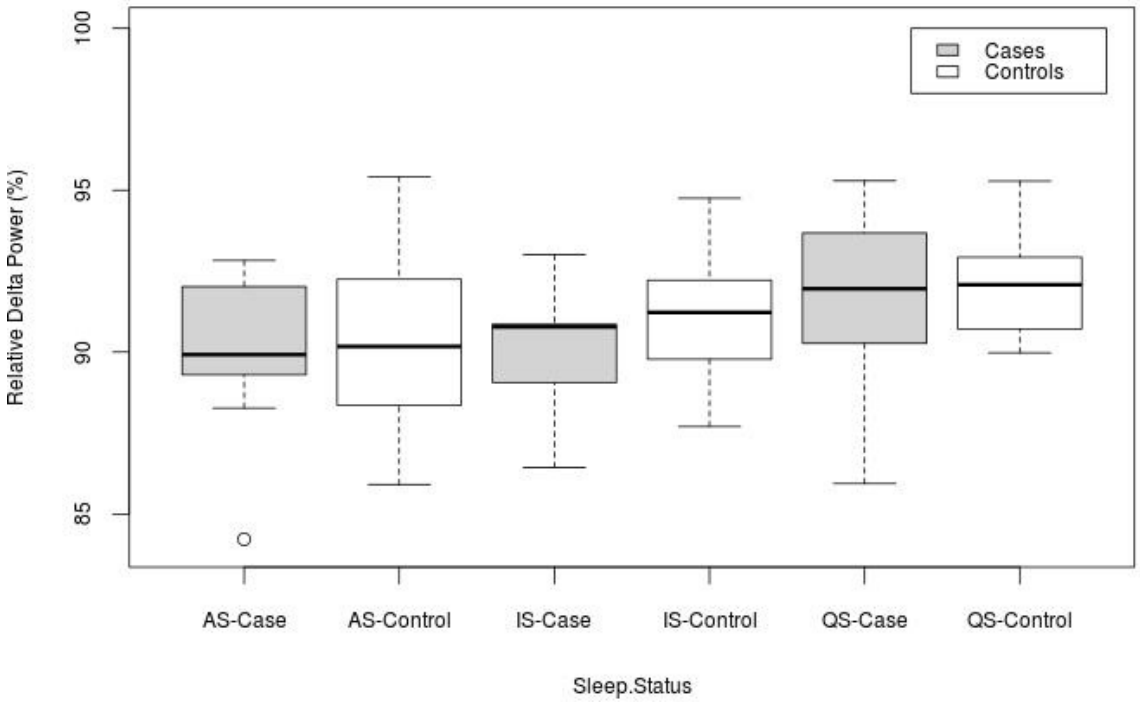

Figure 60: Box plots for relative delta power (0-4 Hz) band power for all three sleep states, with cases shown in grey. The top and bottom of the boxes show the 1st (Q1) and 3rd (Q3) quartile respectively, while the whiskers show Q1 or Q3 ±1.5 of the interquartile range. The black line within the box indicates the median value and outliers are shown by small circles. AS: active sleep; IS: indeterminate sleep; QS: quiet sleep.

	Cases		Controls		p-value	95% Confidence intervals of the
	n	Median (%)	n	Median (%)		difference (cases minus controls)
Active	13	89	18	90	0.89	(-2.22, 2.06)
Indeterminate	17	91	20	91	0.15	(-1.88, 0.48)
Quiet	14	92	19	92	0.91	(-1.42, 1.36)

Table 27: Results of Mann-Whitney U tests comparing relative delta band power for cases and controls for each sleep state.

No statistical difference was found between the relative delta power medians for any sleep state. This indicates that there was no difference identifiable between the study groups using this methodology.

Relative Delta Low (0-2 Hz) Band Power

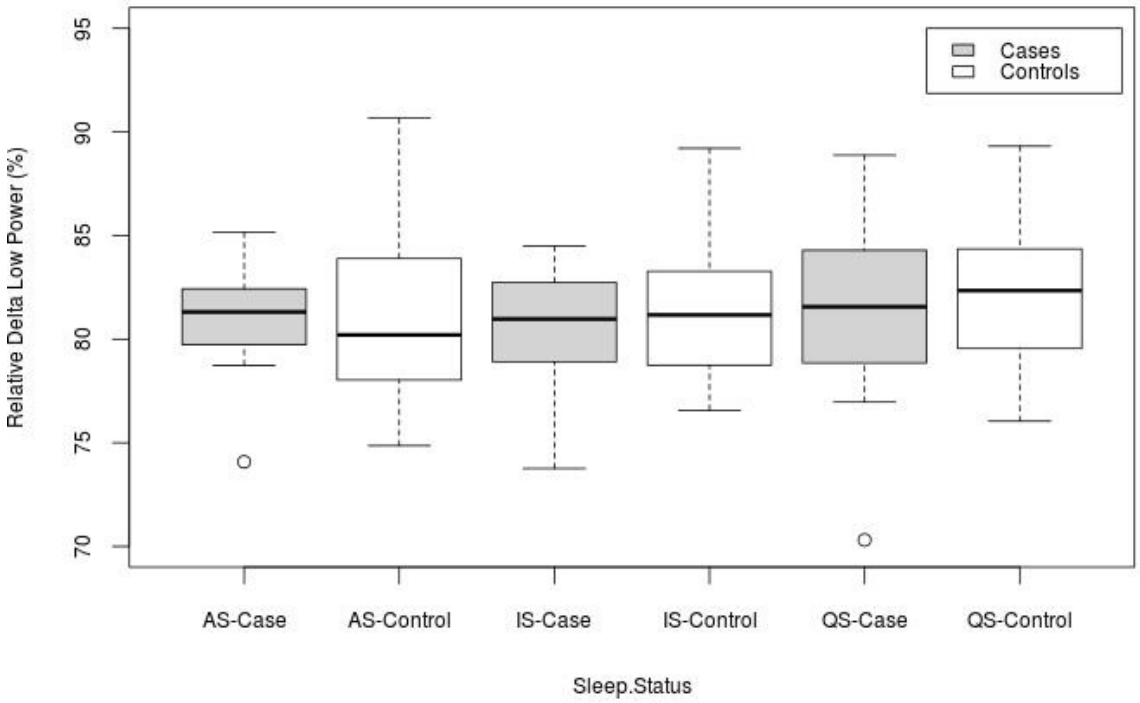

Figure 61: Box plots for relative low delta power (0-2 Hz) band power for all three sleep states, with cases shown in grey. The top and bottom of the boxes show the 1st (Q1) and 3rd (Q3) quartile respectively, while the whiskers show Q1 or Q3 ±1.5 of the interquartile range. The black line within the box indicates the median value and outliers are shown by small circles. AS: active sleep; IS: indeterminate sleep; QS: quiet sleep.

	Cases		Controls		p-value	95% Confidence intervals of the
	n	Median (%)	n	Median (%)		difference (cases minus controls)
Active	13	81.3	18	80.2	0.77	(-2.89, 3.35)
Indeterminate	17	81.0	20	81.2	0.70	(-3.02, 1.54)
Quiet	14	81.6	19	82.3	0.77	(-3.20, 2.34)

Table 28: Results of Mann-Whitney U tests comparing relative delta low band power for cases and controls for each sleep state.

No statistical difference was found between the relative low delta power medians for any sleep state again indicating that there was no difference identifiable between the study groups using this methodology.

Relative Delta High (2-4 Hz) Band Power

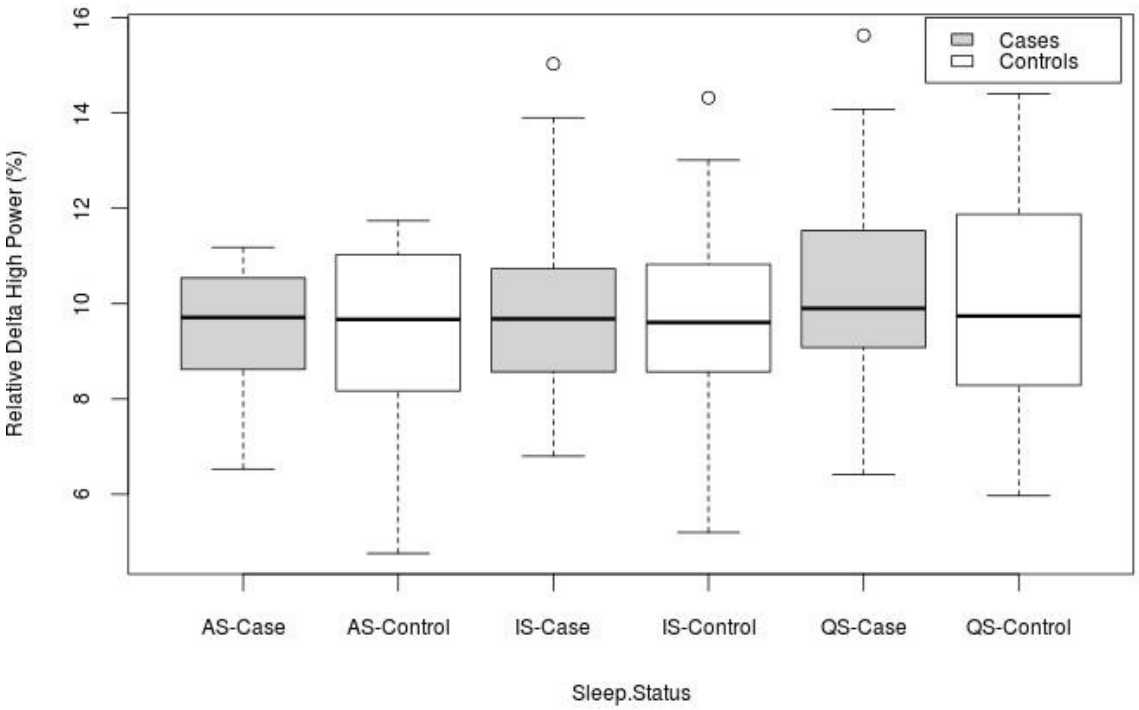

Figure 62: Box plots for relative high delta power (2-4 Hz) band power for all three sleep states, with cases shown in grey. The top and bottom of the boxes show the 1st (Q1) and 3rd (Q3) quartile respectively, while the whiskers show Q1 or Q3 ±1.5 of the interquartile range. The black line within the box indicates the median value and outliers are shown by small circles. AS: active sleep; IS: indeterminate sleep; QS: quiet sleep.

	Cases		Controls		p-value	95% Confidence intervals of the
	n	Median (%)	n	Median (%)		difference (cases minus controls)
Active	13	9.71	18	9.67	0.86	(-1.21, 1.22)
Indeterminate	17	9.68	20	9.61	0.84	(-1.44, 1.21)
Quiet	14	9.90	19	9.74	0.65	(-1.50, 2.16)

Table 29: Results of Mann-Whitney U tests comparing relative delta high band power for cases and controls for each sleep state.

No statistical difference was found between the relative high delta power medians for any sleep state. This indicates that there was no difference identifiable between the study groups using this methodology.

Relative Theta (4-8 Hz) Band Power

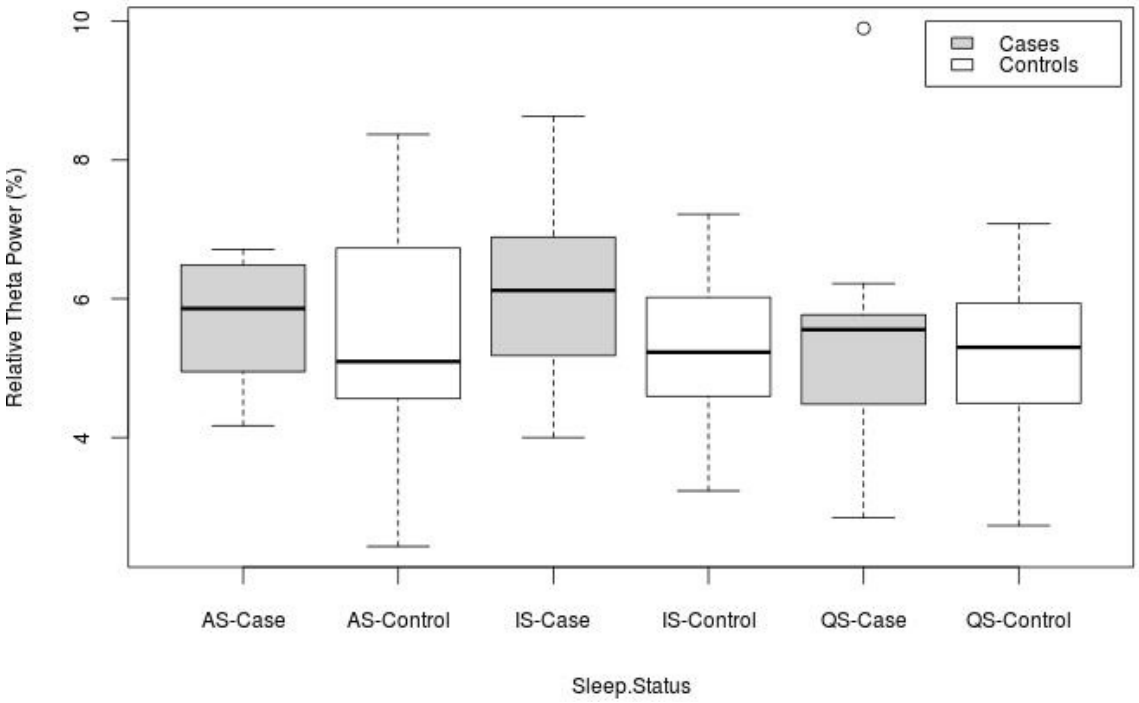

Figure 63: Box plots for relative theta power (4-8 Hz) band power for all three sleep states, with cases shown in grey. The top and bottom of the boxes show the 1st (Q1) and 3rd (Q3) quartile respectively, while the whiskers show Q1 or Q3 ±1.5 of the interquartile range. The black line within the box indicates the median value and outliers are shown by small circles. AS: active sleep; IS: indeterminate sleep; QS: quiet sleep.

	Cases		Controls		p-value	95% Confidence intervals of the
	n	Median (%)	n	Median (%)		difference (cases minus controls)
Active	13	5.86	18	5.10	0.72	(-0.87, 1.39)
Indeterminate	**17**	**6.12**	**20**	**5.23**	**0.05**	**(-0.02, 1.64)**
Quiet	14	5.56	19	5.30	0.99	(-0.36, 0.33)

Table 30: Results of Mann-Whitney U tests comparing relative theta band power for cases and controls for each sleep state.

No statistical difference was found between the relative theta power medians for any sleep state, although relative theta, as for absolute theta was closest to having a statistical significance. However these results still indicate no difference identifiable between the study groups using this statistical methodology.

Relative Alpha (8-12 Hz) Band Power

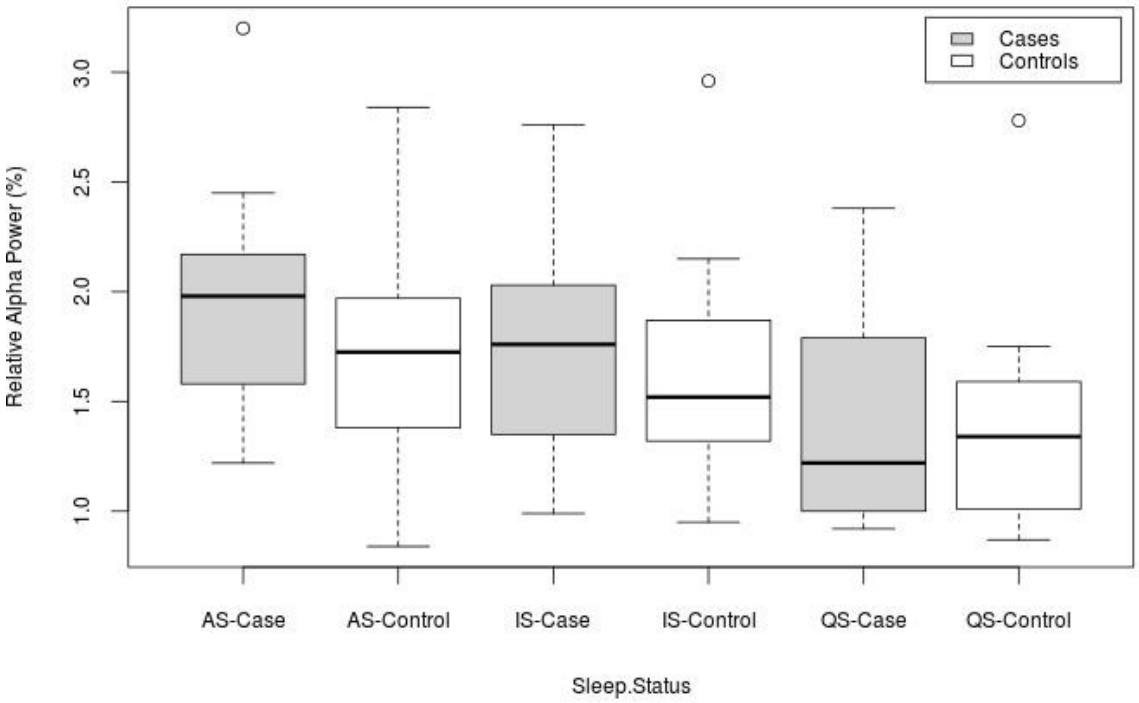

Figure 64: Box plots for relative alpha power (8-12 Hz) band power for all three sleep states, with cases shown in grey. The top and bottom of the boxes show the 1st (Q1) and 3rd (Q3) quartile respectively, while the whiskers show Q1 or Q3 ±1.5 of the interquartile range. The black line within the box indicates the median value and outliers are shown by small circles. AS: active sleep; IS: indeterminate sleep; QS: quiet sleep.

	Cases		Controls		p-value	95% Confidence intervals of the
	n	Median (%)	n	Median (%)		difference (cases minus controls)
Active	13	1.98	18	1.73	0.41	(-0.28, 0.54)
Indeterminate	17	1.76	20	1.52	0.42	(-0.14, 0.42)
Quiet	14	1.22	19	1.34	0.99	(-0.36, 0.33)

Table 31: Results of Mann-Whitney U tests comparing relative alpha band power for cases and controls for each sleep state.

No statistical difference was found between the relative alpha power medians for any sleep state, once again indicating that there was no difference identifiable between the study groups using this methodology.

Relative Beta (12-30 Hz) Band Power

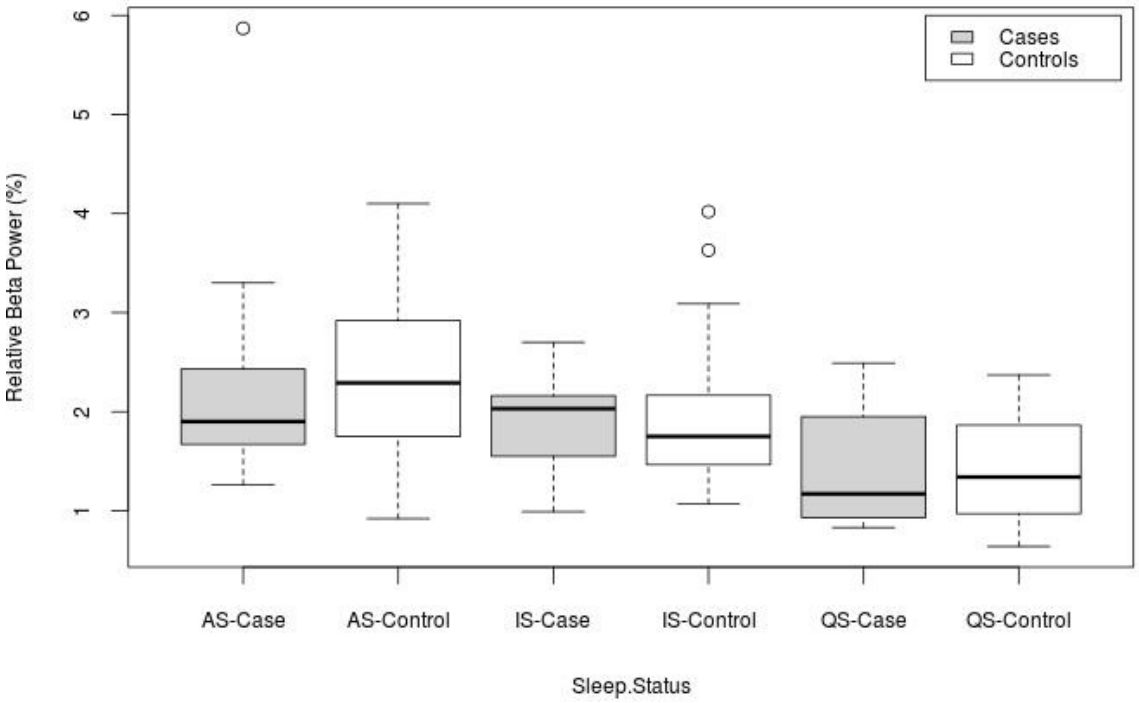

Figure 65: Box plots for relative beta power (12-30 Hz) band power for all three sleep states, with cases shown in grey. The top and bottom of the boxes show the 1st (Q1) and 3rd (Q3) quartile respectively, while the whiskers show Q1 or Q3 ±1.5 of the interquartile range. The black line within the box indicates the median value and outliers are shown by small circles. AS: active sleep; IS: indeterminate sleep; QS: quiet sleep.

	Cases		Controls		p-value	95% Confidence intervals of the
	n	Median (%)	n	Median (%)		difference (cases minus controls)
Active	13	1.90	18	2.29	0.36	(-0.97, 0.36)
Indeterminate	17	2.03	20	1.75	0.76	(-0.40, 0.42)
Quiet	14	1.17	19	1.34	0.99	(-0.36, 0.33)

Table 32: Results of Mann-Whitney U tests comparing relative beta band power for cases and controls for each sleep state.

As before, no statistical difference was found between the relative beta power medians for any sleep state, again indicating that there was no difference identifiable between the study groups using this methodology.

Average Spectral Edge Frequency (0.5-30 Hz)

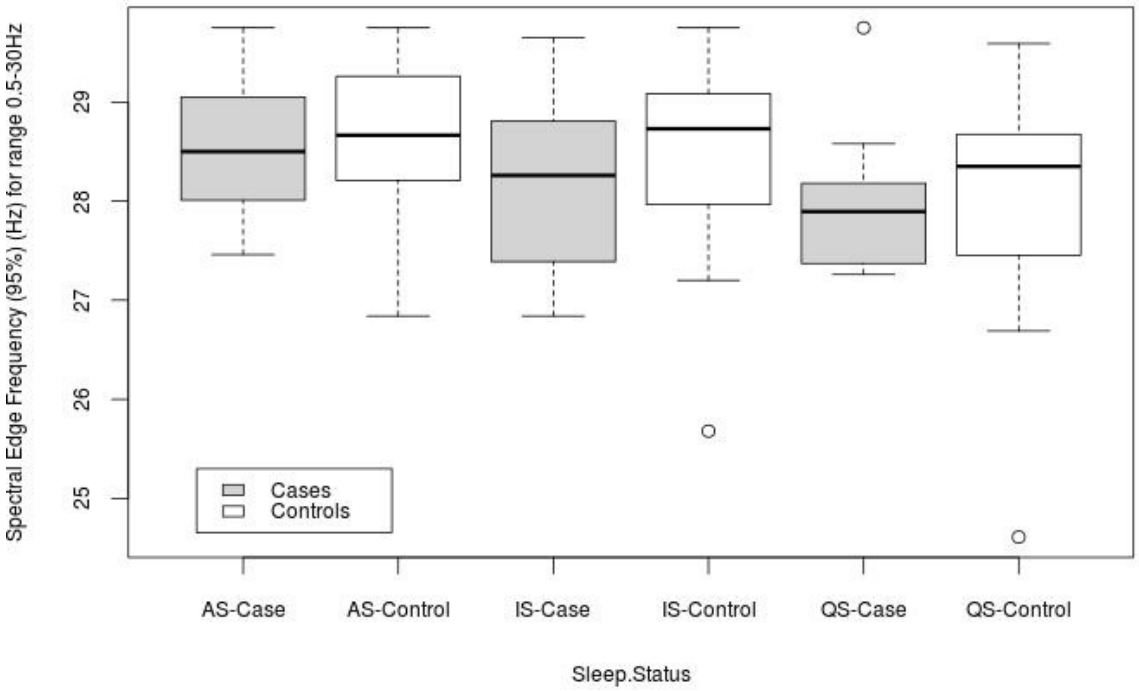

Figure 66: Box plots for spectral edge frequency 95% (0.5-30 Hz) band power for all three sleep states, with cases shown in grey. The top and bottom of the boxes show the 1st (Q1) and 3rd (Q3) quartile respectively, while the whiskers show Q1 or Q3 ±1.5 of the interquartile range. The black line within the box indicates the median value and outliers are shown by small circles. AS: active sleep; IS: indeterminate sleep; QS: quiet sleep.

	Cases		Controls		p-value	95% Confidence intervals of the difference (cases minus controls)
	n	Median (Hz)	n	Median (Hz)		
Active	13	28.5	18	28.7	0.51	(-0.76, 0.46)
Indeterminate	17	28.3	20	28.7	0.26	(-0.94, 0.25)
Quiet	14	27.9	19	28.4	0.34	(-0.91, 0.41)

Table 33: Results of Mann-Whitney U tests comparing spectral edge frequency (0.5-30 Hz) for cases and controls for each sleep state.

None of the comparisons showed a statistical difference. Bell et al., (1991), showed the SEF 95% for healthy term neonates was 22.4 – 26 Hz during active sleep. This study shows higher medians for SEF 95% indicating that the total power between these frequencies is more dispersed than for the Bell et al., (1991) study i.e. more activity in the higher frequency ranges (theta, alpha and beta), suggesting that these study neonates do not reach the same depth of sleep compared with healthy neonates.

Average Spectral Edge Frequency (2-20 Hz)

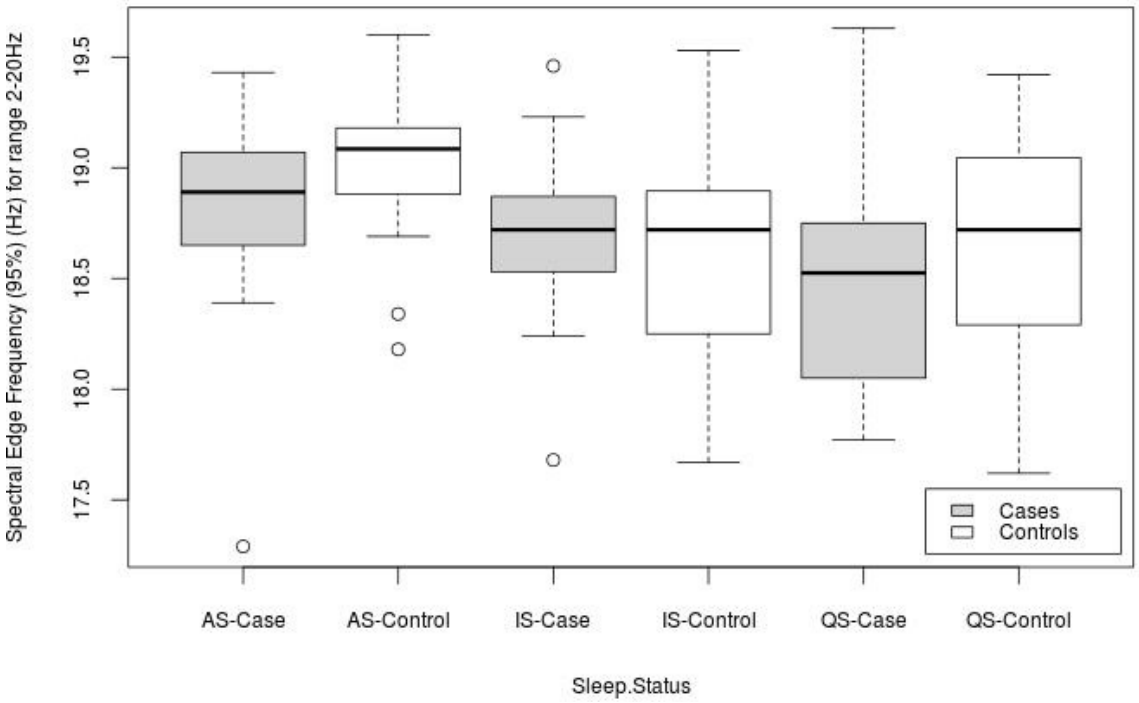

Figure 67: Box plots for spectral edge frequency 95% (2-20 Hz) band power for all three sleep states, with cases shown in grey. The top and bottom of the boxes show the 1st (Q1) and 3rd (Q3) quartile respectively, while the whiskers show Q1 or Q3 ±1.5 of the interquartile range. The black line within the box indicates the median value and outliers are shown by small circles. AS: active sleep; IS: indeterminate sleep; QS: quiet sleep.

	Cases		Controls		p-value	95% Confidence intervals of the
	n	Median (Hz)	n	Median (Hz)		difference (cases minus controls)
Active	13	18.9	18	19.1	0.15	(-0.47, 0.10)
Indeterminate	17	18.7	20	18.7	0.70	(-0.20, 0.40)
Quiet	14	18.5	19	18.7	0.35	(-0.59, 0.22)

Table 34: Results of Mann-Whitney U tests comparing spectral edge frequency (2-20 Hz) for cases and controls for each sleep state.

In this analysis, SEF 95% for 2-20 Hz showed no statistical difference between groups. This range is more suitable for electrically noisy environments such as NICU, so the passband is not as wide as the method suggested by Bell et al., (1991). However delta activity is the predominant frequency in the sleeping neonate (Scher, 1996), so to have a cut off at 2 Hz loses all low frequency band power (0-2 Hz).

7.3.4 EEG Frequency Domain Median Comparisons

The tables that follow (tables 35, 36 and 37) highlight the relative difference between each variable, as a guide to how they differ from each other. Their purpose is to show any large differences when the previous statistical analysis has shown none. The method of calculating the percentage median is shown in equation 13, with the results of the comparison shown below.

$$Relative\ Difference = \frac{(Case\ Median - Control\ Median)}{Case\ Median} \times 100 \quad (13)$$

EEG Frequency Domain Median Comparison for Active Sleep

Variable	Cases (n=20)	Controls (n=25)	Relative Difference (%)
Absolute Delta Power 0-4 Hz (μV^2/Hz)	1499	1382	7.8
Absolute Delta Low Power 0-2 Hz (μV^2/Hz)	1377	1251	9.2
Absolute Delta High Power 2-4 Hz (μV^2/Hz)	**147**	**105**	**28.6**
Absolute Theta Power 4-8 Hz (μV^2/Hz)	62	55	11.3
Absolute Alpha Power 8-12 Hz (μV^2/Hz)	20	18	10.0
Absolute Beta Power 12-30 Hz (μV^2/Hz)	20	18	10.0
Absolute Total Power (μV^2/Hz)	1587	1489	6.2
Average SEF 95% (0.5-30 Hz) Hz	28.5	28.7	-0.7
Average SEF 95% (2-20 Hz) Hz	18.9	19.1	-1.1

Table 35: Relative differences in median values between cases and controls for active sleep. In all but one of the variables, the cases median values were higher than the controls, especially in the high delta band (2-4 Hz), highlighted in bold. A positive percentage difference indicates that the cases have higher medians than the controls.

EEG Frequency Domain Median Comparison for Indeterminate Sleep

Variable	Cases (n=20)	Controls (n=25)	Relative Difference (%)
Absolute Delta Power 0-4 Hz (μV^2/Hz)	1268	1132	10.7
Absolute Delta High Power 2-4 Hz (μV^2/Hz)	1140	1048	8.1
Absolute Delta Low Power 0-2 Hz (μV^2/Hz)	**129**	**96**	**25.6**
Absolute Theta Power 4-8 Hz (μV^2/Hz)	**69**	**50**	**27.5**
Absolute Alpha Power 8-12 Hz (μV^2/Hz)	17	15	11.8
Absolute Beta Power 12-30 Hz (μV^2/Hz)	17	15	11.8
Absolute Total Power 0-30 Hz (μV^2/Hz)	1372	1201	12.5
Average SEF 95% (0.5-30 Hz) Hz	28.3	28.7	-1.4
Average SEF 95% (2-20 Hz) Hz	18.7	18.7	0

Table 36: Relative differences in median values between cases and controls for indeterminate sleep. In all but one of the variables, the cases median values were higher than the controls, especially in the absolute low delta (0-2 Hz) and theta (4-8 Hz) bands, highlighted in bold. A difference indicates that the cases have higher medians than the controls.

EEG Frequency Domain Median Comparison for Quiet Sleep

Variable	Cases (n=20)	Controls (n=25)	Relative Difference (%)
Absolute Delta Power 0-4 Hz (μV^2/Hz)	1687	1370	18.8
Absolute Delta High Power 2-4 Hz (μV^2/Hz)	**1528**	**1212**	**20.7**
Absolute Delta Low Power 0-2 Hz (μV^2/Hz)	138	141	-2.2
Absolute Theta Power 4-8 Hz (μV^2/Hz)	72	66	8.3
Absolute Alpha Power 8-12 Hz (μV^2/Hz)	18	17	5.6
Absolute Beta Power 12-30 Hz (μV^2/Hz)	18	17	5.6
Absolute Total Power 0-30 Hz (μV^2/Hz)	1794	1477	17.7
Average SEF 95% for (0.5-30 Hz) Hz	27.9	28.4	-1.8
Average SEF 95% for (2-20 Hz) Hz	18.5	18.7	-1.1

Table 37: Relative differences in median values between cases and controls for quiet sleep. There are large differences between groups for absolute high delta (2-4 Hz), highlighted in bold. The large difference in delta power would account for the difference shown in delta power (0-4 Hz) and the total power (0-30 Hz). A positive difference indicates that the cases have higher medians than the controls.

The largest differences between the groups are summarised below:

- Active sleep: 28.6 % greater delta high power in cases.
- Indeterminate sleep: 25.6 % greater delta low power, and 27.5 % greater theta power in cases.
- Quiet sleep: 20.7 % greater delta high power in cases.

These results show that during sleep, the cases had larger amplitude activity in the delta band (0-4 Hz) for all sleep states. This increased activity is also shown in that the total power for the cases is higher than for the controls. Absolute theta power (4-8 Hz) activity for the cases is also higher in the indeterminate sleep stages. These raised levels in the cases may be an indicator of abnormal sleep states, indicative of impaired homoeostatic regulation of the autonomic nervous system.

7.4 Summary

The two groups were matched on a number of factors during recruitment (gestation, birth weight and socio-economic status), ensuring that the two study groups were similar. The results of the EEG analysis show that there were no differences between the study groups using spectral analysis and comparing medians with non-parametric tests. However, non-statistically significant observations can be seen in the sleep states between groups, with the cases showing greater absolute power than controls in the absolute delta and theta bands.

8 ECG and CVT Experiments

8.1 Introduction

This chapter describes the recording, interpretation and analysis of the ECG and vagal tone. It covers equipment, software used, the recording parameters and justification for their use and methodology used to acquire data. Finally the results of the analysis are given.

8.2 Methods

8.2.1 Experimental Set Up

The ECG was recorded as part of the PSG, and was described in section 7.2.1. Briefly this involved attaching three electrodes on the chest of the infant to record the electrical activity of the heart during sleep, and identifying the RR intervals necessary for HRV analysis. The sampling frequency of the Xltek PSG equipment was 256 Hz, and the recording length was approximately one hour, with the aim of capturing all three sleep states.

Epochs were selected for analysis based on sleep state as determined by EEG. Interpretation of the EEG was undertaken by a consultant paediatric neurologist, blinded to the infant's prenatal drug exposure group and subsequent clinical course. Selected epochs included quiet, active and indeterminate sleep. Ideally epoch lengths of 120 seconds or greater should be selected, but very few scored sections of this length could be found without movement artefact. An epoch length of 60 seconds was chosen as a compromise between being too short to be able to identify the overall trend of the ECG, and so long that it would include artefact: shorter epoch lengths with no artefact were

considered more desirable than longer epochs containing artefact. Removal of artefact was not considered as this would often introduce mismatch between start and end points, and would distort the baseline voltage.

8.2.2 ECG Analysis

HRV analysis is defined as the variation in the time interval between heart beats, or RR intervals as seen on the ECG. Prior to analysis, the points in time where the R wave occurs are identified and marked. Although this can be done manually, it is more usual to perform an automated RR interval extraction, thus allowing consideration of a large number of peaks within a data set (see section 5.4.2). This peak to peak dataset is then the basis for analysis in either the time or frequency domain.

8.2.3 Software Used

The three software requirements for the analysis were as follows.

1. Accurate estimation of the RR interval from the ECG recording.
2. Analysis of HRV in the time domain.
3. Analysis of HRV in the frequency domain.

The applications chosen to satisfy these requirement were EDF browser for RR interval extraction, and Kubios HRV software for time and frequency domain analysis, both of which have been described in section 5.4.2.

8.2.4 ECG Time Domain Variables

The time domain analysis was based on direct measurements of the RR interval file produced from the EDF browser software, and analysed by the Kubious HRV software. The variables used for the time domain are shown in Table 38. Note that NN is the time

between successive R waves, when the ECG is considered normal, so for a normal ECG, RR and NN are interchangeable.

Parameter	Abbreviation
Mean heart rate	HR
Standard deviation of the mean heart rate	HR_stdev
Mean RR interval	MeanRR
Standard deviation of the RR intervals	SDNN
Root mean squared of successive differences of the RR interval	RMSSD
Poincaré plot standard descriptor 1 & 2	SD1 & 2

Table 38: HRV time domain variables used in this analysis.

8.2.5 ECG Frequency Domain Variables

The frequency domain analysis was also performed using the Kubios HRV software and based on power spectral density estimation using the Welch method (Welch periodogram) described by Welch, (1967). This technique uses windowing to taper the beginning and the end of the epoch to reduce noise in the estimated power spectrum, but at the cost of reducing the frequency resolution. It is a technique that is more suited for identifying trends over longer windows (such as 60 seconds) than finding short bursts of activity such as spikes.

For this analysis, the window chosen was 4 seconds, acquired at 256 Hz, giving 1024 data-points per window. Since the length of the epoch was 60 seconds, 15 analysis windows (each 4 second long) were used to cover the epoch. This approach was similar to Doyle et al., (2009), although they used a Lomb periodogram as opposed to a Welch periodogram.

Band power was then estimated from the periodogram using the ranges set out by the European Society Guidelines for HRV analysis (Force, 1996). The ranges are shown in Table 39.

Frequency Band	Lower Limit (Hz)	Upper Limit (Hz)
Very low frequency (VLF)	0	0.04
Low frequency (LF)	0.04	0.15
High frequency (HF)	0.15	0.40

Table 39: Band power ranges and parameters used for the HRV analysis.

However there is variation between studies concerning limits, as shown in Table 40.

Study	ULF (Hz)	VLF (Hz)	LF or MF (Hz)	HF (Hz)	Total Power (ms^2/Hz)	LF/HF
(Mehta et al., 2002)	<0.0033	0.0033-0.04	0.04-0.15	0.15-0.40	¸	¸
(Schäffer et al., 2008)	<0.003	0.003-0.04	0.04-0.24	0.24-1.04	¸	¸
(Longin et al., 2005)	-	0.01-0.05 (LF)	0.05-0.2 (MF*)	0.2-1.0	¸	MF/HF
(Spassov et al., 1994)	-	0.01-0.034 (LF*)	0.04-0.1 (MF*)	0.125-0.34	-	-
(Doyle et al., 2009)	-	0.01-0.04	0.04-0.2	>0.2	-	¸
(Selig et al., 2011)	-	Used but not defined	Used but not defined	Used but not defined	-	¸
* Note that some studies used LF or MF to mean the same frequency range.						

Table 40: Variables and ranges used for spectral analysis across a range of neonatal HRV studies. ULF- ultra low frequency; VLF – very low frequency; LF – low frequency; MF - mid frequency; HF – high frequency.

As a guide, high frequency (HF) represents parasympathetic activity, low frequency (LF) sympathetic activity, very low frequency (VLF), mainly parasympathetic activity, and the low frequency/ high frequency ration (LF/HF) is considered as a marker of sympathetic-parasympathetic balance (Schäffer et al., 2008).

The variables used for both the frequency domain analysis are shown in table Table 41.

Parameter	Abbreviation
Frequency analysis – Very low frequency (VLF)	Spec_VLF
Frequency analysis – Low frequency (LF)	Spec_LF
Frequency analysis – High frequency (HF)	Spec_HF
Frequency analysis – Total power	Spec_Total
Frequency analysis – LF/HF ratio	Spec_LF/HF

Table 41: HRV frequency domain variables used in this analysis.

8.2.6 CVT Analysis

The Neuroscope™ TONE software (version 3.14f) by Medifit Instruments Ltd was used to produce the vagal tone measurements (www.medifitgroup.com/Neurology.htm). Prior to analysis two steps of pre-processing were performed. These steps were applied to the raw ECG file in EDF file format. Since the Neuroscope™ software incorporates an RR extraction facility, it was not necessary to use the EDF browser function.

The first step removed DC shift or any decaying baseline. The second step applied a simple five point smoothing algorithm, each point with equal weight. This latter step removed or smothed any unsual peaks or spikes that might have been apparent during the visual scoring of PSG and selection of apparently artefact free sleep epochs. An example of the Neuroscope™ software can be seen in Figure 68. Both pre-processing steps were performed using custom propriety software written by Dr Stig Hansen, Department of Clinical Physics and Bioengineering at the Southern General Hospital, Glasgow.

As the software was originally designed to run on a standard PC running Microsoft MS-DOS and was not Microsoft Windows XP compatible, it was run within the DOSbox emulation application (www.dosbox.com).

For each epoch, the start and the end points were highlighted manually, as seen by the dotted vertical lines in Figure 68. The CVT and its standard deviation were then calculated using the method developed by Julu, (1992). As the selection of epochs was performed manually, any small artefact that was not identified during the PSG scoring, or altered by the pre-processing was carefully avoided at this stage.

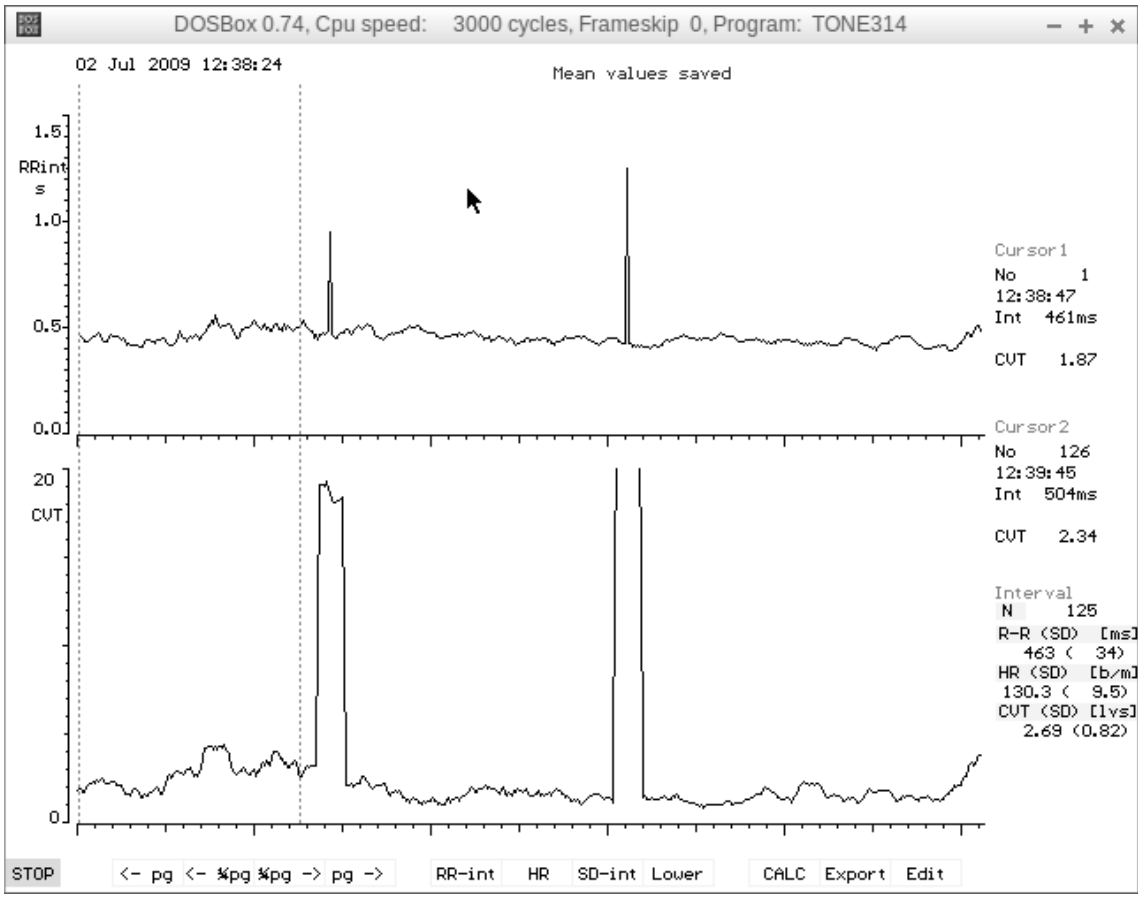

Figure 68: The Neuroscope software running within the DOSbox emulation software. A one minute epoch used has been selected between the dotted vertical lines, to avoid the large artefacts. The estimate of vagal tone is shown in the right hand column.

The variables used for CVT analysis are shown in table Table 42.

Parameter	Abbreviation
Cardiac vagal tone (CVT)	CVT
Standard deviation of CVT	CVT_stdev

Table 42: Cardiac vagal tone variables used in this analysis.

The final output was a comma separated value (*.csv) file which was then imported into a database for later analysis.

8.2.7 Data Management and Statistics

When data from the Kubios HRV and Neuroscope™ software were complete, the results were transferred into a spreadsheet (LibreOffice Calc 4.1) before being imported into the VIDI study database for re-linking and merging with the other study data.

On completion of the data management phase, the database was locked, and the dataset was prepared for statistical analysis. This was done using a combination of the R programming language (R Core Team, 2013) and the R-Commander graphical user interface (Fox, 2005).

8.3 Results

Data were grouped according to *in utero* drug exposure and sleep state (quiet, active and intermediate), giving six groups for analysis and comparison. To understand the nature of the data before statistical analysis, the following section is a description of the different groups in relation to each other.

8.3.1 Statistical Analysis

Normality Testing

The first part of the analysis consisted of testing the subsets of data to see if they were normally distributed. This was done by using a combination of histograms and Shapiro-Wilk normality testing (Shapiro and Wilk, 1965). The results are shown in the tables below. A dataset can be considered normally distributed if the p-value >= 0.05. It was apparent from the results of statistical testing as well as visual inspection of the histograms that much of the data was not normally distributed. Attempts were made to transform the data (x2 and log10), but these proved unsuccessful and it was therefore decided to use non-parametric tests for data analysis.

Table 43 and Table 44 show the results of the normality testing with the normally distributed variables shown in bold. The results show that there are both normally and normally distributed variables within the dataset.

	Active Sleep		Quiet Sleep		Indeterminate Sleep	
Variable	W Score	p-value	W Score	p-value	W Score	p-value
CVT	0.91	0.17	0.83	**0.01**	0.46	**0.00**
CVT_stdev	0.77	**0.00**	0.84	**0.02**	0.35	**0.00**
MeanHR	0.94	0.48	0.82	**0.01**	0.94	0.27
MeanHR_stdev	0.56	**0.00**	0.85	**0.02**	0.71	**0.00**
MeanRR	0.94	0.50	0.78	**0.00**	0.91	0.08
RMSSD	0.81	**0.01**	0.90	0.11	0.84	**0.01**
SD1	0.86	**0.04**	0.90	0.10	0.84	**0.01**
SD2	0.93	0.31	0.96	0.71	0.92	0.11
SDNN	0.92	0.24	0.96	0.71	0.91	0.10
Spec_VLF	0.90	0.12	0.82	**0.01**	0.75	**0.00**
Spec_LF	0.87	0.05	0.78	**0.00**	0.55	**0.00**
Spec_HF	0.71	**0.00**	0.86	**0.04**	0.67	**0.00**
Spec_Total	0.90	0.12	0.85	**0.03**	0.67	**0.00**
Spec_LF/HF	0.85	**0.03**	0.63	**0.00**	0.88	**0.02**

Table 43: Shapiro-Wilk normality tests of cases for the ECG variables. A p-value equal to or greater than 0.05 indicates adequate normality in the distribution. The table shows that not every variable is normally distributed. Bold text indicates normally distributed data.

	Active Sleep		Quiet Sleep		Indeterminate Sleep	
Variable	W Score	p-value	W Score	p-value	W Score	p-value
CVT	0.91	0.17	0.83	**0.01**	0.46	**0.00**
CVT_stdev	0.77	**0.00**	0.84	**0.02**	0.35	**0.00**
MeanHR	0.94	0.48	0.82	**0.01**	0.94	0.27
MeanHR_stdev	0.56	**0.00**	0.85	**0.02**	0.71	**0.00**
MeanRR	0.94	0.50	0.78	**0.00**	0.91	0.08
RMSSD	0.81	**0.01**	0.90	0.11	0.84	**0.01**
SD1	0.86	**0.04**	0.90	0.10	0.84	**0.01**
SD2	0.93	0.31	0.96	0.71	0.92	0.11
SDNN	0.92	0.24	0.96	0.71	0.91	0.10
Spec_VLF	0.65	**0.00**	0.87	**0.02**	0.63	**0.00**
Spec_LF	0.78	**0.00**	0.93	**0.16**	0.55	**0.00**
Spec_HF	0.63	**0.00**	0.50	**0.00**	0.89	**0.02**
Spec_Total	0.76	**0.00**	0.82	**0.00**	0.70	**0.00**
Spec_LF/HF	0.90	0.06	0.78	**0.00**	0.68	**0.00**

Table 44: Shapiro-Wilk normality tests of controls for the ECG variables. A p-value equal to or greater than 0.05 indicates adequate normality in the distribution. The table shows that not every variable is normally distributed. Bold text indicates normally distributed data.

8.3.2 ECG Time & Frequency Domain Results

Each variable has been described graphically (box plots) for visual comparison, and presented in a table showing the results of the Mann-Whitney test for non-parametric data. Where the Mann-Whitney test showed a statistically significant differences, Bonferroni corrections were applied.

Mean Heart Rate

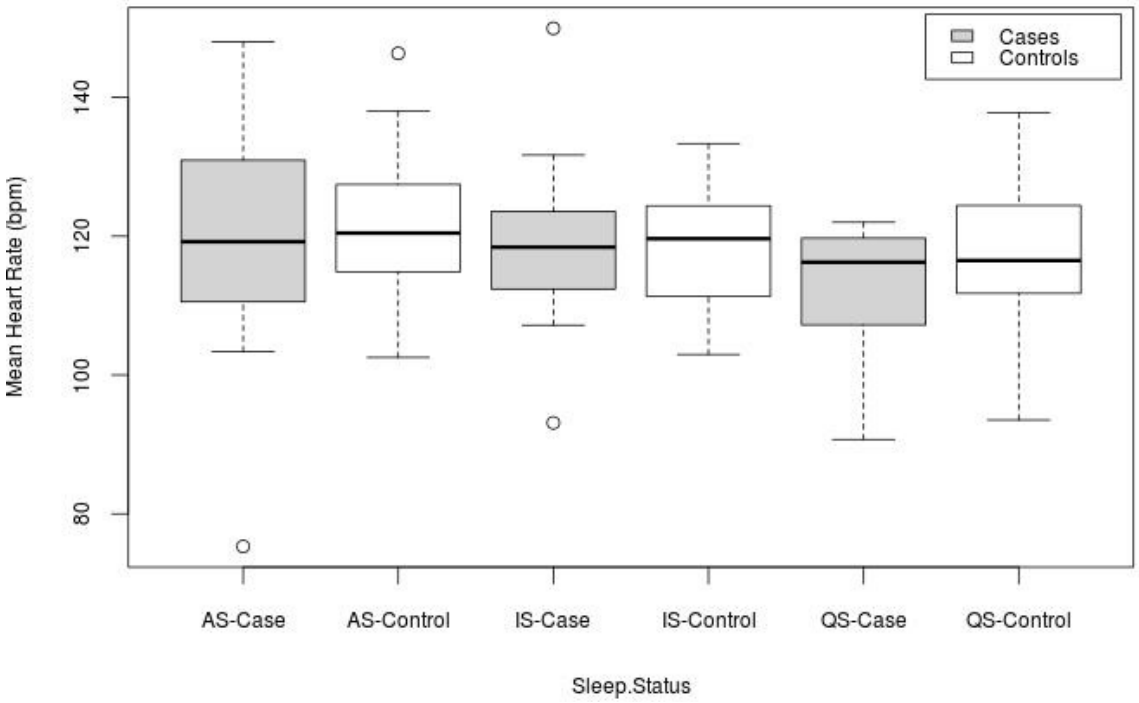

Figure 69: Box plots for mean heart rate for all three sleep states, with cases shown in grey. The top and bottom of the boxes show the 1st (Q1) and 3rd (Q3) quartile respectively, while the whiskers show Q1 or Q3 ±1.5 of the interquartile range. The black line within the box indicates the median value and outliers are shown by small circles. AS: active sleep; IS: indeterminate sleep; QS: quiet sleep.

	Cases		Controls		p-value	95% Confidence intervals of the
	n	Median (bpm)	n	Median (bpm)		difference (cases minus controls)
Active	13	119	19	120	0.88	(-10.70, 8.03)
Indeterminate	18	118	20	120	0.78	(-6.83, 5.54)
Quiet	14	116	19	116	0.42	(-12.61, 3.73)

Table 45: Results of Mann-Whitney U tests comparing median values for mean heart rate for cases and controls for each sleep state.

No statistical difference was found between the median values of mean heart rate for any sleep state. This indicates that there was no difference identifiable between the study groups using this statistical methodology.

Mean Heart Rate (Standard Deviation) SDNN

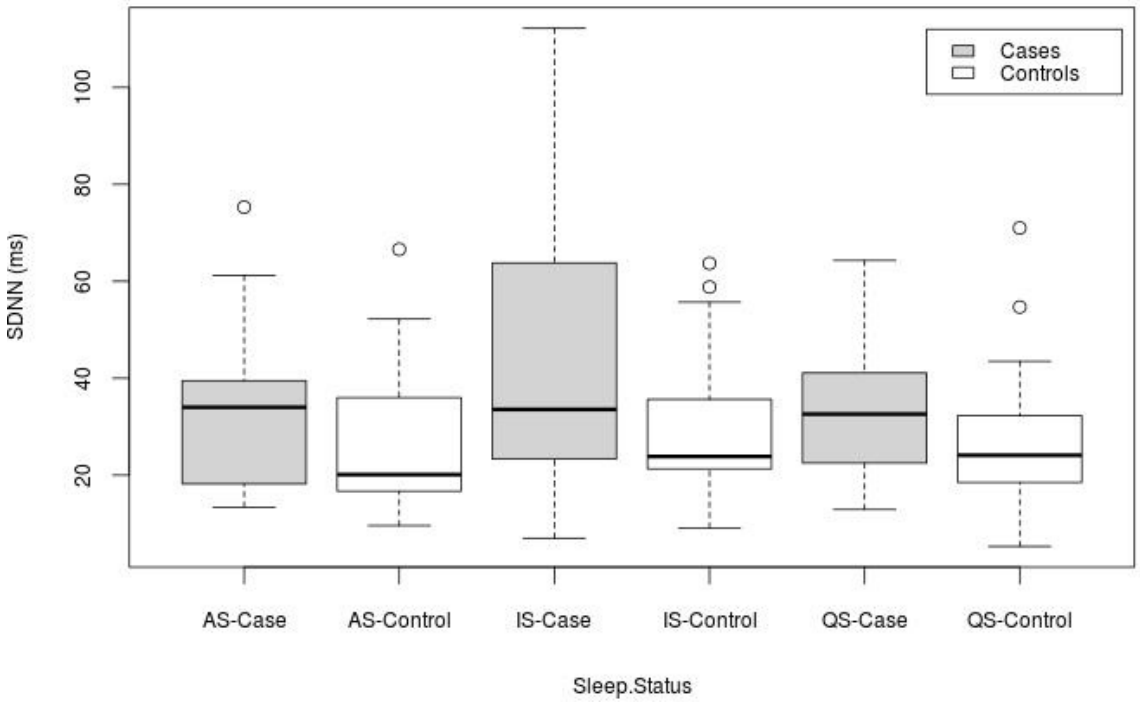

Figure 70: Box plots for mean heart rate standard deviation (SDNN) for all three sleep states, with cases shown in grey. The top and bottom of the boxes show the 1st (Q1) and 3rd (Q3) quartile respectively, while the whiskers show Q1 or Q3 ±1.5 of the interquartile range. The black line within the box indicates the median value and outliers are shown by small circles. AS: active sleep; IS: indeterminate sleep; QS: quiet sleep.

	Cases		Controls		p-value	95% Confidence intervals of the difference (cases minus controls)
	n	Median (ms)	n	Median (ms)		
Active	13	34.0	18	20.1	0.27	(-3.4, 20.3)
Indeterminate	17	33.6	20	23.9	0.10	(-2.1, 21.7)
Quiet	14	32.6	19	24.1	0.12	(-1.9, 16.7)

Table 46: Results of Mann-Whitney U tests comparing median values for mean heart rate (standard deviation) for cases and controls for each sleep state.

No statistical difference was found between the median values of mean heart rate (standard deviation) for any sleep state. This indicates that there was no difference identifiable between the study groups using this statistical methodology.

Mean RR Interval

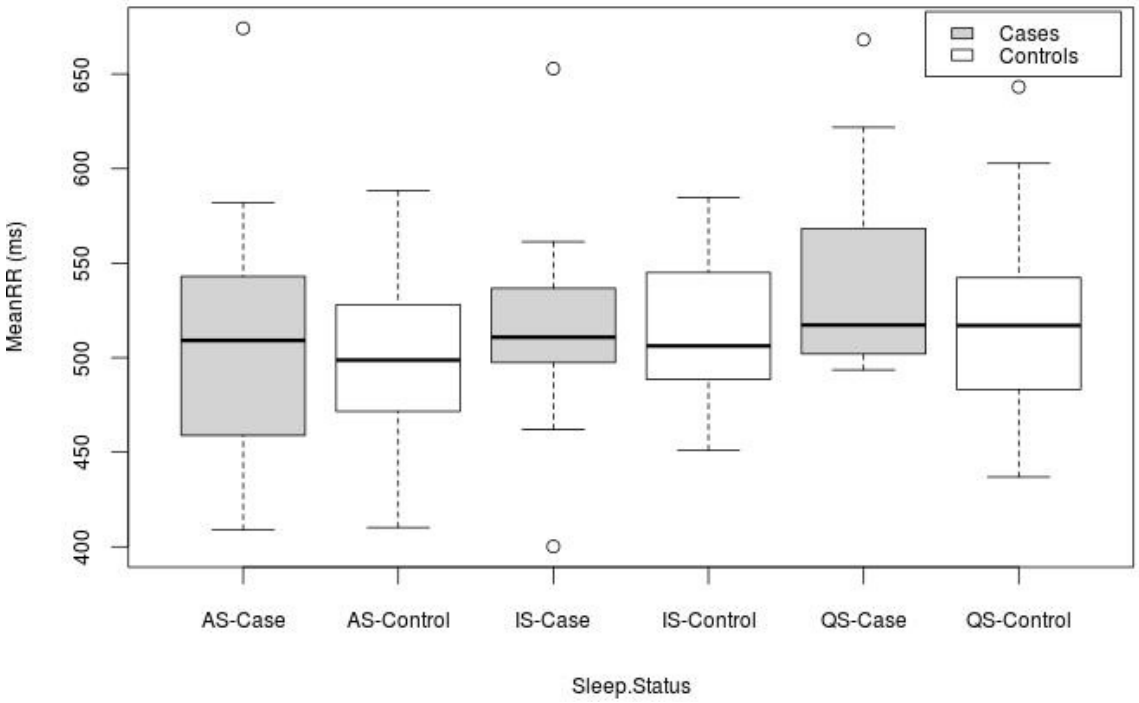

Figure 71: Box plots for mean RR interval for all three sleep states, with cases shown in grey. The top and bottom of the boxes show the 1st (Q1) and 3rd (Q3) quartile respectively, while the whiskers show Q1 or Q3 ±1.5 of the interquartile range. The black line within the box indicates the median value and outliers are shown by small circles. AS: active sleep; IS: indeterminate sleep; QS: quiet sleep.

	Cases		Controls		p-value	95% Confidence intervals of the
	n	Median (ms)	n	Median (ms)		difference (cases minus controls)
Active	13	509	19	499	0.79	(-31.2, 46.5)
Indeterminate	18	511	20	506	0.70	(-23.5, 32.5)
Quiet	14	517	19	517	0.38	(-17.6, 54.1)

Table 47: Results of Mann-Whitney U tests comparing the medians of the mean RR intervals for cases and controls for each sleep state.

No statistical difference was found between the median values of mean RR interval for any sleep state. This indicates that there was no difference identifiable between the study groups using this statistical methodology.

RMSSD

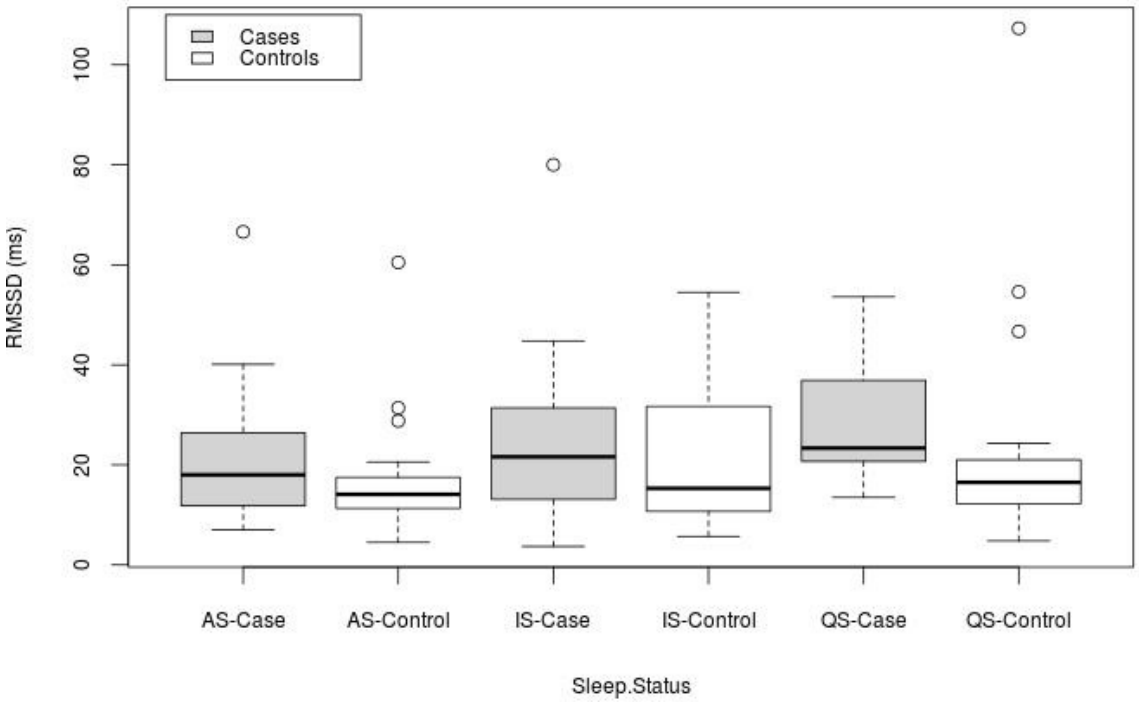

Figure 72: Box plots for RMSSD for all three sleep states, with cases shown in grey. The top and bottom of the boxes show the 1st (Q1) and 3rd (Q3) quartile respectively, while the whiskers show Q1 or Q3 ±1.5 of the interquartile range. The black line within the box indicates the median value and outliers are shown by small circles. AS: active sleep; IS: indeterminate sleep; QS: quiet sleep.

	Cases		Controls		p-value	95% Confidence intervals of the
	n	Median (ms)	n	Median (ms)		difference (cases minus controls)
Active	13	18.0	19	14.1	0.27	(-2.5, 10.3)
Indeterminate	18	21.6	20	15.3	0.51	(-6.10, 11.2)
Quiet	**14**	**23.4**	**19**	**16.5**	**0.032**	**(0.7, 17.4)**

Table 48: Results of Mann-Whitney U tests comparing the medians of RMSSD for cases and controls for each sleep state.

Although quiet sleep showed a statistically significant difference between groups, on the application of the Bonferroni correction (3 sleep states x 0.032 = 0.096), the difference was no longer statistically significant. Otherwise, no difference was found between the median values of RMSSD values for any sleep state using this statistical methodology.

Poincaré Plots (SD1)

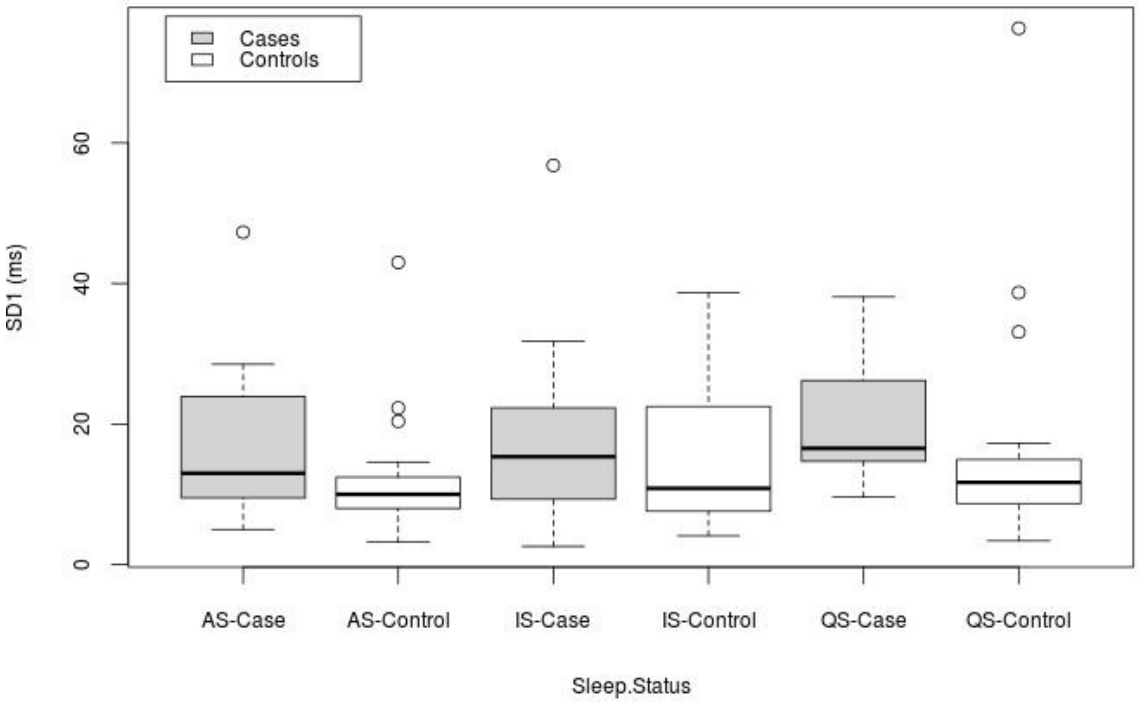

Figure 73: Box plots for Poincaré plot SD1 for all three sleep states, with cases shown in grey. The top and bottom of the boxes show the 1st (Q1) and 3rd (Q3) quartile respectively, while the whiskers show Q1 or Q3 ±1.5 of the interquartile range. The black line within the box indicates the median value and outliers are shown by small circles. AS: active sleep; IS: indeterminate sleep; QS: quiet sleep.

	Cases		Controls		p-value	95% Confidence intervals of the difference (cases minus controls)
	n	Median (ms)	n	Median (ms)		
Active	13	13.0	19	10.0	0.11	(-1.0, 9.8)
Indeterminate	18	15.4	20	10.9	0.51	(-4.4, 8.0)
Quiet	**14**	**16.6**	**19**	**11.7**	**0.03**	**(0.7, 17.4)**

Table 49: Results of Mann-Whitney U tests comparing the medians of Poincaré Plot SD1 for cases and controls for each sleep state

Although quiet sleep showed a statistically significant difference, on the application of the Bonferroni correction (3 sleep states x 0.032 = 0.096), the difference was no longer significant. No statistical difference was therefore found between the median values of SD1 for any sleep state. This indicates that there was no difference identifiable between the study groups using this statistical methodology.

Poincaré Plots (SD2)

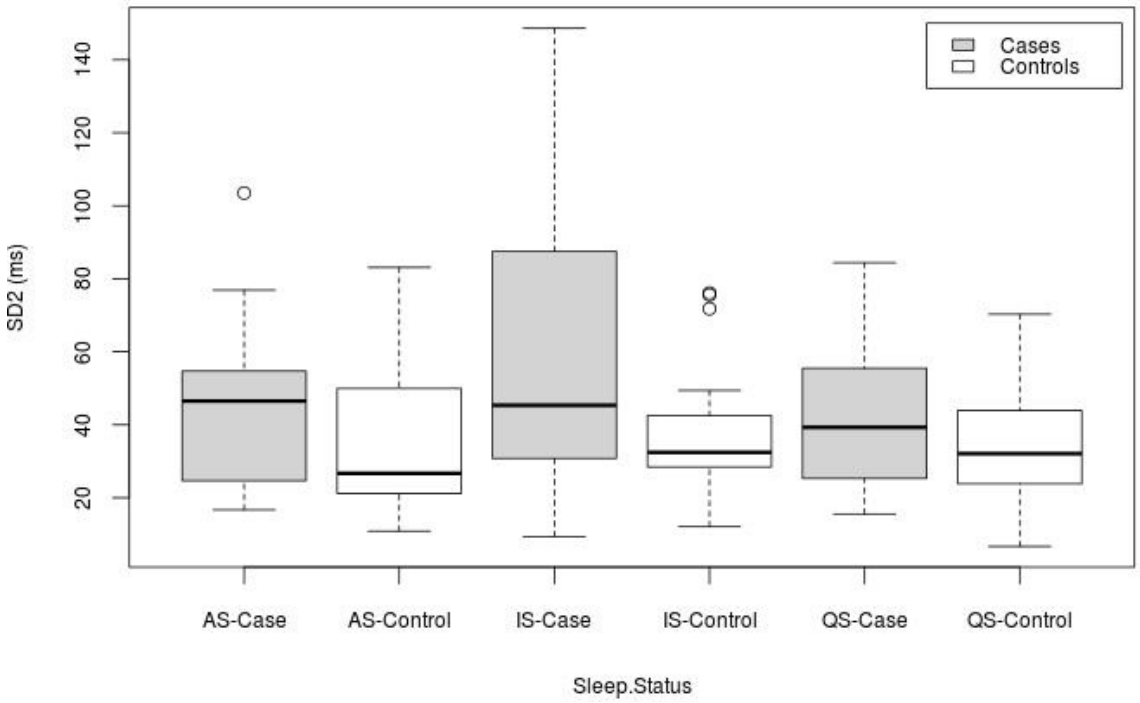

Figure 74: Box plots for Poincaré plot SD2 for all three sleep states, with cases shown in grey. The top and bottom of the boxes show the 1st (Q1) and 3rd (Q3) quartile respectively, while the whiskers show Q1 or Q3 ±1.5 of the interquartile range. The black line within the box indicates the median value and outliers are shown by small circles. AS: active sleep; IS: indeterminate sleep; QS: quiet sleep.

	Cases		Controls		p-value	95% Confidence intervals of the difference (cases minus controls)
	n	Median (ms)	n	Median (ms)		
Active	13	46.5	19	26.7	0.27	(-5.1, 27.6)
Indeterminate	18	45.4	20	32.5	0.07	(-1.5, 27.2)
Quiet	14	39.3	19	32.1	0.21	(-4.4, 23.0)

Table 50: Results of Mann-Whitney U tests comparing the medians of Poincaré Plot SD2 for cases and controls for each sleep state.

No statistical difference was found between the median values of Poincaré SD2 for any sleep state. This indicates that there was no difference identifiable between the study groups using this statistical methodology.

Spectral Analysis – VLF

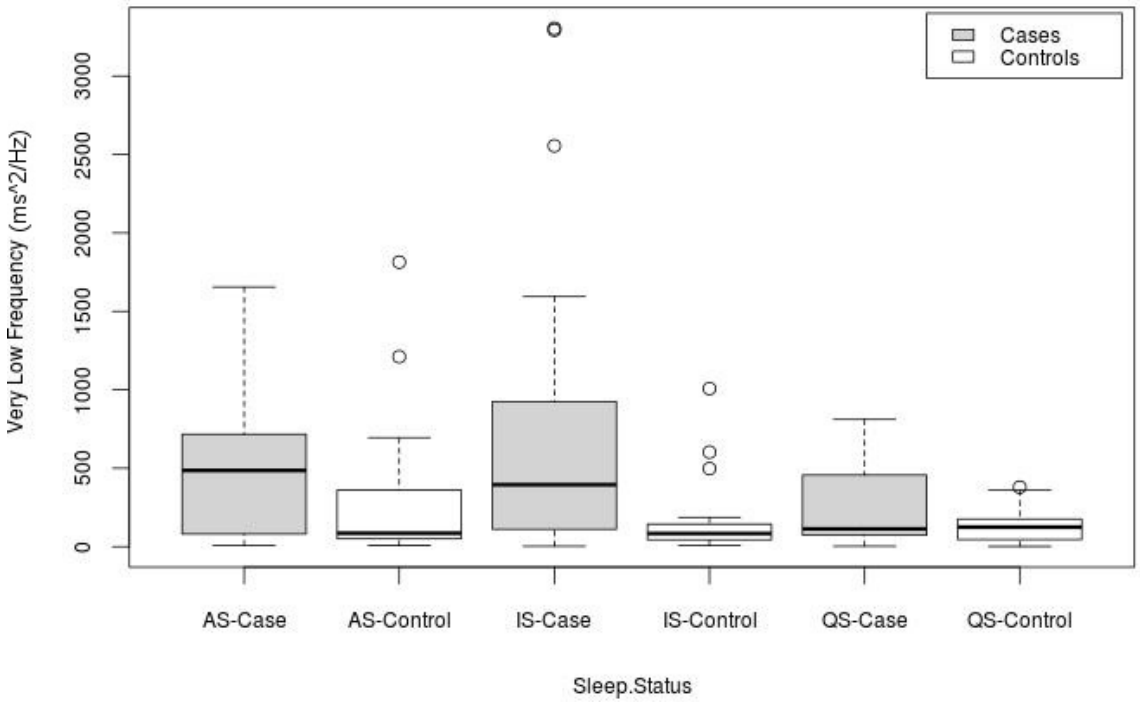

Figure 75: Box plots for VLF for all three sleep states, with cases shown in grey. The top and bottom of the boxes show the 1st (Q1) and 3rd (Q3) quartile respectively, while the whiskers show Q1 or Q3 ±1.5 of the interquartile range. The black line within the box indicates the median value and outliers are shown by small circles. AS: active sleep; IS: indeterminate sleep; QS: quiet sleep.

	Cases		Controls		p-value	95% Confidence intervals of the
	n	Median (ms^2/Hz)	n	Median (ms^2/Hz)		difference (cases minus controls)
Active	13	486	19	86	0.19	(-41, 529)
Indeterminate	**18**	**395**	**20**	**84**	**0.02**	**(26, 781)**
Quiet	14	114	19	125	0.44	(-49, 191)

Table 51: Results of Mann-Whitney U tests comparing the medians of VLF for cases and controls for each sleep state.

Although indeterminate sleep showed a statistically significant difference, on the application of the Bonferroni correction (3 sleep states x 0.02 = 0.06), the difference was no longer significant. No statistical difference was found between the median values of VLF for any sleep state. This indicates that there was no difference identifiable between the study groups using this statistical methodology.

Spectral Analysis – LF

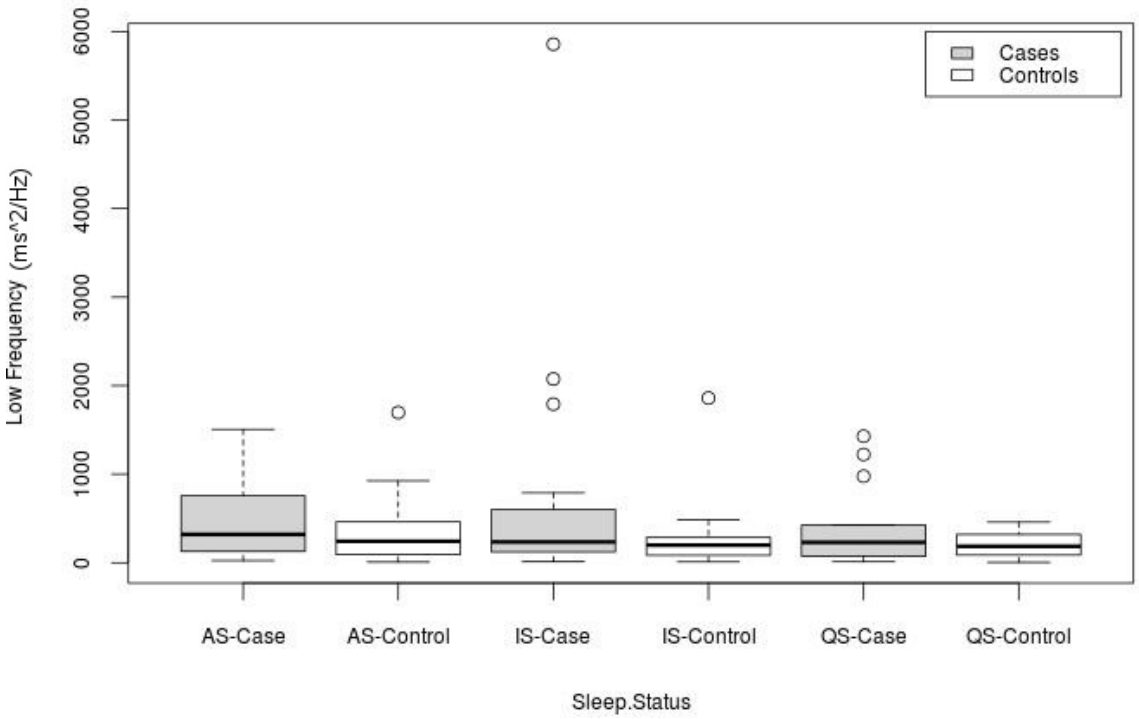

Figure 76: Box plots for LF for all three sleep states, with cases shown in grey. The top and bottom of the boxes show the 1st (Q1) and 3rd (Q3) quartile respectively, while the whiskers show Q1 or Q3 ±1.5 of the interquartile range. The black line within the box indicates the median value and outliers are shown by small circles. AS: active sleep; IS: indeterminate sleep; QS: quiet sleep.

	Cases		Controls		p-value	95% Confidence intervals of the
	n	Median (ms^2/Hz)	n	Median (ms^2/Hz)		difference (cases minus controls)
Active	13	319	19	242	0.56	(-141, 354)
Indeterminate	18	234	20	199	0.17	(-48, 371)
Quiet	14	230	19	185	0.72	(-88, 253)

Table 52: Results of Mann-Whitney U tests comparing the medians of LF for cases and controls for each sleep state

No statistical difference was found between the median values of LF for any sleep state. This indicates that there was no difference identifiable between the study groups using this statistical methodology.

Spectral Analysis – HF

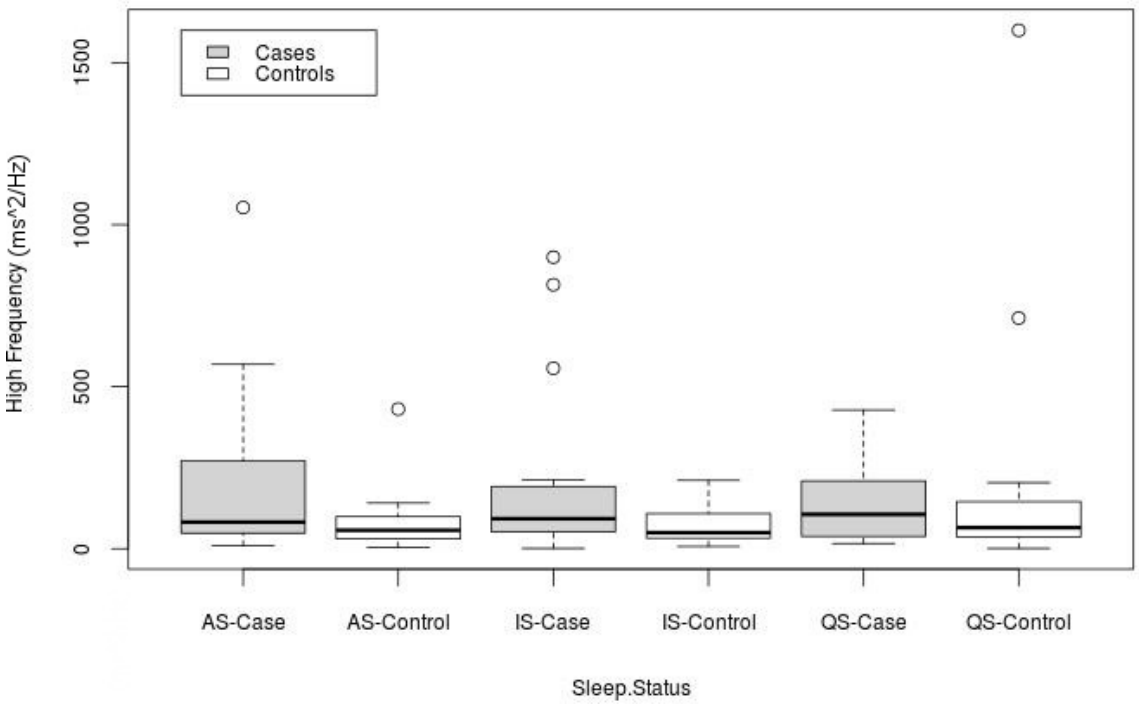

Figure 77: Box plots for HF for all three sleep states, with cases shown in grey. The top and bottom of the boxes show the 1st (Q1) and 3rd (Q3) quartile respectively, while the whiskers show Q1 or Q3 ±1.5 of the interquartile range. The black line within the box indicates the median value and outliers are shown by small circles. AS: active sleep; IS: indeterminate sleep; QS: quiet sleep.

	Cases		Controls		p-value	95% Confidence intervals of the
	n	Median (ms^2/Hz)	n	Median (ms^2/Hz)		difference (cases minus controls)
Active	13	82	19	57	0.30	(-19, 157)
Indeterminate	18	93	20	50	0.24	(-20, 87)
Quiet	14	106	19	65	0.64	(-48, 87)

Table 53: Results of Mann-Whitney U tests comparing the medians of HF for cases and controls for each sleep state.

No statistical difference was found between the median values of HF values for any sleep state. This indicates that there was no difference identifiable between the study groups using this statistical methodology.

Spectral Analysis – LF/HF Ratio

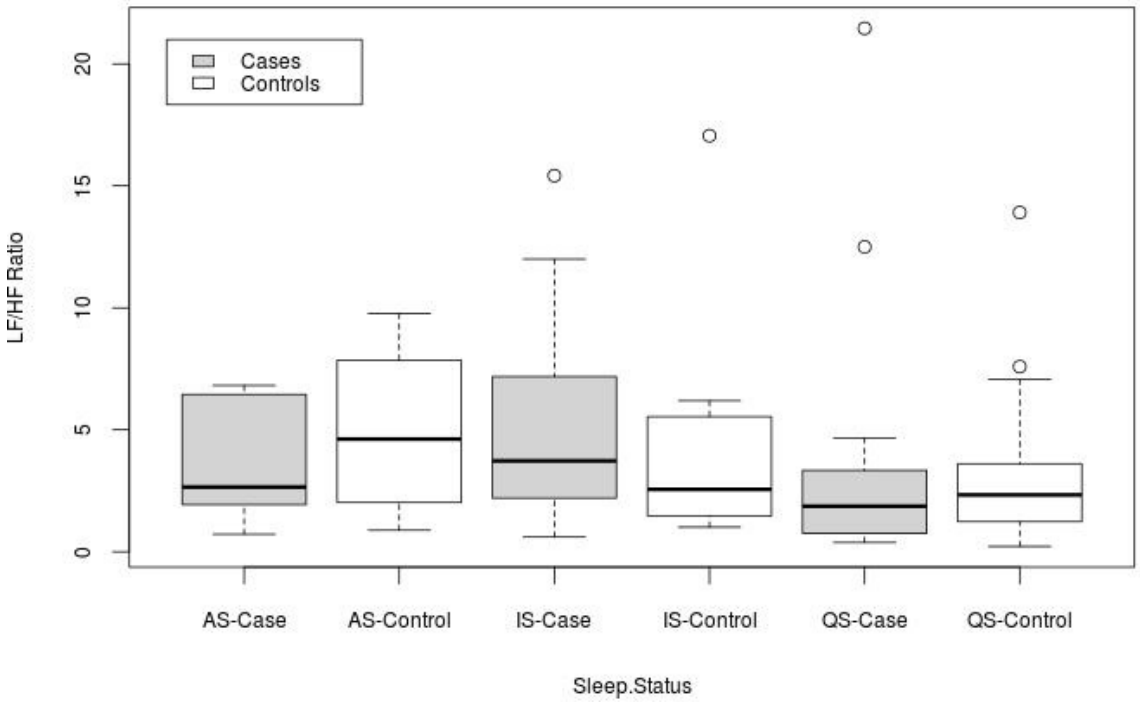

Figure 78: Box plots for LF/HF ratio for all three sleep states, with cases shown in grey. The top and bottom of the boxes show the 1st (Q1) and 3rd (Q3) quartile respectively, while the whiskers show Q1 or Q3 ±1.5 of the interquartile range. The black line within the box indicates the median value and outliers are shown by small circles. AS: active sleep; IS: indeterminate sleep; QS: quiet sleep.

	Cases		Controls		p-value	95% Confidence intervals of the difference (cases minus controls)
	n	Median	n	Median		
Active	13	2.6	19	4.6	0.20	(-3.54, 0.61)
Indeterminate	18	3.7	20	2.6	0.19	(-0.68, 2.80)
Quiet	14	1.9	19	2.3	0.77	(-1.62, 1.14)

Table 54: Results of Mann-Whitney U tests comparing the medians of LF/HF ratio for cases and controls for each sleep state.

No statistical difference was found between the median values of LF/HF ratio values for any sleep state. This indicates that there was no difference identifiable between the study groups using this statistical methodology.

8.3.3 ECG Time and Frequency Domain Median Comparisons

The median values were presented for each variable for each sleep state (ECG time domain - Table 55, Table 56, Table 57, ECG frequency domain - Table 58, Table 59, Table 60). The difference between the two groups for a sleep state was shown indicating what percentage magnitude the cases differ from the controls, and is calculated using equation 13 on page 190. A positive difference shows that the median value for the case is larger.

ECG Time Domain Median Comparison for Active Sleep

Variable	Cases (n=20)	Controls (n=25)	Relative Difference (%)
Mean Heart Rate (bpm)	119	120	-0.8
Mean Heart Rate (bpm) standard deviation SDNN	34.0	20.1	40.9
Mean RR interval (ms)	509	499	2.0
RMSSD (ms)	18.0	14.1	21.7
Poincarè Plot – SD1 (ms)	13.0	10.0	23.1
Poincarè Plot – SD2 (ms)	46.5	26.7	42.6

Table 55: Relative differences in ECG time domain medians between cases and controls for active sleep. A positive percentage difference indicates that the cases have higher medians than the controls. The largest difference shown is the SDNN, indicating that the variability between cases and controls is largest during active sleep.

ECG Time Domain Median Comparison for Indeterminate Sleep

Variable	Cases (n=20)	Controls (n=25)	Relative Difference (%)
Mean Heart Rate (bpm)	118	120	-1.7
Mean Heart Rate (bpm) standard deviation SDNN	33.6	23.9	28.9
Mean RR interval (ms)	511	506	1.0
RMSSD (ms)	21.6	15.3	29.2
Poincarè Plot – SD1 (ms)	15.4	10.9	29.2
Poincarè Plot – SD2 (ms)	45.4	32.5	28.4

Table 56: Relative differences in ECG time domain medians between cases and controls for indeterminate sleep. A positive percentage difference indicates that the cases have higher medians than the controls. Here the SNDD, and Poincarè plot output (SD1 and SD2) are highest, again indicating increased variability between cases and controls.

ECG Time Domain Median Comparison for Quiet Sleep

Variable	Cases (n=20)	Controls (n=25)	Relative Difference (%)
Mean Heart Rate (bpm)	116	116	0.0
Mean Heart Rate (bpm) standard deviation SDNN	32.6	24.1	26.1
Mean RR interval (ms)	517	517	0.0
RMSSD (ms)	23.4	16.5	29.5
Poincarè Plot – SD1 (ms)	16.6	19	-14.5
Poincarè Plot – SD2 (ms)	39.3	32.1	18.3

Table 57: Relative differences in ECG time domain medians between cases and controls for quiet sleep. A positive percentage difference indicates that the cases have higher medians than the controls. SDNN and RMSSD, two measures of variability are shown to be greater in the cases.

ECG Frequency Domain Median Comparison for Active Sleep

Variable	Cases (n=20)	Controls (n=25)	Relative Difference (%)
Very Low Frequency (VLF) ms^2/Hz	**486**	**86**	**82.3**
Low Frequency (LF) ms^2/Hz	319	242	24.1
High Frequency (HF) ms^2/Hz	82	57	30.5
LF/HF Ratio	2.6	4.6	-76.9

Table 58: Relative differences in ECG frequency domain medians between cases and controls for active sleep. A positive percentage difference indicates that the cases have higher medians than the controls. The VLF difference in the controls is larger than in the cases, indicating greater parasympathetic activity. The LF/HF ratio is greater in the controls.

ECG Frequency Domain Median Comparison for Indeterminate Sleep

Variable	Cases (n=20)	Controls (n=25)	Relative Difference (%)
Very Low Frequency (VLF) ms^2/Hz	**395**	**84**	**78.7**
Low Frequency (LF) ms^2/Hz	234	199	15.0
High Frequency (HF) ms^2/Hz	93	50	46.2
LF/HF Ratio	3.7	2.6	29.7

Table 59: Relative differences in ECG frequency domain medians between cases and controls for indeterminate sleep. A positive percentage difference indicates that the cases have higher medians than the controls. As with active sleep, the VLF value is greater in the controls, indicating more parasympathetic activity.

ECG Frequency Domain Median Comparison for Quiet Sleep

Variable	Cases (n=20)	Controls (n=25)	Relative Difference (%)
Very Low Frequency (VLF) ms^2/Hz	114	125	-9.6
Low Frequency (LF) ms^2/Hz	230	185	19.6
High Frequency (HF) ms^2/Hz	**106**	**65**	**38.7**
LF/HF Ratio	1.9	2.3	-21.1

Table 60: Relative differences in ECG frequency domain medians between cases and controls for quiet sleep. A positive percentage difference indicates that the cases have higher medians than the controls. In quiet sleep the HF is larger in the controls indicating more parasympathetic activity.

Summary

The conventional measurement of heart rate (mean RR and RR interval) showed very little difference between the two groups, although the measures of variability (SDNN and RMSSD) showed larger differences, indicating greater variability in the cases. The Poincarè plot parameters SD1 and SD2 showed a higher degree of variability for active and indeterminate sleep, but not quiet sleep.

The spectral analysis showed larger differences between the groups, especially in measurement of VLF, an indicator of parasympathetic activity. In active and indeterminate sleep the cases had 82 % and 79 % greater values than the controls, whilst in quiet sleep, the controls had greater parasympathetic responses, denoted by HF.

8.3.4 Comparison of the ECG Results with Other Studies

Table 61 shows a summary of ECG studies in the neonate that have included a comprehensive time domain HRV analysis, and in some cases a frequency domain analysis. With the exception of the studies by Selig et al., (2011) and Vandeput et al., (2009) that included preterm infants, all were performed on healthy term infants. For comparison purposes, only the cases and controls from the current study have been included in this table.

What is apparent, is that many of the normative studies do not record sleep stages with any detail, and give results over a 24 hour recording. This introduces considerable variability between studies even for commonly used HRV analysis such as RR interval (456 – 495 ms) and mean HR (109 – 131 bpm). A lack of standardisation in the recording and analysis of neonate HRV data precludes precise cross study comparisons. However, in general terms, although the study group had been recruited from a very specific population, the results do not differ greatly from other published studies.

The data from other studies are more variable when examining the frequency domain results. This is because of the varied methods and protocols used for the generation of the spectra and band power calculations. Some studies only publish the relative band power results (the percentage of power), and do not show the absolute values from which these are based. Although relative power values may be of more use, for completeness, the absolute values would be more complete.

Study	This study		Mehta *et al.* (2002)	Schäffer *et al.* (2008)	Longin *et al.* (2005)	Spassov *et al.* (1994)		Doyle *et al.* (2009)		Vandeput *et al.* (2009)		Selig *et al.* (2011)	
Age Group	Neonate term controls	Neonate term cases	Neonate	Neonate	Neonate	Neonate		Neonate (normal)		Preterm (Mean GA 32 weeks)		Term	Preterm
Sleep Status	AS, QS & IS	AS, QS & IS	Awake & asleep	-	Undefined but eyes closed	QS	AS	QS	AS	AS	QS	Awake & asleep	Awake & asleep
Time domain results													
RR (ms)	499-517	509-517	456	457	495	498	472	-	-	408	432	485.3	411.2
SDNN (ms)	20.1-24.1	18.5-18.9	47.0	63.9	49.7	35.2	29.9	14.8	23.8	26.7	12.2	22.6	13.8
HR (bpm)	117-121	116-119	130	131	122	-	-	110	114	-	-	-	-
RMSSD (ms)	14.1-16.5	18.0-23.4	21.6	19.3	20.5	-	-	11.9	11.4	8.0	7.2	11.1	5.9
SD1 (ms)	10.0-11.7	13.0-16.6	-	-	-	-	-	33.7	129.9	-	-	-	-
SD2 (ms)	26.7-32.5	39.3-46.5	-	-	-	-	-	76.1	32.4	-	-	-	-
Frequency domain results													
Relative VLF (%)	23.1-26.7	26.8-53.3	24.2	34.7*	-	-	-	32.9	41.3	-	-	46.6*	47.3*
Relative LF (%)	11.3-54.6	35.0-54.0	12.4	15.2*	-	18.4	10.8	36.4	46.4	-	-	41.5*	47.9*
Relative HF (%)	13.6-15.0	11.6-19.2	5.3	3.8*	-	16.2	23.1	32.2	13.0	-	-	11.8*	11.4*
LF/HF	2.33-4.6	1.9-2.6	2.7	3.75	-	1.4	0.5	1.65	4.38	-	-	4.7	7.6
** indicates that the value was computed from the results presented in the original paper.*													

Table 61: Other relevant studies involving HRV analysis for preterm and term infants, both in the time and frequency domains, involving a neonatal population. QS - quiet sleep; AS - active sleep; IS - indeterminate sleep.

8.3.5 CVT Results

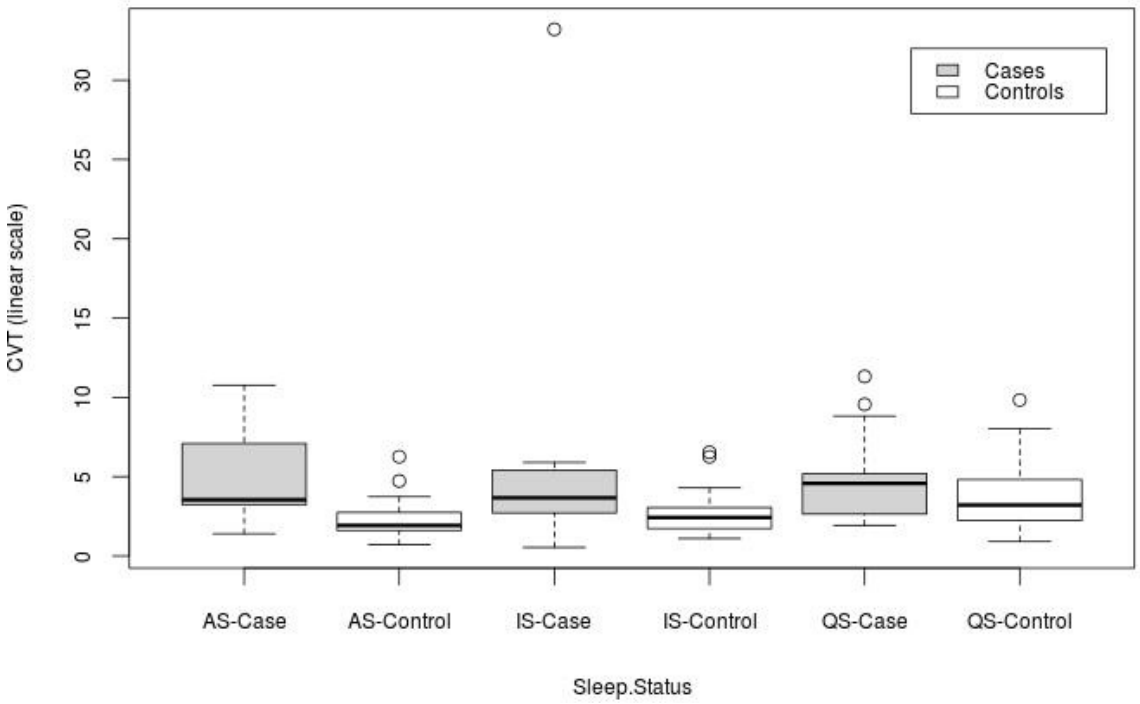

Figure 79: Box plots for CVT for all three sleep states, with cases shown in grey. The top and bottom of the boxes show the 1st (Q1) and 3rd (Q3) quartile respectively, while the whiskers show Q1 or Q3 ±1.5 of the interquartile range. The black line within the box indicates the median value and outliers are shown by small circles. AS: active sleep; IS: indeterminate sleep; QS: quiet sleep.

	Cases		Controls		p-value	95% Confidence intervals of the
	n	Median	n	Median		difference (cases minus controls)
Active	**13**	**3.5**	**19**	**1.9**	**0.002**	**(0.81, 4.27)**
Indeterminate	**18**	**3.7**	**20**	**2.4**	**0.03**	**(0.06, 2.62)**
Quiet	14	4.6	19	3.2	0.37	(-0.52, 2.42)

Table 62: Results of Mann-Whitney U tests comparing the medians of CVT for cases and controls for each sleep state.

The statistical analysis showed that during active sleep, CVT scores were statistically different between the cases and controls, although this was not the case for quiet sleep. Bonferroni corrections demonstrated that cases had significantly higher CVT during active sleep (p=0.006) and a trend towards higher CVT during indeterminate sleep (p=0.099).

CVT Standard Deviation

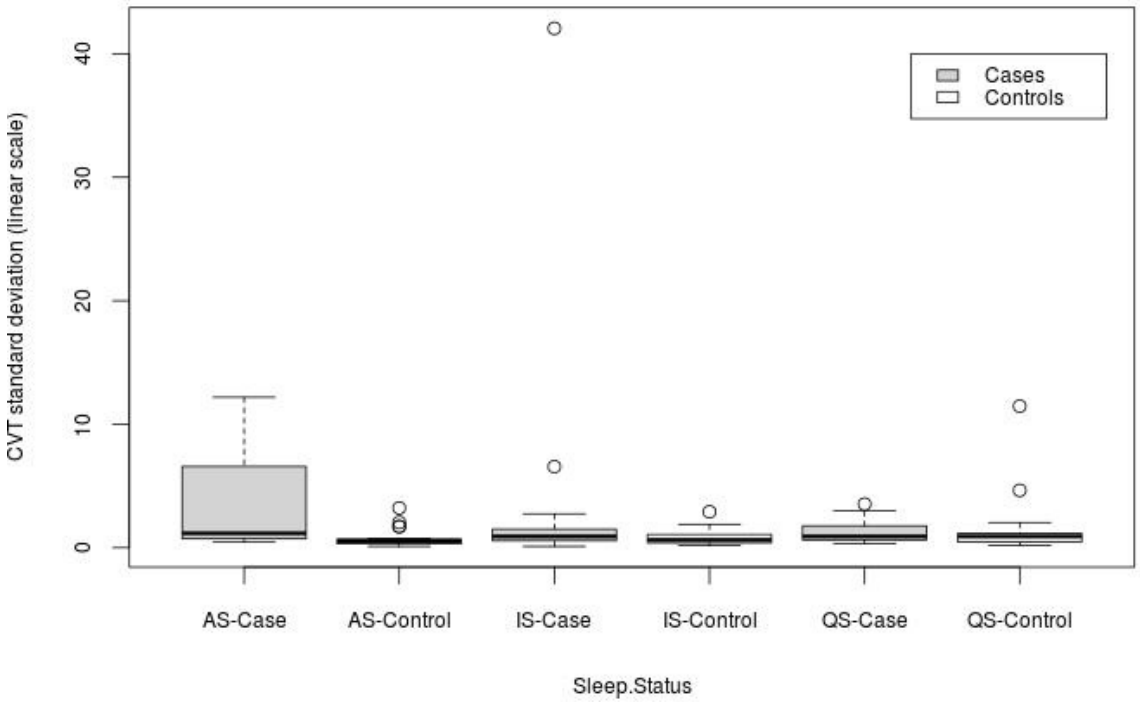

Figure 80: Box plots for CVT standard deviation for all three sleep states, with cases shown in grey. The top and bottom of the boxes show the 1st (Q1) and 3rd (Q3) quartile respectively, while the whiskers show Q1 or Q3 ±1.5 of the interquartile range. The black line within the box indicates the median value and outliers are shown by small circles. AS: active sleep; IS: indeterminate sleep; QS: quiet sleep.

	Cases		Controls		p-value	95% Confidence intervals of the difference (cases minus controls)
	n	Median	n	Median		
Active	**13**	**1.2**	**19**	**0.5**	**0.005**	**(0.2, 5.9)**
Indeterminate	18	0.9	20	0.6	0.21	(-0.1, 0.7)
Quiet	14	0.9	19	0.9	0.48	(-0.31, 0.68)

Table 63: Results of Mann-Whitney U tests comparing the medians of CVT (standard deviation) for cases and controls for each sleep state.

After application of Bonferroni corrections the cases demonstrated significantly higher CVT SD (i.e. CVT variability) during active sleep (p=0.015).

The two CVT measurements – median CVT, and variability of CVT – showed the greatest difference between cases and controls, specifically for active sleep, and is the basis for the analysis that follows.

8.3.6 Comparison of Cases who Subsequently Required Treatment for NAS Versus Cases who Did Not Require Treatment

The analysis so far compared methadone-exposed infants (cases) with unexposed controls. The cases can also be divided into infants who did (n=5) or did not (n=45) go on to develop significant NAS (requiring treatment). Although five cases received oral morphine for the treatment of signs and symptoms of NAS, three of these (#43, #47 and #74) had to be excluded from analysis because no PSG was achieved due to irritability or the infant not sleeping. Table 64 shows the individual results of the two treated infants for each sleep state, in comparison with the medians for the not-treated cases.

Variable	Sleep Stage	Not treated (medians) n=13	infant #54 (medians)	infant #112 (medians)
CVT	AS	4.41	3.44	3.54
	IS	3.24	3.82	5.90
	QS	4.52	5.19	*
VLF (ms^2/Hz)	AS	486	302	906
	IS	328	498	2555
	QS	96	457	*
* Indicates that the QS was not found for this infant during PSG scoring				

Table 64: CVT and VLF results for the two infants that were treated for NAS.

For the two infants who were subsequently treated for NAS there is not obvious relationship difference in CVT or VLF compared to those infants who did not develop significant NAS. Clearly this subset of data (n=2) is very small; more data would be required to determine if there truly is no difference. Infants who subsequently required treatment might very well have been more irritable during the PSG, and thus have proved more difficult to record PSG data from. A larger study set would be needed to confirm the preliminary findings that CVT/VLF does not predict severity of NAS.

8.3.7 Comparison of CVT and Length of Stay for the Treated Group

The results can be seen in Table 65. This shows that the length of stay for exposed infants is over twice as long as for controls, and their CVT is significantly higher: however, Figure 81 shows that CVT is not an indicator of length of stay.

	Mean (days)	Range (days)	CVT	CVT range
Case	8.1	(3-19)	5.10	0.5-33.2
Control	3.0	(2-4)	2.95	0.7-9.8

Table 65: Mean length of stay in relation to CVT for the study infants.

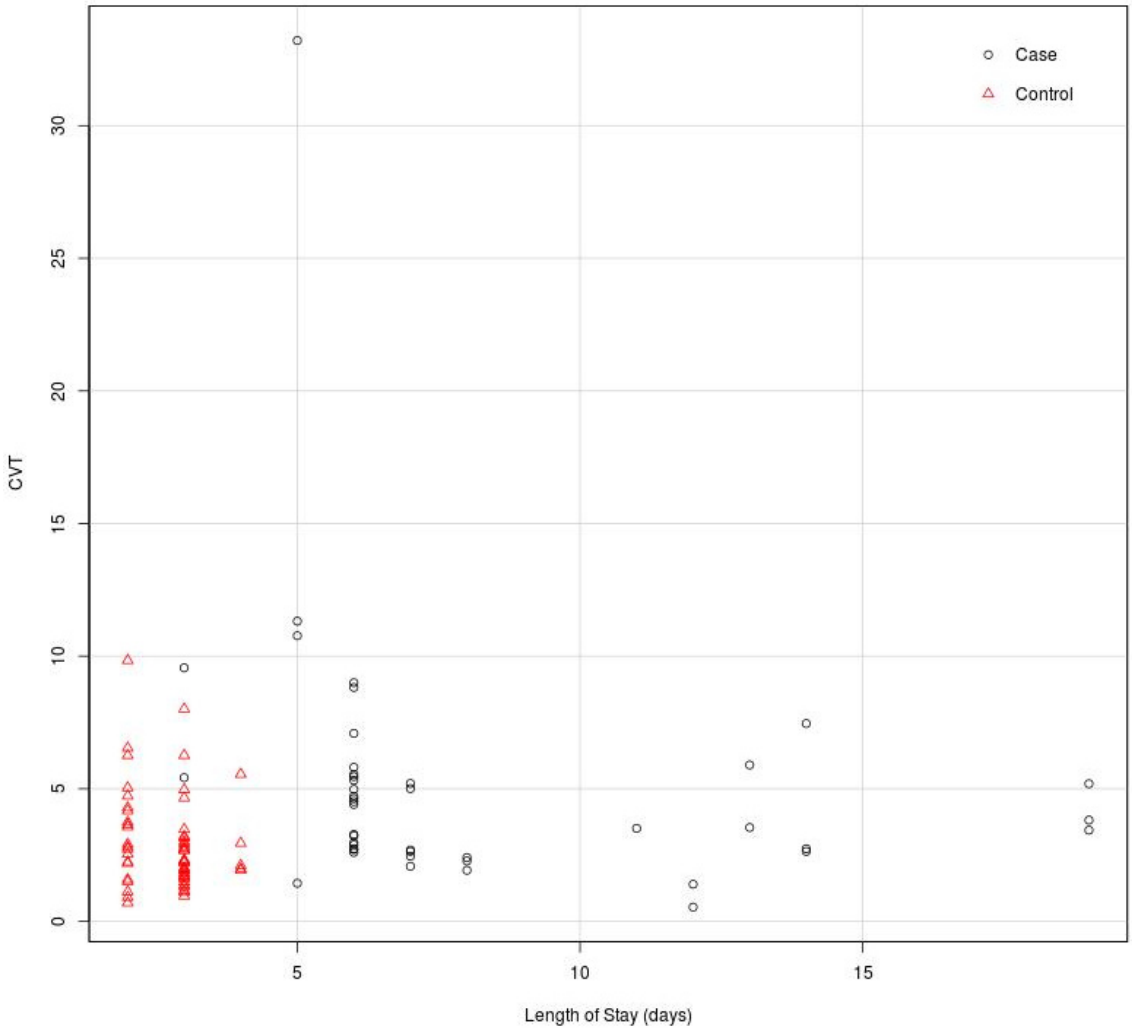

Figure 81: A scatter plot showing the length of hospital stay for cases and controls in relation to their test CVT score.

Similarly, the VLF spectral power band was close to showing a trend between groups, with a statistical difference p-value of 0.056.

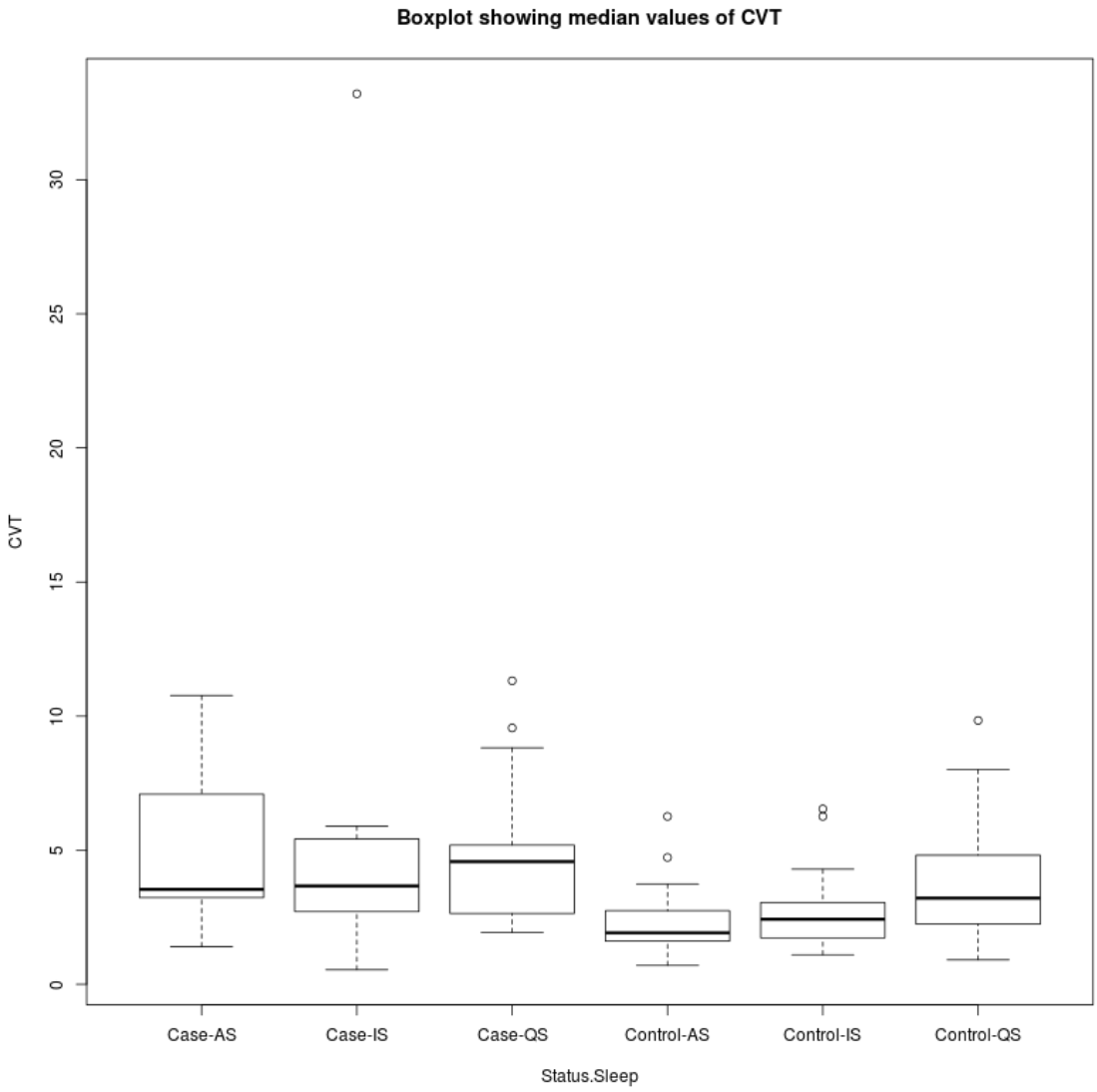

Figure 82: Cardiac vagal tone for cases versus controls for each sleep state. The upper boundary (upper hinge) of the box represents the 75th percentile, the lower boundary (lower hinge) the 25th percentile and the black line the median. The upper and lower whiskers represent the limits of the nominal range inferred from the upper and lower quartiles. The small circles represent outliers.

Variability of CVT for the cases was greater, and the medians higher, for each sleep state relative to controls. This is despite those measurements displayed here being made when the infant was settled, and the sleep epochs identified as artefact free. This variability of CVT amongst the cases indicates that the parasympathetic nervous system

was in a less stable state than in the controls, suggesting impaired or damaged homeostatic regulation.

Figure 83 shows increased level of variability amongst the cases, with wider nominal ranges, and raised medians compared with the controls. Although the differences did not achieve statistical significance (p-value=0.056), the trend is in line with CVT data, confirming the validity of the latter measurements.

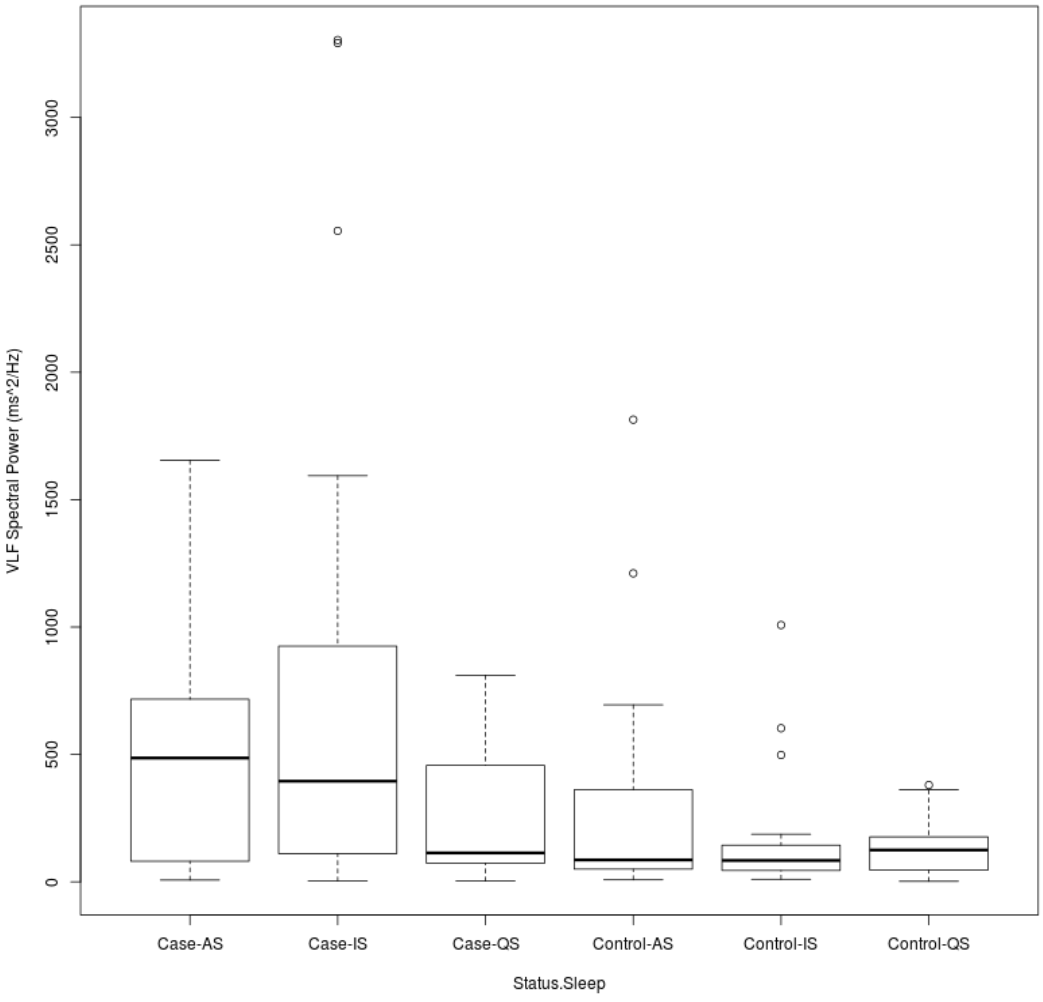

Figure 83: A box plot of VLF (very low frequency) spectral power (ms^2/Hz) for cases versus controls for each sleep state.

It suggests that the parasympathetic regulation that occurs during quiet sleep is less

adversely affected than during active and indeterminate sleep. From a practical point of view, the infants were far more settled during periods of quiet sleep than active/indeterminate sleep, with an EEG is defined by high voltage, low frequency signals. There may be less need for the parasympathetic nervous system to regulate during these more settled periods.

8.3.8 The Relationship Between CVT and VLF

As both CVT and VLF are considered representative of parasympathetic activity, it was necessary to test the presence of a relationship. This relationship was explored by producing the scatter plot shown in Figure 84. On visual inspection of the graph it can be seen that the cases, represented by small circles appear more scattered than the controls. Controls tended to be grouped together with lower VLF and CVT scores. This could indicate that in the control group there is less variation, suggesting highly variable levels amongst the cases.

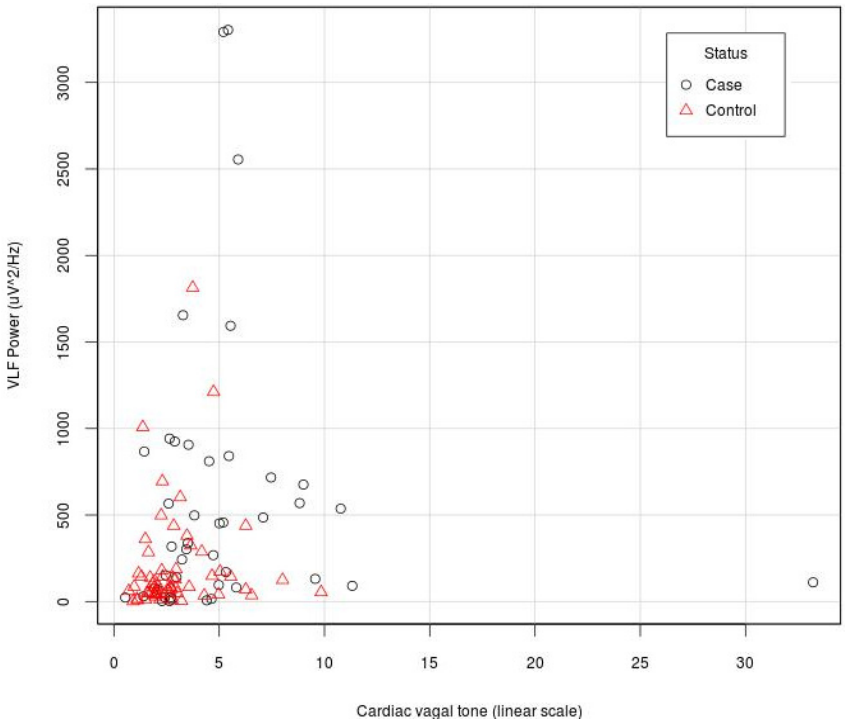

Figure 84: Scatter plot of VLF power versus cardiac vagal tone for cases and controls. Cases are represented by circles, and controls by triangles.

8.3.9 Sensitivity & Specificity

From this study, cardiac vagal tone has been shown to have the most statistically significant difference between the exposed and unexposed groups. With this data a 2x2 contingency table was constructed to identify CVTs capacity to accurately predict exposure. The structure of a 2x2 table is shown in Figure 58.

Test	Condition Positive	Condition Negative	
Outcome positive	True Positive	False Positive	Precision
Outcome negative	False Negative	True Negative	Negative predictive value (NPV)
	Sensitivity	Specificity	

Table 66: The structure of a 2x2 contingency table.

If a CVT ≥ 3.0 from the active sleep dataset is used as a cut-off, the following 2x2 table was constructed.

Test	Exposed (n=13)	Not Exposed (n=19)	
CVT ≥ 3.0	10	3	Precision = 76.9%
CVT < 3.0	3	16	NPV = 84.2%
	Sensitivity = 76.9 %	Specificity = 84.2 %	

Table 67: 2x2 contingency table using CVT>=3 during active sleep.

Figure 56 shows that the sensitivity, or the percentage correctly predicted to have been exposed, is 76.9%, whilst the specificity, which is the percentage correctly predicted to have not been exposed is 84.2%.

8.3.10 Receiver Operator Characteristic (ROC) Curve

ROC curves are visual representations of the data shown in 2 x 2 contingency tables. They are used to show a how good a predictive technique is in relation to the number of errors it makes. For different cut-off levels, a curve can be constructed showing the relationship between the sensitivity and 1-specificity of a test. For the ROC curve to reflect a more-useful-than-chance predictive technique, it should lie to the left of the diagonal, or 45 degree line, shown on Figure 86 as the red line running from (0,0) to (1,1). A useful indicator of the goodness of a predictive test is the area under the ROC curve (AUROC). In the example shown in Figure 85, the numerical integration methods using the trapezoidal rule was used to calculate AUROC.

As CVT was found to be the most significant variable as a predictive test, an ROC curve was constructed for a range of values from 2 to 6. Contingency tables were constructed for each cut-off point with the results being shown in Figure 86. The calculations were performed in LibreOffice Calc 4.2.

Cutoff	3		
	True Case	False Control	Totals
Positive	10	3	13
Negative	3	16	19
	13	19	

Precision		0.769
Positive Predictive Value	PPV	0.769
Negative Predictive Value	PNV	0.842
Sensitivity	(TPR)	0.769
Specificity	(TNR)	0.842

	y		x	AUC
CVT	Sensitivity	Specificity	1-Specificity	Trapezoid
2	0.923	0.579	0.421	0.223
3	0.769	0.842	0.158	0.032
4	0.462	0.895	0.105	0.022
5	0.385	0.947	0.053	0.000
6	0.308	0.947	0.053	
		An estimate of AUROC		0.083

Figure 85: An example calculation for the ROC curve showing CVT during active sleep with a CVT cut-off of 3. The 2x2 is shown at the top, followed by the values calculated for sensitivity and specificity. The table at the bottom is a summary of sensitivity and specificity results for cut off values between 2 and 6, and were used for plotting the ROC curve.

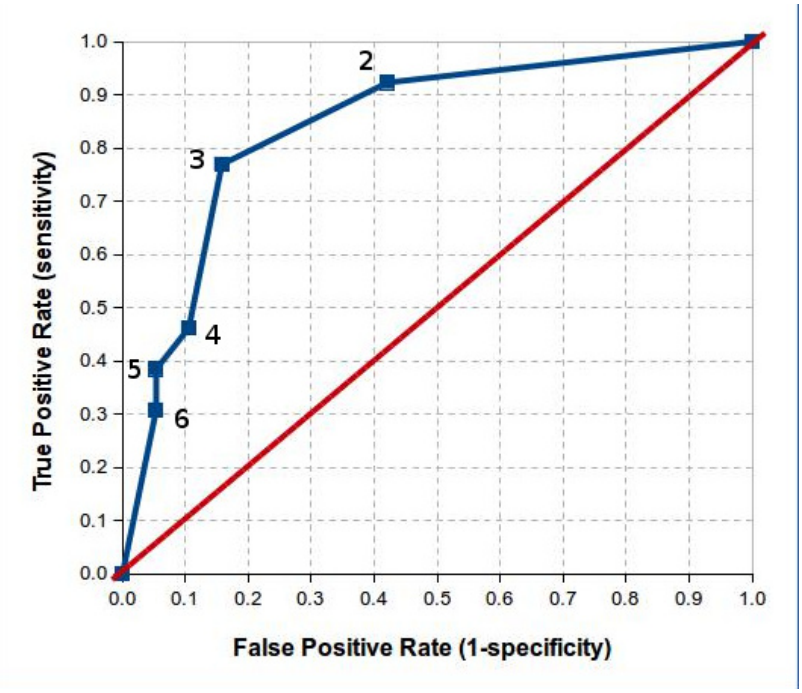

Figure 86: An ROC curve for CVT with a range of cut-off values (2-6) during active sleep.

The AUROC was calculated to be 0.834 or 83 %. It must be noted that the ROC curve has been constructed with only five points because the sample size was small, and values between the integer cut-off's showed very little, if any, change in the sensitivity and 1-specificity values. Also, the AUROC is only an approximation of the true area under the curve. However, as a predictive test, as shown by the ROC curve, CVT shows promise in isolating which infants were exposed, and more likely to develop NAS.

8.4 Summary

For each group of *in utero* drug exposed cases or control infants, none of the conventional time or frequency domain measurements based on the ECG showed a statistically significant difference between sleep states.

However, CVT was significantly higher in the exposed group than in the unexposed group.

- AS Cases 3.5 (3.0-7.2) vs 1.9 (1.6-2.7) p-value 0.002.
- IS Cases 3.7 (2.7-5.4) vs 2.4 (1.8-2.9) p-value 0.033.

9 Discussion & Conclusion

9.1 EEG Discussion

The final analysis of the EEG spectral analysis showed no statistically significant difference between the two groups for any sleep stage, but relative percentage differences highlighted areas of difference. These are summarised in Table 68, where the percentage difference is positive if the cases value is larger.

	Relative difference for each sleep state		
EEG variable	Active	Indeterminate	Quiet
Absolute Delta Power 0-4 Hz ($\mu V^2/Hz$)	7.8 %	10.7 %	18.8 %
Absolute Delta Low 0-2 Hz ($\mu V^2/Hz$)	9.2 %	8.1 %	20.7 %
Absolute Delta High 2-4 Hz ($\mu V^2/Hz$)	28.6 %	25.6 %	-2.2 %
Absolute Theta 4-8 Hz ($\mu V^2/Hz$)	11.3 %	27.5 %	8.3 %
Absolute Alpha 8-12 Hz ($\mu V^2/Hz$)	10.0 %	11.8 %	5.6 %
Absolute Beta 12-30 Hz ($\mu V^2/Hz$)	10.0 %	11.8 %	5.6 %
Absolute Total Power ($\mu V^2/Hz$)	6.2 %	12.5 %	17.7 %
SEF 95% (0.5-30 Hz) Hz	-0.7 %	-1.4 %	-1.8 %
SEF 95% (2-20 Hz) Hz	-1.1 %	0 %	-1.1 %

Table 68: A summary showing how the cases median EEG band power median values differed from the controls in terms of relative difference percentage. A positive indicates that the cases value is greater than the control equivalent.

Examining the data shows that cases values are higher than controls for all but quiet sleep absolute delta high power and for both SEF 95% ranges. This would indicate that cases have more energetic EEG over the frequency bands measured. In the three delta bands, levels are considerably greater indicating that delta activity has been modified by exposure. Delta power is composed of high amplitude, slow wave voltages (SWS – slow wave sleep), often related to cellular regeneration and in the infant dominates the

neonatal EEG (Scher et al., 1994). This difference might suggest that the mechanisms involved in delta activity and sleep regulation are affected by exposure although the neural underpinnings SWS delta activity remain uncertain (Knyazev, 2012).

The higher frequency bands (theta, alpha and beta) were also been affected showing more activity in the cases. This would indicate that in the exposed infants, faster EEG activity is present at times when lower levels in these frequency bands would be more normal. These higher frequencies may explain why there is a higher level of arousal during periods when a infant should be in settled sleep, and would in part explain why drug exposed neonates are less likely to have settled to sleep.

9.2 ECG Discussion

The analysis of the ECG data can be divided into three categories, conventional analysis of the ECG in both the time and frequency domains, and analysis and measurement of parasympathetic activity using estimates of cardiac vagal tone.

9.2.1 Time Domain Analysis

Examining the data, it is apparent that for nearly all the ECG time domain variables that describe heart rate variability (SDNN, mean HR standard deviation, RMSSD, SD1 & SD2), the cases have higher median values. However, the mean HR and mean RR interval were not greatly affected. This indicates that average time between successive R wave peaks (mean HR and RR interval) are poor indicators of the variation within the heart rates for this study group, and describe only the basic mechanism for regulating the rate.

The main differences are summarised in Table 69.

	Relative difference for each sleep state		
ECG variable	Active	Indeterminate	Quiet
Mean HR (bpm)	-0.8 %	-1.7 %	0.0 %

Mean HR Standard Deviation (bpm) SDNN	40.9 %	28.9 %	26.1 %
Mean RR interval (ms)	2.0 %	1.0 %	0.0 %
RMSSD (ms)	21.7 %	29.2 %	29.5 %
Poincarè Plot – SD1 (ms)	23.1 %	29.2 %	-14.5 %
Poincarè Plot – SD2 (ms)	42.6 %	28.4 %	18.3 %

Table 69: A summary showing how the cases median HRV values differed from the controls. A positive value indicates that the cases value is greater than the controls.

When statistical testing was performed comparing the medians (using non parametric tests) between the two groups, none of the comparisons showed statistically significant differences (where p<=0.05). However this was more likely due to the small sample sizes involved, and greater numbers may well elicit a statistically significant difference. Note that even though the data was not normally distributed, and non-parametric tests were used for the statistics where medians are more applicable, mean RR and mean HR are standard ECG variables used across the literature. This means that a median value of a group of mean HR is acceptable.

9.2.2 Frequency Domain Analysis

The summary analysis of the frequency domain results showed a similar picture to the time domain in that nearly all variables. During AS and IS, the VLF band showed 82.3% and 78.7% increases amongst the cases compared with the controls. Although no neonatal data could be found indicating the significance of these raised VLF values, in an adult population, Bigger et al., (1992) showed that increased VLF was strongly associated with sudden arrhythmic death syndrome (SADS).

	Relative difference for each sleep state		
ECG variable	Active	Indeterminate	Quiet
Very Low Frequency (VLF) ms^2/Hz	82.3 %	78.7 %	-9.6 %
Low Frequency (LF) ms^2/Hz	24.1 %	15.0 %	19.6 %
High Frequency (HF) ms^2/Hz	30.5 %	46.2 %	38.7 %
LF/HF	-76.9 %	29.7 %	-21.1 %

Table 70: A summary showing how the cases median HRV values differed from the controls. Positive values indicate that the cases values was greater than the controls.

Only during QS was this pattern of higher medians not reproduced for VLF, although there was only a 9% increase in the controls compared with the cases. This is not all that surprising as QS is characterised by slower more rhythmic breathing, little movement and no REM activity. Consequently a more regular and consistent HR is expected during QS, so there would be less variability during this phase.

As with the time domain analysis, the results showed no statistical difference (where $p<=0.05$) between the groups, although VLF showed the most significant difference ($p=0.057$) between cases and controls. This matches the high percentage difference observed for VLF during AS and IS.

9.3 CVT Discussion

Of all the parameters examined the one that showed the greatest difference in medians was cardiac vagal tone. The median CVT for each sleep state were higher in the exposed group when compared with the control group. This was statistically significant (p-value =0.002 for AS and 0.033 for IS). Again QS was shown not be significantly different, and as stated before, this sleep state is the deepest where physiological variability is at a minimum.

As CVT was considered the most promising variable as a predictive test, a receiver operator characteristic (ROC) curve, shown in Figure 86 using varying levels of CVT from 2 – 6 was prepared. The AUROC was 0.83 or 83% indicating that CVT was shown to be a good indicator of prior exposure, although the sample was small.

One of the aims of this work was to develop an electrophysiological method that could identify differences between groups. CVT showed the strongest difference between the groups.

Overall, the ECG results often showed the exposed group to have higher or more ‘energetic’ values. However, ECG is the product of autonomic nervous system activity, containing indicators of the level of activity from a number of different systems. The electrophysiological test that showed the most significant difference was that of cardiac vagal tone, an indicator of parasympathetic activity alone. This would suggest that the PNS is affected most, and therefore is the most important factor in assessing the exposed infants.

Before more patient focused treatment of NAS can be developed, a more objective test indicating the level of withdrawal that the infant is undergoing is needed. CVT could be a useful tool in assessing how successful treatment for NAS is using existing drugs such as Oromorph.

9.3.1 The Relationship Between CVT and VLF

Although CVT and VLF power were derived using different methods, CVT from a time domain analysis, and VLF from a frequency analysis, they are both powerful indicators of parasympathetic nervous system activity, and are consequently related. It strengthens the observation that parasympathetic activity in the cases is modified in that two different parameters, derived using different methods, show similar results.

9.3.2 Physiological Explanation for the Results

A plausible explanation for the differences between the exposed cases and the controls is that the level of nerve fibre myelination differs between the two groups. This would consequently have an effect on both the development of the brain and the nervous system. In a study examining how vagal nerve fibres develop in the first year of life, Pereyra et al., (1992) found that the number of myelinated fibres increased by a third,

whilst the number of unmyelinated fibres changed only slightly. This showed that the vagal nerve is not fully developed at the time of birth. Consequently any factor, such as irregular myelination, affecting the growth of the vagal nerve could well affect the neuro-development of the infant.

In a study looking at the effects of methadone on the development of the early stages of myelination, Vestal-Laborde et al., (2014) found that early myelination in the developing rat brain was altered by perinatal exposure to therapeutic doses of methadone. They conclude that “while the long-term effects of these observations remain unknown, accelerated or increased myelination could disrupt the complex sequence of synchronized events leading to normal connectivity in the developing brain.”

Not only has methadone been implicated in abnormal myelination development, the same group also found that buprenorphine had a similar effect (Eschenroeder et al., 2012). Like methadone, it is also an opioid, but is a partial antagonist compared to methadone which is a full antagonist. This means that buprenorphine does not active mu receptors to the same extent as methadone and thus its effectiveness reaches a ceiling at a lower dose. It is often more suited to drug addicts who have used lower doses of opioids, and in pregnant women has been shown to produce less severe NAS compared with methadone (Jones et al., 2005).

However, in a study on the pups of pregnant rats, Sanchez et al., (2008) showed that exposure to buprenorphine caused myelination to be altered in the exposed group. On examination of the pups, corpus callosum, the exposed group had a “significant increase in the calibre of the mylinated axons”, although the measured axons showed a disproportionately thinner myelin sheath, suggesting an alteration to myelination. This reduction in the myelinated sheath would affect the resistance of the coating of the axon, and thus affect its conductivity. Such a reduction could cause 'leaky circuits' where current leaks from poorly insulated axons, thus affecting the signal propagation to the vagal nerve.

This would be seen electrophysiologically in a number of ways. If conductivity along nerve fibres such as the vagus nerve were affected, then neuronal firing would be irregular and inconsistent. This lack of regularity could be an explanation for why the

results of this work showed higher electrophysiological values for nearly all of the EEG, ECG and CVT parameters investigated. This would also explain why the CVT results had a far greater spread or variability within the exposed group.

From a clinical perspective, this may be related to why the exposed infants have a higher risk of developing SUDI. The vagus nerve is an important component in respiratory control, and it has been long thought that cardio/respiratory factors underline the cause of SUDI. Sachis et al., (1981) found that the number of myelinated vagus fibres (axon and myelin) in SUDI victims were 'strikingly lower', although they did point out that it was unknown if this was a cause or effect of the SUDI. Further work by Becker et al., (1993) showed that there was delayed maturation of the vagus nerve in infants that succumb to SUDI. They examined the vagus nerves of 30 SUDI victims under post mortem, and found that in SUDI infants, “more small and fewer large myelinated fibres were found than in controls, suggesting that the vagus nerve in SUDI is relatively immature.” This explanation would appear to link with Porges polyvagal theory as disinhibition of the dorsal vagal complex can lead to lethal apnoea and bradycardia in mammals (Porges, 2001).

Overall this study has shown that the EEG, ECG and CVT have all been altered by *in utero* exposure to methadone and other illicit drugs. Of these measurements, CVT proved the most promising as a prognostic tool, as by using a non invasive test such as ECG coupled with a method of identifying sleep state, CVT could be a useful clinical biomarker for identifying which infants would require further treatment for NAS. Although not a predictive test for NAS, it is still a useful method that could be used to measure the effectiveness of future treatments and has the potential to aid in developing patient specific management regimens.

The longer term effects of impaired parasympathetic regulation in the neonate can only be surmised, but having a tool to show which infants are already at risk would be useful in their clinical management.

9.4 Conclusions

This body of work has shown that electrophysiology has a role to play in the monitoring of drug-exposed infants. It has highlighted that in a group of neonates all exposed to methadone, erratic parasympathetic function in the form of high and variable CVT is present, even during periods of settled sleep.

Concerning the original aims of the study (section 1.6), the first two hypothesis related to finding differences between the two groups using EEG or ECG were not proven using statistical testing, although the EEG data suggested that both delta wave activity had been modified and higher frequency activity was present in the exposed group. In relation to the ECG and HRV analysis, again no statistically significant measurement was found. However, VLF as an indicator of autonomic function could be a direction for future work.

The third hypothesis was proven to be correct in that CVT could be used to measure autonomic nervous function and, in the case of the exposed group, was a tool for measuring dysfunction.

Finally the fourth hypothesis that at least one of these electro-physiological tests could be used to predict the onset of NAS withdrawal was not proven, but VLF and especially CVT has been shown to be useful in identifying drug exposure, and may be key components in understanding which neonates might be pre-disposed to NAS withdrawal.

Future Work

This study has shown that CVT, when measured during periods of recognisable sleep, is useful in identifying drug exposure non-invasively in the neonate. A development of this would be to estimate CVT prenatally by using the mothers' ECG and separating the QRS component of the unborn child. From this, an estimate of foetal CVT could be established. This would be useful in developing a better understanding of the effects of drugs on the unborn infant, especially in understanding the relationship between

maternal drug dose and potential NAS withdrawal.

At present, methadone is the primary treatment for opioid addiction, but if alternatives were investigated, such as Naltrexone, using CVT as an indicator of autonomic dysfunction would be a novel way of comparing the treatments.

10 References

Abel, E.L., 1980. Smoking during pregnancy: a review of effects on growth and development of offpring. Hum. Biol. n/a, 593–625.

Acharya, U., Kannathal, N., Sing, O.W., Ping, L.Y., Chua, T., 2004. Heart rate analysis in normal subjects of various age groups. Biomed Eng Online 3, 24.

Ajayi, T., 2008. Drug Misuse and Dependence: UK Guidelines on Clinical Management. Psychiatr. Bull. 32, 360–360.

Akaike, H., 1969. Fitting autoregressive models for prediction. Ann. Inst. Stat. Math. 21, 243–247.

Allen, M.C., 1984. Developmental outcome and followup of the small for gestational age infant. Semin Perinatol 8, 123–156.

Anders, T.F., 1982. Neurophysiological studies of sleep in infants and children. J Child Psychol Psychiatry 23, 75–83.

Baar, A.L. van, Fleury, P., Soepatmi, S., Ultee, C.A., Wesselman, P.J., 1989. Neonatal behavior after drug dependent pregnancy. Arch Child 64, 235–240.

Bailey, J.J., Berson, A.S., Garson Jr, A., Horan, L.G., Macfarlane, P.W., Mortara, D.W., Zywietz, C., 1990. Recommendations for standardization and specifications in automated electrocardiography: bandwidth and digital signal processing. A report for health professionals by an ad hoc writing group of the Committee on Electrocardiography and Cardiac Electrophysiology of the Council on Clinical Cardiology, American Heart Association. Circulation 81, 730.

Bauer, L.O., 1998. Effects of chronic opioid dependence and HIV-1 infection on pattern shift visual evoked potentials. Drug Alcohol Depend. 50, 147–155.

Becker, L.E., Zhang, W., Pereyra, P.M., 1993. Delayed maturation of the vagus nerve in sudden infant death syndrome. Acta Neuropathol. (Berl.) 86, 617–622.

Bell, A.H., McClure, B.G., McCullagh, P.J., McClelland, R.J., 1991. Spectral edge frequency of the EEG in healthy neonates and variation with behavioural state. Biol Neonate 60, 69–74.

Bigger, J.T., Fleiss, J.L., Steinman, R.C., Rolnitzky, L.M., Klieger, R.E., Rottman, J.N., 1992. Frequency domain measures of heart period variability and mortality after mycocardial infarction. Circulation 85, 164–171.

Brennan, M., Palaniswami, M., Kamen, P., 2001. Do existing measures of Poincare plot geometry reflect nonlinear features of heart rate variability? Biomed. Eng. IEEE Trans. On 48, 1342–1347.

Burns, L., Mattick, R.P., Lim, K., Wallace, C., 2007. Methadone in pregnancy: treatment retention and neonatal outcomes. Addiction 102, 264–270.

Butkov, N., Lee-Chiong, T.L., Technologists, A.A. of S., 2007. Fundamentals of Sleep Technology: Endorsed by the American Association of Sleep Technologists (AAST). Lippincott Williams & Wilkins.

Castellanos, F.X., Rapoport, J.L., 2002. Effects of caffeine on development and behavior in infancy and childhood: a review of the published literature. Food Chem Toxicol 40, 1235–1242.

Christov, I., 2004. Real time electrocardiogram QRS detection using combined adaptive threshold. Biomed. Eng. OnLine 3, 28.

Crowell, D.H., Group, C.S., 2003. An Atlas of Infant Polysomnography, Encyclopedia of Visual Medicine Series. Parthenon Pub. Group.

Darmani, N.A., Schnoll, S.H., Pandey, U., Martin, B.R., 1992. Chronic prenatal methadone exposure alters central opioid μ-receptor affinity in both fetal and maternal brain. Neurotoxicol. Teratol. 14, 265–271. doi:10.1016/0892-0362(92)90006-V

Dashe, J., 2002. Relationship between maternal methadone dosage and neonatal withdrawal. Obstet. Gynecol. 100, 1244–1249. doi:10.1016/S0029-7844(02)02387-6

DeGangi, G.A., DiPietro, J.A., Greenspan, S.I., Porges, S.W., 1991. Psychophysiological characteristics of the regulatory disordered infant. Infant Behav.

Dev. 14, 37–50.

De Weerd, A., Despland, P., Plouin, P., 1999. Neonatal EEG. The International Federation of Clinical Neurophysiology. Electroencephalogr. Clin. Neurophysiol. Suppl. 52, 149.

Dinges, D.F., Davis, M.M., Glass, P., 1980. Fetal exposure to narcotics: Neonatal sleep as a measure of nervous system disturbance. Science 209, 619–621.

Di Pietro, J.A., Larson, S.K., Porges, S.W., 1987. Behavioral and heart rate pattern differences between breast-fed and bottle-fed neonates. Dev. Psychol. 23, 467.

Doyle, O.M., Greene, B.R., Murray, D.M., Marnane, L., Lightbody, G., Boylan, G.B., 2007. The effect of frequency band on quantitative EEG measures in neonates with hypoxic-ischaemic encephalopathy. Conf Proc IEEE Eng Med Biol Soc 2007, 717–721. doi:10.1109/IEMBS.2007.4352391

Doyle, O.M., Korotchikova, I., Lightbody, G., Marnane, W., Kerins, D., Boylan, G.B., 2009. Heart rate variability during sleep in healthy term newborns in the early postnatal period. Physiol Meas 30, 847–860. doi:10.1088/0967-3334/30/8/009

Dryden, C., Young, Hepburn, M., Mactier, H., 2009. Maternal methadone use in pregnancy: factors associated with the development of neonatal abstinence syndrom and implications for healthcare resources. BJOG Int. J. Obstet. Gynecol. 116, 665–671.

Dumermuth, G., Molinari, L., 1987. Spectral analysis of the EEG. Some fundamentals revisited and some open problems. Neuropsychobiology 17, 85–99.

Eap, C.B., Buclin, T., Baumann, P., 2002. Interindividual variability of the clinical pharmacokinetics of methadone: implications for the treatment of opioid dependence. Clin Pharmacokinet 41, 1153–1193. doi:10.2165/00003088-200241140-00003

Ebner, A., Sciarretta, G., Epstein, C., Nuwer, M., 1999. EEG Instrumentation. The International Federation of Clinical Neurophysiology. Electroencephalogr. Clin. Neurophysiol. Suppl. 52, 7.

Engle, W., others, 2004. Age terminology during the perinatal period. Pediatrics 114, 1362.

Epstein, C., others, 2006. Guideline 1: minimum technical requirements for performing clinical electroencephalography. J Clin Neurophysiol 23, 86–91.

Eschenroeder, A.C., Vestal-Laborde, A.A., Sanchez, E.S., Robinson, S.E., Sato-Bigbee, C., 2012. Oligodendrocyte responses to buprenorphine uncover novel and opposing roles of μ-opioid- and nociceptin/orphanin FQ receptors in cell development: implications for drug addiction treatment during pregnancy. Glia 60, 125–136. doi:10.1002/glia.21253

Fajemirokun-Odudeyi, O., Sinha, C., Tutty, S., Pairaudeau, P., Armstrong, D., Phillips, T., Lindow, S.W., 2006. Pregnancy outcome in women who use opiates. Eur. J. Obstet. Gynecol. Reprod. Biol. 126, 170–175. doi:10.1016/j.ejogrb.2005.08.010

Fell, J., Röschke, J., Mann, K., Schäffner, C., 1996. Discrimination of sleep stages: a comparison between spectral and nonlinear EEG measures. Electroencephalogr Clin Neurophysiol 98, 401–410.

Finnegan, L., Connaughton Jr, J., Kron, R., Emich, J., 1974. Neonatal abstinence syndrome: assessment and management. Addict. Dis. 2, 141–158.

Fischer, G., Ortner, R., Rohrmeister, K., Jagsch, R., Baewert, A., Langer, M., Aschauer, H., 2006. Methadone versus buprenorphine in pregnant addicts: a double-blind, double-dummy comparison study. Addiction 101, 275–281. doi:10.1111/j.1360-0443.2006.01321.x

Force, T., 1996. Heart rate variability: standards of measurement, physiological interpretation and clinical use. Task Force of the European Society of Cardiology and the North American Society of Pacing and Electrophysiology. Circulation 93, 1043–65.

Fox, J., 2005. The R Commander: A Basic Statistics Graphical User Interface to R. J. Stat. Softw. 14, 1–42.

Gareri, J., Lynn, H., Handley, M., Rao, C., Koren, G., 2008. Prevalence of fetal ethanol exposure in a regional population-based sample by meconium analysis of fatty acid ethyl esters. Ther. Drug Monit. 30, 239–245.

Grigg-Damberger, M., Gozal, D., Marcus, C.L., Quan, S.F., Rosen, C.L., Chervin, R.D.,

Wise, M., Picchietti, D.L., Sheldon, S.H., Iber, C., 2007. The visual scoring of sleep and arousal in infants and children. J Clin Sleep Med 3, 201–240.

Gritz, E.R., Shiffman, S.M., Jarvik, M.E., Haber, J., Dymond, A.M., Coger, R., Charuvastra, V., Schlesinger, J., 1975. Physiological and psychological effects of methadone in man. Arch Gen Psychiatry 32, 237–242.

Hamilton, R., McGlone, L., MacKinnon, J.R., Russell, H.C., Bradnam, M.S., Mactier, H., 2010. Ophthalmic, clinical and visual electrophysiological findings in children born to mothers prescribed substitute methadone in pregnancy. Br J Ophthalmol 94, 696–700. doi:10.1136/bjo.2009.169284

Health and Social Care Information Centre, 1 Trevelyan Square, 2012. Website Search [WWW Document]. URL http://www.hscic.gov.uk/article/2021/Website-Search?productid=13673&q=statistics+on+drug+misuse&sort=Relevance&size=10&page=1&area=both#top (accessed 11.17.14).

Held-Egli, K., Rüegger, C., Das-Kundu, S., Schmitt, B., Bucher, H.U., 2009. Benign neonatal sleep myoclonus in newborn infants of opioid dependent mothers. Acta Paediatr 98, 69–73. doi:10.1111/j.1651-2227.2008.01010.x

Herzlinger, R.A., Kandall, S.R., Vaughan, H.G., 1977. Neonatal seizures associated with narcotic withdrawal. J Pediatr 91, 638–641.

Hoppenbrouwers, T., Harper, R.M., Hodgman, J.E., Sterman, M.B., McGinty, D.J., 1978. Polygraphic studies on normal infants during the first six months of life. II. Respiratory rate and variability as a function of state. Pediatr Res 12, 120–125. doi:10.1203/00006450-197802000-00011

Hormuzdi, S.G., Filippov, M.A., Mitropoulou, G., Monyer, H., Bruzzone, R., 2004. Electrical synapses: a dynamic signaling system that shapes the activity of neuronal networks. Biochim. Biophys. Acta BBA-Biomembr. 1662, 113–137.

Hunt, R.W., Tzioumi, D., Collins, E., Jeffery, H.E., 2008. Adverse neurodevelopmental outcome of infants exposed to opiate in-utero. Early Hum Dev 84, 29–35. doi:10.1016/j.earlhumdev.2007.01.013

Iber, C., 2007. The AASM manual for the scoring of sleep and associated events: rules, terminology and technical specifications. American Academy of Sleep Medicine.

Inturrisi, C.E., Max, M.B., Foley, K.M., Schultz, M., Shin, S.-U., Houde, R.W., 1984. The Pharmacokinetics of Heroin in Patients with Chronic Pain. N. Engl. J. Med. 310, 1213–1217. doi:10.1056/NEJM198405103101902

Jackson, L., Ting, A., McKay, S., Galea, P., Skeoch, C., 2004. A randomised controlled trial of morphine versus phenobarbitone for neonatal abstinence syndrome. Arch Child Fetal Neonatal Ed 89, F300–F304. doi:10.1136/adc.2003.033555

Jansson, L.M., Dipietro, J.A., Elko, A., Velez, M., 2007. Maternal vagal tone change in response to methadone is associated with neonatal abstinence syndrome severity in exposed neonates. J. Matern. Fetal Neonatal Med. 20, 677–685.

Jansson, L.M., DiPietro, J., Elko, A., others, 2005. Fetal response to maternal methadone administration. Am J Obstet Gynecol 193, 611–7.

Jasper, H., 1958. Report of the committee on methods of clinical examination in electroencephalography. Electroenceph Clin Neurophysiol 10, 370–375.

Jones, H.E., Johnson, R.E., Jasinski, D.R., O'Grady, K.E., Chisholm, C.A., Choo, R.E., Crocetti, M., Dudas, R., Harrow, C., Huestis, M.A., Jansson, L.M., Lantz, M., Lester, B.M., Milio, L., 2005. Buprenorphine versus methadone in the treatment of pregnant opioid-dependent patients: effects on the neonatal abstinence syndrome. Drug Alcohol Depend. 79, 1–10. doi:10.1016/j.drugalcdep.2004.11.013

Julu, P.O., 1992. A linear scale for measuring vagal tone in man. J. Auton. Pharmacol. 12, 109–115.

Julu, P.O.-O., Little, C.J.L., 1998. Apparatus and method for measuring cardiac vagal tone. WO1998022020 A1.

Kandall, S.R., Gaines, J., Habel, L., Davidson, G., Jessop, D., 1993. Relationship of maternal substance abuse to subsequent sudden infant death syndrome in offspring. J. Pediatr. 123, 120–126.

Kandel, E.R., Schwartz, J.H., Jessell, T.M., others, 2000. Principles of neural Science.

McGraw-Hill New York.

Katona, P.G., Jih, F., 1975. Respiratory sinus arrhythmia: noninvasive measure of parasympathetic cardiac control. J. Appl. Physiol. 39, 801–805.

Katona, P.G., Poitras, J.W., Barnett, G.O., Terry, B.S., 1970. Cardiac vagal efferent activity and heart period in the carotid sinus reflex. Am J Physiol 218, 1030–1037.

Kay, S.M., Marple, J., S. L., 1981. Spectrum analysis—A modern perspective. IEEE 69, 1380–1419. doi:10.1109/PROC.1981.12184

Klem, G.H., Lüders, H., Jasper, H., Elger, C., others, 1999. The ten-twenty electrode system of the International Federation. The International Federation of Clinical Neurophysiology. Electroencephalogr. Clin. Neurophysiol. Suppl. 52, 3.

Knyazev, G.G., 2012. EEG delta oscillations as a correlate of basic homeostatic and motivational processes. Neurosci. Biobehav. Rev. 36, 677–695.

Lee, H.-K., B. B., 2002. Effects of sponge bathing on vagal tone and behavioural responses in premature infants. J. Clin. Nurs. 11, 510–519.

Lee, H.-K., 2009. Cardiac Vagal Tone as an Index of Autonomic Nervous Function in Healthy Newborn and Premature Infants. J. Korean Acad. Child Health Nurs. 15, 299–305.

Lessard, C.S., 2006. Signal Processing of Random Physiological Signals, Synthesis Lectures on Biomedical Engineering. Morgan & Claypool Publishers.

Lifschitz, M.H., Wilson, G.S., Smith, E.O., Desmond, M.M., 1985. Factors Affecting Head Growth and Intellectual Function in Children of Drug Addicts. Pediatrics 75, 269–274.

Lipsitz, P.J., 1975. A proposed narcotic withdrawal score for use with newborn infants a pragmatic evaluation of its efficacy. Clin. Pediatr. (Phila.) 14, 592–594.

Longin, E., Schaible, T., Lenz, T., König, S., 2005. Short term heart rate variability in healthy neonates: normative data and physiological observations. Early Hum. Dev. 81, 663–671.

Mactier, H., 2011. The management of heroin misuse in pregnancy: time for a rethink? Arch Child Fetal Neonatal Ed 96, F457–F460. doi:10.1136/adc.2009.181057

Mactier, H., McGlone, L., Hamilton, R., MacKinnon, J.R., 2012. Neonatal abstinence syndrome can be a problem. BMJ 344, e4200.

Manfredi, L.G., Rocchi, R., Panerai, A.E., Martini, A., Vegni, C., Lodi, M.L., Ferraris, G., Marini, A., Franchini, A.M., 1983. EEG sleep patterns and endogenous opioids in infants of narcotic-addicted mothers. Rev Electroencephalogr Neurophysiol Clin 13, 199–206.

Marieb, E.N., Hoehn, K., 2007. Human anatomy & physiology. Pearson Education.

Mattick, R.P., Breen, C., Kimber, J., Davoli, M., Breen, R., 2003. Methadone maintenance therapy versus no opioid replacement therapy for opioid dependence.

McCarthy, J.J., Leamon, M.H., Parr, M.S., Anania, B., 2005. High-dose methadone maintenance in pregnancy: material and neonatal outcomes. Am. J. Obstet. Gynecol. 193, 606–610.

McGlone, L., Hamilton, R., McCulloch, D.L., Boulton, R., Bradnam, M.S., Weaver, L.T., Mactier, H., 2013. Neonatal visual evoked potentials in infants born to mothers prescribed methadone. Pediatrics 131, e857–e863.

McGlone, L., Hamilton, R., McCulloch, D.L., MacKinnon, J.R., Bradnam, M., Mactier, H., 2014. Visual outcome in infants born to drug-misusing mothers prescribed methadone in pregnancy. Br J Ophthalmol 98, 238–245. doi:10.1136/bjophthalmol-2013-303967

McGlone, L., Mactier, H., Hamilton, R., Bradnam, M.S., Boulton, R., Borland, W., Hepburn, M., McCulloch, D.L., 2008. Visual evoked potentials in infants exposed to methadone *in utero*. Arch Child 93, 784–786. doi:10.1136/adc.2007.132985

Mehta, S.K., Super, D.M., Connuck, D., Salvator, A., Singer, L., Fradley, L.G., Harcar-Sevcik, R.A., Kirchner, H.L., Kaufman, E.S., 2002. Heart rate variability in healthy newborn infants. Am J Cardiol 89, 50–53.

Mirmiran, M., 1995. The function of fetal/neonatal rapid eye movement sleep. Behav

Brain Res 69, 13–22.

Mitra, J., O'Brien, C.P., Sloviter, H.A., 1981. The effects of methadone on cortical and subcortical EEG in the rat. Electroencephalogr Clin Neurophysiol 52, 345–352.

Mizrahi, E.M., Hrachovy, R.A., Kellaway, P., 2003. Atlas of Neonatal Electroencephalography, LWW medical book collection. Lippincott Williams & Wilkins.

Nijhuis, J.G., 2003. fetal behavior. Neurobiol. Aging 24, 541–546.

Nokes, L., Jennings, D., Flint, T., Turton, B., 1995. Introduction to medical electronics applications. Butterworth-Heinemann.

Novák, D., Lhotská, L., Eck, V., Sorf, M., 2004. EEG and VEP signal processing. Cybern. Fac. Electr. Eng n/a, 50–53.

Nunez, P.L., Srinivasan, R., 2005. Electric fields of the brain: the neurophysics of EEG. Oxford University Press, USA.

Nuwer, M.R., Comi, G., Emerson, R., Fuglsang-Frederiksen, A., Guérit, J.M., Hinrichs, H., Ikeda, A., Luccas, F.J., Rappelsburger, P., 1998. IFCN standards for digital recording of clinical EEG. International Federation of Clinical Neurophysiology. Electroencephalogr Clin Neurophysiol 106, 259–261.

O'Brien, C.M., Jeffery, H.E., 2002. Sleep deprivation, disorganization and fragmentation during opiate withdrawal in newborns. J Paediatr Child Health 38, 66–71.

Ornoy, A., Michailevskaya, V., Lukashov, I., Bar-Hamburger, R., Harel, S., 1996. The developmental outcome of children born to heroin-dependent mothers, raised at home or adopted. Child Abuse Negl. 20, 385–396.

Ornoy, A., Segal, J., Bar-Hamburger, R., Greenbaum, C., 2001. Developmental outcome of school-age children born to mothers with heroin dependency: importance of environmental factors. Dev. Med. Child Neurol. 43, 668–675. doi:10.1111/j.1469-8749.2001.tb00140.x

Osborn, D.A., Jeffery, H.E., Cole, M.J., 2010. Opiate treatment for opiate withdrawal in newborn infants. Cochrane Database Syst Rev 10, n/a.

Parikh, R., Hussain, T., Holder, G., Bhoyar, A., Ewer, A., 2011. Maternal methadone therapy increases QTc interval in newborn infants. Arch. Dis. Child.-Fetal Neonatal Ed. 96, F141–F143.

Pereyra, P.M., Zhang, W., Schmidt, M., Becker, L.E., 1992. Development of myelinated and unmyelinated fibers of human vagus nerve during the first year of life. J. Neurol. Sci. 110, 107–113.

Peters, T.M., Williams, J.C., Bates, J.H.T., 1998. The Fourier Transform in Biomedical Engineering, Applied and Numerical Harmonic Analysis. Birkhäuser.

Pinto, F., Onofrj, M., Pola, P., Tempesta, E., Torrioli, M., 1986. Fetal addiction to methadone: postnatal abstinence syndrome and development of visual evoked potentials. Drug Alcohol Depend. 18, 1–10.

Pinto, F., Torrioli, M.G., Casella, G., Tempesta, E., Fundarò, C., 1988. Sleep in babies born to chronically heroin addicted mothers. A follow up study. Drug Alcohol Depend 21, 43–47.

Porges, S.W., 1985. Method and apparatus for evaluating rhythmic oscillations in aperiodic physiological response systems. US4510944 A.

Porges, S.W., 2001. The polyvagal theory: phylogenetic substrates of a social nervous system. Int. J. Psychophysiol. 42, 123–146.

Porter, F.L., Porges, S.W., Marshall, R.E., 1988. Newborn pain cries and vagal tone: parallel changes in response to circumcision. Child Dev. n/a, 495–505.

Prechtl, H.F., 1974. The behavioural states of the newborn infant (a review). Brain Res 76, 185–212.

R Core Team, 2013. R: A Language and Environment for Statistical Computing. R Foundation for Statistical Computing, Vienna, Austria.

Rechtschaffen, A., Kales, A., 1968. A manual of standardized terminology, techniques, and scoring systems for sleep stages of human subjects. citeyoulike.org n/a, n/a.

Reed, S.F., Ohel, G., David, R., Porges, S.W., 1999. A neural explanation of fetal heart rate patterns: a test of the polyvagal theory. Dev. Psychobiol. 35, 108–118.

Rennie, J.M., Hagmann, C.F., Robertson, N.J., 2008. Neonatal Cerebral Investigation. Cambridge University Press.

Robinson, S.R., Smotherman, W.P., 1997. Stimulus contingencies that permit classical conditioning of opioid activity in the rat fetus. Behav. Neurosci. 111, 1086–1097. doi:10.1037/0735-7044.111.5.1086

Rosen, T.S., Johnson, H.L., 1982. Children of methadone-maintained mothers: follow-up to 18 months of age. J. Pediatr. 101, 192–196.

Rowan, A.J., Tolunsky, E., 2003. Primer of EEG: With a Mini-atlas. Butterworth-Heinemann.

Sachis, P.N., Armstrong, D.L., Becker, L.E., Bryan, A.C., 1981. The vagus nerve and sudden infant death syndrome: a morphometric study. J. Pediatr. 98, 278–280.

Sanchez, E.S., Bigbee, J.W., Fobbs, W., Robinson, S.E., Sato-Bigbee, C., 2008. Opioid addiction and pregnancy: perinatal exposure to buprenorphine affects myelination in the developing brain. Glia 56, 1017–1027.

Sanei, S., Chambers, J.A., 2007. EEG Signal Processing. Wiley-Interscience.

Sarfi, M., Martinsen, H., Bakstad, B., Røislien, J., Waal, H., 2009. Patterns in sleep-wakefulness in three-month old infants exposed to methadone or buprenorphine. Early Hum. Dev. 85, 773–778.

Schäffer, L., Burkhardt, T., Müller-Vizentini, D., Rauh, M., Tomaske, M., Mieth, R.A., Bauersfeld, U., Beinder, E., 2008. Cardiac autonomic balance in small-for-gestational-age neonates. Am. J. Physiol.-Heart Circ. Physiol. 294, H884–H890.

Scher, M.S., 1996. Normal electrographic-polysomnographic patterns in preterm and fullterm infants. Semin Pediatr Neurol 3, 2–12.

Scher, M.S., 2004. Automated EEG-sleep analyses and neonatal neurointensive care. Sleep Med 5, 533–540. doi:10.1016/j.sleep.2004.07.002

Scher, M.S., Sun, M., Steppe, D.A., Guthrie, R.D., Sclabassi, R.J., 1994. Comparisons of EEG spectral and correlation measures between healthy term and preterm infants. Pediatr Neurol 10, 104–108.

Schlogl, A., Brunner, C., 2008. BioSig: a free and open source software library for BCI research. Computer 41, 44–50.

Schulman, C.A., 1969. Alterations of the sleep cycle in heroin-addicted and “suspect” newborns. Neuropaediatrie 1, 89–100.

Schwartz, P.J., Garson, A., Jr, Paul, T., Stramba-Badiale, M., Vetter, V.L., Wren, C., European Society of Cardiology, 2002. Guidelines for the interpretation of the neonatal electrocardiogram. A task force of the European Society of Cardiology. Eur Heart J 23, 1329–1344.

Selig, F.A., Tonolli, E.R., Silva, É.V.C.M. da, Godoy, M.F. de, 2011. Heart rate variability in preterm and term neonates. Arq. Bras. Cardiol. 96, 443–449.

Semmlow, J.L., 2004. Biosignal and Biomedical Image Processing: MATLAB-Based Applications, Signal Processing and Communications. CRC.

Shapiro, S.S., Wilk, M.B., 1965. An analysis of variance test for normality (complete samples). Biometrika 52, 591–611.

Sharbrough, F., Chatrian, G., Lesser, R., Lüders, H., Nuwer, M., Picton, T., 1991. American Electroencephalographic Society guidelines for standard electrode position nomenclature. J Clin Neurophysiol 8, 200–202.

Shellhaas, R., Chang, T., Tsuchida, T., Scher, M., Riviello, J., Abend, N., Nguyen, S., Wusthoff, C., Clancy, R., Shellhaas, R., 2011. The American Clinical Neurophysiology Society’s Guideline on Continuous EEG Monitoring in Neonates. J. Clin. Neurophysiol. 28, 611.

Sisson, T., Wickler, M., Tsai, P., Rao, I., Vaughan, V., 1974. Effect of narcotic withdrawal on neonatal sleep patterns. Pediatr. Res. 8, 451–451.

Spassov, L., Curzi-Dascalova, L., Clairambault, J., Kauffmann, F., Eiselt, M., M?digue, C., Peirano, P., 1994. Heart rate and heart rate variability during sleep in small-for-gestational age newborns. Pediatr Res 35, 500–505.

Stringer, J., Welsh, C., Tommasello, A., 2009. Methadone-associated QT interval prolongation and torsades de pointes. 66 n/a, 825–833.

Tarvainen, M., Niskanen, J., 2008. Kubios HRV Version 2.0 User's Guide. Dep. Phys. Univ. Kuopio Kuopio Finl. n/a, n/a.

Team, G.R.O. for S.W., 2013. General Register Office for Scotland - 2012 [WWW Document]. Gen. Regist. Off. Scotl. URL http://www.gro-scotland.gov.uk/statistics/theme/vital-events/deaths/drug-related/2012/index.html (accessed 11.17.14).

Teberg, A.J., Walther, F.J., Pena, I.C., 1988. Mortality, morbidity, and outcome of the small-for-gestational age infant. Semin Perinatol 12, 84–94.

Teplan, M., 2002. Fundamentals of EEG measurement. Meas. Sci. Rev. 2, 1–11.

Thordstein, M., Löfgren, N., Flisberg, A., Bågenholm, R., Lindecrantz, K., Kjellmer, I., 2005. Infraslow EEG activity in burst periods from post asphyctic full term neonates. Clin Neurophysiol 116, 1501–1506. doi:10.1016/j.clinph.2005.02.025

Tong, S., Thakor, N.V., 2009. Quantitative EEG Analysis Methods and Clinical Applications, Engineering in Medicine & Biology. Artech House.

Tonner, P.H., Bein, B., 2006. Classic electroencephalographic parameters: median frequency, spectral edge frequency etc. Best Pr. Res Clin Anaesthesiol 20, 147–159.

Trambaiolli, L., Lorena, A., Fraga, F., Kanda, P., Nitrini, R., Anghinah, R., 2011. Does EEG montage influence Alzheimer's disease electroclinic diagnosis? Int. J. Alzheimers Dis. 2011, 1–6.

Vandeput, S., Naulaers, G., Daniels, H., Van Huffel, S., 2009. Heart rate variability during REM and non-REM sleep in preterm neonates with and without abnormal cardiorespiratory events. Early Hum. Dev. 85, 665–671.

Van Drongelen, W., 2006. Signal Processing for Neuroscientists: An Introduction to the Analysis of Physiological Signals. Academic Press.

Vanhatalo, S., Tallgren, P., Andersson, S., Sainio, K., Voipio, J., Kaila, K., 2002. DC-EEG discloses prominent, very slow activity patterns during sleep in preterm infants. Clin Neurophysiol 113, 1822–1825.

Vatury, O., Barg, J., Slotkin, T.A., Yanai, J., 2004. Altered localization of choline

transporter sites in the mouse hippocampus after prenatal heroin exposure. Brain Res. Bull. 63, 25–32. doi:10.1016/j.brainresbull.2003.11.004

Vestal-Laborde, A.A., Eschenroeder, A.C., Bigbee, J.W., Robinson, S.E., Sato-Bigbee, C., 2014. The Opioid System and Brain Development: Effects of Methadone on the Oligodendrocyte Lineage and the Early Stages of Myelination. Dev. Neurosci. 36, 409–421. doi:10.1159/000365074

Villa, M.P., Calcagnini, G., Pagani, J., Paggi, B., Massa, F., Ronchetti, R., 2000. Effects of sleep stage and age on short-term heart rate variability during sleep in healthy infants and children. Chest 117, 460–466.

Walhovd, K.B., Watts, R., Amlien, I., Woodward, L.J., 2012. Neural tract development of infants born to methadone-maintained mothers. Pediatr. Neurol. 47, 1–6.

Welch, P., 1967. The use of fast Fourier transform for the estimation of power spectra: a method based on time averaging over short, modified periodograms. Audio Electroacoustics IEEE Trans. On 15, 70–73.

Whitham, E.M., Pope, K.J., Fitzgibbon, S.P., Lewis, T., Clark, C.R., Loveless, S., Broberg, M., Wallace, A., DeLosAngeles, D., Lillie, P., others, 2007. Scalp electrical recording during paralysis: quantitative evidence that EEG frequencies above 20Hz are contaminated by EMG. Clin. Neurophysiol. 118, 1877–1888.

Whitham, J.N., Spurrier, N.J., Sawyer, M.G., Baghurst, P.A., Taplin, J.E., White, J.M., Gordon, A.L., 2010. The effects of prenatal exposure to buprenorphine or methadone on infant visual evoked potentials. Neurotoxicol Teratol 32, 280–288. doi:10.1016/j.ntt.2009.09.001

Wilson, G.S., McCreary, R., Kean, J., Baxter, J.C., 1979. The development of preschool children of heroin-addicted mothers: A controlled study. Pediatrics 63, 135–141.Abel, E.L., 1980. Smoking during pregnancy: a review of effects on growth and development of offpring. Hum. Biol. n/a, 593–625.